14 1-34 Y

QF 3-

īne

:-UTT),

'E''y, a

imi sys Mationsi

of p-087 y

Pre probe

amalytic

Casses,

Diential

• • •

Diservance Irres

sulfonyl 4

i.dies.

flworide (

10th form

imatio

:::eryatio

erine also

ABSTRACT

Ву

Michael Norman Liebman

The three-dimensional structure of α -chymotrypsin (α -CHT), a representative enzyme of the serine protease family, as determined by Tulinsky <u>et al.</u>, provided an ideal system in which to examine the structure-function relationship. The existence of two independent molecules of α -CHT within the crystalline dimer permitted an extensive probe of specificities within the binding and catalytic regions of the active site using two inhibitor classes, irreversible, covalently-linked inhibitors and potential transition-state analogs, while allowing the observance of structural variability.

Irreversible inhibition of α -CHT by phenyl alkyl sulfonyl fluorides has been established in solution studies. The compounds studied, p-toluene sulfonyl fluoride (TOS) and phenyl methyl sulfonyl fluoride (PMS) both form covalent sulfonyl ester bonds with SER 195. Examination of the structure of the complexes allowed observation of definitive covalent linkages with SER 195 while also allowing the study of those interactions

responsitions of the property of the property

Catyl Bor Ellowed f

ime inter

incase o

ing at a

and corre

::-35:5

10013547

responsible for specificity. Structural analysis emphasized the similar but independent molecules within the crystalline dimer while recognizing two unique but consistent binding orientations across the two-fold axis. Observation of the SER 195 interaction allowed evaluation to be made of the applicability of the potential transition-state analogs.

As α -CHT is expected to involve a tetrahedral intermediate in its catalytic mechanism, it has been proposed that phenyl alkyl boronic acid derivatives would be isosteric with normal substrates and allow observation of the bound state by crystallographic methods. Variation of the phenyl alkyl group, phenyl ethane boronic acid (PEBA), phenyl propyl boronic acid (PPBA) and phenyl butyl boronic acid (PBBA), as well as pH with PEBA, allowed for the observation that at pH 5.4 and pH 7.3, the interaction more closely resembled the covalent linkage of TOS, but formed a weaker complex at pH 3.6. Further studies involving PPBA and PBBA established the limiting features of the specificity pocket of α -CHT and correlations with previous kinetic studies.

The direction of the research has been to establish the basis of enzyme recognition and specificity, with emphasis on molecular organization and conformational adaptability. Towards these goals, the method of

::spanal

Forier a

;f 3-01,7

diagonal plots was expanded to incorporate difference Fourier analysis and in this manner the domain structure of $\alpha\text{-CHT}$ was further studied.

AN X-RAY CRYSTALLOGRAPHIC EXAMINATION OF THE INTERACTIONS OF α -CHYMOTRYPSIN WITH IRREVERSIBLE INHIBITORS AND POTENTIAL TRANSITION-STATE ANALOGS

Ву

Michael Norman Liebman

A DISSERTATION

Submitted to

Michigan State University
in partial fulfillment of the requirements

for the degree of

DOCTOR OF PHILOSOPHY

Department of Chemistry



6107080

In Memory of My Father

The a appreciation pridence a To Or author would sarly supplied in the appreciation for the visitance of the appreciation for the appre

various pi for her to faring th

> Supp National Study is

Pe Lower

of the au

ACKNOWLEDGMENTS

The author wishes to express his sincerest appreciation to Dr. Alexander Tulinsky for his constant guidance and support, enthusiasm and friendship.

To Dr. S. N. Timasheff and Dr. R. B. Beard, the author would like to extend his appreciation for their early support and encouragement. To Dr. Richard L. Vandlen, the author extends particular appreciation for his interactions and encouragement in the early part of this work. The author would like to express appreciation for their many helpful discussions to Dr. Irene Moustakali, Dr. Aristides Mavridis, Mr. Lawrence Weber and Mr. Lyndon Hibbard.

The author would like to thank Mr. Paul Hunt, Mr. Tom Smith, for their technical assistance during various phases of this study and Ms. Janet L. Sayers for her technical assistance and helpful discussions during the final stages of this work.

Support of the Molecular Biology Section of the National Science Foundation during the course of this study is gratefully acknowledged as is the support of the Lower Merion Township Scholarship Fund for support of the author's undergraduate education.

: :NTR00

A. G

3. 3

Ç. 3

). T

II. EXPER

A. C

8. D

C. 0

III. METH

Å. E

B. E

C. E

0.

E. 1

i. RESUL

Å. I

TABLE OF CONTENTS

																								Page
I.	INTRO	DUCT	101	۱.	•		•	•	•	•	•			•	•	•				•	•	•	•	1
	Α.	Gene	ral	•		•	•		•	•				•	•			•	•		•			1
	В.	α-Ch	ymc	tr	ур	s i	n	(c	1 – 1	СН	T)	:		Cł	ı e	mi	S 1	tr	y	•	•	•	•	1
	С.	α-Ch	ymc	tr	ур	s i	n:		С	ry	s t	: a	11	0 9	gra	a p	hy	/	•	•	•	•	•	18
	D.	Tran	sit	io	n –	St	a t	e	Α	n a	10	g	s	a r	nd	α	. – (CH	T	•	•		•	29
II.	EXPE	RIME	NTA	\L	•		•		•	•		,	•	•	•	•		•	•		•		•	36
	Α.	Crys	tal	1 i	z a	ti	o n	(o f	α	- 0	H	Т	•	•	•		•	•	•	•	•		36
	В.	Data	Co	11	еc	ti	o n	١.	•	•	•	,			•	•			•		•	•	•	41
	С.	Data	Pr	ос	e s	s i	n g	١.		•				•	•	•		•	•		•		•	49
III.	MET	THODS	0 F	Α	ΝA	LY	SI	S		•	•					•			•	•	•	•	•	64
	Α.	Emph	asi	S	o f	A	na	1)	/ S	is	•		•	•	•	•				•	•	•	•	64
	В.	Exam Acti																				•	•	66
	С.	Exam Acco																					•	74
	D.	Inhi Mole											n •	th •	e •	I •			•	en d			•	82
	Ε.	Inhi	bit	or	0	ri	e n	ta	t	i o	n	D	e f	ir	۱i	ti	o r	١s	•		•	•	•	82
IV.	RESU	JLTS	AND	D	ΙS	CU	SS	IC	N	•	•		•	•		•		•	•	•	•	•	•	87
	Α.	Irre	ver	s i	b 1	е	Ιn	h i	i b	it	o r	`S		•		•		•	•	•	•	•	•	87
		1.	Su TO	bs S																	•	•	•	87
		2.		i e																				92

TABLE OF CONTENTS

																		rage
		3.	Comp TOS											•	•	•	•	105
	В.	•	etiti sitio											•	•	•	•	110
		1.	Subs PEBA												•		•	110
		2.	Orie inte func	rac	tio	n w	vith	α	-CH	IT	a s	a			i	•	•	118
		3.	Eval stat															130
		4.	Comp (nat														•	138
		5.	Phen tion leng	as	a	fun	icti											142
		6.	Orient pheny active	nta yl a	tio: alk:	na yl	nd bor			аc		S .	i n	th	ne	•	•	144
		7.	Subs	tra	te :	spe	cif	ic	ity	0	f	x – (CHI	Γ.		•	•	150
V . D	IAGO	NAL I	PLOT	ANAI	LYS	IS.	•	•		•	•	•	•	•	•	•	•	161
	Α.		sis (•		161
		with	arison Panci of Dis	reat	tic	Tr	yps	in	Ιn	hi	bit	toı	r t	ЭУ		•	•	174
			urbat mpany															182
REFER	RENCE	s			•		•	•		•	•			•	•	•	•	200

PPENDIX A

mendix e

DEFACIX C

TABLE OF CONTENTS

			<u>Page</u>
APPENDIX	Α.	Coordinates of Inhibitors Determined in This Study (a = 49.2 Å, b = 67.2 Å, c = 65.95 Å, β = 101.8°)	208
APPENDIX	В.	Calculated van der Waals Contacts of TOS, PMS, TOS (MRC), PEBA pH 3.6, PEBA pH 5.4, PEBA pH 7.3, PPBA and PBBA	218
APPENDIX	С.	Coordinates of Difference Fourier Peaks Used in Calculation of Difference Diagonal Plots (a = 49.2 Å, b = 67.2 Å, c = 65.95 Å,	226
		$\beta = 101.8$)	226

LIST OF TABLES

<u>Table</u>		<u>Page</u>
1	Specificity of $\alpha\text{-CHT}$ with Respect to Methyl Esters of Some N-Acetyl-L-Amino Acids	6
2	Sequence Homology in the Vicinity of Active Site Residues Among Several Serine Proteases	14
3	Classes of Derivatives Studied in $\alpha\text{-CHT}$	21
4	Comparison of Lattice Parameters for $\alpha\text{-}Chymotrypsin$ with Addition of Dioxane	23
5	Possible Configuration of Tetrahedral Centers for Interaction with SER 195	32
6	Lattice Parameters of the $\alpha\text{-CHT}$ Derivative Crystals Used in This Study	48
7	Comparison of Derivative Crystal Characteristics in This Study	50
8	Comparison of Derivative Crystal $ \Delta F $ Distribution Statistics	55
9	Comparison of Cell Parameters of Irreversibly Inhibited $\alpha\text{-CHT.}$	87
10	Comparison of the Centroid Positions of Substitution Density in the Active Sites of Molecules 1 and 1' (TOS and PMS)	91
11	Orientation Angles Determined for the Inhibitor-Enzyme Structures	93
12a	Summary of van der Waals Contacts (\leq 3.5 Å) Between Native $\alpha\text{-CHT}$ and the Inhibitor Molecules	95
12b	Summary of Inhibitor Contacts with Specific Residues of Native α -CHT (< 3.5 Å)	96

25

LIST OF TABLES

<u>Table</u>		<u>Page</u>
13	Comparison of Unit Cell Parameters of TOS (MSU) and TOS (MRC)	106
14	Comparison of Contacts Within van der Waals Distances Between Tosyl and $\alpha\text{-CHT}$ in MSU and MRC Studies	111
15	Comparison of Cell Parameters of PEBA at pH 3.6, 5.4 and 7.3	112
16	Comparison of Peak Heights of Difference Electron Density Regions in the Active Site of PEBA pH 3.6, 5.4 and 7.3	113
17	Comparison of Centroid Positions of Substitution Density in the Active Sites of Molecules 1 and 1' (PEBA pH 3.6, PEBA pH 5.4 and PEBA pH 7.3)	117
18	Cell Parameters for PPBA and PBBA	142
19	Comparison of Peak Heights of Difference Electron Density in the Active Sites of the PPBA and PBBA Derivatives	143
20	Comparison of Centroid Positions of Substitution Density in the Active Sites of Molecules 1 and 1' (PPBA and PBBA)	147
21	Comparison of Homologous Series of Inhibitors, Substrates and Potential Transition-State Analogs of $\alpha\text{-CHT}$	153
22	Structural Features of $\alpha\text{-CHT}$ Diagonal Plot	165
23	Intersection of Mirror Planes with Diagonal of Distance Plot of $\alpha\text{-CHT.}$	167
24	Intrachain Loop Palindromy	169
25	Residues in Proximity of Localized Sulfate Ions	173

<u> 30 le</u>	
26	Se Do
27	In El
28	Co De Wi

Appendix A

Eppendix A.

imendix B.

locendix B-

ippendix C

LIST OF TABLES

<u>Table</u>					Page
26	Domair	n A Bas	ed on A	of PTI and α -CHT lignment of Distance	e 179
27	Electr	on Den		of Difference stance Diagonal	192
28	Densit	y Peak	s (Othe	Difference Electron r Than Substitution ite Region of α -CHT.)
Appendix	A-1	in Thi	s Study	f Inhibitors Determ (a = 49.2 Å, b = 5.95 Å, β = 101.8°)	
Appendix	A-2		tors De	s and Bond Angles of termined in This	f 216
Appendix	B-1	Between Inhibi	n Nativ tors (T	n der Waals Contacts e α -CHT and Irrevers OS and PMS) Inhibitorom Appendix	sible or
Appendix	B-2	Between	n α-CHT	n der Waals Contacts (MRC) and Tosyl C Results) (49)	s 225
Appendix	. C	Peaks Differed 49.2 A	Used in ence Di , b = 6	f Difference Fourier Calculation of agonal Plots (a = 7.2 Å, c = 65.95 Å,	
		~ 10	, .		

91.19

A:

E

R

ς γ

LIST OF FIGURES

<u>Figure</u>		Page
1	Amino Acid Sequence of $\alpha\text{-Chymotrypsinogen}$.	. 3
2	Activation and Autolytic Reactions of $\alpha\text{-Chymotrypsinogen A (4)}$. 4
3	pH-Activity Profile of $\alpha\text{-CHT}$ Catalyzed Hydrolysis of a) N-acetyl-L-tryptophan amide, and b) N-acetyl-L-phenylalanine amide in water at 25°C (10)	. 10
4	Early Ideas of Serine 195 Participation in Anomalous Activity	. 17
5	Charge-Relay Mechanism of Blow et al. (31)	. 19
6	3D Derivatives of $\alpha\text{-CHT}$ at 2.8 $\overset{\circ}{A}$ Resolution	. 20
7	Schematic Packing Diagram of $\alpha\text{-CHT}$ Viewed Along a*-Direction. Non-crystallographic Dimer = I and I' or II and II' (41)	. 22
8	Variation of Unit Cell Parameters of $\alpha\text{-CHT}$ with pH (43)	. 24
9	Distance Diagonal Plotoof Native $\alpha\text{-CHT}$ (45), Contoured at 15 A (Solid Regions)	. 27
10	Potential Transition-State Analogs	. 34
11	Preparation of Crystals of Native $\alpha\text{-Chymotrypsin}$. 37
12	Procedure for Preparation and Verification of Derivative $\alpha\text{-CHT}$ Crystals	. 39
13	Inhibitor Molecules Used in This Study	. 40
14	Crystal Selection and Data Collection Procedures	. 43
15	Distribution of Diffracted Intensities Along Principal Axes of α-CHT Complexes Used in This Study	. 45

23

24

H

A C

LIST OF FIGURES

<u>Figure</u>		<u>P a</u>	ge
16a	Data ProcessingReduction of Intensities to F 's	. 5	1
16b	Data ProcessingConversion of F 's to F's	. 5	2
17	Histograms of Derivative Crystal $ \Delta F $ Distribution Statistics	. 5	6
18	Absorption Correction CurvesPEBA pH 3.6, Crystal G-67-SI-3	. 5	9
19	Schematic of y-z Projections of the Difference Electron Density in the Active Site Region for TOS $\alpha\text{-CHT}.$. 6	7
20	Comparison of Composite Projections of the TOS Difference Electron Density in the Active Sites of the α -CHT Dimer; Contoured at 0.15 eA-3, Positions of TOS 1 and TOS 1' are Arbitrary in z	. 6	8
21 a	Comparison of Composite Projections of the Substitution Electron Density of TOS and PMS in the Active Site of Molecule 1; Contoured at 0.15 eA-3	. 6	9
216	Comparison of Composite Projections of the Substitution Electron Density of TOS and PMS in the Active Site of Molecule 1'; Contoured at 0.15 eA-3	. 7	0
22	Model of TOS as Fitted to Weighted Centroid Projections of the Difference Electron Density	. 7	3
23	Distance Diagonal Plot, r_{ij} , of α -CHT, Contoured at 15 Å only (45) and Exhibiting Dimer	. 7	6
24	Schematic Representation of $\alpha\text{-CHT}$ Domains	. 7	8

34

DOC 20 SIFF BO SIFF PER CONTROL PER CONTRO

D a

LIST OF FIGURES

Figure		<u>Page</u>
25	Intermolecular Domain Contacts in $\alpha\text{-CHT}$ Crystalline Dimera) Schematic of Cross-Distance Diagonal Plot, and b) Linear Packing of Dimers and Domains of $\alpha\text{-CHT}$. 79
26	Definitions for Diagonal Distance Plotand for Difference Distance Plots	. 81
27a	Difference Distance Plot of Conformational Changes on Increasing the Native, pH = 3.6 α -CHT Crystal to pH = 7.3 in the Presence of PEBA	. 83
27b	Substitution Distance Plot of Substitution of PEBA Observed on Increasing the Native, pH = 3.6 α -CHT Crystal to pH = 7.3	. 84
28	Definition of Orientation Angles for Comparison of Inhibitor Orientation	. 85
29	Variability Between Irreversible Inhibitors Viewed Down y,z-Axis, Contoured at 0.15 eA- with Approximate Two-Fold Representation .	- 3
30	TOS and PMS Orientation in x-z Projection of Active Site	. 98
31	TOS (MRC) Orientation in x-z Projection of Active Site (MRC)	. 108
32	TOS (MSU) vs. TOS (MRC) Position	. 109
33a	PEBA in Region of Active Site, Molecule 1, Viewed Down y,z-Axis, Contoured at 0.15 eÅ-3	. 115
33Ь	PEBA in Region of Active Site, Molecule 1', Viewed Down y,z-Axis, Contoured at 0.15 eA-3	. 116
34	PEBA pH 3.6 Orientation in x-z Projection of Active Site	. 119

35 35 37 38**a** 38b р У А; 39 P: 10 S. ir 47 Di 42 Di pi Co 43 ეე 44 00 1-45 Di

46

Id of Di

::<u>,,re</u>

LIST OF FIGURES

Figure		<u>Page</u>
35	PEBA pH 5.4 Orientation in x-z Projection of Active Site	. 120
36	PEBA pH 7.3 Orientation in x-z Projection of Active Site	. 121
37	Energy Diagram of Proposed Enzymatic Mechanism Involving a Transition-State for Catalysis (96)	. 132
38a	PPBA in Region of Active Site, Viewed Down y,z-Axis, Contoured at 0.15 eA-3, with Approximate Two-Fold Representation	. 145
38b	PBBA in Region of Active Site, Viewed Down y,z-Axis, Contoured at 0.15 eA-3, with Approximate Two-Fold Representation	. 146
39	PPBA and PBBA Orientation in x-z Projection of Active Site	. 149
40	Substrate/Inhibitor Side-Chain Specificity in $\alpha\text{-CHT}$. 157
41	Distance Diagonal Plot Definitions	. 162
42	Distance Diagonal Plot of α -CHT Dimer Depicting Representative Structural Features, Contoured at 15 Å (Solid Regions)	. 163
43	Domain Configuration of $\alpha\text{-CHT}$ Dimer	. 171
44	Comparison of Distance Diagonal Plots of $\alpha\text{-CHT}$ and PTI	. 177
45	Difference Diagonal Plots	. 185
46	Identification of Diagonal Plot Features of Native $\alpha\text{-CHT}$ to be Compared in Differenc Diagonal Plots	e . 191

espects o

re activ

the source

re ating

I. INTRODUCTION

A. General

The chemical processes of living systems are almost entirely dependent on the catalytic activity of enzymes. Two fundamental questions in biochemistry are: What are enzymes and how do they operate? One answer that has emerged is that enzymic activity depends on the structure of the molecule and particularly on the chemical nature of that part of the enzyme which comes into contact with the substrate and is generally referred to as the active site. The purpose of the present work is to utilize X-ray diffraction in studying two specific structural aspects of α -chymotrypsin (α -CHT): the interaction at the active site upon binding of substrate/inhibitor, and the source of the specificity of the enzyme.

B. α -Chymotrypsin (α -CHT): Chemistry

 α -CHT is a proteolytic enzyme which is found in pancreatic tissue and pancreatic juice. Its empirical formula, $C_{1113}N_{300}0_{349}H_{1752}S_{12}$, indicates a molecular weight of 25,300 amu and corresponds to a total polypeptide chain length of 241 amino acid residues. As with other enzymes, α -CHT is secreted in an inactive form, or zymogen, in this case, alpha-chymotrypsinogen (α -CTN). The amino acid sequence of this zymogen is used as a

runbering

determinativerified b

revision b

Blow et al

established form of the part involved and three poly 131, and 9

disulfide

actions.

Kunit 1935 and c be examine ease of ot parity who become on However,

only to a

to all ca

^{Deen} de.

numbering basis for α -CHT (Figure 1). The sequence determination was performed by Hartley <u>et al</u>. (1), and verified by Meloun <u>et al</u>. (2), with a final minor revision based on examination of the X-ray results of Blow <u>et al</u>. (3).

All though the activation scheme for α -CTN has been established (Figure 2) (4), the exact function of each form of the enzyme is not yet known. The activation to α -CHT involves the removal of two dipeptides, SER 14-ARG 15 and THR 147-ASN 148, by tryptic and chymotryptic hydrolysis of α -CTN. The final structure consists of three polypeptide chains, A, B, and C, containing 13, 131, and 97 residues, respectively, connected by five disulfide bridges and various polar and non-polar interactions.

Kunitz and Northrop (5) first isolated α-CHT in

1935 and crystals of the enzyme were among the first to

be examined by X-ray diffraction (6). Because of the

ease of obtaining the alpha form and its relatively high

purity when prepared from bovine sources, α-CHT has

become one of the most extensively studied enzymes.

However, it is beyond the scope of this work to allude

to all of the observations reported and the intention is

only to deal with some of the results which have been

observed consistently and with the theories which have

been developed to explain them.

SER THR SER THR PRO

THR CYS

SER TRP GLY SER SER

GLY ILE VAL

LEU VAL

ALA TRP THR

GLY

LYS ASN

CYS LYS

201

ALA ASN

THR LEU ALA

ASN TRP VAL

LEU VAL

THR ALA I

ARG

TYR ALA

GLY VAL

226

25 CYS GLY VAL PRO ALA ILE GLN PRO VAL LEU SER GLY LEU SER ARG"ILE VAL ASN GLY GLU GLU ALA VAL PRO GLY TRP WAL VAL THR ALA ALA HIS CYS GLY VAL THR SER ASP VAL VAL VAL ALA GLY GLU PHE ASP GLN GLY SER SER GLU LYS ILE GLN LYS LEU LYS ILE ALA LYS VAL PHE LYS ASN SER LYS TYR ASN SER LEU THR ILE ASN ASP ILE THR LEU LEU LYS LEU SER THR ALA ALA SER PHE SER GLN THR VAL SER ALA VAL CYS LEU PRO SER GLY LEU THR ARG TYR THR ASN ALA ASN THR PRO ASP ARG LEU GLN GLN ALA SER LEU PRO LEU LEU SER ASN THR ASN CYS LYS LYS TYR TRP GLY THR LYS SER SER CYS MET GLY ASP SER GLY GLY PRO LEU VAL or or SER TRP PRO TRP GLN VAL SER LEU GLN ASP LYS THR GLY PHE HIS PHE CYS GLY GLY SER LEU ILE ASN ALA ALA GLY THR THR CYS VAL THR THR GLY TRP SER GLY VAL ILE CYS ALA GLY ALA 踞 ILE LYS ASP ALA MET ASP ASP SER **5**6 21 9/ 126 176 101 151

COMPOSITION

P 80 ÆT LEU LYS 19 10 ALA ARG ASN ASP CYS GLN GLU GLY HIS 2 4 14 9 10 10

Total number of residues = 245

(*) This residue is lost during activation to $\alpha\text{-chymotrypsin.}$

DISULFIDE BRIDGES

1-122, 42-58, 136-201, 168-182, 191-220

C-chain B-chain — | |-|-|-A-chain ---CHAIN DESIGNATION

FIGURE 1. Amino Acid Sequence of lpha-Chymotrypsinogen

CHT -

Flaure 2

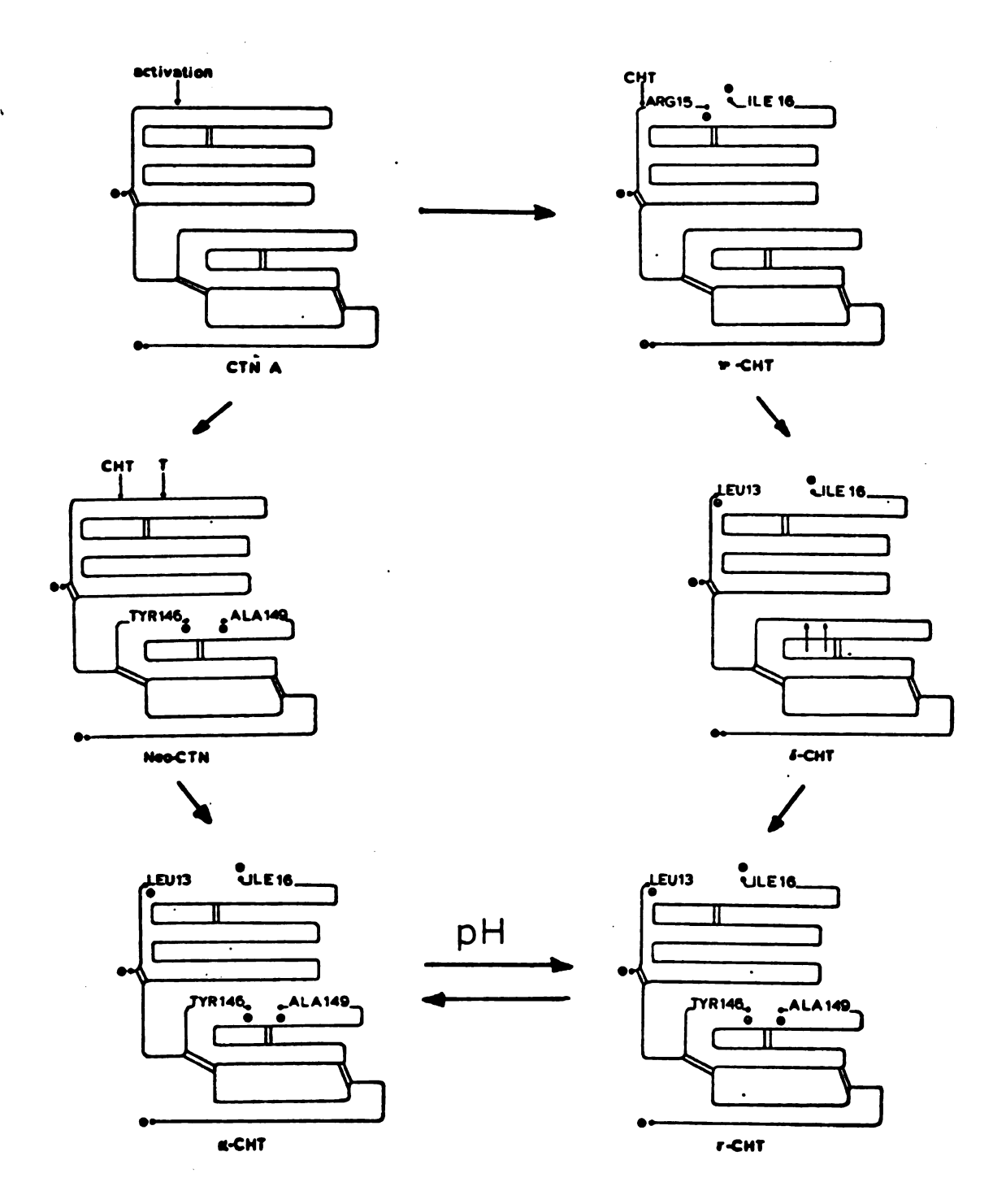


FIGURE 2. Activation and Autolytic Reactions of α -Chymotrypsinogen A (4)

cheim cectid cataly

2

of car

The so

an and

of spe

ine ef from w

^{phobi}c

al thoug

charact

:atalys

1/2roly

₹5°0 fo

 α -CHT catalyzes the hydrolysis of proteins and their derivatives, polypeptides and amides, as an endopeptidase. <u>In vitro</u>, α -CHT has also been noted to catalyze the hydrolysis of esters. Bergmann and Fruton (1936) (7) first observed the α -CHT catalyzed hydrolysis of carbobenzyloxyglycyl-L-tyrosyl glycinamide, proving that synthetic peptides could be used as substrates. The specificity of α -CHT for aromatic peptide side-chains has been observed and associated with the presence of an aromatic binding pocket in the active site; the order of specificity is summarized in [1] below.

 R_2 : Aromatic > Cycloalkyl > Alkyl

The effect of this specificity is seen in Table 1 (8), from which it can also be seen that other large, hydrophobic peptides are susceptible to chymotryptic attack, although at a greatly reduced catalytic rate. The characteristic rate enhancement observed in enzyme catalysis is seen in N-acetyl-L-tyrosine ethyl ester hydrolysis, where the rate constant is 0.45 min $^{-1}$ at 25°C for standard base catalysis (NaOH), and 0.12 x 10^5

TABLE 1 Specificity of $\alpha\text{-CHT}$ with Respect to Methyl Esters

of Some N-Acetyl-L-Amino Acids (8)

Acyl Group	Side-Chain Structure	$k_{cat}/K_m (M^{-1}s^{-1})$	К _т (mм)
N-Acetyl-L- tryptophanyl	CH ₂ -	4.2 × 10 ⁵	0.1
N-Acety]-L- tyrosyl	H0 CH2-	3.65 x 10 ⁵	0.7
N-Acetyl-L- hexahydro- phenylalanyl	CH2-	8.0 × 10 ⁴	0.5

Table 1 (cont'd.)

lable 1 (cont.d.)

Table 1 (cont'd.)

2	מאוו + טויא טיימאט פויים אין	(L-1, N/ N/ 1	(WE)
Acy i aroup	סומפינוו סרומנים פ	rcat' m ''' 3 /	(E
N-Acetyl-L- phenylalanyl	CH ₂ -	4.2 × 10 ⁴	1.2
N-Acetyl-L- methionyl	сн3-5-сн2-сн2-	2.3 × 10 ²	
N-Acetyl-L- leucyl	сн ₃ сн-сн ₂ -	1.59 × 10 ²	3.1
N-Acetyl-S- methyl-L- methionyl	сн ₃ >s ⁺ -сн ₂ -сн ₂ -	2.1 × 10 ⁻¹	

Table 1 (cont'd.)

K_m (mM)

Table ! (conf'd.)

Table 1 (cont'd.)

Acyl Group	Side-Chain Structure	$k_{cat}/K_{m} (M^{-1}s^{-1})$	K _m (mM)
N-Acetyl-L- glutamyl	- 2 - С - С н 2 - С н 2 -	3.5 × 10 ⁻²	
N-Acetyl-L- glycyl	H-	9.8 × 10 ⁻³	96

Where k_{cat} = catalytic rate constant K_m = Michaelis binding constant

studies
tion of
by the

E) Shows a

betweer separat

tenavid near op

reactio

3

The pos

positio

^{ey}perim A

> active diisopr

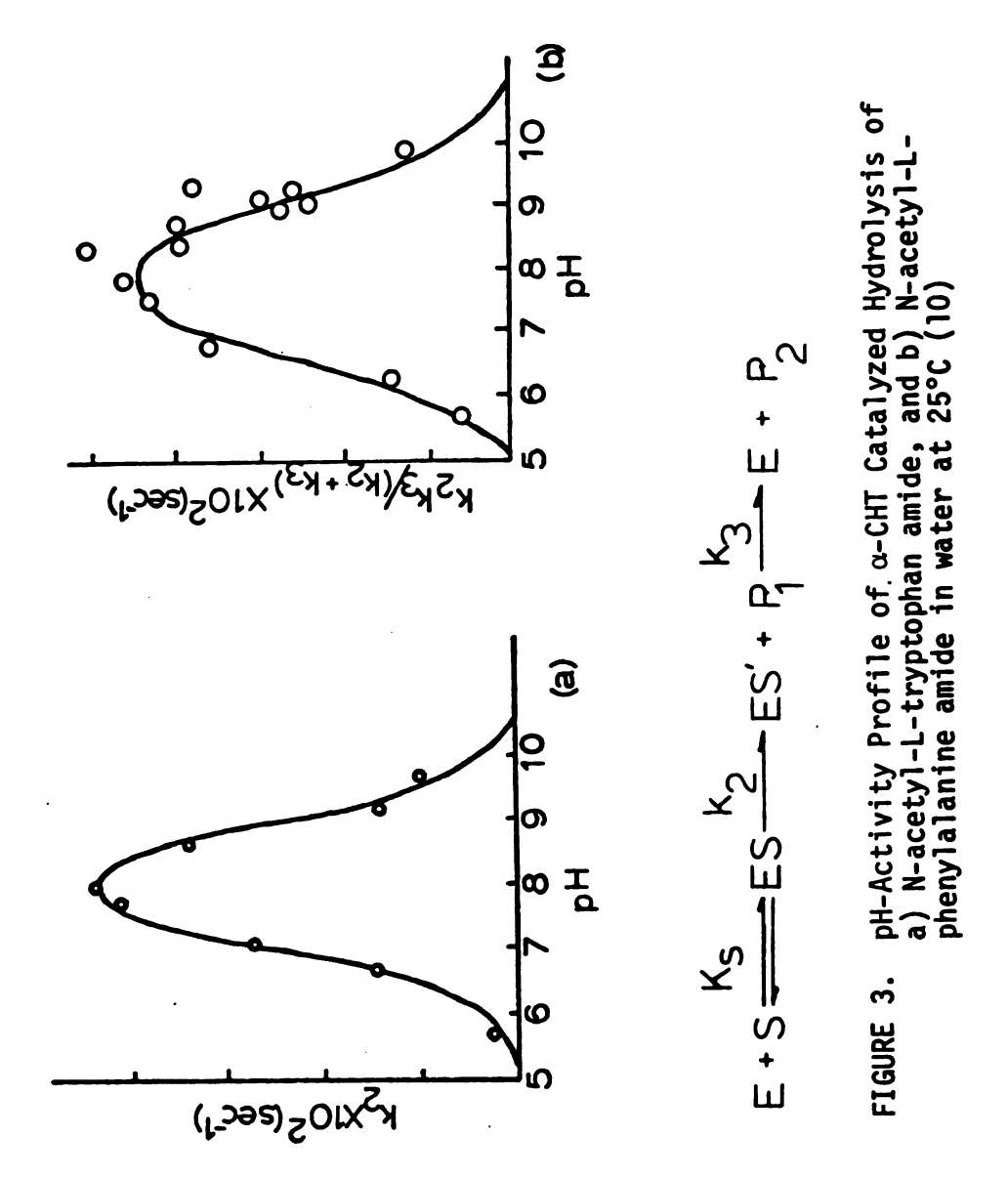
min⁻¹ at 25°C for α -CHT catalysis (9). Other solution studies have yielded information concerning the composition of the active site of α -CHT, which has been verified by the crystallographic results.

Examination of the activity profile of α -CHT vs. pH shows a bell-shaped behavior with a maximum occurring between pH 7.5 and pH 8.5 (Figure 3) (10), with two separate ionizing groups apparently controlling this behavior. When a carboxylic acid is placed in a solution near optimal pH containing 0^{18} -enriched water, the reaction, shown by [2] (11), takes place.

$$R-C00^{-} + H_{2}0^{18} --- R-C00^{18} + H_{2}0$$
 [2]

The positioning of amino acids in the active site must account for these observations, and locating their positions can only be accomplished by careful chemical experimentation.

A unique serine residue, SER 195, was located in the active site as a result of inhibition studies with disopropyl fluorophosphate (DFP) [3].



Jansen <u>et</u> staionian reaction (13) reve SER 195. that the was analo the acety men to b ::erest: ot susce 4 a-047, Stemical : anhydr of the s been impl directly HIS Joon the d

eliminates (6.0) for

as the gri

for the c

of Schoel

9-087 **ar** 1

Jansen et al. (1949) (12) first observed that α -CHT was stoichiometrically inactivated in a (1:1) manner by reaction with DFP. Later work by Shaffer et al. (1953) (13) revealed that this was due to the acylation of SER 195. Oosterbaan and von Adrichem (1958) (14) showed that the acylation step of the reaction with substrate was analogous to the reaction with DFP when comparison of the acetyl peptide and phosphoryl peptide segments proved them to be identical. These results were particularly interesting since under ordinary conditions, serine is not susceptible to acylation or phosphorylation, while in α -CHT, one serine of twenty-eight is reactive (15). Chemical conversion of SER 195 to ALA in the production of anhydro-chymotrypsin eliminates catalytic activity but not the substrate binding capability. SER 195 has thus been implicated as a catalytic residue of α -CHT but not directly involved in the specificity of binding.

HIS 57 was first implicated in catalytic function upon the observation that photo-oxidation of this residue eliminates enzyme activity (16). Due to the unique pK (6.0) for histidine residues, HIS 57 has been assigned as the group responsible for the control of the low pH leg of the activity profile. The strongest evidence for the definition of its role in catalysis was the work of Schoellman and Shaw (17), who alkylated HIS 57 in α -CHT and also in trypsin (T), a related enzyme, using

eleglating specificit.

2-141
4-042-04

¢ =

Recent X-r

School liner through ing seem carri activity (

1-CHT reve

isplication rather than

ASP 1

the origin of the hom

porcine el

led to a n

this resig

thange rel

still sub

alkylating agents which take advantage of enzyme specificity and are shown in [4] below.

$$\frac{\alpha - CHT}{\phi - CH_2 - CH - C - CH_2 - C1} = \frac{T}{CH_2 - CH_2 -$$

Recent X-ray studies of α -CHT in the presence of the Schoellman-Shaw reagent have established some new ideas concerning this work (18). Methylation of HIS 57 has also been carried out but without total loss of enzymatic activity (19,20). Solution studies of HIS 57-methylated α -CHT reveal a slight reduction of the acylation rate constant but no reduction in the binding constant, thus implicating HIS 57 in a catalytic role similar to SER 195, rather than participation in substrate binding (20).

ASP 102 was misinterpreted to be asparagine (ASN) in the original amino acid sequencing work (3). Comparison of the homologous enzymes trypsinogen, thrombin, and porcine elastase, coupled with crystallographic results led to a reassessment of the observations associated with this residue and its reassignment to aspartic acid.

ASP 102 has also been assigned a catalytic role in the charge relay system of Blow et al. (3), but its role is still subject to debate.

It should be sold tryps in oge tryps in oge tryps in an vicinity of the encyme and several as "senine activity of side chain that the vin panchea from a com

In ree investigations of the control of the control

Articular

ine conver

i/drolysi intonir

ine maxi-

It should be noted that several enzymes, some of them isolable from pancreatic juices, including chymotrypsinogen A and B, chymotrypsin A and B, trypsinogen, trypsin and elastase, have homologous sequences in the vicinity of SER 195, HIS 57, and ASP 102 (Table 2) (21). The enzymes indicated in Table 2, subtilisin, thrombin and several other proteases, constitute a class denoted as "serine proteases," all of which exhibit proteolytic activity centered around the serine, but with varying side chain specificities (22). It has been suggested that the variation in specificity of the proteases found in pancreatic juice is an example of divergent evolution from a common precursor, while the other proteases, particularly those of bacterial origin, are examples of the convergent evolution of similar enzymes (23).

Three other amino acid residues of α -CHT have been in vestigated for possible involvement in the catalytic activity of α -CHT although they are not necessarily homologous with other serine proteases. MET 192 has been implicated in enzymic activity on the basis of selective $0 \times i$ dation experiments. Oxidation of MET 192 by either photo-oxidation or chemical means affects substrate hydrolysis without alteration of MET 180, the only other methionine in α -CHT. Koshland et al. (24) showed that the maximal velocity of hydrolysis of the substrate

The Book of the fift fit and the con-

:::::<u>:</u> 191 But the set to the fit fit we have

ereviations:

Deletic Region Bovine Porcine Thromb Bovine Bovine Porcine Elastar a-Lytin

TABLE 2 Sequence Homology in the Vicinity of Active Site Residues Among Several Serine Proteases (21)

<u>Protease</u>	<u>55 56 57 58 59</u>	<u>100 101 102 103 104</u>
BT	ALA ALA HIS CYS TYR	ASN ASN ASP ILE MET
PT	ALA ALA HIS CYS TYR	ACD ACD ACD TIE ALA
TH	ALA ALA HIS CYS -	ASP ASP ASP ILE ALA
BCA BCB	ALA ALA HIS CYS GLY ALA ALA HIS CYS GLY	ASN ASP ASP ILE THR
PCA	ALA ALA HIS CYS GLY ALA ALA HIS CYS GLY	ARG ASP ASP ILE THR
E	ALA ALA HIS CYS VAL	GLY ASP ASP ILE ALA
LP	ALA GLY HIS CYS GLY	GLY ASP ASP ARG ALA
S	ASN SER HIS GLY THR	GLN ASP ASP ASN SER
_		
Protease	<u>191 192 193 194 195 196 197 198</u>	<u>213 214 215 216 217 218</u>
Protease BT PT	CYS GLN GLY ASP SER GLY GLY PRO	VAL SER TRP GLY SER X
BT	CYS GLN GLY ASP SER GLY GLY PRO CYS GLN GLY ASP SER GLY GLY PRO	VAL SER TRP GLY SER X
BT PT	CYS GLN GLY ASP SER GLY GLY PRO CYS GLN GLY ASP SER GLY GLY PRO	VAL SER TRP GLY SER X
BT PT TH	CYS GLN GLY ASP SER GLY GLY PRO CYS GLN GLY ASP SER GLY GLY PRO CYS GLU GLY ASP SER GLY GLY PRO	VAL SER TRP GLY SER X ALA VAL SER TRP GLY GLU X
BT PT TH BCA BCB PCA	CYS GLN GLY ASP SER GLY GLY PRO CYS GLN GLY ASP SER GLY GLY PRO CYS GLU GLY ASP SER GLY GLY PRO CYS MET GLY ASP SER GLY GLY PRO	VAL SER TRP GLY SER X ALA VAL SER TRP GLY GLU X VAL SER TRP GLY SER SER
BT PT TH BCA BCB PCA E	CYS GLN GLY ASP SER GLY GLY PRO CYS GLN GLY ASP SER GLY GLY PRO CYS GLU GLY ASP SER GLY GLY PRO CYS MET GLY ASP SER GLY GLY PRO CYS MET GLY ASP SER GLY GLY PRO CYS - GLY ASP SER GLY GLY PRO CYS GLN GLY ASP SER GLY GLY PRO	VAL SER TRP GLY SER X ALA VAL SER TRP GLY GLU X VAL SER TRP GLY SER SER
BT PT TH BCA BCB PCA	CYS GLN GLY ASP SER GLY GLY PRO CYS GLN GLY ASP SER GLY GLY PRO CYS GLU GLY ASP SER GLY GLY PRO CYS MET GLY ASP SER GLY GLY PRO CYS MET GLY ASP SER GLY GLY PRO CYS - GLY ASP SER GLY GLY PRO	VAL SER TRP GLY SER X ALA VAL SER TRP GLY GLU X VAL SER TRP GLY SER SER VAL SER TRP GLY SER SER

Abbreviations:

- (X) Deletion (-) Region unclear BT Bovine Trypsin Porcine Trypsin

TH - Thrombin

BCA - Bovine Chymotrypsin A BCB - Bovine Chymotrypsin B PCA - Porcine Chymotrypsin A

Ε - Elastase

- α -Lytic Protease LP

Subtilisin

remains unchanged although substrate binding is increased by a factor of five upon oxidation with $\rm H_2O_2$. Scramm and Lawson (25) observed normal α -CHT inhibition by DFP although MET 192 had been alkylated by benzyl bromide. More recent work by Taylor et al. (26) using $\rm Cl_3CSO_2Cl$, a specific MET 192 oxidizing agent, renewed interest in the role of MET 192. Their observations indicate that the oxidized enzyme retains maximum catalytic activity over a broader pH range.

GLY 216 occurs in a region of the enzyme which shows variability in sequence among the serine proteases (Table 2). As this residue has its alpha carbon atoms positioned at the entrance of what appears to be the specificity pocket of the enzyme, the observed variation suggests a source for the varied specificities. If a larger side-chain, such as valine in elastase, is present at this position, the specificity is altered from that of an aromatic group in α -CHT to a small hydrophobic group in elastase (e.g., alanine) (27).

TYR 146 is the exposed carboxylic acid terminal residue of the B-chain which is formed during the activation process from α -CTN. It is not involved in the catalytic mechanism since its removal by carboxypeptidase has no effect on the catalytic rate (28). However, TYR 146 is apparently critical for dimerization of α -CHT which predominates in solution at low pH, and which is observed in the crystal structure at pH 3.6; the removal of TYR 146 prevents dimerization in solution.

:::

*e\$

:":

::-<u>i`</u>.

:ne :es:

50m.

ir.

Pos

r¹75

Sis Tanga Subsa

3:11

Tin

±71;

,52; Q

The first proposed mechanisms of α -CHT analysis attempted to deal with the anomalous reactivity of SER 195. It was believed that the unexpected reactivity was the result of the incorporation of the serine hydroxyl group into intermediate covalent ring structures. Rydon (29) proposed the formation of an oxazoline ring (Figure 4a). Cohen et al. (30) as well as Schneider (30) and Smith et al. (30) had predicted that an internal ester link between the serine hydroxyl and the carbonyl of ASP 194 was responsible for its reactivity (Figure 4b). A fused ring structure with the serine hydroxyl protruding was proposed by Bernhard et al. (Figure 4c) (31). In all cases, the ring structures were presumed to open before the catalytic process was complete since isolation of the acylated or phosphorylated serine peptide sequence never revealed these ring structures.

The observation that imidazole catalyzes ester hydrolysis in solution by general base catalysis suggested the manner in which HIS 57 might participate in α -CHT catalysis. Gutfreund and Sturtevant (32) suggested that HIS 57 was a cationic group which was not transiently acylated, but rather acted as a base catalyst for the acylation and deacylation of the SER 195 hydroxyl group.

In the work of Blow \underline{et} \underline{al} . (3), which re-assigned residue 102 as aspartic acid, a charge relay mechanism

³³³€ 4. €

FIGURE 4. Early Ideas of Serine 195 Participation in Anomalous Activity

The PMC has Pt diffe

Poplem. Priodure

::::ernin :::,37,38

Pransly Dethey

:::hemic

ine ws

inte to

involving SER 195, HIS 57, and ASP 102 evolved. The charge relay system (Figure 5) involves the hydrogen bonding of ASP 102 to HIS 57 which is further hydrogen bonded to SER 195. The strong nucleophilic character of SER 195 would then be a result of the stabilization of hydrogen transfer through the histidine to the negatively charged aspartic acid (pK 1.5) (33). This interpretation resulted from observations of an inhibited derivative of α -CHT, tosyl- α -CHT (TOS), and is subject to re-evaluation based on the structure of native- α -CHT (NAT), as determined by Tulinsky et al. (34).

C. α -Chymotrypsin: Crystallography

The crystallographic determination of the structure of α -CHT has been the result of two efforts, both independent and differing fundamentally in their approaches to the problem. D. M. Blow's group at the MRC (35) described the structure initially, as well as some of the early ideas concerning the structure-function relationship of α -CHT (36,37,38,39). A. Tulinsky's group at MSU (40) has been primarily concerned with the details of the structure and how they relate to several classes of chemical and/or biochemical behavior (Table 3, Figure 6) (18,41,42,43). In the MSU approach, individual members of the classes prove to be only as important as their contribution to the overall understanding of the behavior of that class.

5)

FIGURE 5. Charge-Relay Mechanism of Blow et al. (31)

Irrevers 161e -

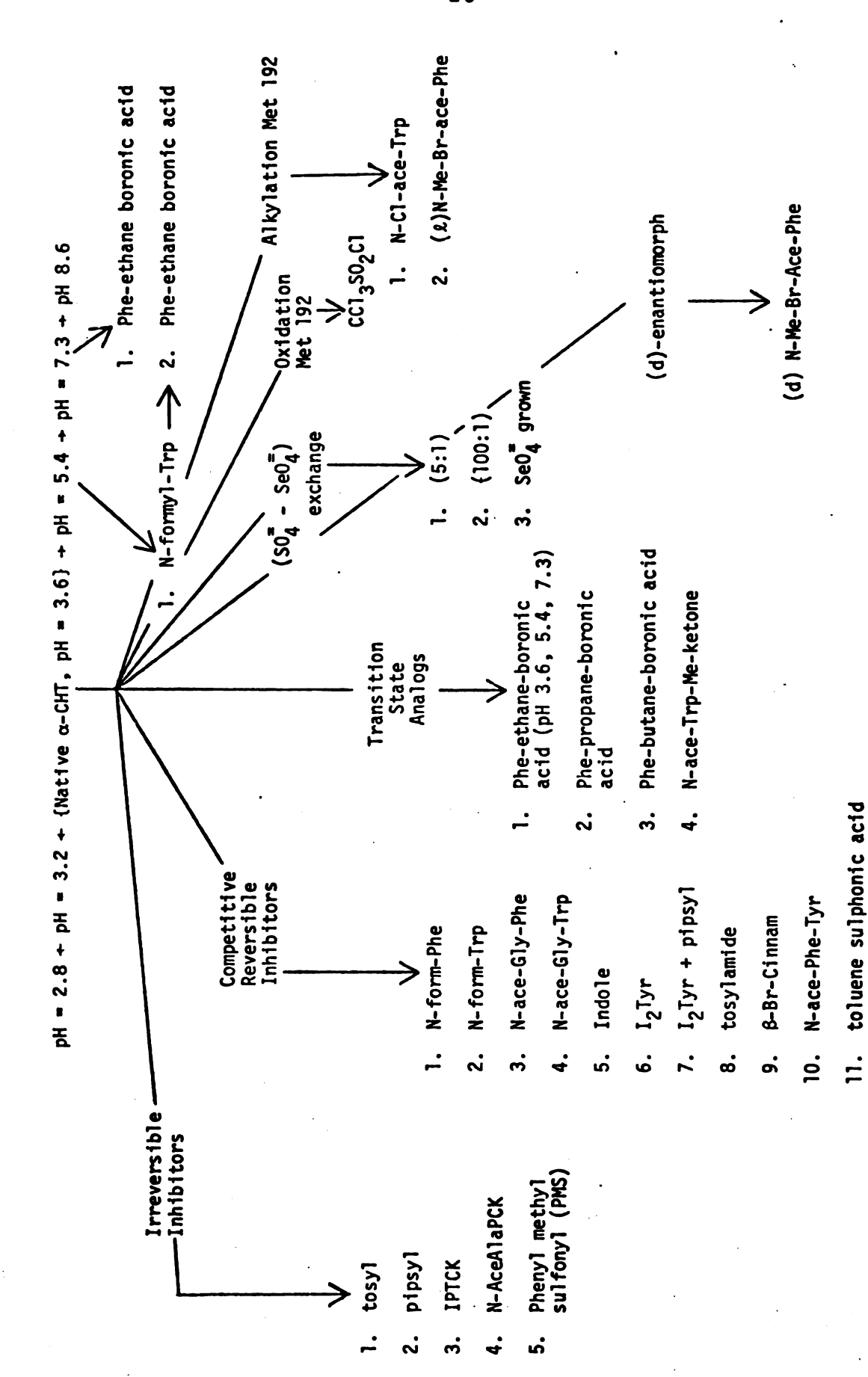


FIGURE 6. 3D Derivatives of $\alpha-\text{CHT}$ at 2.8 A Resolution

300

ire z

:::a)

ard

Wis of

Borety

ંલ સ્ટોફ

Dier /e:

:° ;⊱e

D39633 ∃`, w

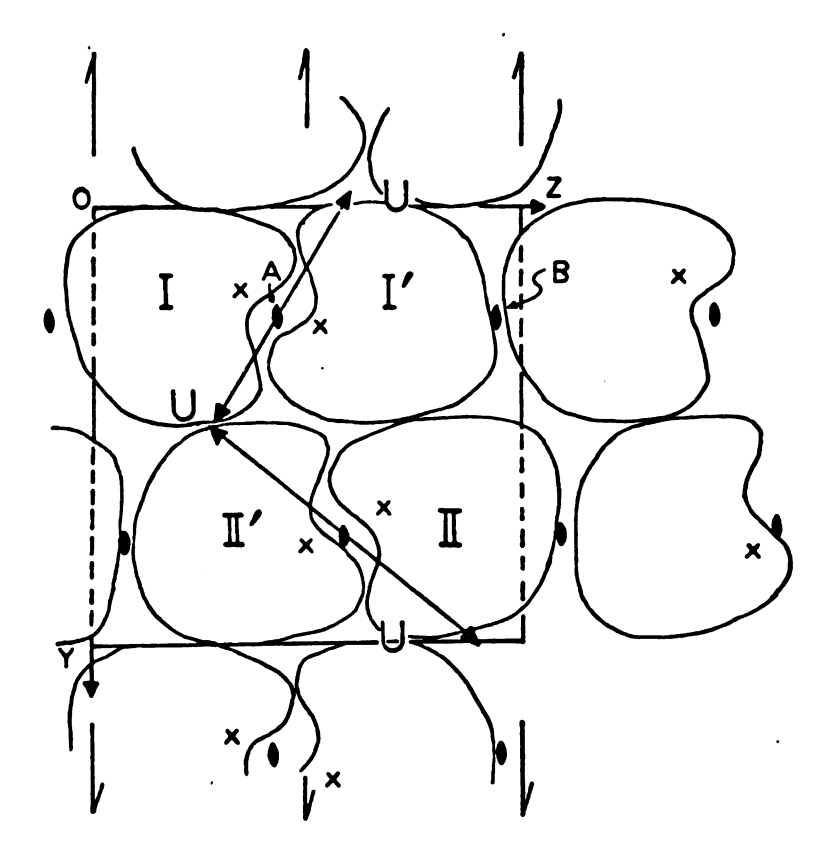
ilio da

ille 5

रे क्इर,

- 1. pH Conformers
- 2. Irreversible Inhibitors
- 3. Competitive Reversible Inhibitors
- 4. Transition-State Analogs
- 5. $S0_4^{-}$ -Se 0_4^{-} Exchange
- 6. Oxidation of MET 192
- 7. Alkylation of MET 192

Both groups have established the same general features of the α -CHT structure. α -CHT crystallizes in the monoclinic crystal system, space group P2 $_1$, with four molecules per unit cell and two molecules per asymmetric unit. A local two-fold axis of non-crystallographic origin exists within the asymmetric unit between the two independent molecules. The two molecules probably resemble the dimer of α -CHT which is observed to form in solution at lower pH values. A schematic of the dimer is shown in Figure 7; however, it does not possess exact two-fold symmetry (42). This view of the unit cell, which is approximately parallel to the a*-axis, is also parallel to the local two-fold axis. The interstitial space between molecules is occupied by solvent (about 36% by weight).



A,B=non-crystallographic dyads
x =active sites
U =uranyl binding sites

FIGURE 7. Schematic Packing Diagram of α -CHT Viewed Along a*-Direction. Non-crystallographic Dimer = I and I' or II and II' (41)

A comdetermined by Tulinsk cell paramiconcarison and the dimensions are given

Co-

MSU. pH 3 dio>

49 67

63 101

213

resembles with the

band c c.

A comparison of the native α -CHT structures as determined by the MSU and MRC groups has been summarized by Tulinsky (34,42). A summary of the changes in the cell parameters as a function of pH (Figure 8), and a comparison with earlier reported cell dimensions of α -CHT, is given by Mavridis et al. (43). The cell dimensions for the NAT crystals as used in this study are given in Table 4. From Figure 7, the molecule

TABLE 4 Comparison of Lattice Parameters for α -Chymotrypsin with Addition of Dioxane

	MSU, Native, pH 3.6, no dioxane	MRC, Native, grown from dioxane (34)	MSU, Native, pH 3.6, addition of 3% (v/v) dioxane
a	49.24(7)Å	49.1(1)Å	48.9(1)Å
 	67.20(10)Å	67.4(1)Å	68.3(1)Å
c	65.94(9)Å	65.9(1)Å	65.8(1)Å
β	101.79(8)°	101.7(1)°	101.8(1)°
٧	213,600(1000)Å ³	214,000(1100)Å ³	215,000(1000)Å ³

resembles a prolate ellipsoid of about 25 x 28 x 33 \check{A} , with the ellipsoid axes corresponding closely to the a*, b and c crystallographic axes.

2:50-Vinc²

2100-

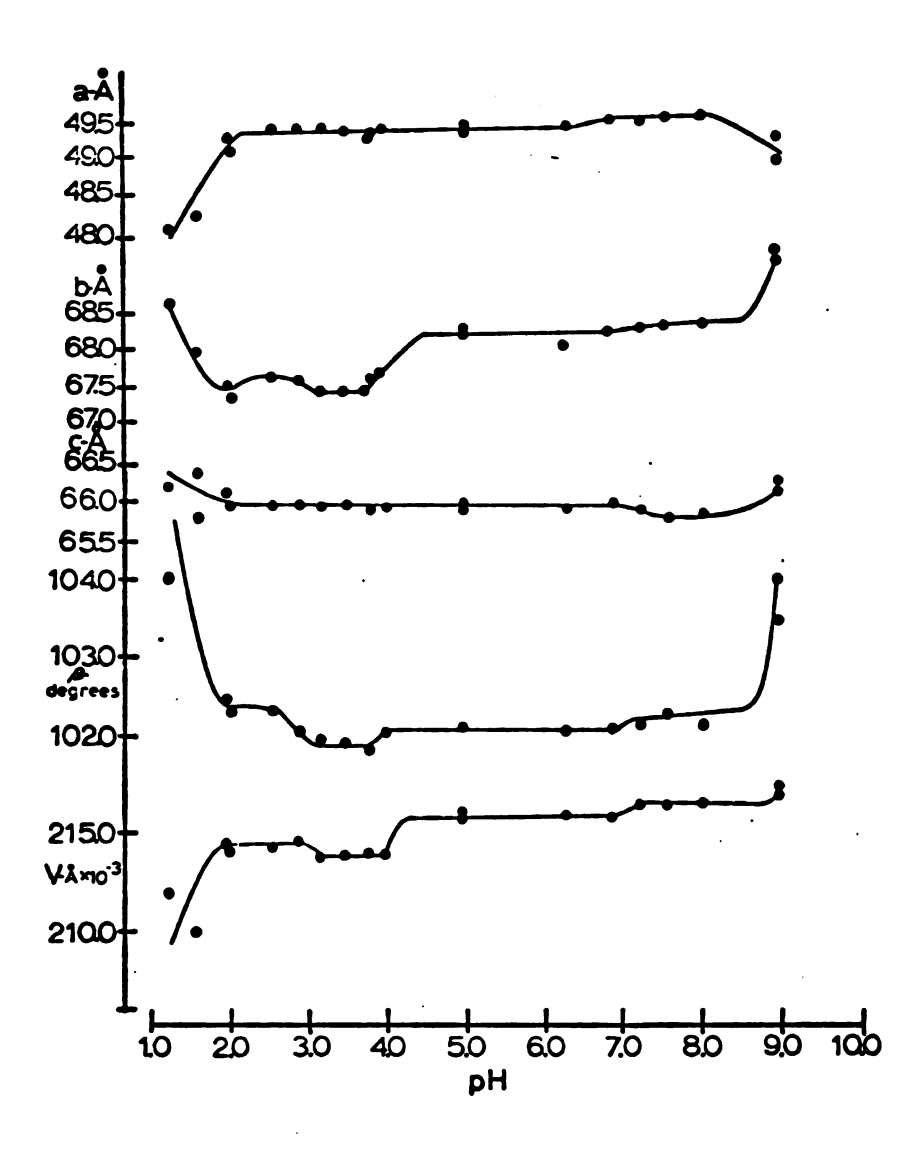


FIGURE 8. Variation of Unit Cell Parameters of $\alpha\text{-CHT}$ with pH (43)

acoroxi is conce torted a distort ieta she and degr Ceviati :ropose 5^heet h of stru 459 194 ionic g tolecul in the of the the exc appear oolar 1

An

termin, pol∕se

on the

tal do

fegior

An examination of the structure of α -CHT reveals approximately 7.5% helix and 34% beta sheet. The helix is concentrated into two regions--10 residues of undistorted alpha helix (236-245) and about 10 residues of distorted helix (164-173). The larger component of beta sheet is observed in 13 segments of varying length and degrees of distortion in the anti-parallel mode. Deviation in both α -CHT and other proteins from the proposed models of tertiary structures for helix and sheet has been a major problem in the correct prediction of structure by spectroscopic techniques. The ILE 16-ASP 194 internal salt bridge and ASP 102 are three major ionic groups which are found in the interior of the molecule, and all are important in that they are involved in the formation of the active site region. The majority of the interior is comprised of non-polar groups with the exception of 18 non-polar groups whose side-chains appear on the surface of the molecule in the company of polar residues. Except for *NH3-ILE 16, the aminoterminal and carboxylic-terminal groups of the three polypeptide chains formed during CTN-activation appear on the surface. The intricate folding of the polypeptide chain has the A-B chain and the C chain forming individual domains with little overlap. Two areas of particular interest occur at the interface of these regions--the active site and a secondary binding site

(tryptop) studies i tre possi two separ is evide in the d interact ™ecule snip in te discur interest inhibito group [b [47] and ireer et

Sev

and have of activ further differen

tion of

tat alt #15 57,

actions

1)

(tryptophan cluster) (42). Detailed conformational studies involving the folding of the backbone indicate the possibility of an evolutionary relationship between two separate domains within the α -CHT molecule. This is evidenced by the presence of an apparent mirror plane in the distance diagonal plot (44) which represents interactions between all the alpha carbons within the molecule (Figure 9). Further analysis of this relationship in light of changes which occur upon binding will be discussed in the present work.

Several other crystallographic studies are of interest in relation to the $\alpha\text{-CHT}$ structure. Several inhibitor: $\alpha\text{-CHT}$ structures have been examined by the MRC group [DFP (39), Tosyl (39,46,49), N-formyl-L-tryptophan (47) and indoleacryloylimidazole (48)]. In addition, Freer et al. (50) have described the structure of $\alpha\text{-CTN}$ and have made some observations concerning the process of activation. Wright (51) has pursued this work further in a detailed comparison of the structural differences between $\alpha\text{-CHT}$ and $\alpha\text{-CTN}$, and an interpretation of the process of activation. He has concluded that although the catalytic triad is intact (SER 195, HIS 57, and ASP 102), four major enzyme-substrate interactions do not occur in $\alpha\text{-CTN}$:

1) binding within an ill-formed specificity pocket;

1

ESIDUE* I

20

,

Macre 9.

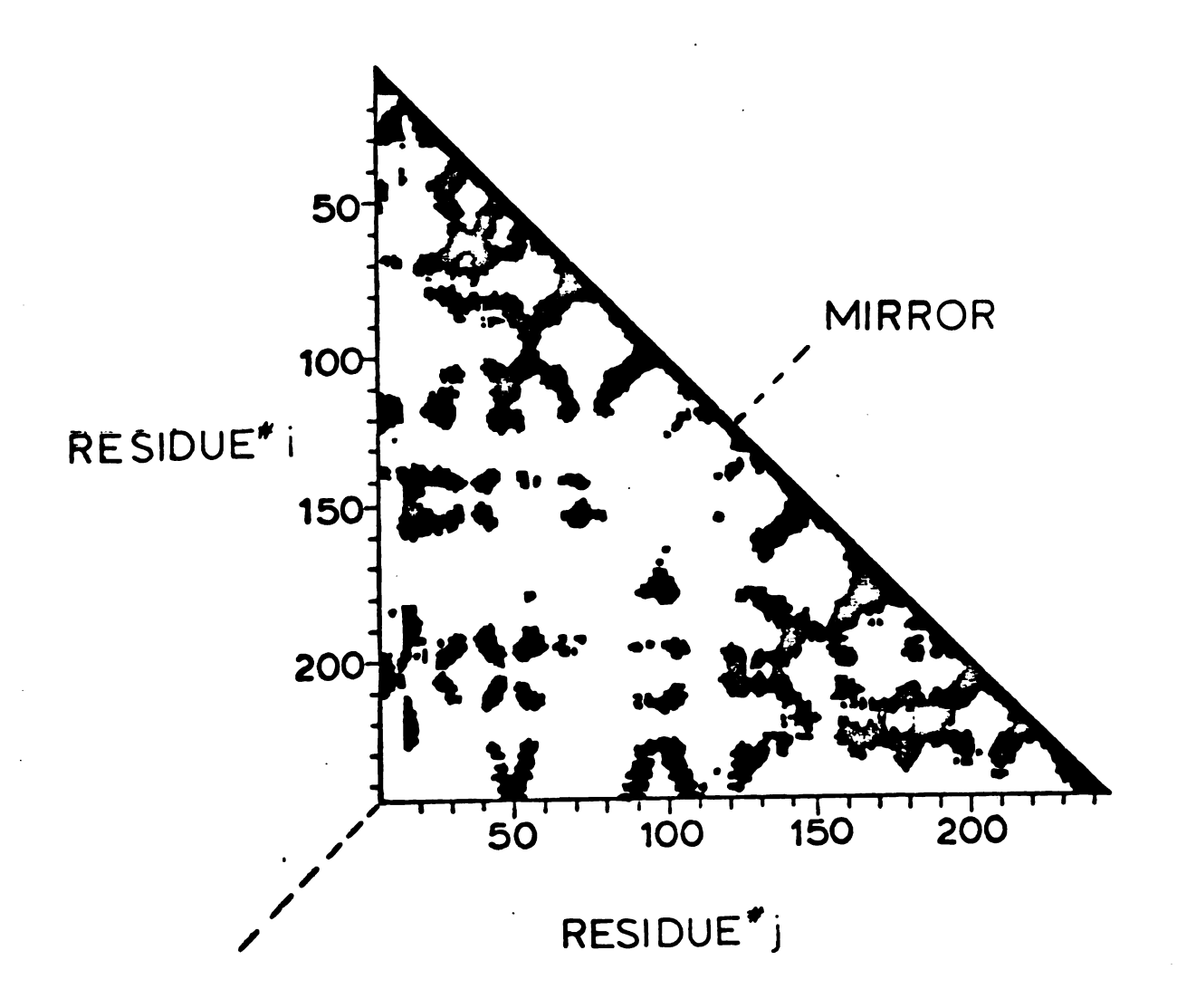


FIGURE 9. Distance Diagonal Plot of Native α -CHT (45), Contoured at 15 Å (Solid Regions)

2)

3)

4)

Ine

(N-CHT) + it reveal

residues

are the

214-216

from the tis work

does not

Other tha

iange sub

Subs

letermine. subtilis:

(%) (55).

to have c

of other

ⁱⁿ Specif

these enz g 20 dite

Trenomenc/

^{externa}l

- 2) the GLY (193)-NH-to-substrate hydrogen bond;
- 3) hydrogen bonds from substrate to GLY (216);
- 4) the inability for interaction of a polypeptide substrate leaving group with MET (192).

The structure of the monomeric gamma-chymotrypsin $(\gamma\text{-CHT})$ has been determined by Segal <u>et al</u>. (52), and it reveals little difference in the positioning of residues in the active site. Of particular interest are the indications of the importance of the segment 214-216 in forming the specificity pocket which results from their inhibitor studies. It can be concluded from this work that the dimerization process in the crystal does not greatly affect the active site configuration other than blocking the active site from interacting with large substrates.

Subsequent X-ray crystallographic studies have determined the structures of other serine proteases, subtilisin (SUB) (53), elastase (E) (54), and trypsin (T) (55). Although SUB is of bacterial origin, it seems to have converged evolutionarily to the catalytic triad of other serine proteases SER-HIS-ASP. The divergence in specificity remains the primary distinction among these enzymes. However, since the pH activity profiles also differ, this suggests an influence from some other phenomenon such as conformational adaptability to external (i.e., pH) change. The understanding of the

requi

:rese

on se

1. <u>T</u>

idea

resu]

State

ite e

to er

tre :

: +

:1

: 6 :

₹.6.0

°5,

requirement for this particular geometric orientation as the only one used in the proteolytic activity of these enzymes remains the goal of the current research on serine proteases.

D. Transition-State Analogs and α -CHT

As early as 1946, Pauling (56) had expressed the idea that the greater efficiency in enzyme catalysis resulted from the complementarity between the transition state of the reaction catalyzed and the active site of the enzyme. This suggestion was the foundation for Wolfenden's application of transition-state analog theory to enzyme catalysis (57).

Of particular interest to enzyme chemists has been the structure of ES^+ and EA^+ [5]:

$$E + S = ES - ES^{+} - ES^{+}$$

where, E = native enzyme,

S = substrate,

ES = initial enzyme-substrate complex

. (Michaelis-Menten)

ES⁺ = transition-state complex,

EA = acylated enzyme,

 P_1 = acylation product, and

P₂ = hydrolysis product.

In 1951, Bender (58) had postulated the existence of a tetrahedral intermediate in ester hydrolysis. The mechanism for the reaction [6] offered an explanation for the isotopic exchange he observed when an alkyl ester

of benzoic acid in 0^{18} -enriched water was catalytically hydrolyzed by OH $^-$, and 0^{18} was incorporated into the unhydrolyzed ester [7].

$$R_1 COOR_2 + O^{18}H^{-} - - \begin{bmatrix} 0 \\ R_1 - C - OR_2 \\ 0^{18}H \end{bmatrix} - - - R_1 COOH + R_2 OH$$
 [7]

The same process has been observed with $\alpha\text{-CHT}$. The possibility of observing the suggested short-lived intermediate has been discarded on the basis of lifetime. However, if the mechanism is correct, the tetrahedral intermediate should also appear during catalysis by $\alpha\text{-CHT}$. To approximate the tetrahedral configuration, aldehydes and ketones with susceptible carbonyl groups had been studied with elastase (59), but they yielded complexes with $\alpha\text{-CHT}$ which were too weak to permit examination of their interaction with SER 195 by crystallographic methods. The tosylated enzyme had a tetrahedral arrangement around the sulfur which is covalently linked to 0_{γ} -SER 195, but the tetrahedral sulfur is not dimensionally

is appa correct enzyme intera actua!

isoster

3

a hydr

to be tetra

Te st

orepa

they to be

the e

35 37

With ٤٠٤ (

in bo

trang

à] 50 of t

وددو

isosteric with a tetrahedral carbon (Table 5) (60). It is apparent that the more closely a model approaches the correct configuration, the more susceptible it becomes to enzyme catalysis, and, the more closely the active site interactions should approximate those which occur in actual catalysis.

Bell (61) had observed that boronic acids equilibrate a hydroxyl group according to [8]:

$$R-B(OH)_2 + OH^- --- R-B(OH)_3^-$$
 [8]

The structure produced in this manner has been observed to be dimensionally isosteric with that proposed for the tetrahedral carbon (Table 5). As boronic acids are easily prepared with varying alkyl- and phenyl-alkyl groups, they appeared to be ideal as transition-state analogs and to be adaptable to meet the specificity requirements of the enzyme. Exceptionally large inhibition constants, as predicted for transition-state analogs, were observed with phenyl ethane boronic acid and both α -CHT (62) and SUB (63). A pH dependence for this inhibition was noted in both studies which reflected the pK of the tetrahedral transformation of $R-B(OH)_2$. This pH-inhibition profile also appears to be a function of the pH-activity profile of the enzyme. Antonov et al. (64,65) studied the effects of pH and variation of the R group in both the

TABLE 5

Possible Configuration of Tetrahedral Centers

for Interaction with SER 195

Enzyme Complex	Bond Distances (60)	Inhibitor/ Substrate
CH ₂ —0—¢—R	r _{R-C} = 1.54 Å r _{C-0} = 1.43 Å	Phenylalanine
ρΗ CH ₂ —0—β—R HΘΗ	$r_{R-B} = 1.57 \text{ Å}$ $r_{B-0} = 1.48 \text{ Å}$	Phenyl Alkyl Boronic Acids
CH ₂ —0 — \$ R	r _{R-S} = 1.83 Å r _{S-0} = 1.47 Å	p-Toluene and Phenyl Methyl Sulfonyl Fluorides

alkyl b
The sid
interact
SER 195
mental
compania
acid, l
that Si
intono
acid c
10), a
fransi
to det
active
(E7) (

exami

boron

:ilis

of th

bindi

≎ocke

tive;

Et 4d

alkyl boronic acid and phenyl alkyl boronic acid series. The side-chain variation allowed for examination of the interactions within the specificity pocket as well as the SER 195 interaction. Although a comparison of the experimental results reveals similar dependencies on pH and a comparable inhibition constant for phenyl ethane boronic acid, Koehler and Lienhard (1971) (66) have predicted that SER 195 is involved in the boronate binding, while Antonov has suggested HIS 57. Phenyl ethane boronic acid closely resembles a phenylalanine peptide (Figure 10), a typical α -CHT substrate. Thus, if PEBA were a transition-state analog, it would be of great interest to determine the details of the interactions within the active site. The X-ray results of Matthews et al. (1975) (67) on the structure of the complexes of benzene boronic acid and phenyl ethane boronic acid with subtilisin BPN' (Novo) provide a further source of comparison of the serine protease class and the specific modes of binding both to SER 195 and within the specificity pocket.

The emphasis of the present study has been to examine the substitution and related changes in enzyme configuration upon the binding of boronic acid derivatives. Because of the specificity of α -CHT for aromatic side-chains, the phenyl alkyl boronic acid series was studied with variation in the alkyl side chain length,

POTENTIAL TRANSITION-STATE ANALOGS

PHENYL ETHANE BORONIC ACID
(PEBA)

@ pH 3.6, pH 5.4, pH 7. 3 (PEBA 3.6) (PEBA 5.4) (PEBA 7.3)

PHENYL PROPYL BORONIC ACID
(PPBA)

PHENYL BUTYL BORONIC ACID
(PBBA)

FIGURE 10. Potential Transition-State Analogs

n = 2,3
of the
been in
To aid
actions
covaler
techan
the mo
the in

involv each r n = 2,3,4 (Figure 10). The effects of pH on the binding of the phenyl ethane boronic acid molecule have also been investigated at three pH values, 3.6, 5.4, and 7.3. To aid in the interpretation of the SER 195-HIS 57 interactions with these inhibitors, the structures of α -CHT covalently linked with a tosyl group and with a phenyl methane sulfonyl group have also been determined, and the molecules were compared. The differences between the interactions in the independent subunits were evaluated. The approach pursued throughout this work involved interpreting the independent interactions within each molecule and then comparing these results.

A. Cr

prepay

modif:

Canit

worth

recry

⊮≟tho

proce

#35 (

(ine

of v

ery s

of t

Tate

cont

of.

];4

, ea

Per

Chy

į'n.

II. EXPERIMENTAL

A. Crystallization of α -CHT

The crystals of native α -CHT used in this study were prepared by the method outlined in Figure 11. This is a modification of the original procedure developed by Kunitz and Northrup (5). α -CHT was obtained from Worthington Biochemical Corporation (68) as three-times recrystallized, salt-free, lyophilized α -CHT and was used without further characterization or purification. procedure, which involves the salting-out of the enzyme, was carried out at pH 3.6, close to the optimum pH for dimerization (69), and corresponds to the pH 3.6 conformer of Mavridis et al. (43). The diamond-shaped platelet crystals reached a size of $1.5 \times 1.0 \times 0.5$ mm within one to two weeks of growth at room temperature. The density of the α -CHT crystals grown in this manner is approximately 1.25 g-cm³ which corresponds to a solution containing 37% mother liquor, or an enzyme concentration of ~ 0.1 M within the crystal. The presence of the mother liquor enables the diffusion of inhibitors, substrates, heavy metal ions and hydrogen ions into crystals and permits the assessment of the catalytic activity of the crystalline enzyme.

Crystals of $\alpha\text{-CHT}$ were modified by addition of inhibitor to the mother liquor, by alteration of the pH

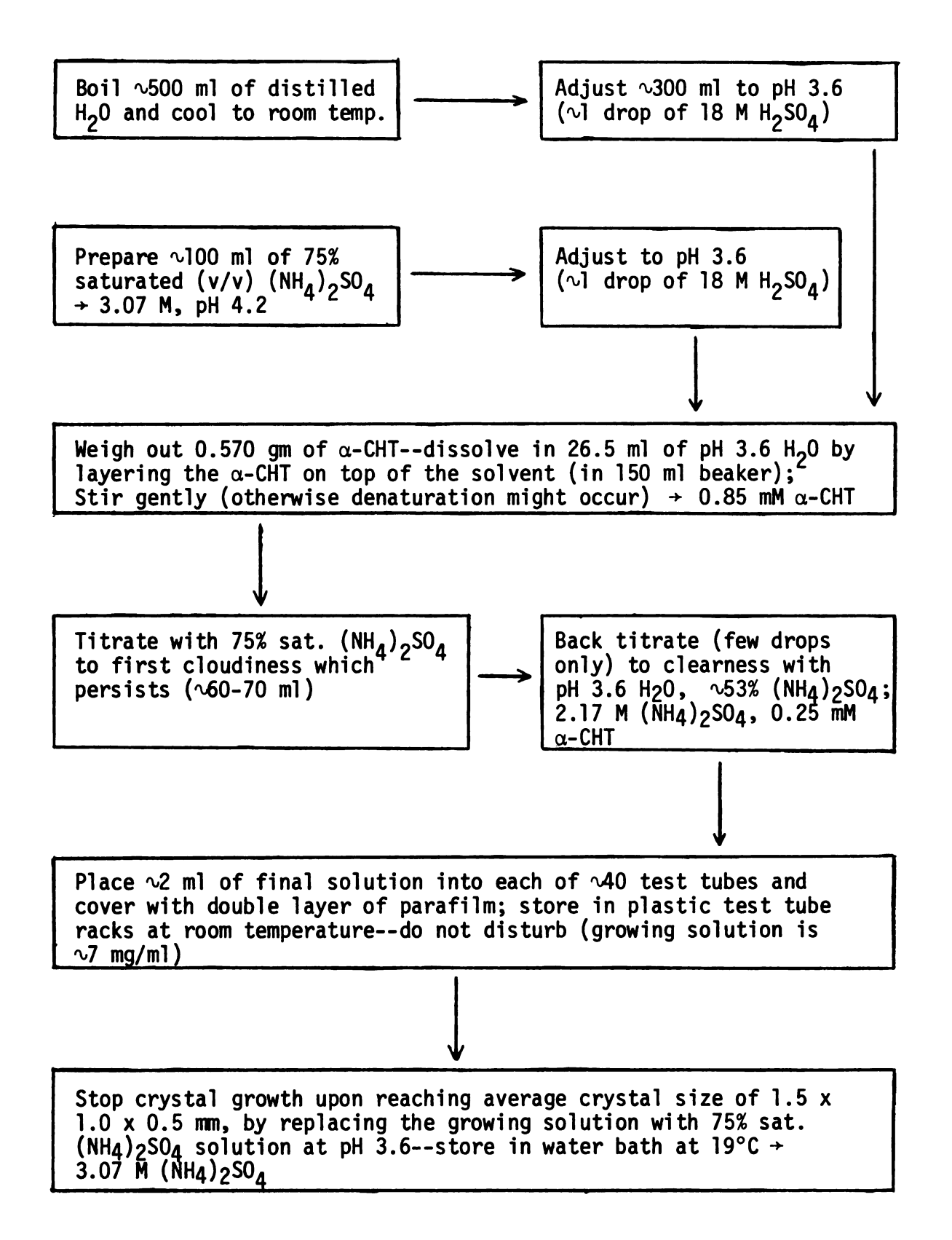
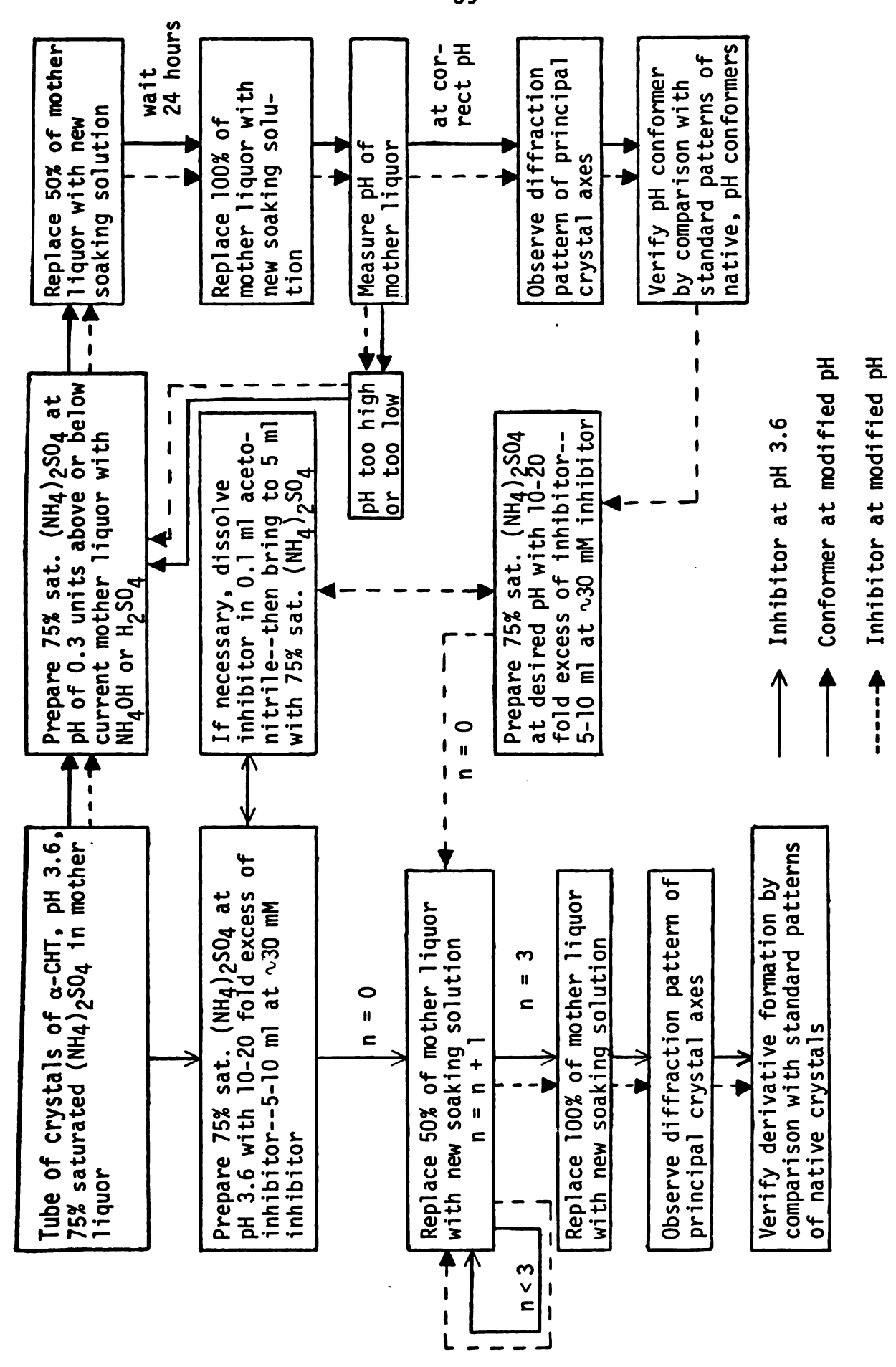


FIGURE 11. Preparation of Crystals of Native α -Chymotrypsin

of the mother liquor, or both (Figure 12). The inhibitors used in this study (Figure 13) were all of non-commercial sources except for the para-toluene sulfonyl fluoride (70). Phenyl methane sulfonyl fluoride (PMS) was the gift of Dr. Lawrence J. Berliner (71); phenyl ethane boronic acid (PEBA) was donated by Dr. Gustav E. Lienhard (72); and Dr. V. K. Antonov (73) donated phenyl propyl boronic acid (PPBA) and phenyl butyl boronic acid (PBBA). All pH measurements were performed using a Leeds-Northrup, Model 7411, general purpose pH meter with temperature compensation and equipped with a miniature Ag/AgCl element combination electrode, Model 117202. Although the manufacturer's specifications state an accuracy of + 0.05 pH units with + 0.02 pH units reproducibility (74), a more conservative estimate for the protein work would be a reproducibility of + 0.05 pH units. The buffers used to standardize the pH meter were Mallinckrodt AR Standard Buffer Solutions, pH 4.01 (#0029) for the range pH = 3.0 to pH = 5.5, and pH 7.00 (#0031) for the range pH = 5.5to pH = 8.5. The pH conformers discussed in the present work are those described by Mavridis et al. (43). derivatives where both the pH of the mother liquor was modified and an inhibitor was added, the change in pH and subsequent verification of equilibrium preceded the inhibitor addition.



Procedure for Preparation and Verification of Derivative $\alpha\text{-CHT}$ Crystals FIGURE 12.

IRREVERSIBLE INHIBITORS

P TOLUENE SULFONYL FLUORIDE (TOS) PHENYL METHYL SULFONYL FLUORIDE (PMS)

POTENTIAL TRANSITION-STATE ANALOGS

PHENYL ETHANE BORONIC ACID (PEBA)

@ pH 3.6, pH 5.4, pH 7. 3 (PEBA3.6)(PEBA5.4)(PEBA7.3)

PHENYL PROPYL BORONIC ACID
(PPBA)

PHENYL BUTYL BORONIC ACID
(PBBA)

FIGURE 13. Inhibitor Molecules Used in This Study

The modified α -CHT crystals were allowed to equilibrate for a minimum period of one to two weeks before X-ray examination. Single crystals were mounted in glass capillaries according to the method of King (75), and the seal was reinforced by the addition of paraffin wax. inclusion of a drop of mother liquor both above and below the crystal maintained a constant humidity level and helped prevent drying the crystal. Further positional stabilization of the crystals mounted in this manner was obtained by allowing the crystals, fixed to the capillary wall by a drop of mother liquor, to stand inverted for a period of several hours. Examination of the crystal included the observation of the diffraction pattern along the principal axes, and the determination of the lattice parameters. Subsequent use of the crystal in intensity data collection came only after allowing further positional stabilization over a 24 hour period. To minimize the effects of unanticipated corrections, the crystals used for data collection were always mounted with the monoclinic b-axis coincident with the phi-axis of the diffractometer.

B. Data Collection

All X-ray work was performed using a Picker Nuclear FACS-1 automated, four-circle diffractometer modified at MSU to replace the slow-operating filter selection wheel

modific include the dis crysta consis of the time of extend An add 60 cm, crysta detect the di examin, The co ^{the} di ⊐odifi the di

with a

lifeti X and de

improv

involv diffra prelim

with a simpler filter-solenoid system. Additional modifications, made during the course of this work, included the repositioning of the balanced filters from the diffracted beam to the incident beam side of the crystal. The X-radiation incident on the crystal now consists of little more than the characteristic wavelength of the copper K_{α} line (1.5418 Å). As a result, the lifetime of a crystal with respect to X-ray decay has been extended without loss of intensity of the diffracted beam. An additional modification involved the placement of a 60 cm, helium-filled tube between the detector and the crystal (43,76). Increasing the distance between the detector and the crystal improves the resolving power of the diffractometer and allows in the present case the examination of crystals with unit cells of up to 180 Å. The constant flow of helium eliminates air absorption of the diffracted beam. The net effect of these two modifications was a slight increase in the intensity of the diffraction pattern peak-to-noise ratio, a marked improvement in resolution and an extension of a crystal's lifetime during X-ray exposure.

X-ray crystallographic examination of the crystals and determination of their lattice parameters initially involved inspecting the relative intensities of the diffraction pattern along the crystal axes (Figure 14). Preliminary evaluation of the quality of a derivative

Mount or capillar forcing

Examine along confine la compane crystal

Coserve diffract verify

Examin Sain s

Collec

1. 1 2. 6 3. 3 4. 6

Se-eroning any as a

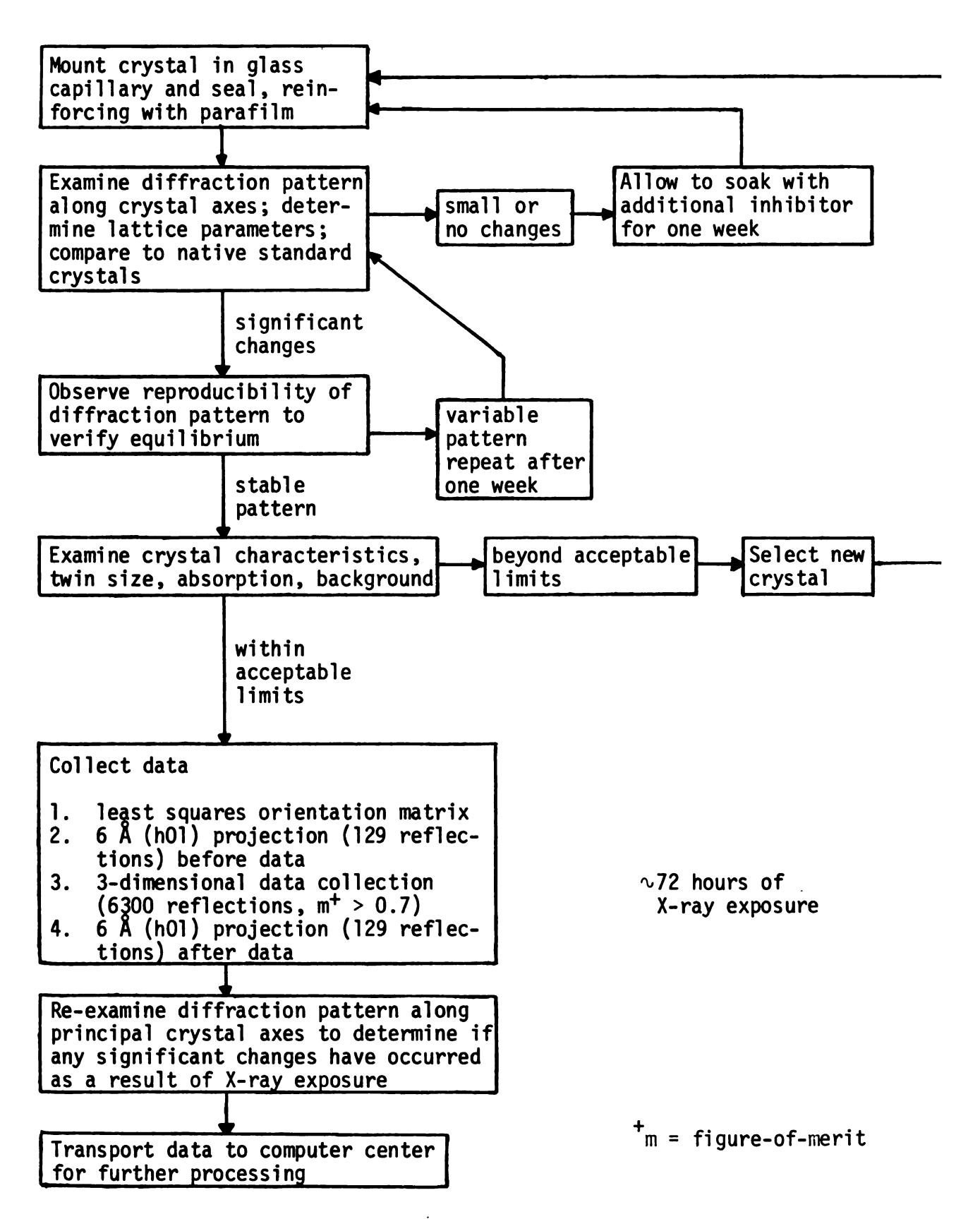


FIGURE 14. Crystal Selection and Data Collection Procedures

lattic same p (Figur in the listed analys for th refle repre exper bindi

involve

has the

veri

inh;

note

dat

eva (in

hi t'w

Sh

W

involved comparison of the axial diffraction pattern and lattice parameters with those of the native enzyme at the same pH. Changes in the distribution of axial intensities (Figure 15) were considered more significant than changes in the lattice parameters alone. The lattice parameters listed in Table 6 were obtained by the least squares analysis of the positions of twelve reflections, except for the native enzyme at pH = 4.6, where only a three reflection matrix was used, and at pH = 3.6, which represents the average of several crystals. In those experiments involving both pH change and inhibitor binding, attainment of the desired pH conformer was verified by comparison to the native enzyme before the inhibitor was added to the soaking solution. It should be noted that the diffraction pattern of the native enzyme has proved to be reproducible over a period of years; the same probably applies to the other pH conformers (43).

Before initiating a full, three-dimensional intensity data collection (Figure 14), each crystal was further evaluated with respect to its ability to diffract X-rays (intensity of diffraction pattern in general, and at higher diffraction angles), size of the crystal and its twin, X-radiation absorption characteristics and peak shape of the reflections. Optimum diffracting ability would allow operating the high intensity X-ray tube at a

	·	

F

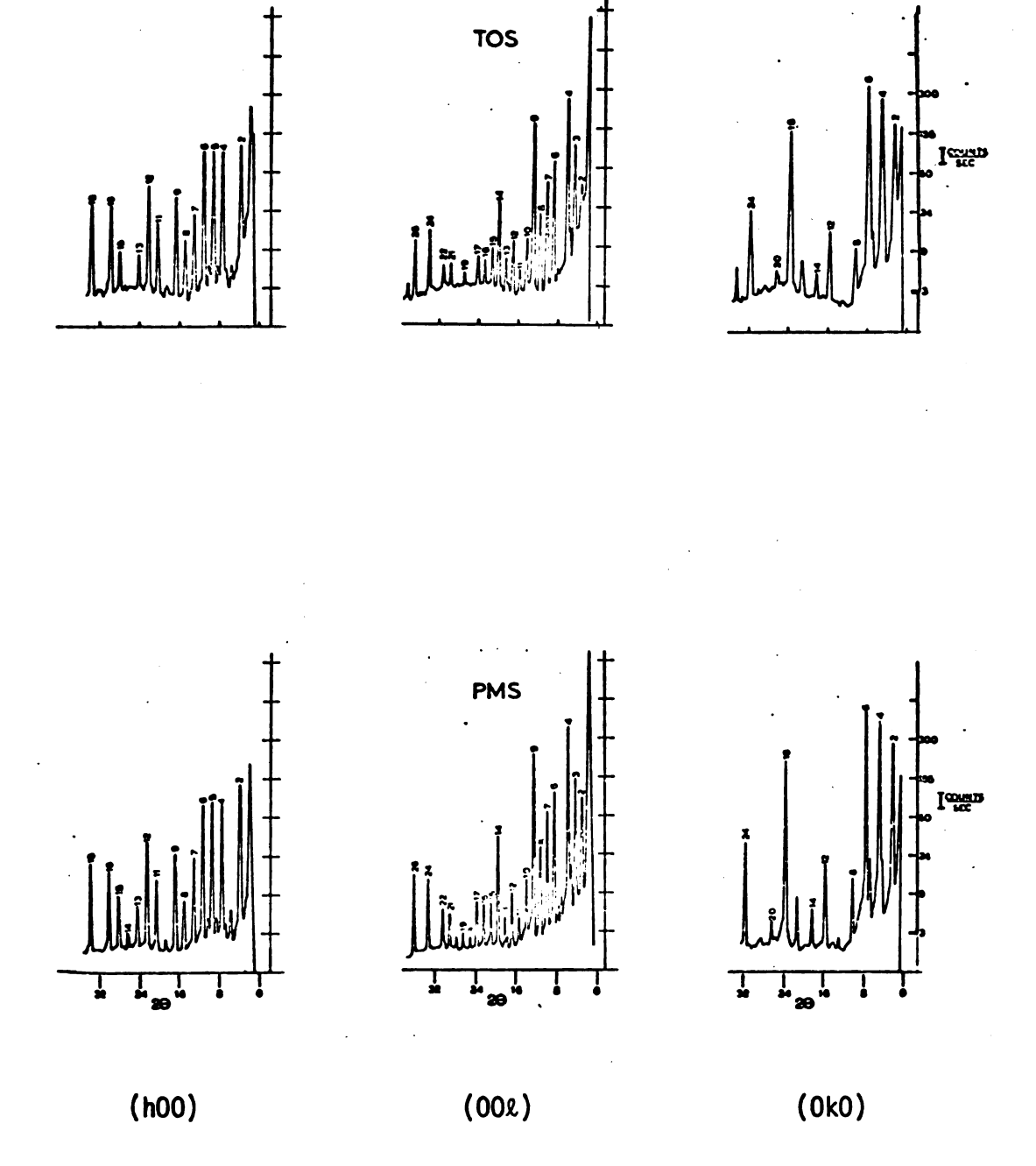
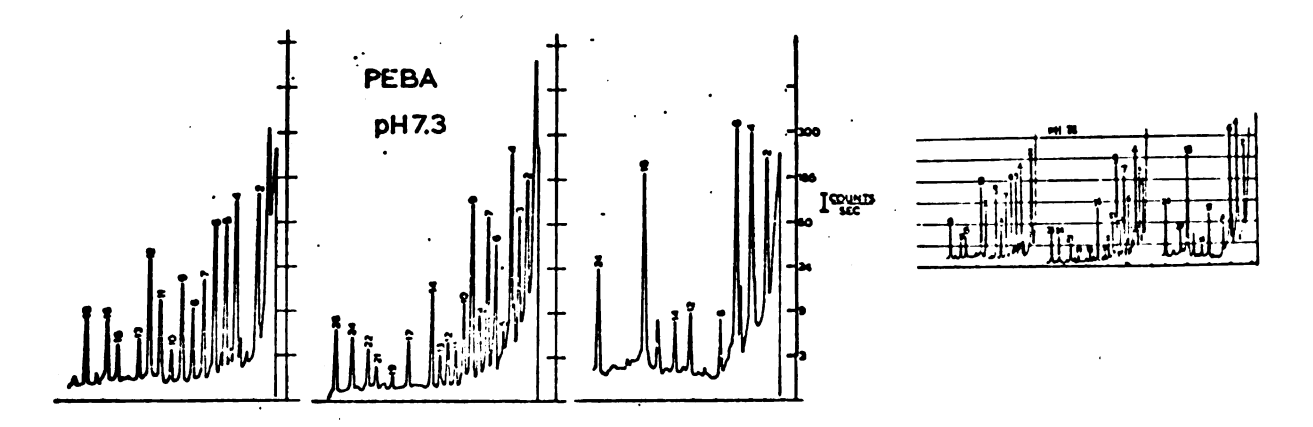
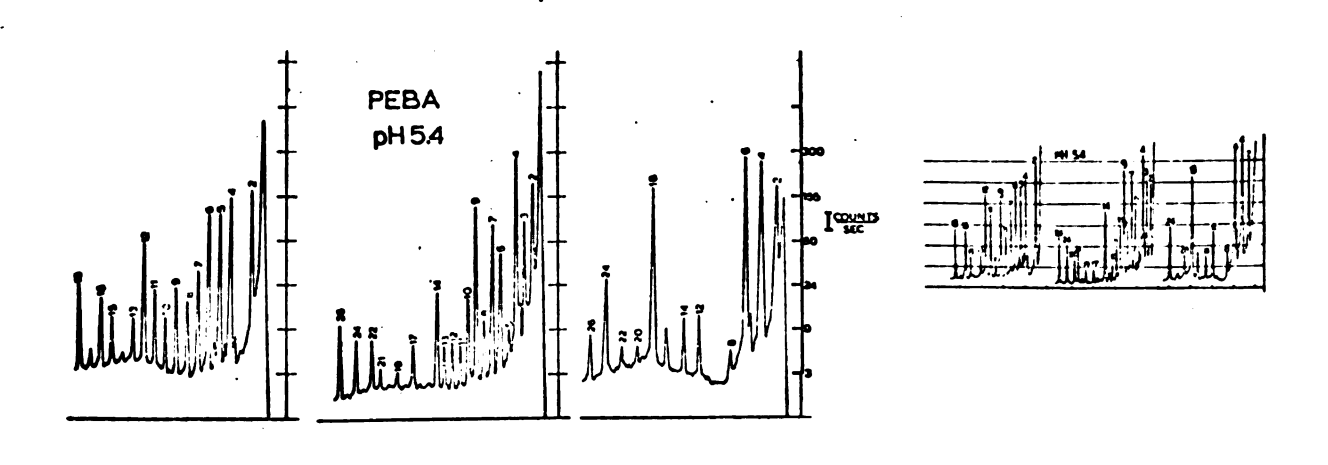
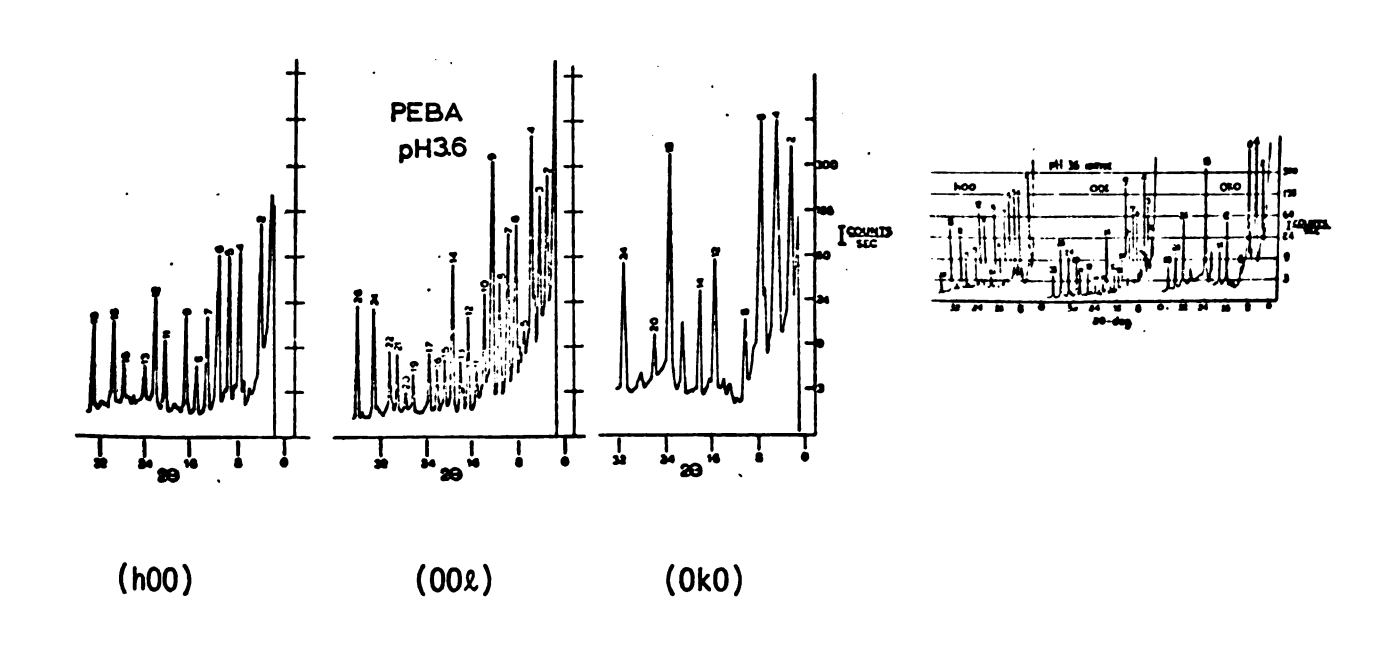


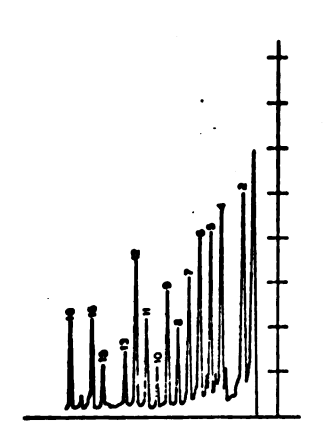
FIGURE 15. Distribution of Diffracted Intensities Along Principal Axes of $\alpha\text{-CHT}$ Complexes Used in This Study

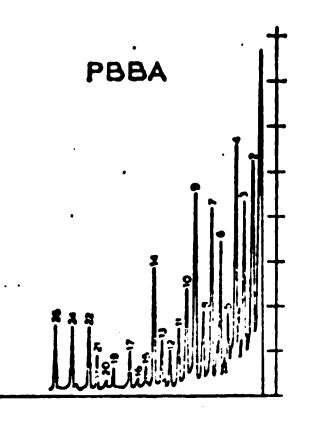
(b) (c)

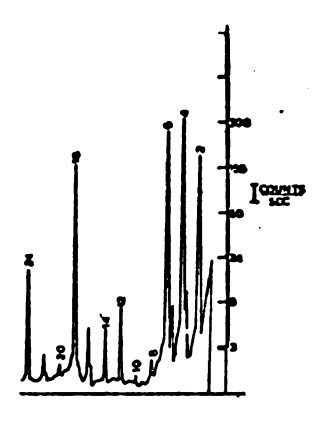


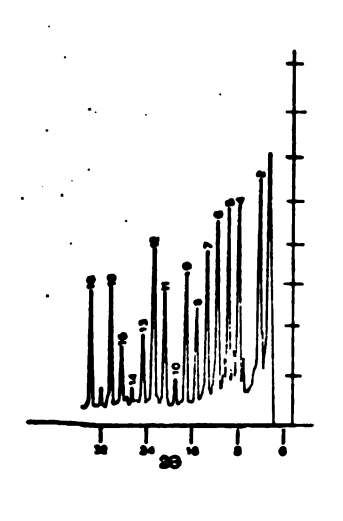




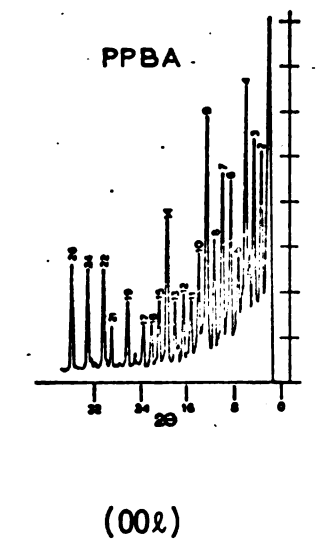


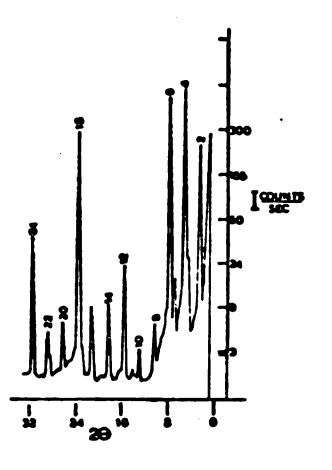






(h00)





(0k0)

TABLE 6 Lattice Parameters of the $\alpha\text{-CHT}$ Derivative

Crystals Used in This Study

Derivative	돐	a(Å)	b(Å)	c(Å)	beta(°)	Volume (ų)
T0S	3.6	49.15(5)	67.02(6)	65.88(9)	101.78(3)	212,400(700)
PMS	3.6	49.36(4)	67.25(5)	65.98(6)	101.78(3)	214,400(600)
PEBA	3.6	49.36(4)	67.43(4)	(9)66.59	101.83(4)	214,900(600)
PPBA	4.6	49.54(4)	67.39(6)	(2)00(9)	101.92(5)	215,600(600)
PBBA	4.6	49.54(2)	67.43(2)	66.03(3)	101.97(4)	215,800(300)
PEBA	5.4	49.37(3)	67.32(4)	65.73(5)	101.92(6)	213,700(500)
PEBA	7.3	49.35(2)	67.68(2)	65.98(3)	102.03(4)	215,500(300)
Native	3.6*	49.24(7)	67.20(10)	65.94(9)	101.79(6)	213,600(1000)
Native	4.6	49.3(1)	67.8(1)	65.9(1)	102.0(1)	215,000(600)
Native	$5.4^{(12)}$	49.13(5)	67.83(7)	65.81(7)	101.92(6)	214,600(700)
Native	7.3(13)	49.24(2)	67.98(3)	65.85(4)	102.03(3)	215,600(400)

* Average of several crystals

⁺ Results of three reflection matrix determinations

00 **n** a t

700

at exp

at.

des

det the

dif

wit

€.

hay sho

res

Fig

I - I 0 b 0 c 0 c Te

Mr 6

=

power setting of 240-480 watts (six to twelve milliamps at 40 kilovolts). The previously detailed instrumental modifications allowed most measurements to be collected at a power setting of 300 watts, further reducing X-ray exposure. The acceptable twin ratio was arbitrarily set at 2:1 (crystal:twin) with a larger ratio being more desirable (Table 7). The absorption characteristics were determined by measuring the intensity of reflections along the \underline{b} -axis, aligned at $X = 90^{\circ}$, as the phi axis of the diffractometer was rotated, which was also coincident with the b-crystallographic axis.

C. Data Processing

The methods used here for data reduction and processing have been described in detail elsewhere (34). A flow chart showing the path from data collection to the comparison of results with a Kendrew model of the enzyme is shown in Figure 16 and is summarized below.

where (A) = data reduction:

TABLE 7 Comparison of Derivative Crystal Characteristics in This Study

		:	:			From siona	From 3-dimensional data@
Derivative	Natio Ratio	Absorp. Max.*	Absorp. Asymm. &	Decay	Scale [%]	B\$	*
T0S	2.2:1	1.72	1.07	0.15	1.25	4.2	1.02
PMS	2.1:1	1.40	1.10	0.19	1.69	1.2	1.06
PEBA pH 3.6	2.8:1	2.00	0.98	0.21	0.52	5.6	0.98
PEBA pH 5.4	8	2.13	1.01	0.25	1.08	-2.4	1.02
PEBA pH 7.3	3.4:1	1.35	1.05	0.28	2.66	-6.0	0.95
PPBA	8.0:1	1.98	0.95	0.35	1.01	-5.0	0.92
PBBA	4.7:1	1.67	1.05	0.10	1.90	-2.8	0.96

Twin Ratio = Intensity of (6 0 0) native Intensity of (6 0 0) twin

Intensity of (6 U U) twin * Absorption maximum = $I(\phi)_{max}/I(\phi)_{min}$

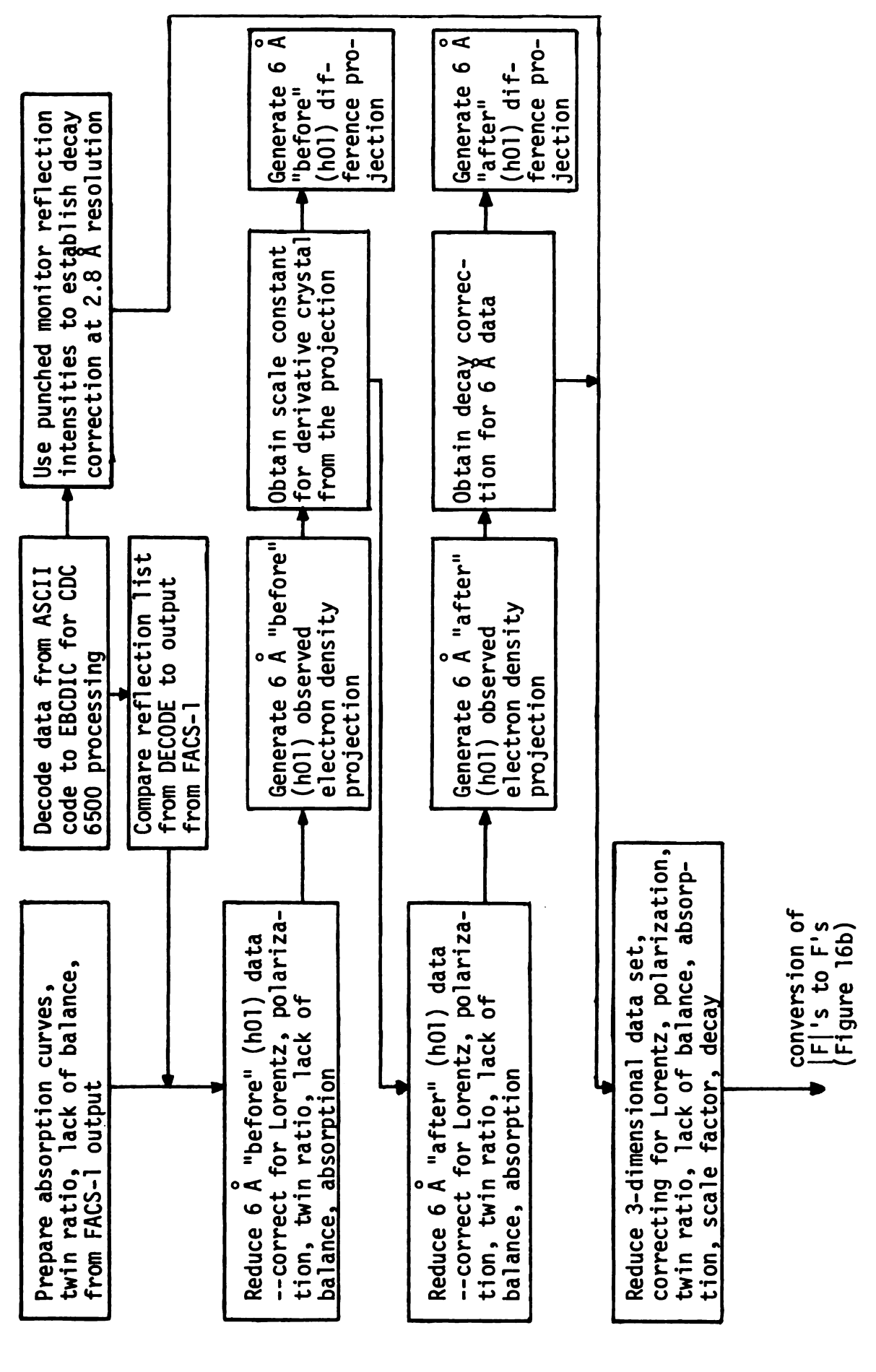
& Absorption Asymmetry = $I(\phi)_a/I(180+\phi)_a$, where ϕ_a = ϕ angle of a-axis

 ϕ Decay = (<I>initial - <I>final)/<I>initial

Scale obtained from 6 Å (h01) projection results

Parameters obtained from 3-dimensional radial distribution fitting to native distribution

 $|F|_{nat}^2 = |F|_{der}^2 k^2 \left[exp(-28sin^2\theta/\lambda^2) \right]$ B = isotropic temperature factor
} K = overall scale factor



Data Processing--Reduction of Intensities to |F|'s FIGURE 16a.

Determine scale constant correction and B thermal parameter for 2

Compare with native

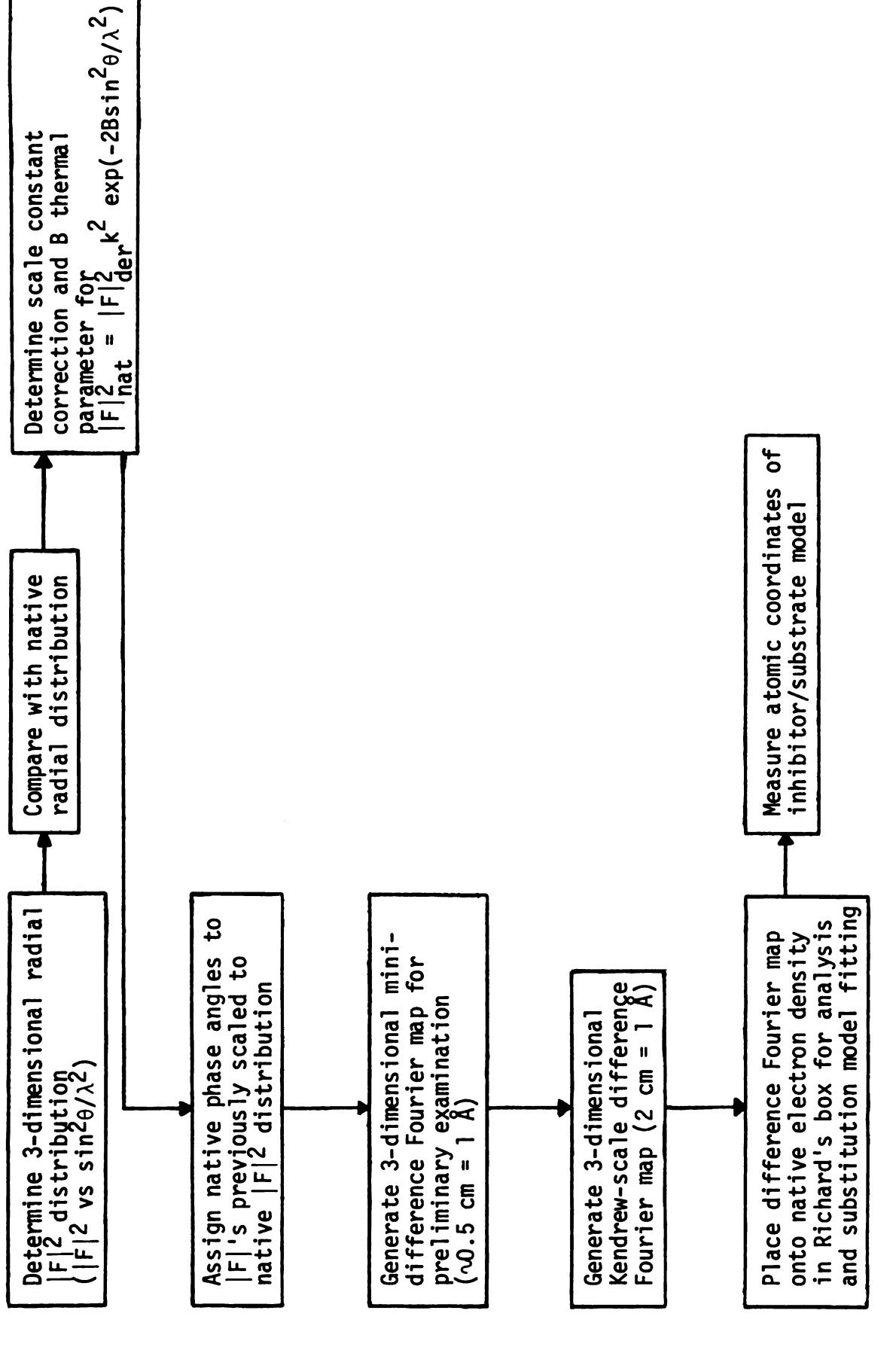


FIGURE 16b. Data Processing--Conversion of |F|'s to F's

1:

ard (€

deriva 's als with scaling and 6 \mathring{A} resolution decay corrections derived from "before" and "after" (h01) electron density projections;

(B) = scaling of the radial distribution of $|F|^2$;

$$|F|_{abs-nat}^2 = |F|_{abs-der}^2 = k^2 |F|_{rel-der}^2 \exp(-2B\sin^2\theta/\lambda^2);$$
(see last two columns, Table 7)

and (C) = assignment of the native phases to the derivative structure amplitudes and generation of "best" difference Fourier coefficients:

$$F_{abs-der} = |F|_{abs-der} \exp(i\alpha_{nat})$$

$$\alpha_{nat} = "best" phase angle,$$

$$\Delta = m(|F|_{abs-der} - |F|_{abs-nat}) \exp(i\alpha_{nat})$$

where Δ is the "best" difference Fourier coefficient and m is the figure of merit.

At the time native phase angles are assigned to the derivative data, the distribution of $\|F\|_{abs-der} - \|F\|_{abs-nat}$ is also determined. The distributions of the derivative

,

S

t v

> t: d:

is br

or na

i T

C٢

₩e th

۲ŗ

14 5 t (

àr

difference coefficients used in this study are listed in Table 8, and in the histograms of Figure 17. From Table 8, it can be seen that the differences are generally observable ($|F|_{unobs}$ = 33 electrons/unit cell) and that excessive changes in intensity are minimal, suggesting good isomorphism.

A series of typical absorption curves from a PEBA pH 3.6 crystal is shown in Figure 18. A comparison of the relative absorption maxima and asymmetry of the derivative crystals used in this study is made in columns 2 and 3 of Table 7. Evaluations of the peak shape of the reflections were based on the appearance of the axial diffraction pattern and reflection centering characteristics. Crystals were rejected if peaks appeared too broad or split. Most omega-spreads of derivative crystals (0.3-0.4°) were slightly larger than those in native crystals (0.2-0.3°), but this did not seem to impair the diffraction pattern in any way (4). Severely cracked crystals were also not used. As experiments were performed on tubes containing ten or more crystals, these evaluations could be repeated until an acceptable crystal was found.

The intensity data collection procedures (Figure 14), including the wandering count-six-drop-two omega step scan, have been extensively discussed by Vandlen and Tulinsky (34,78). The data collection system used

Comparison of Derivative Crystal $\left| \triangle F \right|^{+}$ Distribution Statistics TABLE 8

			 ∆	$ \Delta F ^{\dagger}$ Distributions (electrons/unit cell)	ribution	ons (ele	ectrons,	unit ce	(11)		
Derivative	<pre># observed # measured</pre>	33	34-	68- 134	135-	201- 267	268- 334	335- 400	401-499	200	Standard error* σ(∆p _{map})(eA-3)
		(%)	(%)	(%)	(%)	(%)	(%)	(%)	(%)	(%)	
T0S	6142 6187	52.7	31.5	14.5	1.6	0.2	•	•		ı	0.012
PMS	6150 6185	50.9	30.1	16.2	2.0	0.7	0.3	0.2	0.1	1	0.015
PEBA pH 3.6	6143 6184	52.8	30.5	15.7	1.5	0.2	•	•	ı	ı	0.012
PEBA pH 5.4	6142 6168	32.1	27.2	30.2	7.3	2.2	0.8	0.3	0.3	0.1	0.022
PEBA pH 7.3	6144 6177	42.0	29.9	24.2	3.7	9.0	0.1	ı	1	1	0.016
PPBA pH 4.6	980 <u>9</u>	47.4	31.0	18.8	2.1	0.3	ı	ı	1	1	0.013
PBBA pH 4.6	6184 6185	49.5	31.3	17.2	1.8	0.2	•	1	ı	ı	0.013
Native pH 5.4 (41)	4 6176 6176	52.8	29.1	15.9	1.7	0.3	0.1	1			0.013
Native pH 7.3 (77)	3 <u>6148</u> 6175	41.6	31.3	23.5	3.5	0.5	0.1	1	1	ı	0.015
+ AF = F abs-der -	abs-der -	F abs-nat	nat	*Sta	*Standard discussed	Standard error in discussed in text.	differ t.	ence el	error in difference electron density map d in text.	density	/ map as

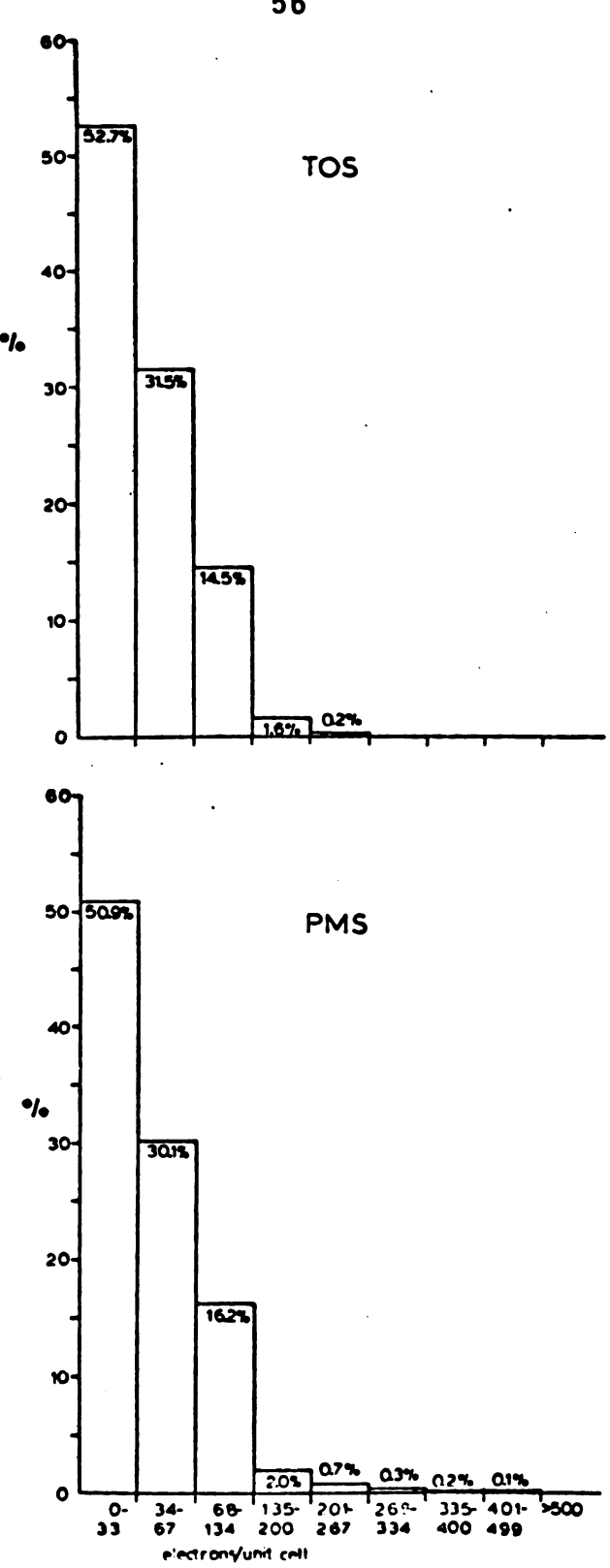
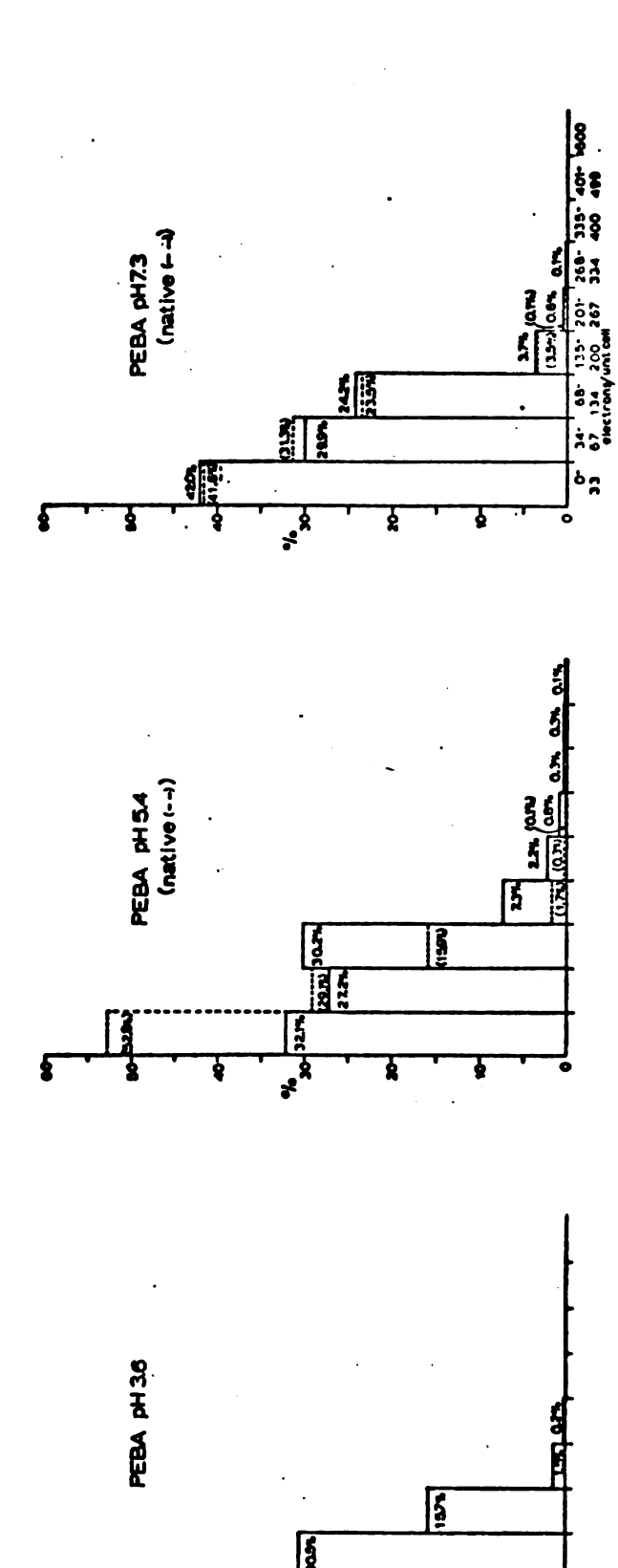
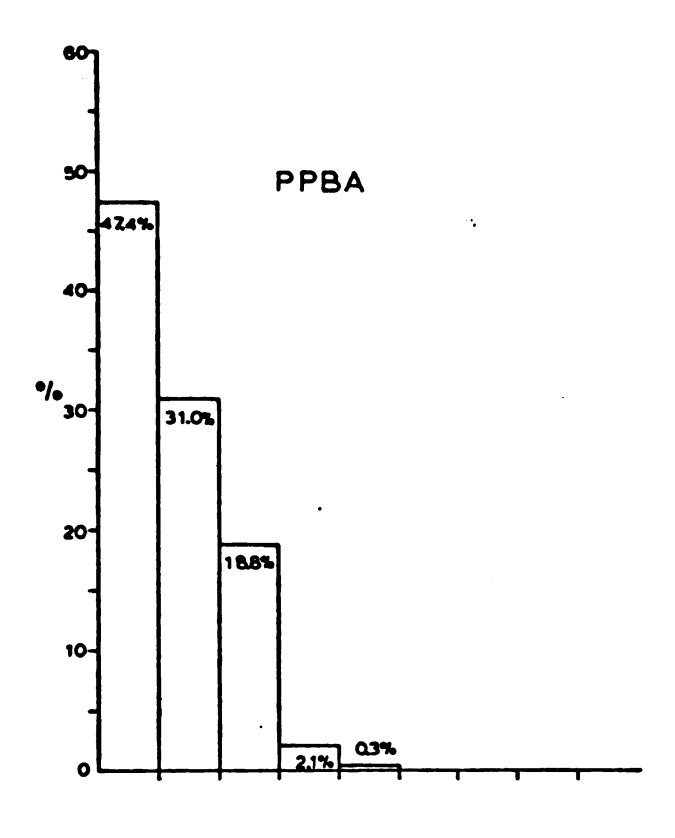
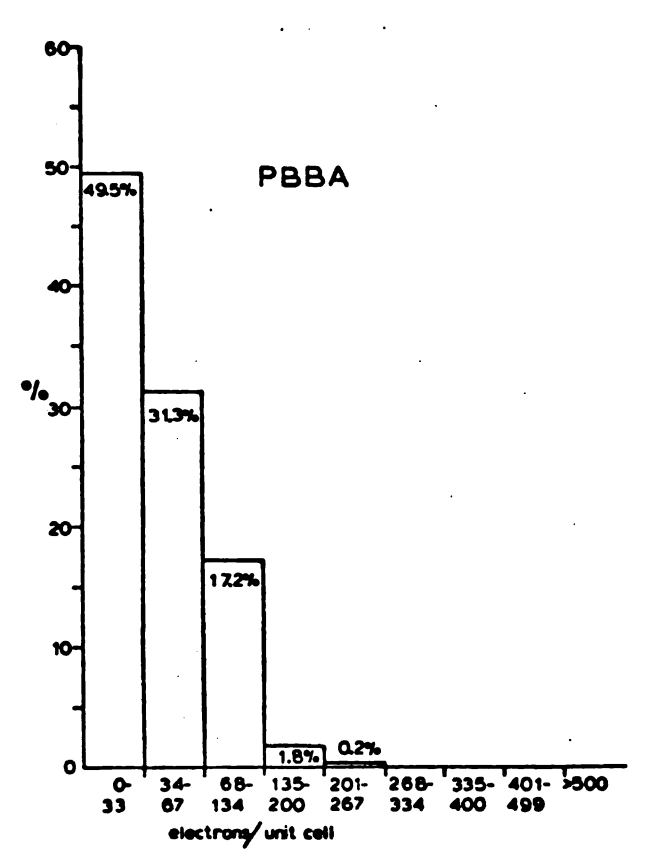


FIGURE 17. Histograms of Derivative Crystal $\left|\Delta F\right|$ Distribution Statistics







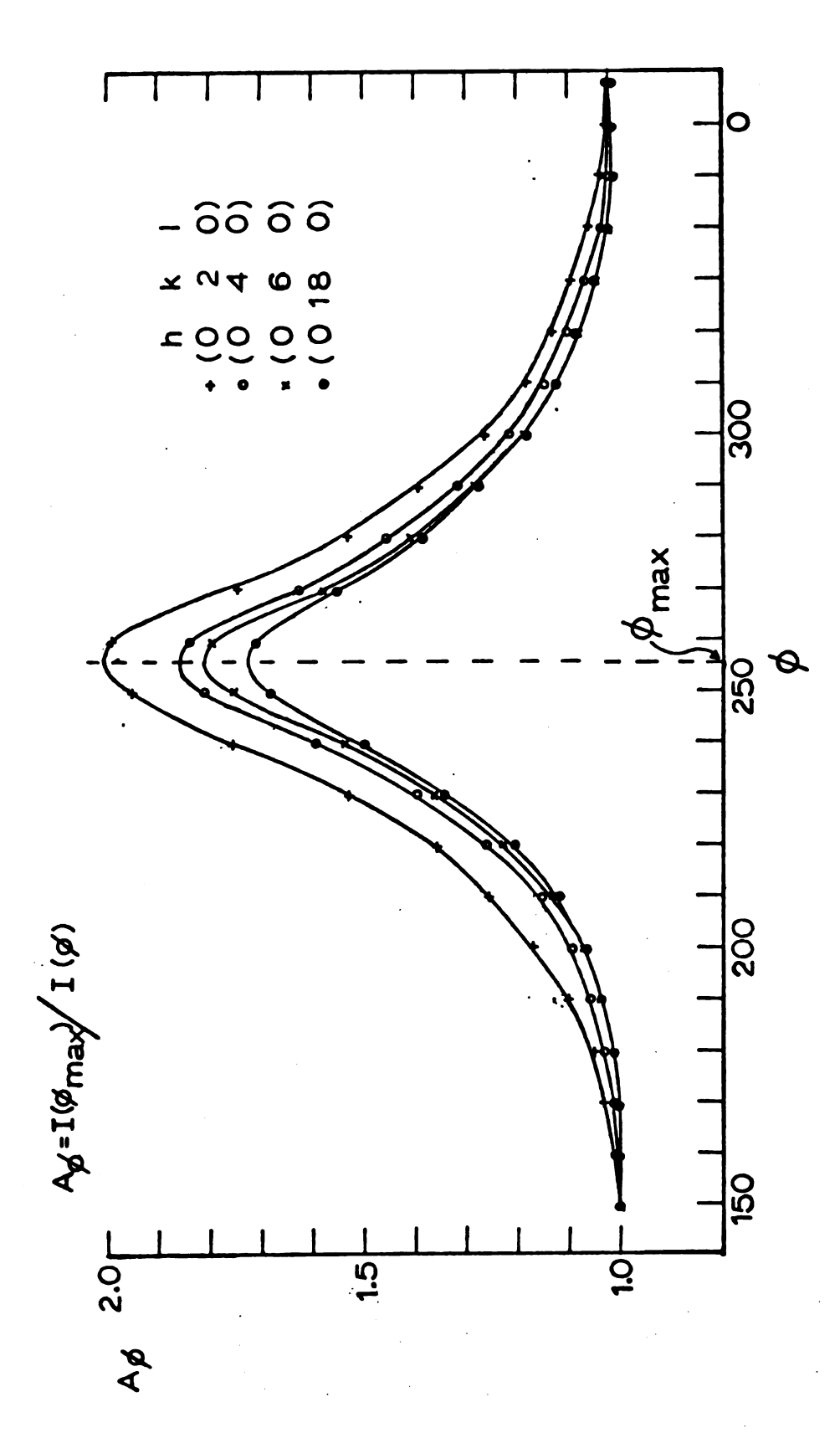


FIGURE 18. Absorption Correction Curves--PEBA pH 3.6, Crystal G-67-SI-3

in this study, which was developed at MSU, permitted the monitoring of the crystal alignment during intensity data collection and the redetermination of the crystal orientation matrix if the crystal apparently moved. In addition, the programs measured a reduced reflection data set which only considered reflections which had a figure of merit greater than 0.7 in the native data (79). hardware and software developments described here and elsewhere made it possible to obtain a complete set of observations from a single crystal, not the five or more crystals required in previous studies. The reduced reflection set included approximately 6300 reflections. The total number of independent reflections is approximately 10,500 at 2.8 Å resolution. The electron density maps calculated with the reduced set of coefficients, whose phase angles were more accurately known, compared well with maps calculated from the native data set containing all reflections with figure of merit greater than 0.3 (approximately 8500 reflections). collections were completed within a three to four day period, averaging 70 to 80 hours of total X-ray exposure to the crystal. In all the derivatives studied, the decay as determined by fall-off in intensity of monitored reflections was 35% or less (Table 7).

For each derivative crystal, the intensity of the 129 reflections of the centrosymmetric (hOl) projection

at 6 \mathring{A} resolution was measured both before and after the three-dimensional intensity data collection. The "before" (h01) projected electron density permitted scaling to the parent native crystal data, normalizing the crystal size and beam intensity. The "after" (h01) projected density allowed the determination of intensity fall-off due to X-ray damage in the 6 \mathring{A} resolution range. These projections also permitted the evaluation of possible changes in inhibitor binding which might have accompanied the extended X-ray exposure. The derivative crystals used in this study did not show the latter changes.

A method of evaluating the error of the difference electron density has been developed by Henderson and Moffat (80), the mean-square-error of the difference density being given by

$$\begin{split} <\Delta \rho^2> &= (2/V^2) \Sigma \Sigma \Sigma [\Delta|F|_{d-n}^2(hk1) + \Delta|F|_{d-n}^2(hk1)(1-m^2(hk1)) \\ &+ \delta^2(hk1)] \\ \text{Where, } \Delta|F|_{d-n} &= |F|_{der-nat} = |F|_{der} - |F|_{nat}| \\ \delta^2 &= \sigma^2(\Delta|F|_{d-n}) \\ &= \text{figure of merit} \\ V &= \text{unit cell volume} \end{split}$$

The first term, $\Delta |F|_{d-n}^2$, represents the error caused by assuming that the phase angles of the parent native

are subs phas (1-6 dete fig the ехре coef deri in T tion esta the i erro note by a cons

of ba

stud

^{noise}

(12),

occur

crys

Alt!

crystals are unchanged in the derivative crystals. Although the structural changes observed in this study are generally small, Luzzati (81) has shown that the substitution could be 50% higher due to this type of phase angle difference. The second term, $(\Delta |F|_{d-n}^2)$ $(1-m^2(hk1))$, corrects for the errors made in the original determination of the native phase angles by using the figure of merit; the latter is related to the error of the phase angle. The third term, δ^2 , represents experimental observational errors in the difference coefficient. The root-mean-square (rms) errors of the derivative difference electron density maps are included in Table 8 (the δ^2 term was not included in the calculation). This error estimation of the maps was used to establish levels of significance in the maps. Although the method has become a standard means of estimating the error in difference electron density maps, it should be noted that the calculation has been shown to be inaccurate by a factor of 2 (82). In the present work, a more conservative approach was employed based on an estimate of background noise in the Fourier maps. Earlier pH studies had indicated that an appropriate random background noise level in the difference map was about $+ 0.05 \text{ eA}^{-3}$ (12), and confidence was placed in those peaks which occurred at about three times this value. The same

proced being

for ea

proces

electr

featur

even m

maps.

were (

procedure was used in the present work, with adjustments being made on the basis of the random background noise for each derivative crystal studied. This screening process, along with the ability to correlate the difference electron density peaks with intelligent structural features of the native structure, will be shown to give even more validity to the interpretation of the difference maps. The significance levels established in this manner were usually about $10 \times \sigma(\Delta \rho)$.

III. METHODS OF ANALYSIS

A. Emphasis of Analysis

The two classes of inhibitors used in this study (sulphonyl halides and boronic acids) and the selection of the compounds within these classes permitted a detailed comparison of the α -CHT:inhibitor complexes with respect to the following important points:

- 1. The orientation of each inhibitor in the independent molecules of the α -CHT dimer and the interactions of the inhibitor in the active site upon binding.
- The perturbation of the native conformation which occurs upon binding in regions removed from the active site, and its relationship to the binding in the active site.
- 3. The effect of varying the side-chain of the inhibitor upon:
 - The binding orientation and interactions within the specificity site,
 - b. The perturbation of the native conformation removed from the active site region.
- 4. The structural and functional variability among the different pH conformers observed in the crystal upon inhibitor binding.

use o inabi

atomi

here.

tions

descr

the c orien

struc

coope

compa

has u the d

the e

elect

diffe

of to :ion

diff

the diagr

5. The evaluation of the suitability of phenyl alkyl boronic acids as potential transitionstate analogs for α -CHT catalyzed hydrolysis.

The present analysis has been based primarily on the use of the difference Fourier method. However, the inability to examine the three-dimensional structure at atomic resolution limits the correlative studies described here. On the other hand, several refinements and innovations to present techniques have been made and will be described below.

The areas of major concern in this study have been the comparison of the inhibitor binding interactions and orientations within the active site and their external structural perturbations which might indicate a form of cooperativity upon active site binding. A detailed comparison of the inhibitor molecule binding orientations has utilized the examination of composite sections of the difference electron density of the substitution and the fit of a model representing the substitution to electron density centroid positions in planes of the difference Fourier electron density map. The examination of the changes which occur in the native α -CHT conformation upon binding has been carried out by the use of a difference diagonal plot method which was developed during the course of this work and which is a variation of the diagonal plot originally proposed by Phillips (83).

B. Examination of the Substitution in the Active Site

Initial examination of inhibitor substitution involved the superposition of the "best" difference electron density map onto the native electron density map in the MSU Richard's box (84). The orientation of the MSU-Kendrew model of α -CHT presented problems in placement of a model of the inhibitor within the electron density. The Fourier map, calculated along the a-direction and stacked along the a*-direction, revealed a more or less "end-on" view of each of the inhibitors used in this work (Figure 19). This made a direct comparison of the various inhibitor substitutions difficult and the same applied to the exact placement of the inhibitor model in the active site. Therefore, the difference electron density was calculated along both the b- and c-directions, and composite projections were constructed as shown in Figure 20. composite projections permitted a simple comparison of the substitution density in each of the independent molecules of the dimer and, also, among the various derivatives (Figure 21). The lowest contour level in the projections is drawn at about three times the noise level previously discussed (0.15 $e^{\mathring{A}-3}$), and only these contours are drawn in each section.

A detailed comparison of the various substitutions was possible after the Kendrew model of the inhibitor was fit to the difference density and the coordinates for the

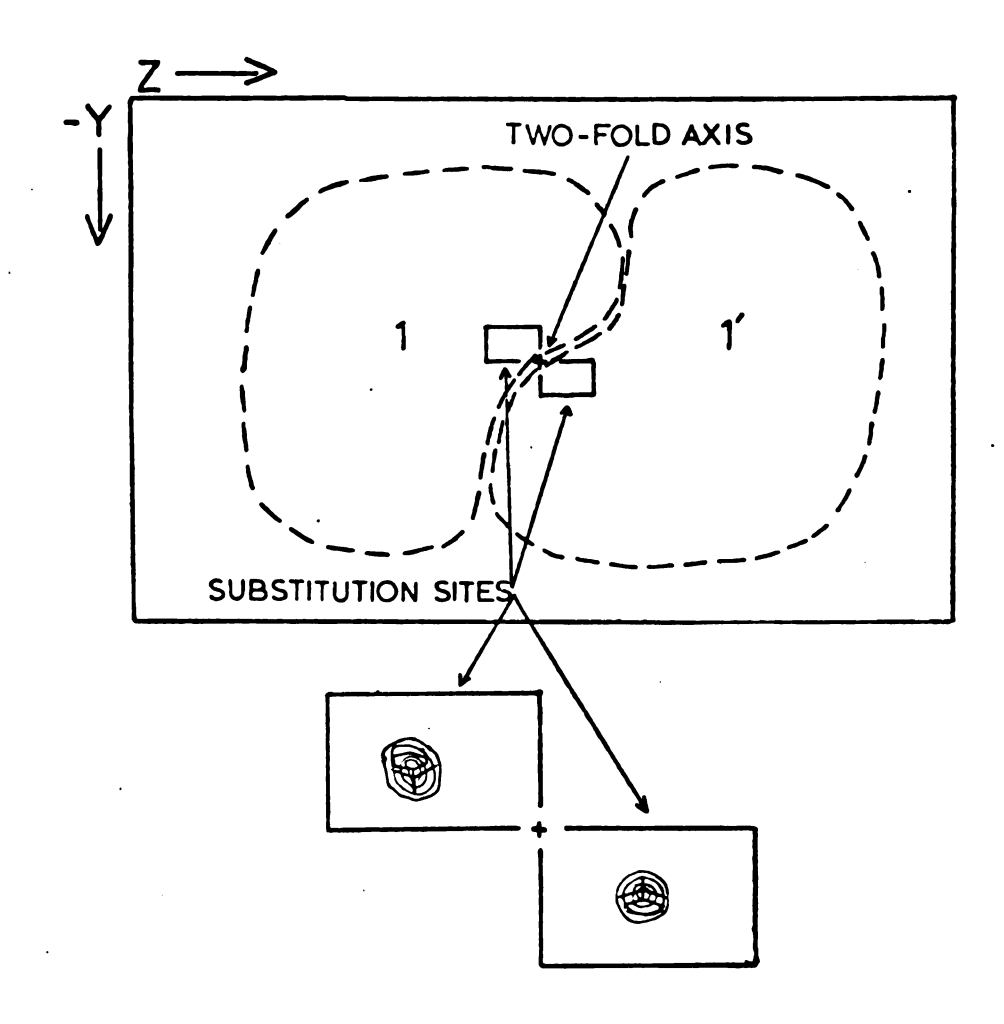


FIGURE 19. Schematic of y-z Projections of the Difference Electron Density in the Active Site Region for TOS $\alpha\text{-CHT}$

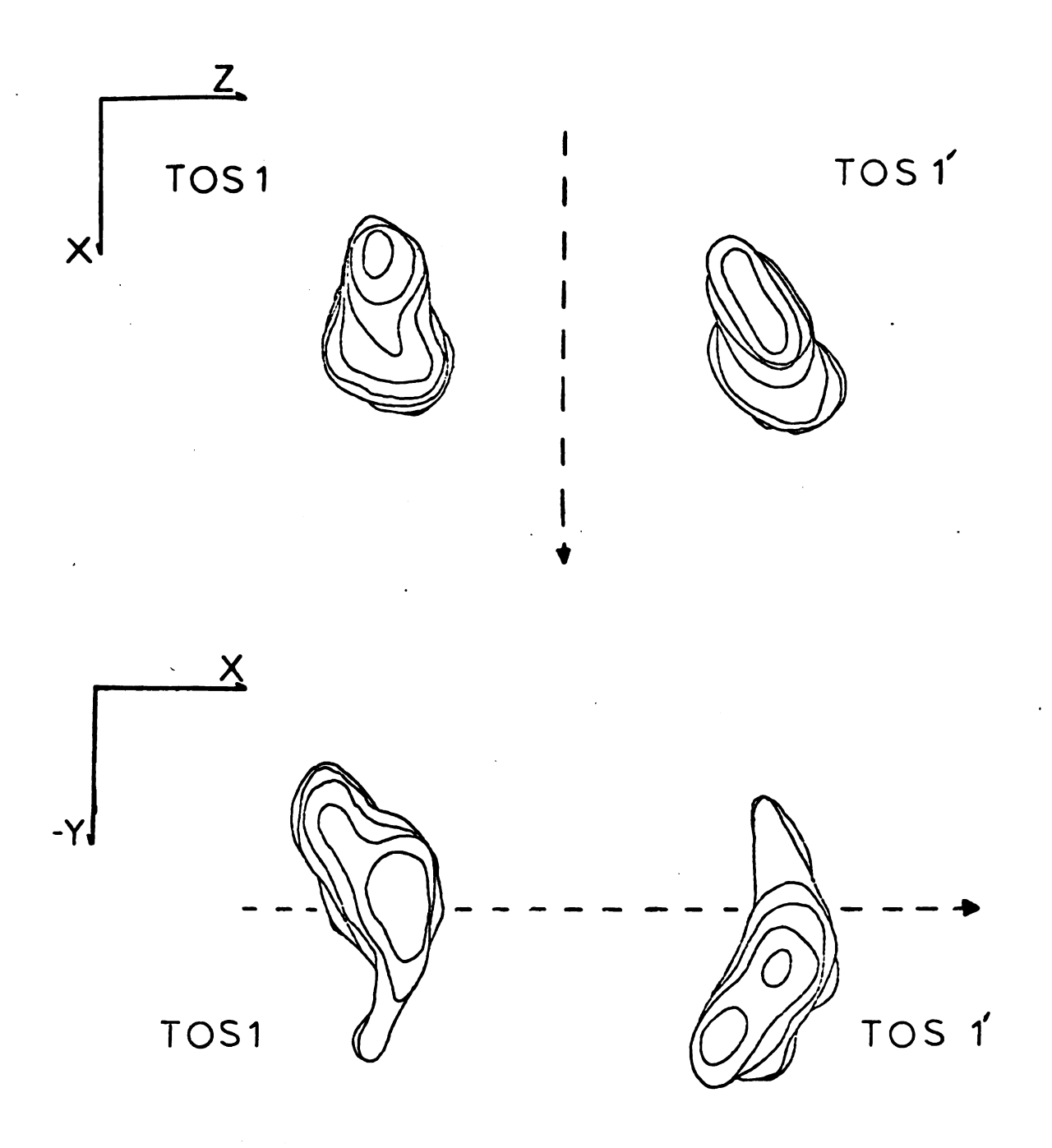
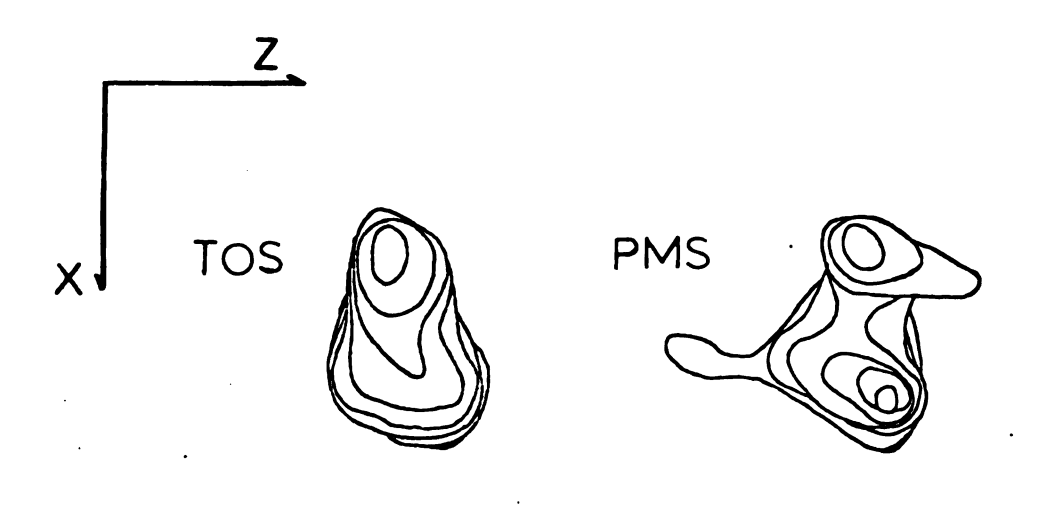


FIGURE 20. Comparison of Composite Projections of the TOS Difference Electron Density in the Active Sites of the α -CHT Dimer; Contoured at 0.15 eA-3, Positions of TOS 1 and TOS 1' are Arbitrary in z

X

-Y

F. GUD



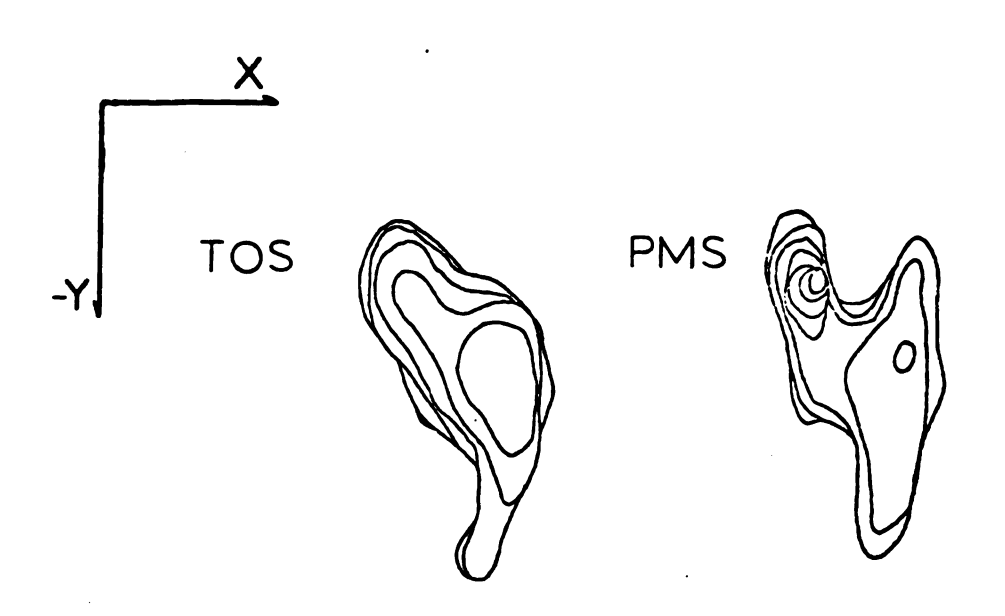
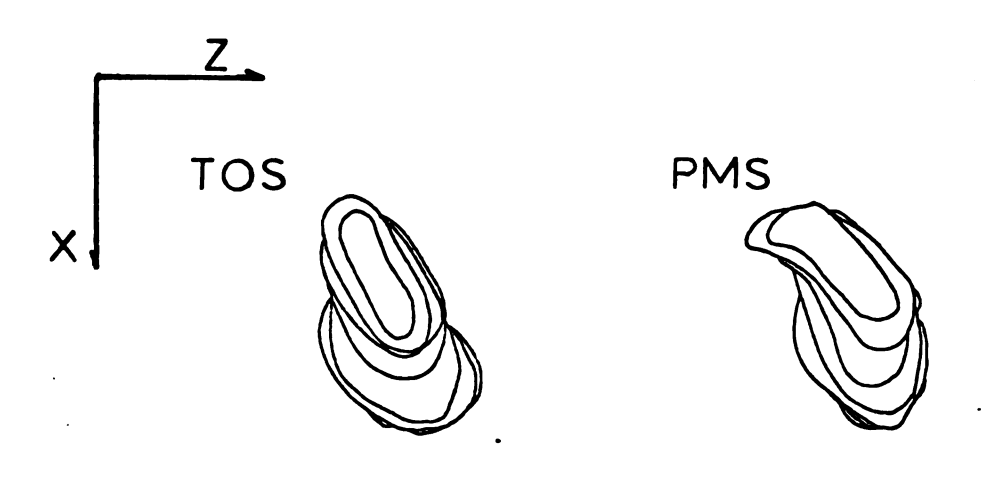


FIGURE 21a. Comparison of Composite Projections of the Substitution Electron Density of TOS and PMS in the Active Site of Molecule 1; Contoured at 0.15 eA-3

X -Y FIGUE



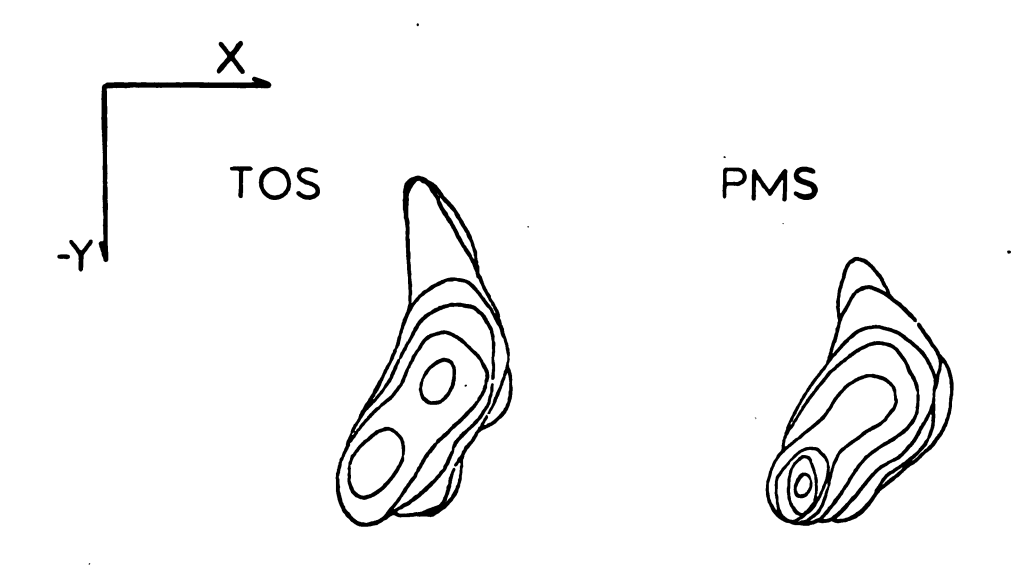


FIGURE 21b. Comparison of Composite Projections of the Substitution Electron Density of TOS and PMS in the Active Site of Molecule 1'; Contoured at 0.15 eÅ $^{-3}$

fitt in t

plot

elec

fo]]

fitted model were obtained. The positioning of the model in the difference electron density used a method of plotting the projections of the calculated difference electron density centroids. The method involved the following scheme:

- 1. For each Fourier section calculated along the \underline{a} direction, line sections are constructed through the peak density position in the region of the substitution in both the y- and z-directions.
- 2. The centroid peak position (maximum of the above plot) for each Fourier section is determined to an accuracy of \pm 0.25 Fourier grid units (0.16 Å in y- and 0.13 Å in z-directions).
- 3. These centroid positions are plotted on a scale of 2 cm = 1 Å in both the x-z and x-y projections. For the centroid position in each section, a boundary occurring at \pm 3 x $\sigma(\Delta\rho)$ is also plotted, establishing a new weighted composite density projection, which is weighted by the difference electron density.
- 4. A Kendrew model of the inhibitor is "fitted" to the three projections and the atom coordinates are measured.

The app

The

COm

vis gca

sys

the

na t coo

Pre eas

٥f

¥3 e

the

er, z

5. Bond distances and angles are calculated and the atomic positions are then adjusted to correct any major disparities from accepted geometries (85). The proper orientation is maintained within the difference electron density centroid projections.

The inhibitor bond distances determined in this manner approach accepted values to within \pm 0.05 Å (A-1, A-2). The fit of tosyl to the centroid density of ρ (TOS- α -CHT) - ρ (α -CHT) is shown in Figure 22.

The method approximates results obtained from a computer analysis of substitution density which uses visual interactive graphics display techniques (86). A goal of both this method and that of the visual display system is to manipulate inhibitor orientations within the difference electron density without disturbing the native model and to obtain an initial set of atomic coordinates for the substitution. Although not quite as precise as the automated techniques, the method is easily applied and has allowed the detailed comparison of the orientation of the substitutions for the inhibitors used in this work.

A detailed analysis of the inhibitor orientation in the active site was accomplished by the use of the native enzyme coordinates measured using the model of α -CHT at

FIGU

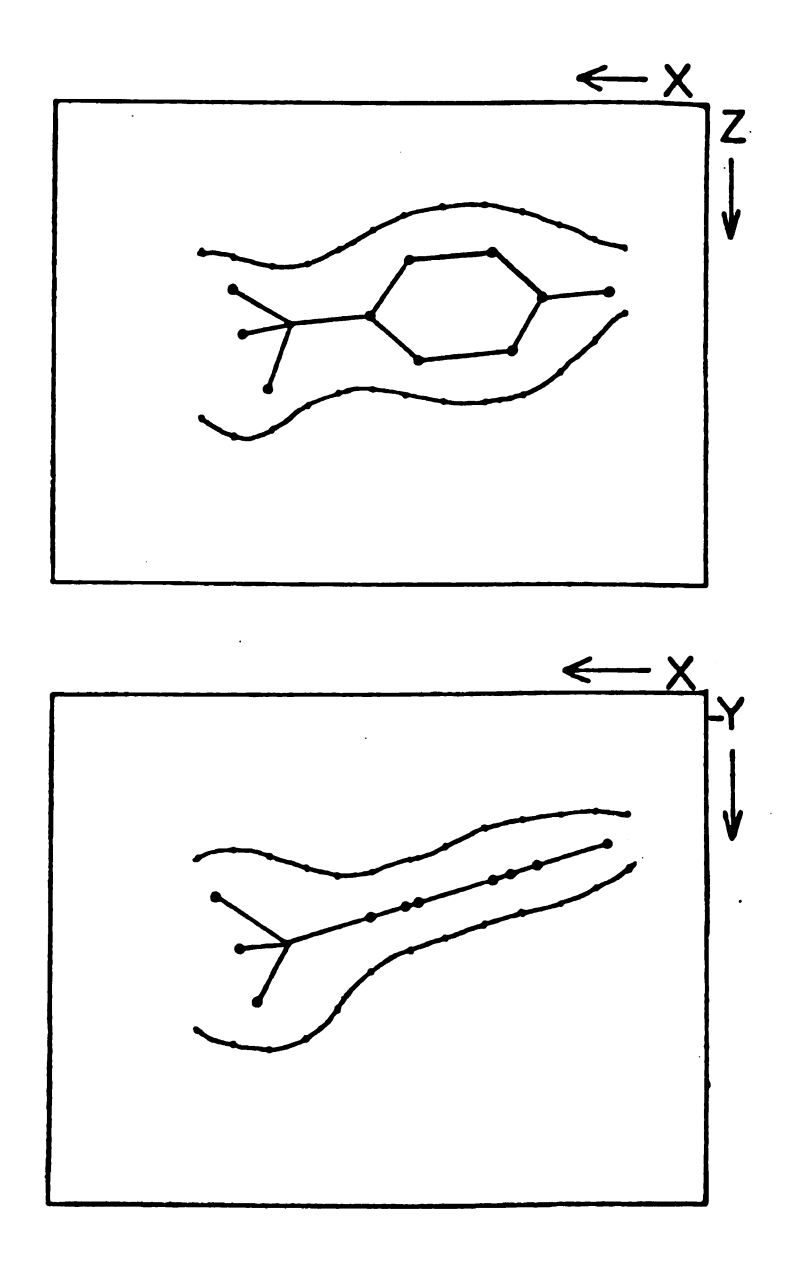


FIGURE 22. Model of TOS as Fitted to Weighted Centroid Projections of the Difference Electron Density

MSU

(87)

the form

the

ξ.

sugg tura

inni

mole syst

the

and i

matj.

of a

inhil as w

are

regi

upon for 1

genas

bind.

be re

MSU (79), and refined by Diamond's program, "Model Build" (87). A comparison of the calculated distances between the inhibitor molecules and the amino acid residues forming the specificity pocket and the catalytic site of the native configuration is made in the Results section.

C. <u>Examination of Conformational Adaptation Accompanying</u> Inhibitor Binding

Kirkwood (88) and Lumry (89), among others, have suggested that enzymes might exhibit a cooperative structural relationship upon the binding of a substrate or inhibitor in the active site of the molecule. The intermolecular cooperativity observed in the hemoglobin system (sigmoidal kinetics) has raised the question of the generality of possible intramolecular cooperativity and molecular recognition. An examination of the conformational changes which might occur upon the interaction of α -CHT with individual members of two classes of inhibitors could provide insight concerning such questions as why large biopolymers, such as the serine proteases, are required for the maintenance of a small active site region. In this respect, particular emphasis is placed upon the domain structure of proteins, as first uncovered for the nucleotide binding domains of lactate dehydrogenase (90) and observed later with other nucleotide binding enzymes. These bio-architectural features can be revealed by a diagonal distance plot (1).

and car

dis the

cha cor

the

as in

res

the dis

do:

st

be

9 e

ti du

th

be in

ir

The diagonal distance plot involves the calculation and representation of the distances separating the alphacarbons (C_{α}) in a protein (polypeptide) molecule. distance map, shown in Figure 23, where r_{ii} represents the distance between residues i and j along the $\alpha\text{-CHT}$ chain, was generated by Nishikawa et al. (44), and was contoured at intervals of 15 Å. This original map used the MRC coordinates of α -CHT and is virtually the same as the map generated using the MSU coordinates. This is in agreement with the comparison of the MSU and MRC results which were within the 15 $\overset{\circ}{\mathsf{A}}$ resolution limit of the distance map. A striking feature of the α -CHT distance plot is the appearance of two similar structural domains, A and B, beginning at residues 1 and 123 (Figure 23) (44). The presence of separate but similar structural features is not restricted to α -CHT and has been observed with elastase (91) and lactate dehydrogenase (92). This structural repetition in the construction of a protein molecule has been attributed to gene duplication with evolutionary differences occurring in the related regions (49).

The potential cooperativity which might occur between domain regions as a result of binding of an inhibitor or substrate, chemical modification or change in the pH or salt content of the mother liquor, has been

100-

ωo

FIG

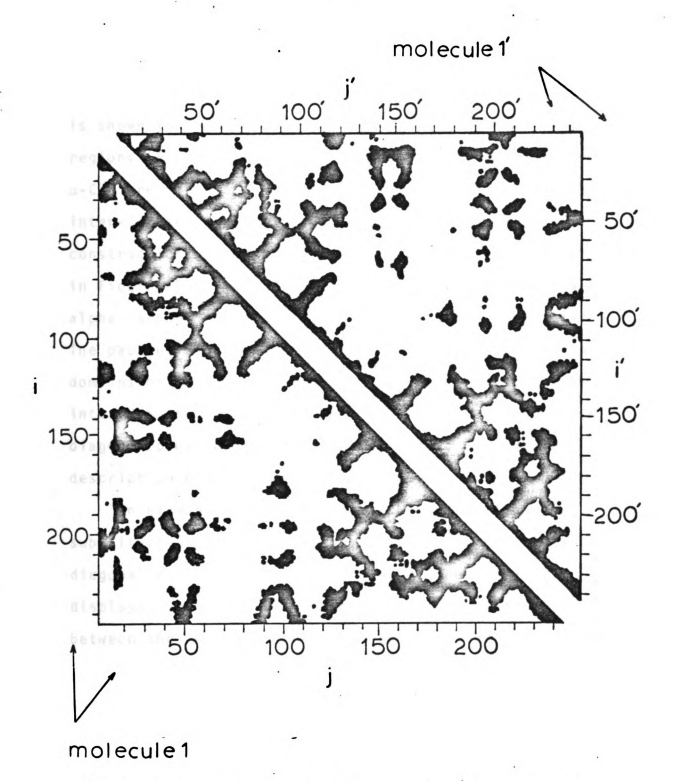


FIGURE 23. Distance Diagonal Plot, r_{ij} , of $\alpha\text{-CHT}$, Contoured at 15 Å only (45) and Exhibiting Dimer

exa

•h

is

re

3-

in

CO

in

al

Th

do

in

di

de

su

di

di

5e

(4

th

di

th.

dj

St

examined in this work. A schematic representation of the domains of the distance diagonal plot of Figure 23 is shown in Figure 24. Both the individual domain regions (A and B) and the inter-domain regions (A-B) of α -CHT are depicted. It is also possible to examine the inter-domain interactions in the dimer of α -CHT by construction of the cross-distance diagonal plot shown in Figure 25a. This method plots r_{ij} where i and j are alpha carbons (C_{α}) from molecules l and l', respectively. The packing along the z-direction of the dimers and the domains of α -CHT is shown in Figure 25b. Although the inter-domain regions have been observed in the distance diagonal plots of other enzymes (92,93), no detailed description of them has been reported.

In examining the structural changes accompanying substitution, some innovations to the original distance diagonal plot have been made. One of these readily displays the variability of conformational changes between the two independent molecules of the α -CHT dimer (42). The method makes use of the inherent symmetry in the diagonal plot (e.g., $r_{ij} = r_{ji}$). Since the distance diagonal plot exhibits structural features arising from the interaction of individual C_{α} atoms, the peaks of a difference Fourier map, which represent changes in the structure of the native enzyme, can be examined for their

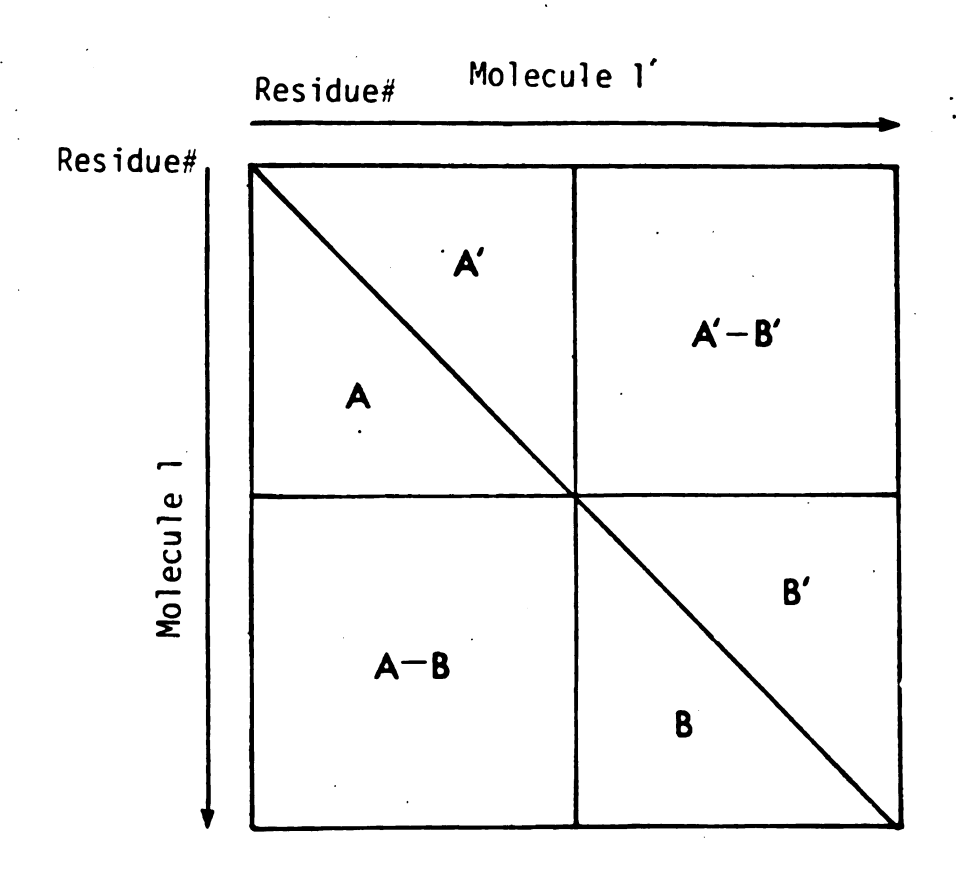
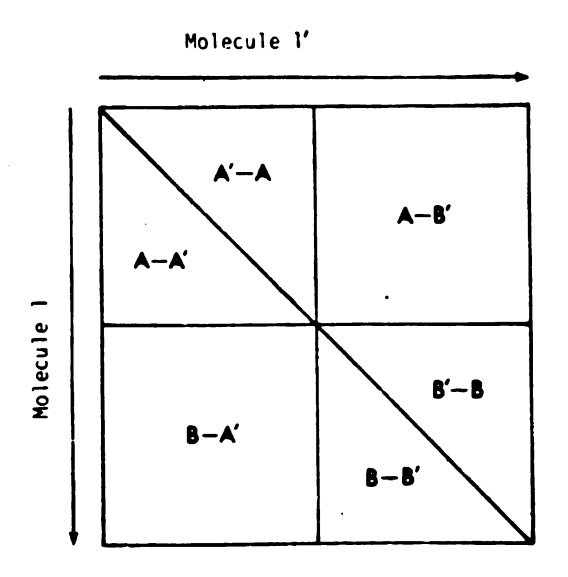


FIGURE 24. Schematic Representation of $\alpha\text{-CHT}$ Domains



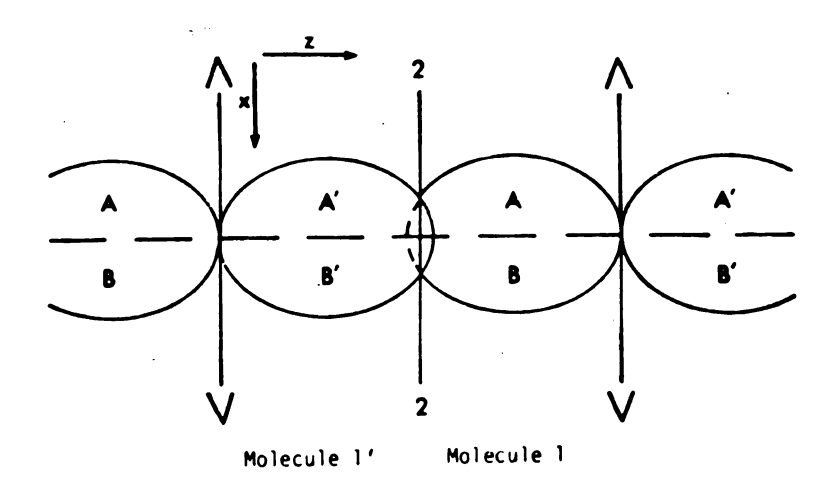


FIGURE 25. Intermolecular Domain Contacts in $\alpha\text{-CHT}$ Crystalline Dimer--a) Schematic of Cross-Distance Diagonal Plot, and b) Linear Packing of Dimers and Domains of $\alpha\text{-CHT}$

9

۲ 2 0

ge be

fr r

tn is

or

R ij mol dia

Īŋ;

d:a

proximity to these atoms. A substitution can also be examined in a similar manner. We have termed these as difference distance plots and difference substitution plots, respectively. The definition of the quantity plotted, R_{ij} , is presented in Figure 26. In the difference distance plot, the \mathbf{C}_{α} atoms, i and j, and the difference Fourier peaks are not simply considered as points. Instead, a prolate ellipsoid surface is generated as an ellipsoid of revolution about the line between i and j. By allowing the sum of the distances from the peak to i and to j to equal the separation, \mathbf{r}_{ij} , increased by 2 $\mathring{\mathbf{A}}$ as appears below

$$R_{ij} = r_{ij} + 2 \mathring{A} \le |r_{pi} + r_{pj}|$$

the equation for the resulting ellipsoid of revolution is

$$x^{2}/(R_{ij}/2)^{2} + y^{2}/((R_{ij}/2)^{2} - (r_{ij}/2)^{2})$$

+ $z^{2}/((R_{ij}/2)^{2} - (R_{ij}/2)^{2}) = 1,$

or

$$x^2/(r_{ij}/4 + r_{ij} + 1) + y^2/(r_{ij} + 1) + z^2/(r_{ij} + 1) \le 1.$$

Thus, if a peak occurs within this surface, its value, R_{ij} , is plotted. Moreover, the R_{ij} of the two independent molecules of $\alpha\text{-CHT}$ dimer are plotted on either side of the diagonal of the distance plot. Thus, deviations from diagonal symmetry represents asymmetrical behavior. An

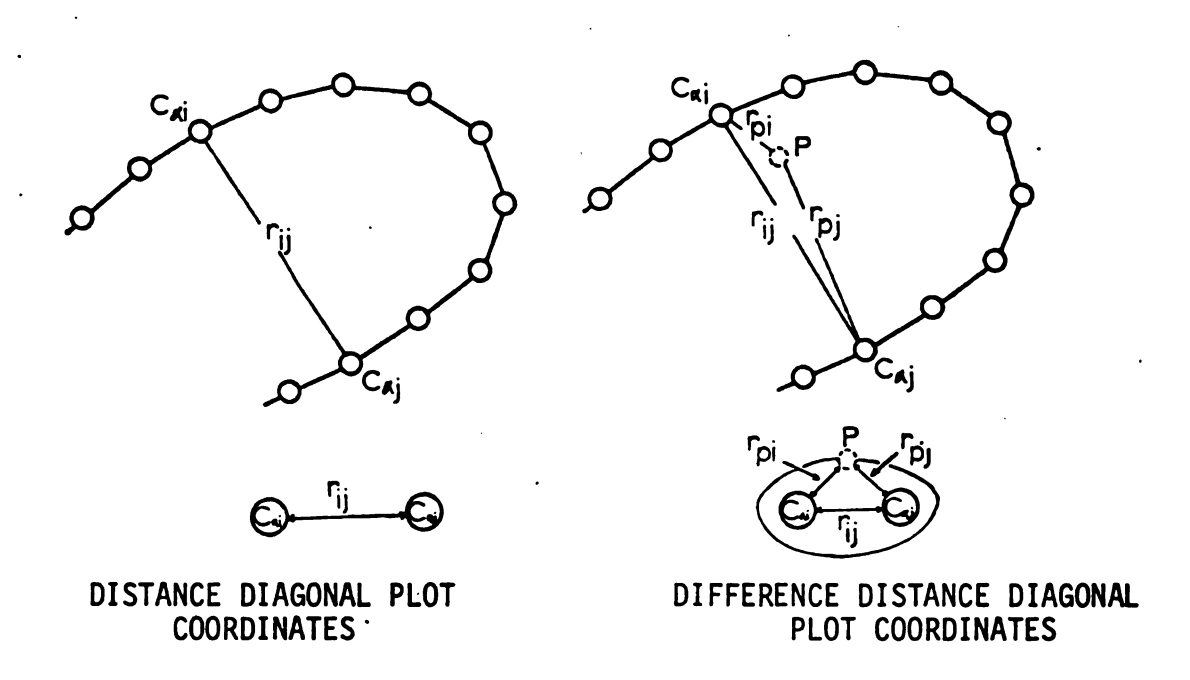


FIGURE 26. Definitions for Diagonal Distance Plot and for Difference Distance Plots

the pH is for its the

exa

٥.

inh

Tab

mo: spe var

Ē.

ne t

inc The beti

ring

non.

example of the difference distance plot calculated from the difference Fourier map obtained from changing the pH of α -CHT from pH 3.6 to pH 7.3 in the presence of PEBA is shown in Figure 27a. The substitution distance plot for PEBA pH 7.3 using the peaks of the substitution itself are shown in Figure 27b. Appendix C contains a list of all difference Fourier peaks used in calculating the difference distance plots of this work along with their peak heights. The substitution peaks are listed in Table A-1.

D. Inhibitor Orientation in the Independent Molecules

The detailed comparison of the orientation of each inhibitor molecule used in this study in the independent molecules of α -CHT dimer probes both the source of the specificity of α -CHT and the effects of the dimeric variability in structure.

E. <u>Inhibitor Orientation Definitions</u>

In comparing the inhibitor orientations, three parameters have been defined and examined, an x-z and x-y inclination angle and an aromatic ring rotation angle.

The inclination angles are defined as the angles formed between a line from the C-l to C-4 positions of the phenyl ring and the x-z or x-y planes, which are parallel to the non-crystallographic two-fold axis (Figure 28). Inhibitors

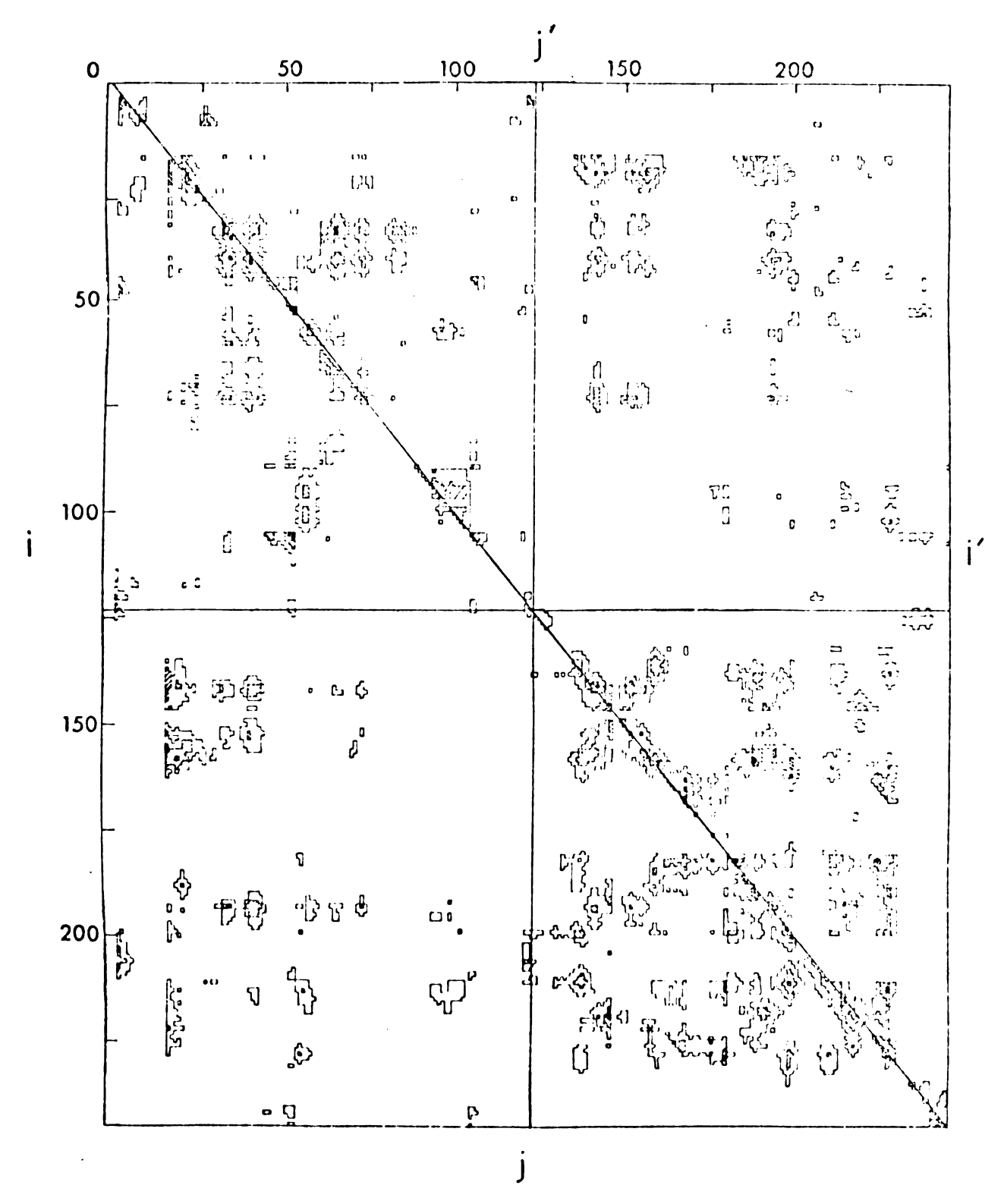


FIGURE 27a. Difference Distance Plot of Conformational Changes on Increasing the Native, pH = 3.6 $\alpha\text{-CHT}$ Crystal to pH = 7.3 in the Presence of PEBA

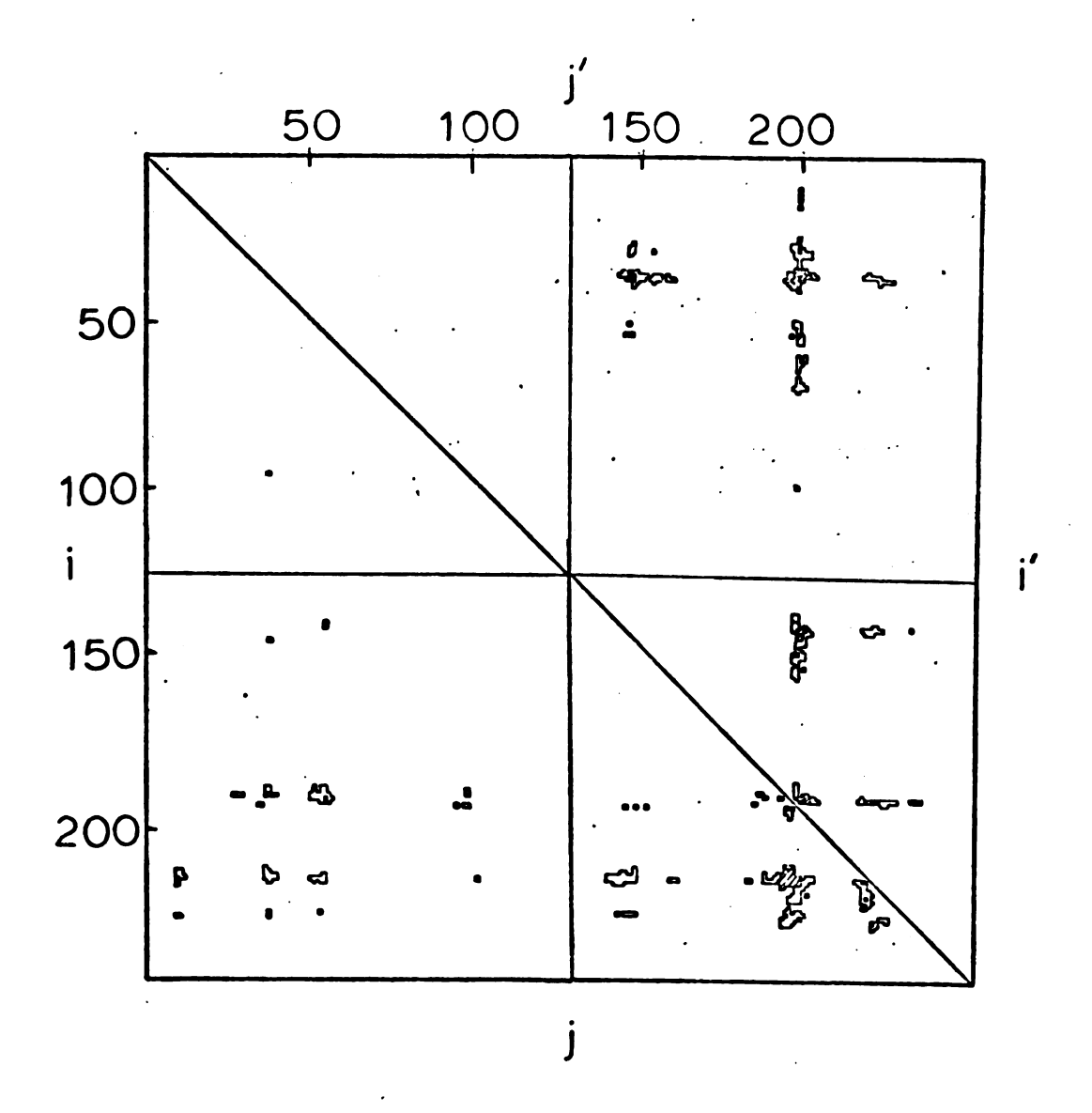
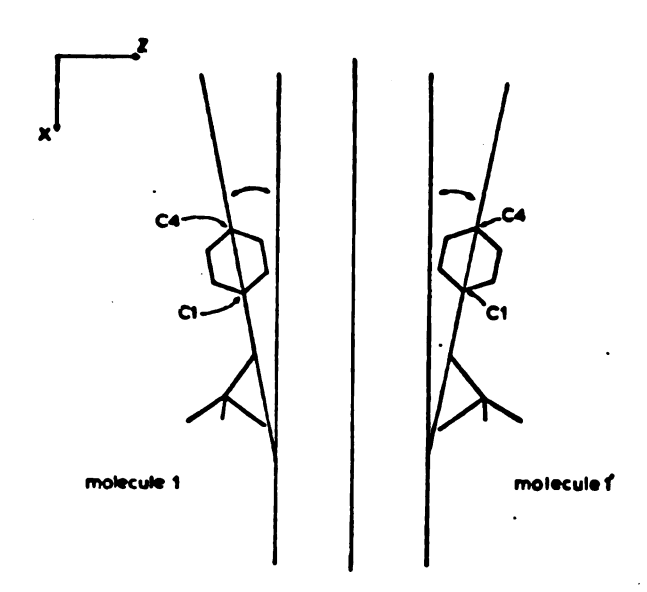
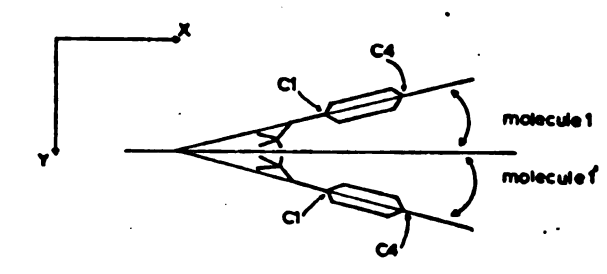


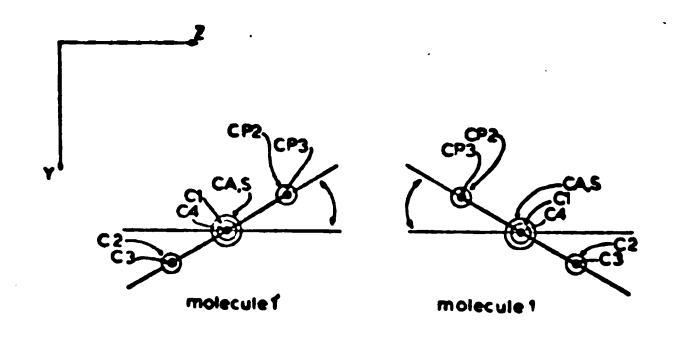
FIGURE 27b. Substitution Distance Plot of Substitution of PEBA Observed on Increasing the Native, pH = $3.6~\alpha$ -CHT Crystal to pH = 7.3



x-y INCLINATION ANGLE



x-z INCLINATION ANGLE



AROMATIC ROTATION ANGLE

FIGURE 28. Definition of Orientation Angles for Comparison of Inhibitor Orientation

which are oriented identically in the specificity sites of the two independent molecules would have inclination angles which are identical in magnitude but opposite in sign. Values of 0° in the inclination angles are observed when the Cl-C4 line is parallel to the two-fold axis in the x-z or x-y plane.

The aromatic ring rotation angle defines the orientation of the phenyl ring of the inhibitor by rotation about the line joining Cl to C4 (also, Cl to CA or Cl or S). It is taken to be 0° when the ring lies in the x-z plane if the x-y inclination angle is set equal to 0°. The positive rotation direction is taken to be a clockwise rotation around the Cl-CA or Cl-S bond when viewed from the Cl side. The rotation angle for two identically oriented inhibitors would also be identical in magnitude but opposite in sign.

A.

the sub

nat

sim hea

uni

cal

TOS PMS NAT

_

The that

appr

The Stru

IV. RESULTS AND DISCUSSION

A. Irreversible Inhibitors

1. Substitution characteristics of TOS and PMS

Initial examination of the diffraction pattern along the principal axes of the TOS and PMS derivatives revealed substantial but similar intensity changes when compared to native α -CHT (Figure 23). Moreover, the changes are similar in magnitude to those observed with isomorphous heavy atom derivatives. The lattice parameters of the unit cells show little difference in dimensions beyond the calculated error (Table 9).

TABLE 9 Comparison of Cell Parameters of Irreversibly Inhibited $\alpha\text{-CHT}$

	a(Å)	b(Å)	c(Å)	β (°)	Volume (Å ³)
TOS pH 3.6	49.15(5)	67.02(6)	65.88(9)	101.78(3)	212,400(700)
PMS pH 3.6	49.36(4)	67.25(5)	65.98(6)	101.78(6)	214,400(600)
NAT pH 3.6	49.24(7)	67.20(10)	65.94(9)	101.79(6)	213,600(1000)

The cell volume of TOS appears to shrink slightly while that of PMS expands slightly; however, both differences approach the limit of error in the native cell volume. The larger standard deviation indicated for the native structure results from the combination of the seven

se wh th

di

de

000

by syr

0.6

Süb

occ Fur

sho

Var

In Wer

nat Exa

dif

str der

ele: des:

and

separate native crystals used in the data collection (34) while the errors for the derivative structures represent the parameters for the one single crystal used for three-dimensional data collection.

A preliminary examination of the difference electron density maps showed that the substitution approaches 100% occupancy, as expected from solution studies of inhibition by aromatic sulfonyl fluorides, with excellent two-fold symmetry with respect to occupancy. The active site substitution of TOS in molecule 1 reaches $0.65 \text{ e}^{\text{A}-3}$ and $0.62 \ e \mathring{\text{A}}^{-3}$ in molecule 1'; while in PMS, the corresponding occupancies are 0.62 e^{A-3} and 0.65 e^{A-3} , respectively. Further study of the substitution density of TOS and PMS showed differences in orientation reminiscent of the variability and asymmetry in the native structure (42). In addition to the substitution density, gradient peaks were observed, indicative of small rearrangements of the native enzyme structure to accommodate the inhibitors. Examination of peaks greater than 3 x $\sigma(\Delta \rho)$ in the difference maps showed more extensive changes in the structure with the PMS derivative than with the TOS derivative.

Construction of x-z and x-y composite difference electron density projections of the substitution, as described in the Methods section, revealed significant and consistent differences in the inhibitor binding

of
tiv
dis
Tab
by
in
cal
the
reg
bas
est

ori

dir obse bel

The

rot

fitt

in t

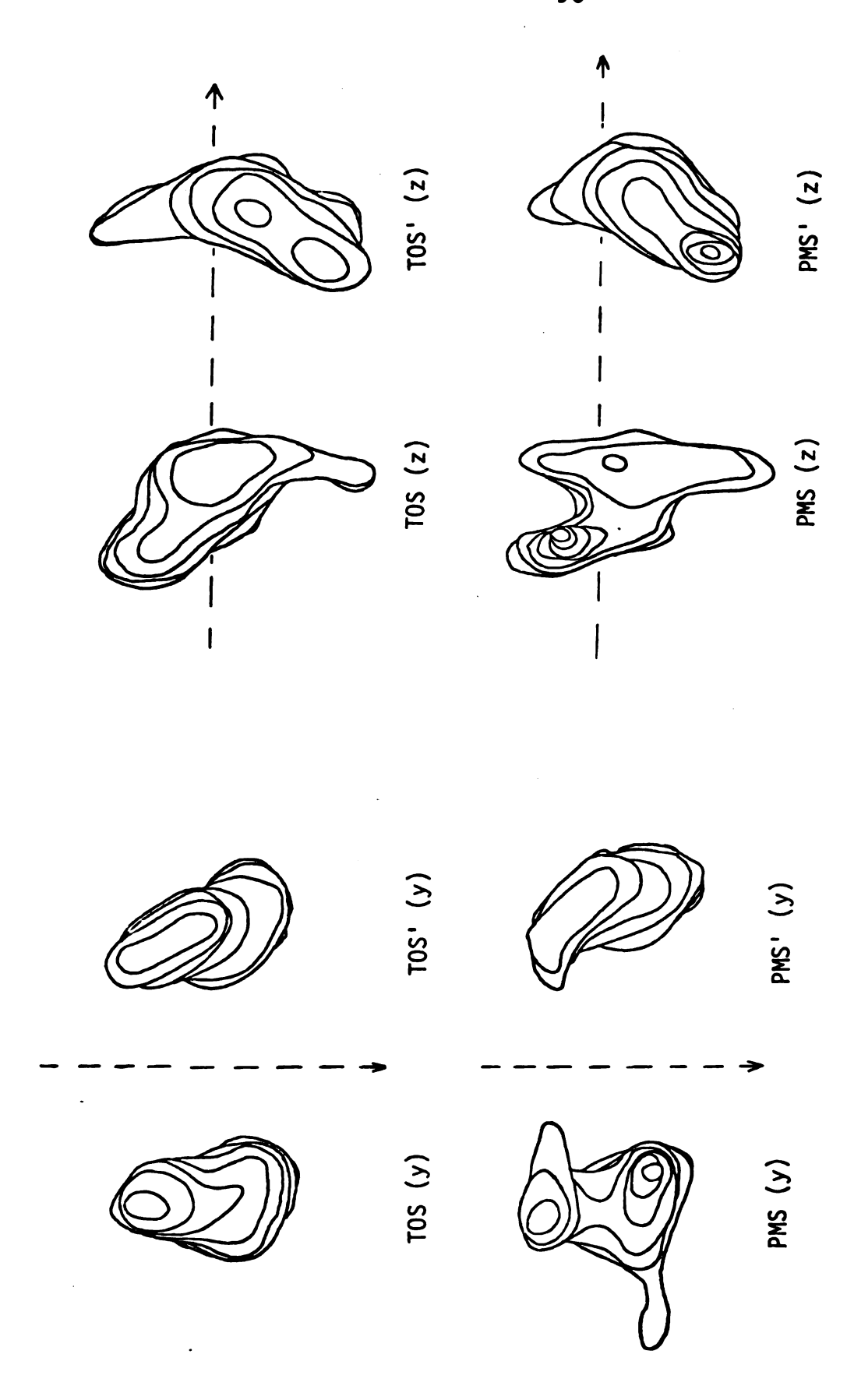
àre

ţanc

orientation both between the two independent molecules of the α -CHT dimer, and between the TOS and PMS derivatives (Figure 29). A detailed comparison of the centroid distribution of the inhibitor density is summarized in Table 10. The comparison within the dimer was accomplished by the rotation of the electron density of the substitution in molecule 1' about the two-fold axis followed by the calculation of the differences in centroid positions in the specificity region (x < 49/76) and in the catalytic region (x > 50/76). These regions were selected on the basis of inhibitor interactions as discussed later. The estimated error in these comparisons is about 0.4 Å; thus, only the differences in the y-direction are significant. The systematic difference across the two-fold axis (the rotated density of molecule 1' is displaced in the (-)ydirection) is compatible with the variability in structure observed in the dimer and will be discussed more fully below.

Kendrew models of the inhibitor molecules were fitted to the composite bounded difference electron density and atomic coordinates were measured as discussed in the Methods section. The atomic coordinates determined in this manner for all the inhibitors used in this study are listed in Table A-1 and these were used in all distance calculations and comparisons. The bond lengths of





Variability Between Irreversible Inhibitors Viewed Down y,z-Axis, Contoured at 0.15 eA⁻³ with Approximate Two-Fold Representation FIGURE 29.

Comparison

TABLE 10

Comparison of the Centroid Positions of Substitution Density in the

Active Sites of Molecules 1 and 1' (TOS and PMS)

(') denotes molecule l'

Comparison of Rotation About Two-Fold Axis of the Substitution in Molecule 1', Followed by Averaging the Deviation from Molecule 1 ъ

<pre>specificity pocket (x < 49/76)</pre>	catalytic pocket	(0//0c = x)
ΔZ = 0.24 Å	δ = 0.41 Å	' SM'
Δ <u>y</u> = -1.25 Å	Δ <u>y</u> = -0.70 Å	PMS '
PMS	SWd	
Δ <u>z</u> = 0.24 Å	Δ z = 0.35 Å	T0S'
۵ <u>۷</u> = -1.25 Å	∆ <u>y</u> = -0.91 Å	10S'

T0S

T0S

Comparison of Irreversible Inhibitor Substitution in Each of the Independent Molecules of the Crystalline $\alpha\text{-CHT}$ Dimer ۵.

<pre>specificity pocket (x < 49/76)</pre>	<pre>catalytic pocket (x > 50/76)</pre>
$\Delta \bar{z} = 0.13 \text{ Å}$	$\Delta \tilde{\mathbf{z}} = 0.05 \text{ Å}$ $T0S'$
∆ <u>y</u> = -0.05 Å	∆ <u>y</u> = -0.19 Å TOS'
PMS '	PMS.
Δ z = -0.13 Å	$\Delta \bar{z} = -0.15 \text{ Å}$
$\Delta \bar{\mathbf{y}} = 0.06 \text{ Å}$	$\Delta \bar{\mathbf{y}} = -0.26 \text{ Å}$
	PMS

The deviation between the centroid positions of TOS in molecules 1 and 1' in the catalytic pocket is -0.91 Å (Δy) and 0.35 Å (Δz). Example:

Ta

th

se

fr a:

to w³

ti

in (

T(

re b

5

đ

i

d a

j

ā

the individual inhibitor molecules are also reported in Table A-2.

2. Orientation of inhibitor molecule and interaction with α -CHT

The orientation angles, as defined in the Methods section, for TOS and PMS and the other inhibitors used in this study are presented in Table 11. It is apparent from this table that the two-fold related pairs, TOS-TOS' and PMS-PMS', exhibit good two-fold symmetry with respect to the x-y and x-z inclination angles, but are asymmetric with respect to the aromatic rotation angle. The orientations of TOS and PMS in each of the independent α -CHT molecules differ in both their x-y inclinations and aromatic rotation angles. The differences between the TOS and PMS derivatives can be related to the specificity requirements of α -CHT, while the two-fold asymmetry in both derivatives can be related to the structural variability of the dimer. A more detailed comparison of the individual inhibitor molecular orientations and interactions with the enzyme, and a full comparison of the TOS derivative results with those reported by the MRC (49), are given below.

The effect of the variability of α -CHT structure on inhibitor orientation can be seen by examining the interactions which occur between α -CHT and the inhibitors. A

TO TO PM

PE PE PE PE

TABLE 11
Orientation Angles Determined for the
Inhibitor-Enzyme Structures

Derivative	Inclination Angle (x-y) (<u>+</u> 5°)	Inclination Angle (x-z) (<u>+</u> 5°)	Aromatic Rotation Angle (<u>+</u> 10°)
TOS MSU	+44	-12	+10
TOS' MSU	-42	+ 9	-30
TOS MRC ¹	+40	-12	+14
PMS	+65	-12	+ 0
PMS'	-65	+ 8	-45
PEBA pH 3.6	+48	-12	+60
PEBA' pH 3.6	-39	+ 8	- 75
PEBA pH 5.4	+48	+ 5	+45
PEBA' pH 5.4	-39	+ 8	-45
PEBA pH 7.3	+45	- 4	+30
PEBA' pH 7.3	-32	+ 8	-20
PPBA	+41	+ 5	+70
PPBA'	-44	- 2	?
PBBA	+41	+ 5	+70
PBBA'	-42	- 2	?

Calculated from coordinates reported by Birktoft and Blow, <u>J. Mol. Biol</u>. <u>68</u>, 187 (1972).

summary of protein:inhibitor contacts which are 3.5 Å or less (van der Waals) of all the inhibitors used in this study is given in Table 12. The individual protein: inhibitor contacts are listed in Table B-1. This table was compiled using the inhibitor coordinates and a set of α -CHT coordinates which resulted from one cycle of Diamond's model-build procedure. Only the coordinates of molecule 1 were used and the analysis was based on the inhibitor interactions in molecule 1 and the known variability in both inhibitor orientation and enzyme conformation (42) as determined from the difference electron density maps.

From Table 12, it is apparent that the majority of van der Waals contacts between the aromatic group of the inhibitor and the protein molecule involve residues TRP 215-GLY 216. The structure of the α -CHT dimer in this region of the specificity pocket (i.e., residues TRP 215-SER 218) shows significant deviations from local two-fold symmetry, due either to repulsive or attractive interactions (42). The orientations of TOS and PMS in x-z projection are shown in Figure 30, which also details some interactions in the specificity pocket. The shortest contacts occur with GLY 216 C_α , thus establishing its importance in defining a boundary to the specificity pocket. This is in agreement with observations in

TABLE 12a

Summary of van der Waals Contacts (≤ 3.5 Å) Between Native lpha-CHT and the Inhibitor Molecules

		Inhibitor	itor Molecule	Molecule Contact Region	egion		Total	Total	
Derivative		Toluyl- Methyl	Aromatic Group	Alkyl Chain	2	က	Specificity Pocket	Catalytic Pocket	Total
TOS MSU	3.5 A 3.0 A	94	13	1 1	14		98	25 16	44
TOS MRC	3.5 3.0 A	0 2	16 2	1 1	12	10	21 2	22 12	43 14
PMS	3.5 A 3.0 A	1 1	14 4	٥ -	15 8	۳ 8	14 4	27 16	41
PEBA pH 3.6	3.5 A 3.0 A	1 1	15 7	4 L	က က	ა 4	15 7	14 8	29 15
PEBA pH 5.4	3.5 A 3.0 A	1 1	26 9	N 22	00 9	11	26 9	26 17	52 26
PEBA pH 7.3	3.5 3.0 A A	1 1	25 12	- D	o 5	ο α	25 12	23 14	48 26
PPBA	3.5 A 3.0 A	1 1	30 17	9 -	92 8	12 9	30	34 18	64 35
PBBA	3.5 A 3.0 A	1 1	26 16	10 6	91	10	26 16	36 21	62

Calculated from coordinates reported by Birktoft and Blow, <u>J. Mol. Biol.</u> <u>68</u>, 187 (1972).

Non-hydrogen bonded interactions in catalytic site (x \geq 50/76).

Potential hydrogen bonded interactions in catalytic site (x \geq 50/76).

Summary of Inhibitor Contacts with Specific Residues of Native $\alpha\text{-CHT}$ (< 3.5 Å) TABLE 12b

							Amino	Amino Acid Residue	Resid	ne Te					
	Derivative	42	57	190	191	192	193	194	195	213	214	215	216	217	220
Toluyl- methyl	TOS MSU TOS MRC ¹	1 1	1 1	1 1	1 1	1 1	1 1	1 1	1 1	1 1	1 1	2 1	ოო	- 2	1 1
Aromati c Group	TOS MSU TOS MRC ¹ PMS PEBA PH 3.6 PEBA PH 5.4 PEBA PH 7.3	1 1 1 1 1 1 1	1 1 1 1 1 1 1	1 1 1 1 9 9 0	- 2 1 1 9 5 5	ורונטוו			-4-1111	1 1	2 1 2 2 1 - 1	224 EL 29	0 K 0 V 4 8 Q	1110011	
Alkyl Chain	PBBA TOS MSU TOS MRC PMS PEBA PH 3.6 PEBA PH 5.4 PEBA PH 7.3 PPBA		1 111111	0 1111111	8 1111-111				1 11162247	1 1 1 1 1 1 1 1		נווווווו	0		

Table 12b. (cont'd.)

Table 12b. (cont'd.)

							Amin	Amino Acid Residue	Resid	ne					
	Derivative	42	22	190	191	192	193	194	195	213	214	215	216	217	220
o e	TOS MSU TOS MRC PMS PEBA PH 3.6 PEBA PH 5.4 PEBA PH 7.3 PEBA PH 3.6 PEBA PH 3.6 PEBA PH 3.6 PEBA PH 3.6 PEBA PH 7.3 PEBA PH 7.3	11111110 1111111	111-1111 -11		-40111-1 1-11111	222111 11111	0 1 C 1 E C C C C C C C C C C C C C C C C	0141	5 5 5 5 7 7 7 7 7 7 7 7 7 7 7 7 7 7 7 7						

Calculated from coordinates reported by Birktoft and Blow, J. Mol. Biol. 68, 187 (1972).

Non-hydrogen bonded interactions in catalytic site (x \geq 50/76).

Potential hydrogen bonded interactions in catalytic site (x \geq 50/76).

		900

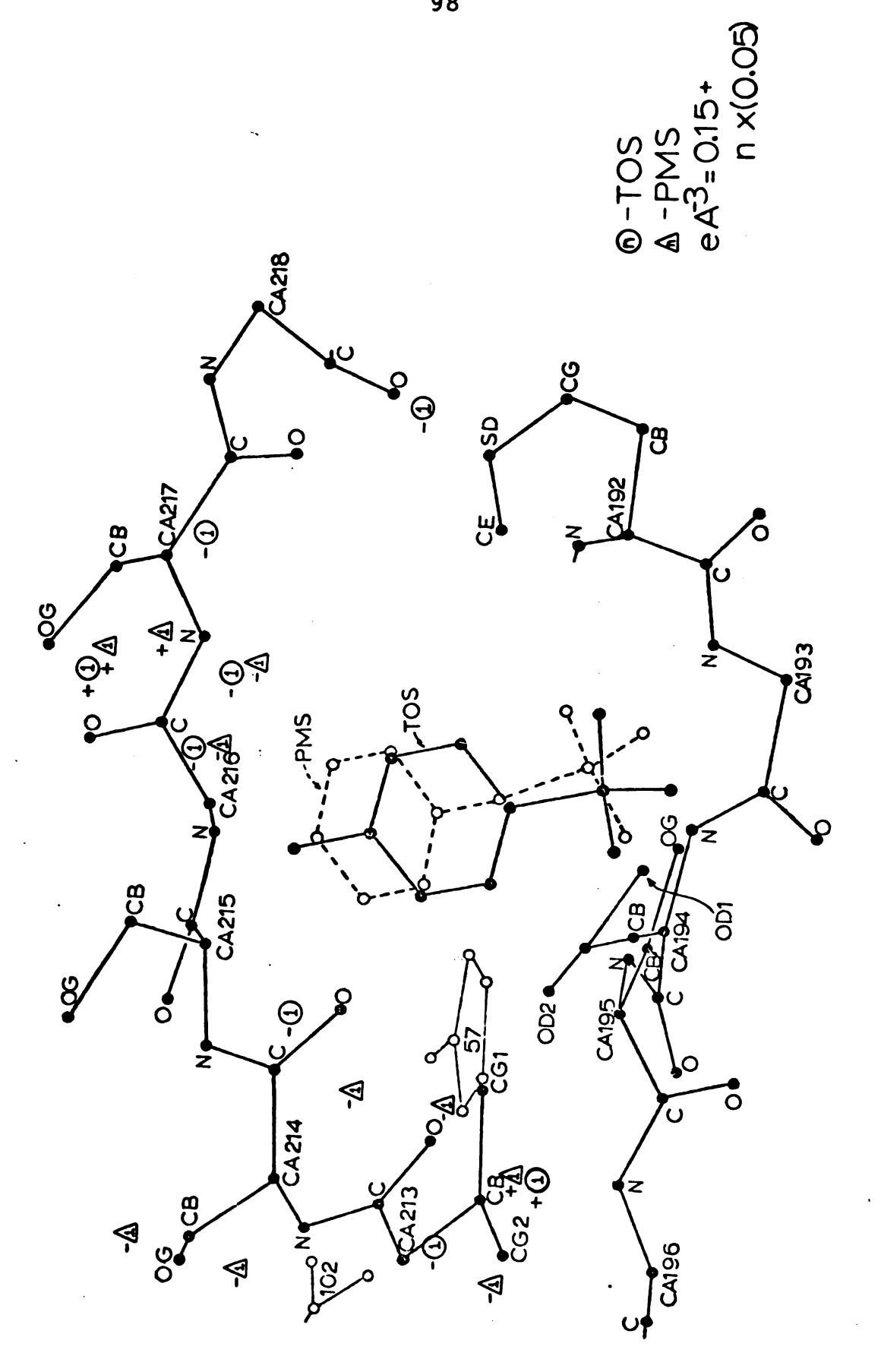


FIGURE 30. TOS and PMS Orientation in x-z Projection of Active Site

the nat sub SER dir SER in (Ta of rot. app, inh enzy dist cont 105 201 to b

aror

14 c

g 2 J

to a

arom

nota

It w

ela

elastase where substitution of this GLY with VAL modifies the specificity by reducing the size but not the chemical nature of the side-chains of acceptable elastase-specific substrates (54). The observed displacement of the TRP 215'-SER 218' chain by approximately 2 \mathring{A} in both the y- and xdirections from the two-fold related position of TRP 215-SER 218 (42) appears to be responsible for the differences in orientation of the aromatic groups of TOS and PMS (Table 11). The observed displacement in the y-direction of the phenyl group (Table 10) and its difference in rotation between molecule 1 and molecule 1' reflects an apparent attempt to maintain maximum contact between the inhibitor phenyl ring and the specificity pocket of the There are approximately 19 contacts within a distance of 3.5 Å to the phenyl group of TOS and 14 contacts to PMS. The main difference in contacts between TOS and PMS comes from six additional contacts of the TOS methyl group; thus, approximately 13 contacts appear to be responsible for maintaining the orientation of the aromatic group of TOS which compares favorably with the 14 contacts observed with PMS. Although there might be a slight difference in orientation between TOS and PMS to accommodate the CA of PMS, the contact region for the aromatic group remains constant. The contact region is notable in that it principally involves main chain atoms. It would therefore appear that the specificity site might

be influenced, or even possibly determined, by the conformation of the main chain. The only polar groups in this region are the carbonyls and amides of the main chain with the remainder being hydrophobic in nature. The side-chains of residues SER 214-SER 217 other than GLY 216 extend away from the pocket. A more detailed examination of the specificity region will be discussed with the PEBA results since this inhibitor more closely resembles a typical substrate.

The difference electron density maps contain peaks other than those attributable to substitution of an inhibitor which occur at much lower electron density levels are are probably associated with changes in the native conformation which accompany the binding of an inhibitor in the active site. These changes are indicated schematically in the x-z projection of the specificity region by circles for TOS and triangles for PMS (Figure 30), the enclosed number giving the peak height of the change in $e\mathring{A}^{-3}$. The difference peaks indicate a small reorientation of the main chain from SER 214-SER 218 to accommodate the inhibitor, and principally involves sections of the polypeptide chain making close van der Waals contacts (< 3.5 Å) between the native enzyme and inhibitor. The changes of molecule 1 do not have exact two-fold correspondence in molecule 1' due to variability in the native structure between TRP 215-SER 218 (42).

The differences observed in molecule 1 are larger and more extensive than those in molecule 1' and suggest a small enlargement of the specificity pocket of molecule 1 to approximate that present in molecule 1'. The asymmetric inhibitor accommodation leads to a dimeric molecule satisfying the two-fold symmetry more exactly. Although the phenyl and the sulfonyl groups are relatively fixed in their interactions in α -CHT, the orientation of the phenyl groups in TOS and PMS must be slightly different to accommodate the additional tetrahedral carbon atom of PMS (C1-CA-S angle is \sim 110°). The difference in orientation between the phenyl groups of TOS and PMS is achieved by the increased flexibility in orientation of the phenyl ring in PMS due to rotational freedom about the C1-CA and CA-S bonds.

The exact orientation of the sulfonyl group in the catalytic site is not immediately discernible from the difference electron density maps due to the limitations imposed by 2.8 Å resolution data, and to the presence of a sulfate ion adjacent to SER 195 0_{γ} in native α -CHT (94) which is displaced by both TOS and PMS. Although the sulfur atom of TOS and PMS must maintain an approximately tetrahedral arrangement utilizing one carbon atom and three oxygen atoms (one of which is SER 195 0_{γ}), this tetrahedral array is not directly observable. To

establish a more accurate and detailed representation of the interactions of the sulfonyl group with SER 195, it was necessary to apply chemical knowledge. Although actual distortions from a tetrahedral sulfur will be somewhat obscured as a consequence, any such distortion should not introduce significant misinterpretation.

Among the factors used in determining the orientation of the sulfonyl group were: 1) optimization of potential interactions generated by rotation about the C1-S bond of TOS or C1-CA and CA-S bonds of PMS; 2) presence of hydrogen-bonding solvent molecules as evidenced by positive difference electron density located adjacent to the sulfonyl electron density; and 3) difference density gradients involving reorientation of SER 195 0_{\odot} .

A positive peak which occurs in the difference electron density map in the immediate vicinity of the sulfonyl group was assigned to a solvent molecule in both the TOS and PMS derivatives and in both molecules 1 and 1'. It is labeled as $\rm H_2O$ in the composite difference electron density projections shown in Figure 29. Assignment of such peaks to water or solvent molecules is common in protein crystallography. In addition to the sulfate ion assignments of MSU α -CHT, where sulfates have been found in particularly ordered positions, counter ions have also been suggested (94). Due to the covalent bond between TOS and SER 195 $\rm O_{_Y}$ with the resultant orientation

С

M) (

fo

in

du.

in

axi it

red in

H H

the chan

SER

of the sulfonyl group, the water molecule appears to be highly ordered and hydrogen-bonded, thus defining the position of one sulfonyl oxygen.

Further evidence for orienting the sulfonyl group (which relates the TOS and PMS derivatives directly) involves a density gradient at the SER 195 0_{γ} position; in the derivatives the SER 195 hydroxyl moves approximately 1.5 Å by a rotation of approximately -60° (counterclockwise) about the C_{α} - C_{β} bond. The native SER 195 0_{γ} position is 2.4 Å from the sulfur in both derivatives, much longer than the accepted S-O bond length ($\sim\!1.4$ Å).

The difference peaks in the vicinity of the sulfonyl in molecule 1' differ from those in molecule 1 similarly for both the TOS and PMS derivatives. This is probably due to the slight difference in positioning of SER 195 and SER 195' (42). In molecule 1' the SER 195 0_γ lies in an x-z plane which passes closer to the local two-fold axis than the similar plane in molecule 1. Once again, it appears that the binding of both TOS and PMS tends to reduce some of the variability of structure which occurs in the dimer. Such effects have also been noted with the pH 5.4 conformer by Vandlen and Tulinsky (41).

The difference electron density map also shows that the native active site conformation undergoes significant changes upon binding TOS and PMS. The catalytic triad, SER 195-HIS 57-ASP 102, appears to transmit the effects of

the covalent involvement of SER 195; HIS 57 rotates counter-clockwise about its C_{α} - C_{β} bond away from the new SER 195 0_{γ} orientation and ASP 102 retracts slightly from its position near HIS 57. The peaks associated with these changes appear somewhat larger in the PMS derivative and probably reflect an additional perturbation caused by the CA position which is only about 4 Å away from HIS 57 NE2. In TOS, the ASP 102 movement is smaller than that observed in PMS and is just above the observable limit. The movements involving HIS 57 and ASP 102 occur similarly in both molecules.

Other significant changes in the active site are associated with residues involved in the dimer interaction. The B-chain carboxyl terminus, TYR 146', is positioned in the active site region of molecule 1 (and vice versa) and interacts via a hydrogen bond from OEE to a sulfate ion, which in turn is hydrogen bonded to SER 195 0_{γ} ; in addition, the carboxylic acid group of TYR 146' interacts with HIS 57. The sulfate is lost on inhibition, expelled by the sulfonyl group of TOS and PMS, and subsequent reorientation of HIS 57 produces changes in TYR 146'. This reorientation is resolved by a rotation of approximately -40° about the C_{α} - C_{β} bond of HIS 57. The change in unit cell volume accompanying the introduction of the methylene group in the PMS

derivative is probably a result of increased interaction with TYR 146 of the two-fold related molecule, which in turn, can affect the dimer interface.

MET 192, which shows an asymmetric orientation about the local two-fold axis in the native dimer to minimize the non-covalent S_{γ} - S_{γ} , contact, exhibits a complex movement on inhibition of the enzyme. The close approach of MET 192 to MET 192' (\sim 3 Å) (42) makes a detailed analysis of this region difficult but it would appear that a rotation occurs about the C_{β} - S_{γ} bond.

Another region displaying electron density changes which occur in both the TOS and PMS derivatives involves the disulfide bridge of CYS 191-CYS 220. Similar observations have been made in other derivative studies in this laboratory (18). Such features might be due to the higher electron density associated with the sulfur atoms in the native structure so that small changes in the position can easily produce observable difference density peaks of 0.20 $e {\rm \mathring{A}}^{-3}$ or larger.

3. Comparison of TOS (MSU) and TOS (MRC)

It has already been noted that the structure of $TOS-\alpha-CHT$ was also determined by the MRC group (49). The TOS derivative was used as the parent compound by the MRC group in phase determination. The approximations concomitant with such an approach have already been detailed

in addition to others such as averaging the structure of the two independent molecules of the dimer.

The unit cell parameters of the MRC and MSU structures are compared in Table 13.

TABLE 13

Comparison of Unit Cell Parameters of TOS (MSU) and TOS (MRC)

	a(Å)	b(Å)	c(Å)	(°)	Volume (Å ³)
MSU					
TOS-pH 3.6 75% saturated Ammonium Sulfate	49.15(5)	67.02(6)	65.88(9)	101.78(3)	212,400(700)
NAT-pH 3.6 (34)	49.24(7)	67.2(1)	65.94(9)	101.79(6)	213,600(1000)
MRC					
TOS-pH 4.2 (49), 65% saturated Ammonium Sulfate, 0.1 M citrate, 2% dioxane	49.3(1)	67.3(1)	65.9(1)	101.8(1)	214,000(1100)
NAT-pH 4.2 (47)	49.1(1)	67.4(1)	65.9(1)	101.7(1)	214,000(1100)

The apparent shrinkage in unit cell volume upon tosylation observed in the present work is not indicated in the MRC work. The changes in the MSU cell parameters, although small, appear significant in comparison with changes

observed as a function of pH. The large standard deviations of the MRC results could possibly arise from the introduction of dioxane into the crystallization solvent.

The TOS orientation, generated from the MRC coordinates, is shown in xz projection in Figure 31. Comparison with the results of this study (Figure 32) shows small (< 0.5 Å) differences in both the placement of the tosyl group in the active site and the orientation of the chain defining the substrate specificity pocket (SER 214-SER 218) (Figure 31). The gradients indicated in Figure 30 suggest shifts which lead to a structure approximating the tosylated α -CHT structure of the MRC group.

A direct comparison of the tosyl orientations is shown in Figure 32, which indicates that the orientation derived from the averaged structure of the tosylated dimer reported by the MRC group is slightly displaced from both tosyl group orientations of the present study. Both the inhibitor orientation in molecule 1 and in molecule 1' after rotation about the local two-fold axis are compared with the MRC results. The van der Waals contacts in MRC TOS (with TOS- α -CHT [MRC]) have been calculated and are fewer in number than those of MSU TOS (with native- α -CHT) using a limit of 3.5 Å (Table B-1). To compensate for the concerted ~ 0.5 Å

90

o

90/

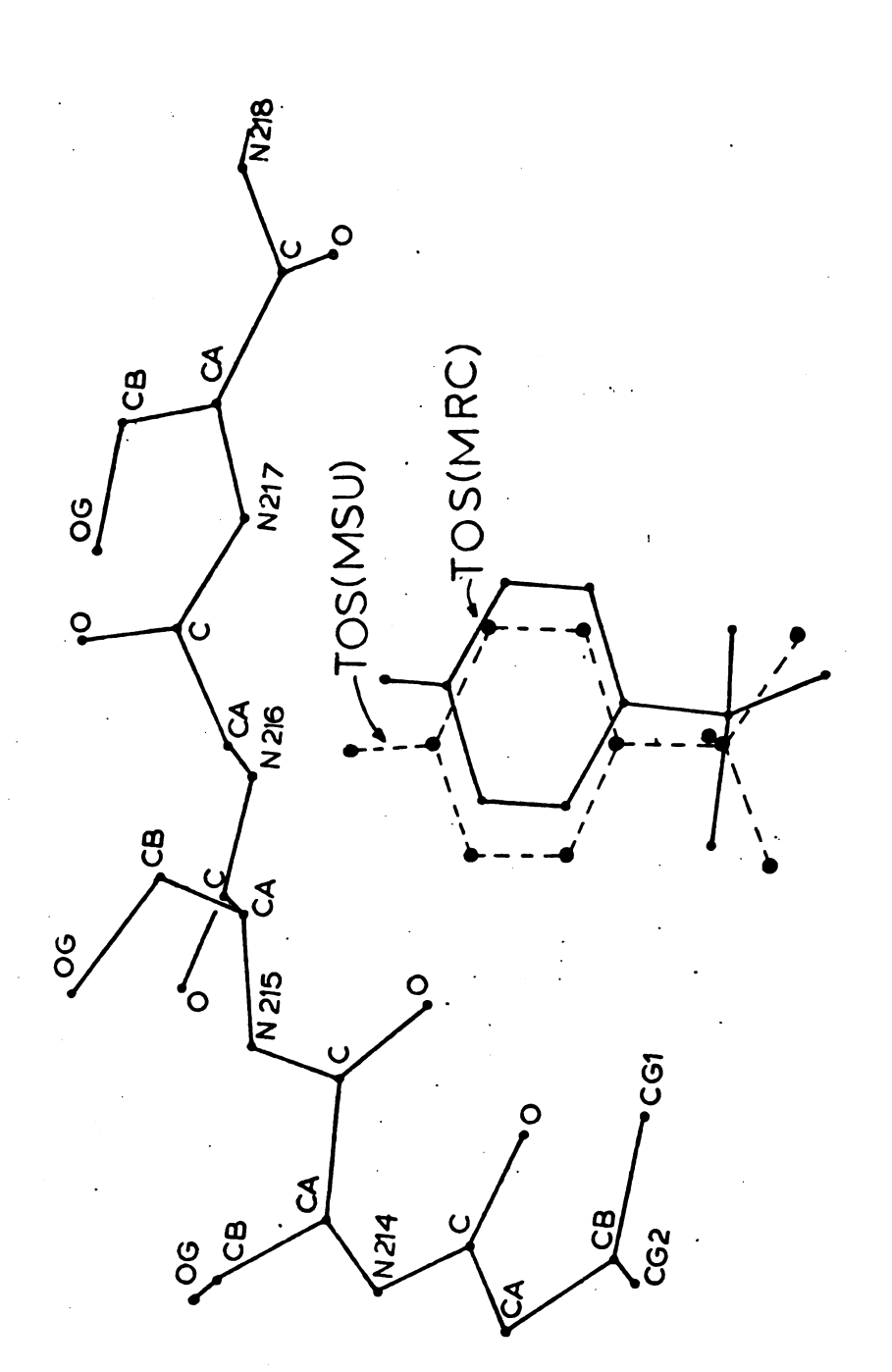
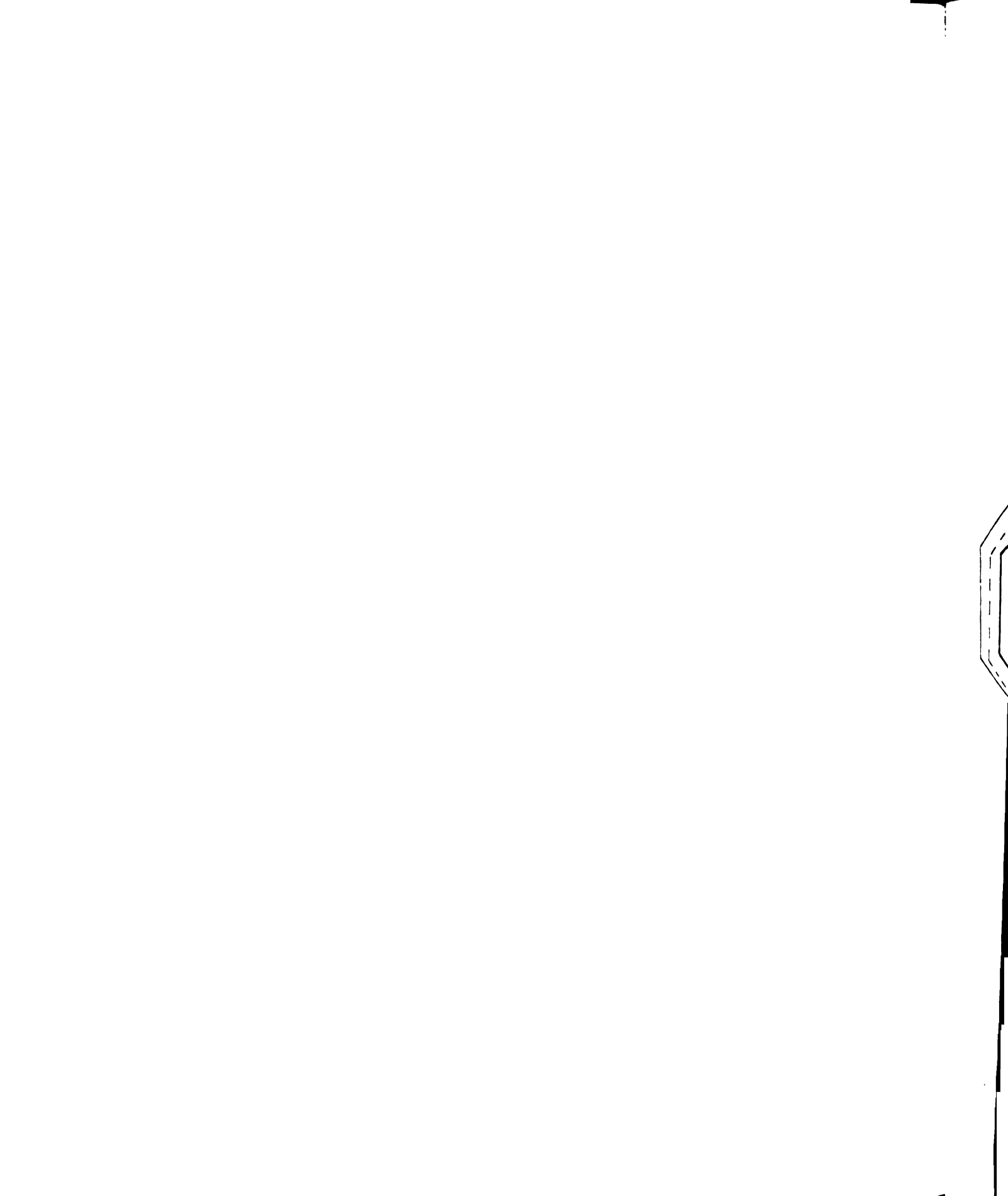


FIGURE 31. TOS (MRC) Orientation in x-z Projection of Active Site (MRC)



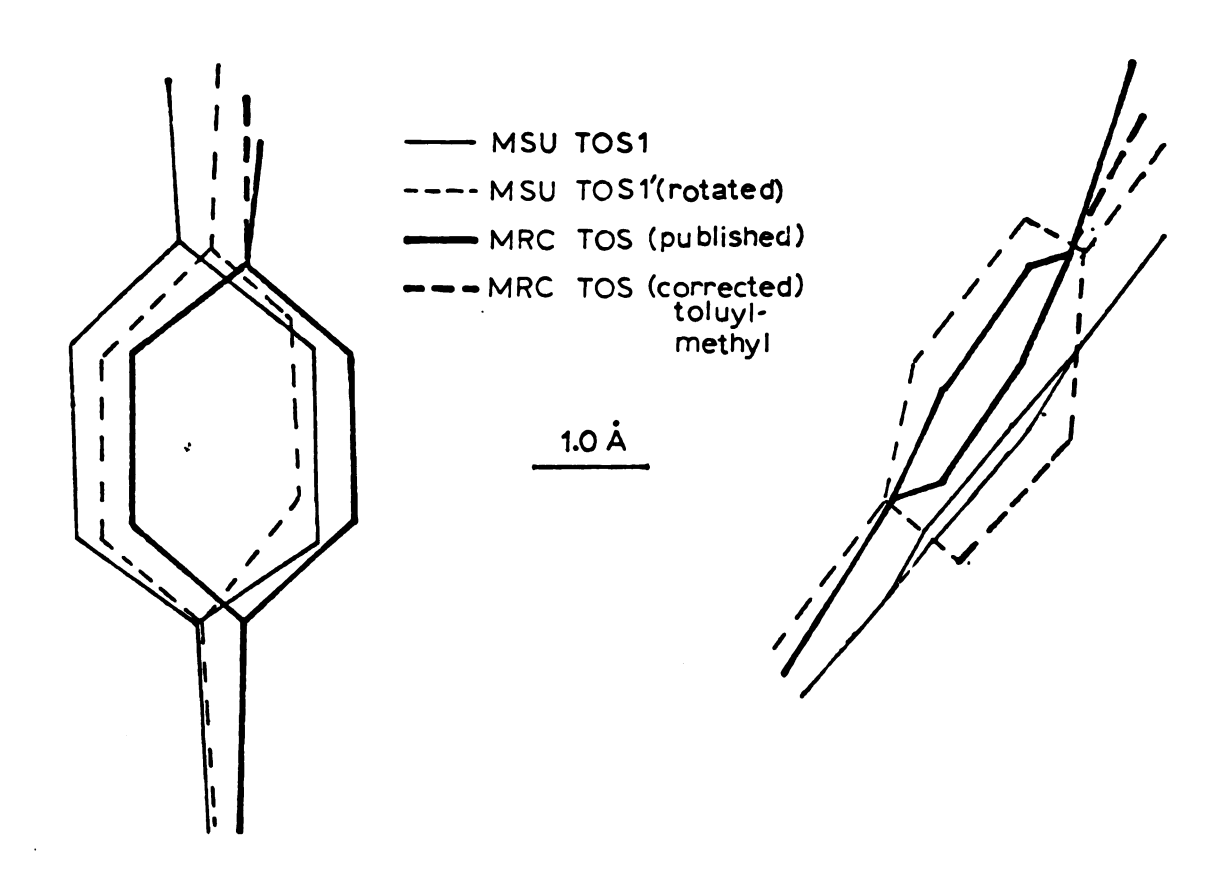


FIGURE 32. TOS (MSU) vs. TOS (MRC) Position

shift in the GLY 216-SER 218 backbone observed in this work upon tosylation, the limit was extended to $4.0\ \mathring{A}$ in examining the MRC results. It can be seen in Table 14 that the number of contacts is comparable in the two studies when the difference in choice of parent enzyme is taken into consideration.

- B. <u>Competitive Reversible Inhibitors:Transition-State</u>
 Analogs
 - Substitution characteristics of PEBA as a function of pH

The α-CHT:PEBA complex was examined with respect to three pH conformers of α-CHT, pH 3.6, pH 5.4, and pH 7.3. As described in the Experimental section, 30 mM PEBA was added to the mother liquor of the desired crystalline pH conformer. The appropriate pH conformer was verified initially by comparison with known axial diffraction patterns and unit cell dimensions. The addition of PEBA produced further significant changes in both the diffraction pattern and unit cell parameters (Table 15).

From Table 15, it can be noted that the addition

Of PEBA to the pH conformers increased the b-axis at

PH 3.6 but decreased it at pH 5.4 and pH 7.3, while the

interaxial angle remained unchanged with the substitution.

These two parameters had proven to be the most sensitive

pH changes in earlier studies, although a pH study

TABLE 14

Comparison of Contacts Within van der Waals Distances Between Tosyl and $\alpha\text{-CHT}$ in MSU and MRC Studies

MRC			21 (49%)	4 (16%)	2 (14%)			22 (51%)	21 (84%)	12 (86%)				
											o	3.0 A	24	14
	CP3)*										o	3.5 A	44	25
tudy	3, C4, C5, CP2,		ı	19 (43%)	8 (33%)	, 03)		1	25 (57%)	16 (67%)	o	4.0 A	ı	43
This Study	(Including atoms Cl, C2, C3, C4, C5, CP2, CP3)*	Total Contacts	4.0 Å	3.5 8	3.0 Å	(Including atoms S, 01, 02, 03)	Total Contacts	4.0 Å	3.5 Å	3.0 Å	Total for all atoms		MSM	MRC

Example: In the MSU study, 43% (19) of the 3.5 Å contacts occur with atoms C1, C2, C3, C4, C5, CP2, CP3. *See Table A-1.

TABLE 15
Comparison of Cell Parameters of PEBA at pH 3.6, 5.4 and 7.3

NAT pH 3.6 49.24(7) 67.20(10) 65.94(9) 101.79(6) 2 PEBA pH 5.4 49.37(3) 67.32(4) 65.73(5) 101.92(6) 2 NAT pH 5.4 49.13(5) 67.83(7) 65.81(7) 101.92(6) 2 PEBA pH 7.3 49.35(2) 67.68(2) 65.98(3) 102.03(4) 2		a(Å)	b(Å)	c(Å)	β(°)	Volume (Å ³)
PEBA pH 7.3 49.35(2) 67.68(2) 65.98(3) 102.03(4) 2		49.36(4) 49.24(7)	67.43(4) 67.20(10)	65.99(6) 65.94(9)	101.83(5) 101.79(6)	215,000(600) 214,000(1000)
PEBA pH 7.3 49.35(2) 67.68(2) 65.98(3) 102.03(4) 2	PEBA pH 5.4	49.37(3)	67.32(4)	65.73(5)	101.92(6)	213,700(500)
	NAT pH 5.4	49.13(5)	67.83(7)	65.81(7)	101.92(6)	214,600(700)
MAI pn 7.3 49.24(2) 67.96(3) 63.65(4) 102.03(3) 2	PEBA pH 7.3	49.35(2)	67.68(2)	65.98(3)	102.03(4)	215,500(300)
	NAT pH 7.3	49.24(2)	67.98(3)	65.85(4)	102.03(3)	215,600(400)

performed on α -CHT specifically oxidized at MET 192 shows effects similar to the b-axis behavior observed here. It should be noted further that among the boronic acid derivatives studied, PEBA, PPBA, and PBBA, those derivatives which do not appear to interact strongly at both the specificity site and the catalytic site (PEBA pH 3.6, PPBA and PBBA as discussed below) show an increase in their respective unit cell volume, while those which appear to interact more strongly at both sites (PEBA pH 5.4 and 7.3) show a decrease in unit cell volume or remain constant. The TOS and PMS derivatives would not necessarily be expected to follow this pattern as they interact covalently with SER 195 and do not meet the specificity requirements of α -CHT.

As with the irreversibly inhibited derivatives, examination of the difference electron density map

revealed small, localized regions of both positive and negative electron density (> 0.15 eÅ^{-3}) accompanying the large substitution density of PEBA at pH 3.6, both in and removed from the active site region. The difference maps calculated from the derivative and native data at pH 5.4 and pH 7.3 revealed more extensive regions of perturbation of the native structure. Due to the separation of the phenyl ring from the boronate group by an ethyl group, two maximum density regions occur. These regions correspond to the phenyl group in the specificity pocket (x \leq 49/76) and to the boronate group near the catalytic site (x \geq 50/76). A comparison of these peak heights is representative of the occupancy and/or ordering of the inhibitor in the two sites (Table 16). The independent

TABLE 16

Comparison of Peak Heights of Difference Electron

Density Regions in the Active Site

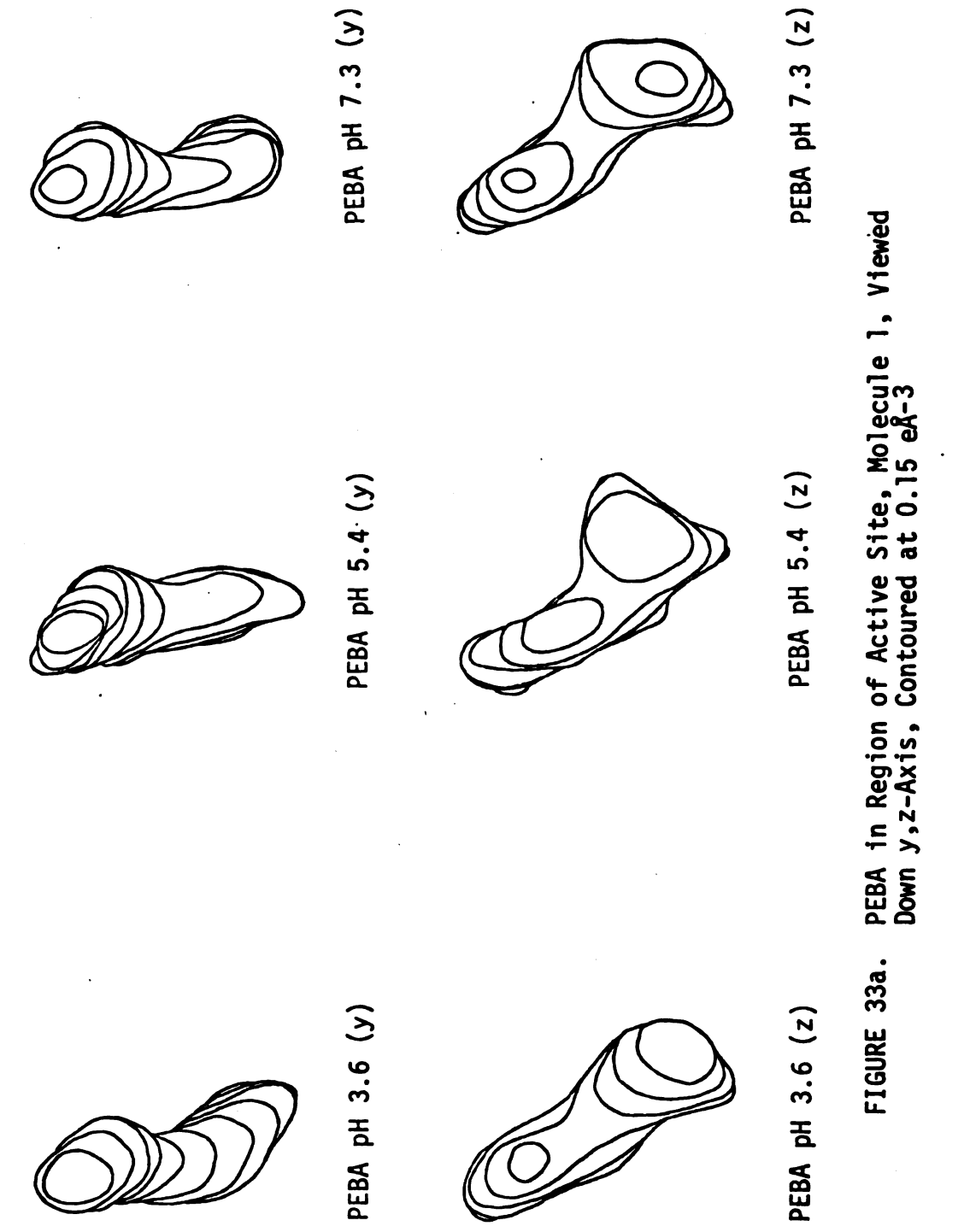
of PEBA pH 3.6, 5.4 and 7.3

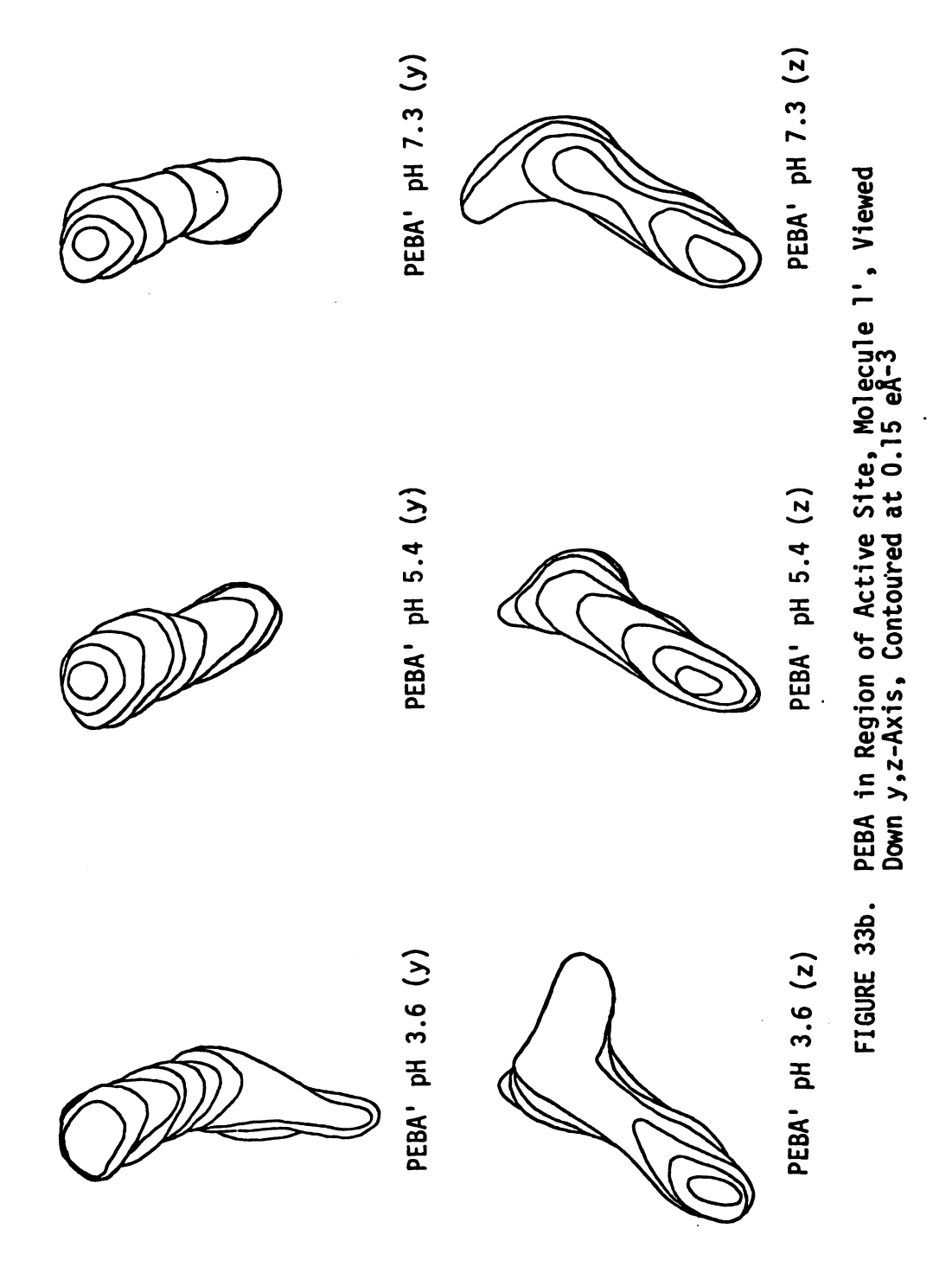
Derivative	Site	Molecule 1	Molecule 1'
PEBA pH 3.6	catalytic	0.47 eÅ ⁻³	0.38 eÅ ⁻³
	specificity	0.37	0.33
PEBA pH 5.4	catalytic	0.46	0.45
	specificity	0.46	0.45
PEBA pH 7.3	catalytic	0.44	0.33
	specificity	0.39	0.45

molecules exhibit good two-fold symmetry in their occupancies only at the higher pH values.

The x-y and x-z composite bounded projections of the difference electron density for the substitution of PEBA at the three pH values are shown in Figure 33, from which it can be seen that there is a striking similarity in the orientation of the phenyl group density in the specificity pocket as a function of pH in the independent α -CHT molecules.

A comparison of the centroids of the difference electron density of PEBA pH conformers across the local two-fold axis shows a significant variation in the ydirection (Table 17) as previously noted with TOS and PMS (Table 10). Again, the estimated error in coordinate is about + 0.4 Å. The above comparison indicates a strong pH effect in the catalytic site; the results at pH 3.6 show a large deviation from local two-fold symmetry (in the y-direction), while at pH 5.4 and 7.3, the deviation is within the limits of error. The constant variation in the specificity site for this series seems indicative of the fact that the side-chain of PEBA approximates that of phenylalanine, an α -CHT specific substrate. The atomic coordinates for PEBA at pH 3.6, 5.4 and 7.3 were determined in a manner similar to that used for TOS and PMS and are given in Table A-1.





specificity
pocket
(x < 49/76)</pre>

catalytic pocket (x > 50/76)

specificity
pocket
(x < 49/76</pre>

catalytic pocket (x ≥ 50/76)

TABLE 17

Comparison of Centroid Positions of Substitution Density in the Active Sites of Molecules 1 and 1' (PEBA pH 3.6, PEBA pH 5.4 and PEBA pH 7.3)

Comparison of Rotation About Two-Fold Axis Performed on the Substitution in Molecule 1', Followed by Averaging the Deviation from Molecule 1

specificity pocket (x < 49/76) catalytic pocket (x > 50/76)				
δ 2	0.13 Å	0.21 Å	Σ∇	PEBA' pH 7.3
Δÿ	-0.92 Å	-0.45 Å	Δÿ	PEBA' pH 7.3
	PEBA pH 7.3	PEBA DH 7.3		
δΖ	0.40 Å	0.07 Å	Z∇	PEBA' pH 5.4
Δÿ	-0.73 Å	-0.25 Å	Δÿ	PEBA' pH 5.4
PEBA pH 5.4 PEBA pH 5.4				
δΖ	0.27 Å	0.35 Å	δŽ	PEBA' pH 3.6
Δÿ	-1.05 Å	-1.19 Å	Δÿ	PEBA' pH 3.6
PEBA pH 3.6 PEBA pH 3.6				

Comparison of Competitive Inhibitor Substitution in Each of the Independent Molecules of the Crystalline lpha-CHT Dimer ۵.

0.22 Å	0.51 Å	0.22 Å	-0.17 Å	¥ 7.3
-0.36 Å	Å 7E.0-	-0.05 Å	-0.42 Å	PEBA' pH 7.3
0.00 Å	0.68 Å	1 5.4 PEBA' pH 5.4	PEBA'	
-0.32 Å	0.05 Å	PEBA' ph		
PEBA' pH 3.6	PEBA' pH 3.6			
-0.07 Å	-0.35 Å	0.07 Å	-0.05 Å	PEBA pH 7.3
0.23 Å	-0.25 Å	0.27 Å		PEBA
-0.14 Å	-0.69 Å	5.4 PEBA pH 5.4	PEBA	
PEBA -0.05 Å -0.14 Å 0.23 Å -0.07 Å pH 3.6	PEBA -1.04 Å -0.69 Å -0.25 Å -0.35 Å	PEBA pH 5.4 PEBA PH 5.4	PEBA DH 5.4	
		PEBA' PEBA' PH 3.6	PEBA' PH 3.6 PEBA' PH 3.6	PEBA' -0.32 Å 0.00 Å PEBA' PH 3.6 PEBA' PH 5.4

The devigtion between the centroid positions of PEBA pH 5.4 and PEBA pH 7.3, both in molecule 1, is 0.27 Å $(\Delta \bar{y})$ and 0.07 Å $(\Delta \bar{z})$ in the specificity pocket and 0.35 A $(\Delta \bar{y})$ and -0.05 Å $(\Delta \bar{z})$ in the catalytic pocket. Example:

2. Orientation of PEBA molecule and interaction with $\alpha\text{-CHT}$ as a function of pH

The PEBA orientations at each pH value are shown in Figures 34-36. The peaks observed in the difference electron density maps of both the native pH conformer and the inhibited conformer are indicated. The enzyme inhibitor contacts for each of the PEBA derivatives have been summarized in Table B-1.

It is apparent from examination of Tables 11, A-1, and B-1 that, although the phenyl group extends into approximately the same translational position at each of the hydrogen ion concentrations studied, significant differences in orientation occur, both among the pH conformers and within the α-CHT dimer. The PEBA results are of particular interest as the phenyl ethyl group resembles the phenylalanine side-chain and the interactions in the hydrophobic pocket should approximate those responsible for substrate specificity. The possible application of PEBA as a transition-state analog for α-CHT-catalyzed ester hydrolysis is partially dependent on this isosterism.

Examination of the inclination angles of PEBA reveals

a similar orientation of the phenyl ring to that of the

tosyl ring in molecule 1 at all the pH's investigated.

It will be seen below that an x-y inclination angle of

45° also occurs with the PPBA and PBBA derivatives in

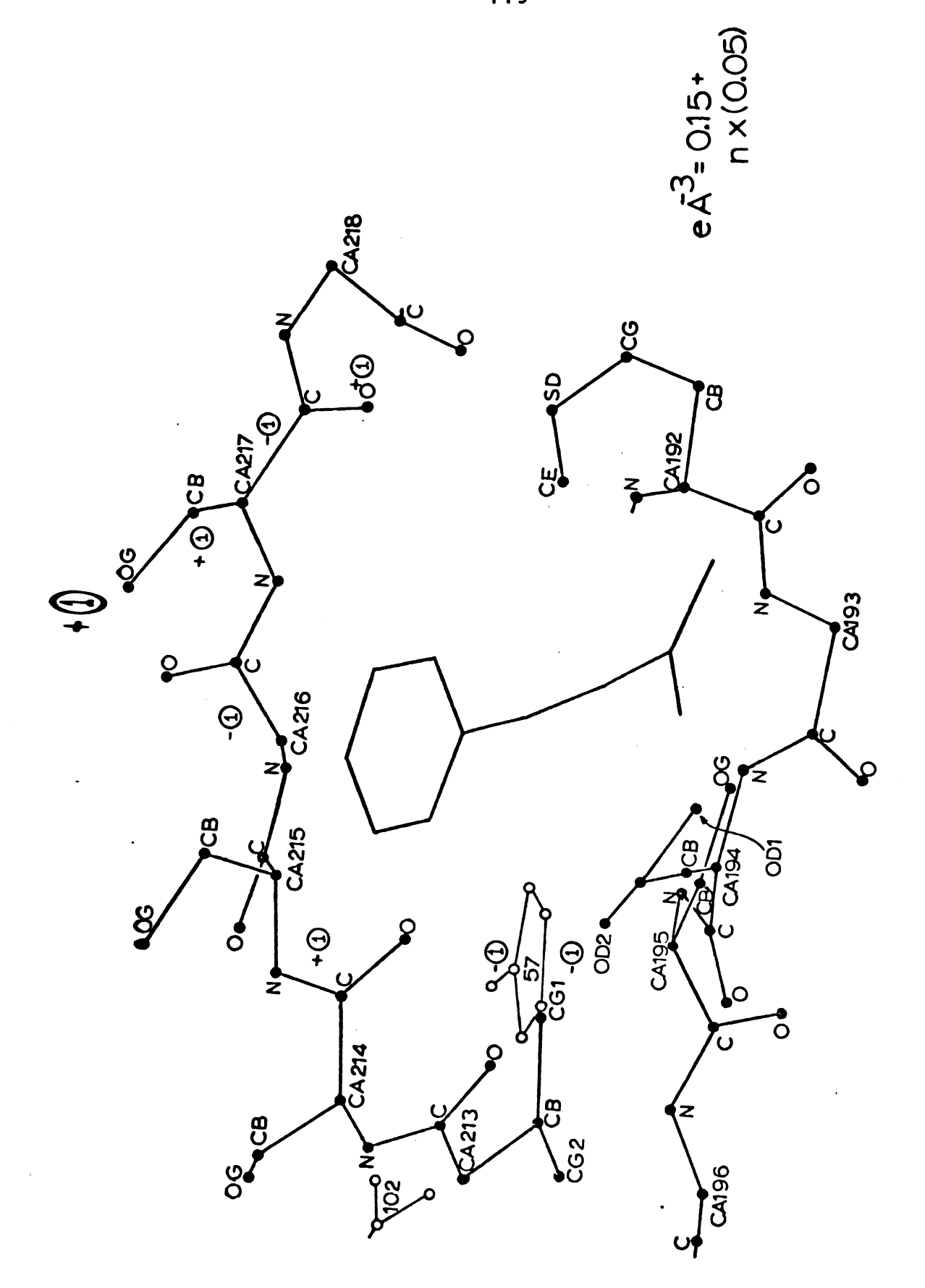


FIGURE 34. PEBA pH 3.6 Orientation in x-z Projection of Active Site

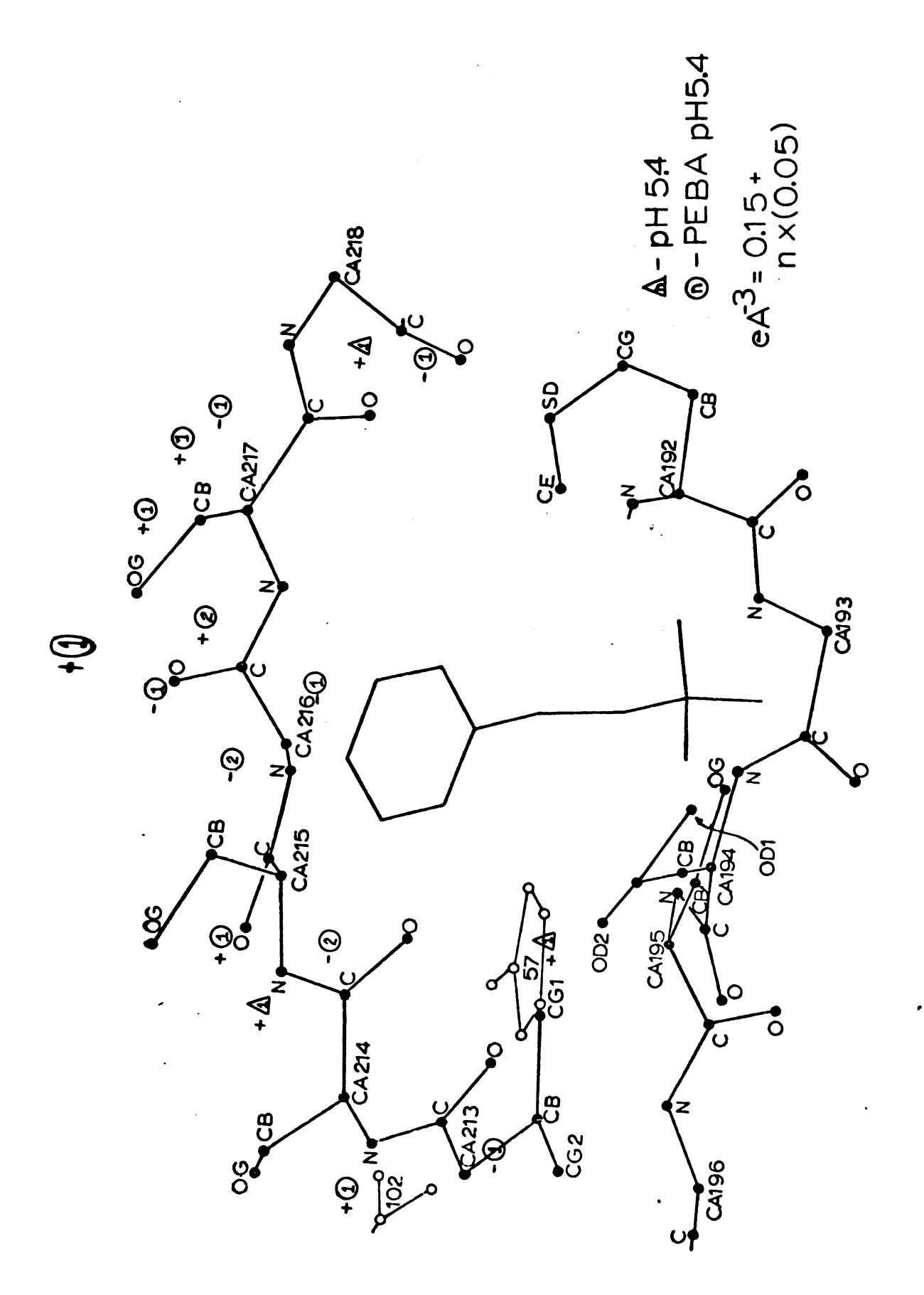


FIGURE 35. PEBA pH 5.4 Orientation in x-z Projection of Active Site

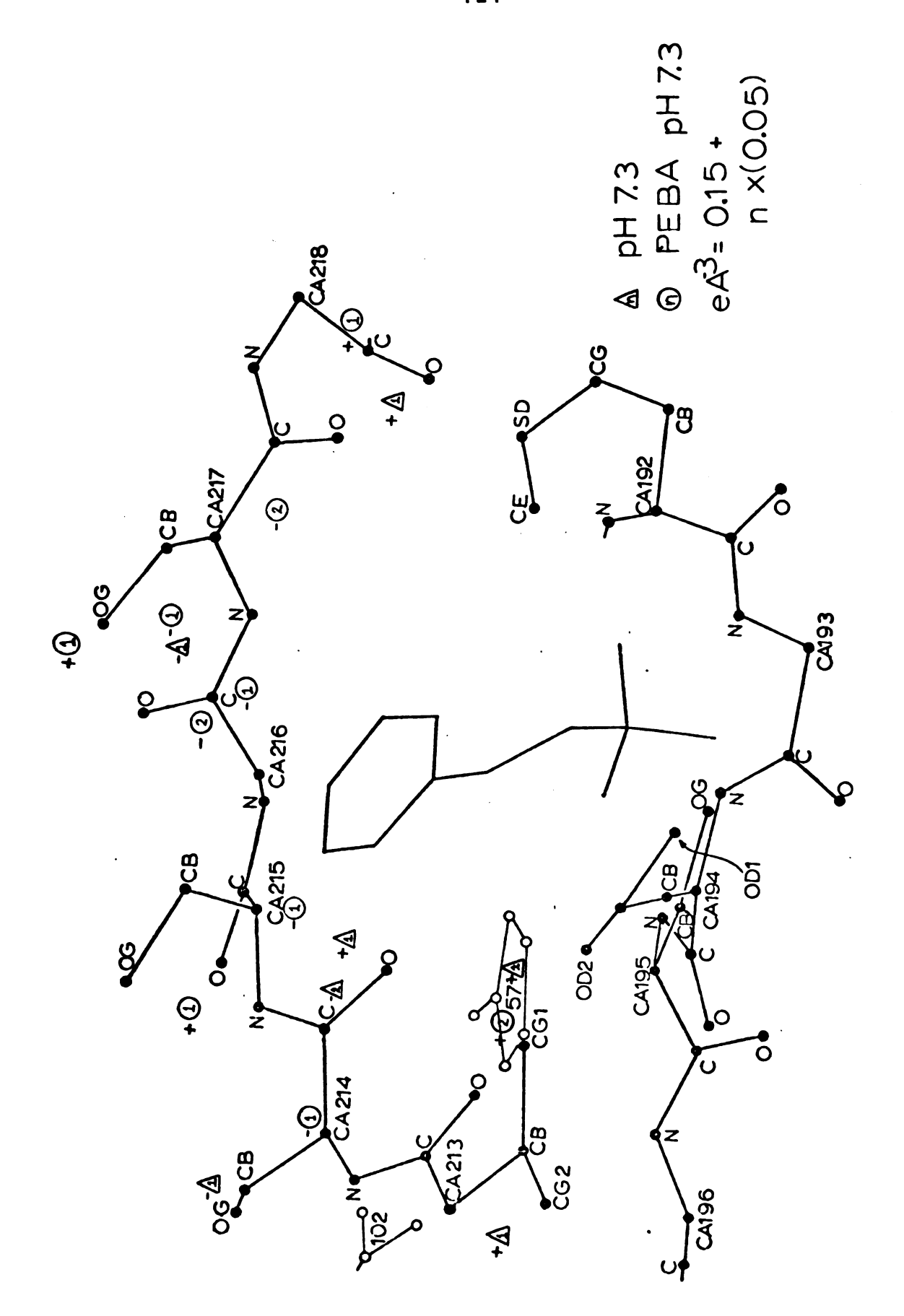


FIGURE 36. PEBA pH 7.3 Orientation in x-z Projection of Active Site

molecule 1, suggesting that this orientation optimizes the interactions between the specificity pocket of α -CHT and the aromatic group of an inhibitor or substrate. The deviation observed in PMS (\sim 65°) is consistent with a tetrahedral configuration about the CA atom (S-CA-C) angle = 110°), and the involvement of a side-chain too long to possess complete orientational freedom and too short to extend properly into the hydrophobic cleft. This further explains the identical x-y inclination angle for PMS in molecules 1 and 1'. The variability exhibited in the orientations in the dimer in all three PEBA derivatives is explainable in terms of the conformational variability of the dimer. The observed displacement of the SER 214'-SER 217' chain in molecule 1' away from SER 195 (along x) orients the aromatic ring with a smaller x-y inclination angle to maximize the contacts within the specificity pocket.

A more substantial variation in the aromatic rotation angle of PEBA is observed with each of the pH conformers. It should be apparent that the contacts listed in Table 12 are responsible for the primary interactions within the specificity pocket. Although little structural change is noted in the SER 214-SER 217 region with pH, the movement which is observed (at pH 5.4) seems to decrease the asymmetry of the dimer, thus possibly accounting for the similarity in aromatic

rotation angle. The anomalous values of the x-z inclination angle for the pH 5.4 conformer is indicative of the asymmetry remaining.

Overall, the introduction of the phenyl ethyl group into the specificity pocket at the hydrogen ion concentrations studied produces movement of the SER 214-SER 217 chain to enlarge the pocket and optimize interactions between enzyme and inhibitor. Although it is not immediately obvious, distance calculations reveal that those changes in orientation which occur as a function of pH result in almost doubling the number of contacts with the phenyl ring (Table 12a). At pH 3.6, the PEBA phenyl ring (15 contacts) interacts at approximately the same extent as the phenyl rings of PMS (14 contacts) and TOS (19 contacts). At pH 5.4 and 7.3, these contact regions expand to include 26 and 25 contacts, respectively (Table 12). As with TOS and PMS, the majority of the contacts within the specificity pocket involve main chain atoms of α -CHT, reinforcing the importance of the main chain conformation. It should also be noted that the pH 5.4 and pH 7.3 PEBA conformers show a substantial increase in the number of contacts in the active site region (29 at pH 3.6, 52 at pH 5.4 and 48 at pH 7.3; Table 12).

The most significant difference in the orientation of PEBA occurs in the catalytic region. Examination of

the composite difference electron density (Figure 33) and the orientation diagrams (Figures 34-36) reveals that as the pH is increased between pH 3.6 and pH 7.3, the boronate group moves toward SER 195, shifting almost 1 Å along the z-direction towards SER 195 0_{γ} . The pH 5.4 structure is intermediate in this movement. The α -CHT PEBA contacts (Table 12) further show that the number of contacts in the catalytic site also increases substantially upon raising the pH above 3.6 (14 contacts at pH 3.6, 26 at pH 5.4 and 23 at pH 7.3).

The orientation of the boronate functional group is not clearly defined at 2.8 Å resolution, similar to the TOS and PMS derivatives. Unlike the tetrahedral sulfonyl fluoride inhibitors, the boronic acids (R-B- $(OH)_2$) exhibit a tendency to accept a hydroxyl group as a function of pH, converting a trigonal boron arrangement to a tetrahedral boronate configuration. Examination of the composite electron density of the PEBA substitution (Figures 34-36) shows the orientational differences of the $-B(OH)_2$ group among the three pH conformers. variability is assumed to be a function of the interaction of the various ionic equilibrium states $(R-B(OH)_2 +$ $OH^- = R-B(OH)_3$) (95) previously observed in solution studies. This structural variability of the boronate group complicates the interpretation of the detailed interaction in the catalytic site because a covalent bond

to SER 195 is not obvious as with TOS and PMS. Evidence for a tight interaction between the boronate group and O_{γ} -(195) is given by the inability to wash out the inhibitor-soaked crystal as discussed below.

The boronate group occupies different orientations in the catalytic site at each of the three pH conformers of the α -CHT dimer studied. At pH 3.6, this group is positioned furthest from SER 195 $\mathbf{0}_{_{\mathbf{Y}}}$ (and 195') as evidenced by fewer contacts less than 3.5 $\mathring{\text{A}}$ between $\alpha\text{-CHT}$ and inhibitor. The difference electron density indicates that a water molecule might be hydrogen bonded to 02 of the boronate and that the separation between the boron and SER 195 $\mathbf{0}_{_{\boldsymbol{\gamma}}}$ is about 3.5 $\mathring{\mathbf{A}}$ after applying a shift to the position of SER 195 as indicated by a difference electron density gradient. Thus, at pH 3.6 SER 195 0_{\odot} is probably involved in a weak interaction with a trigonal $-B(OH)_2 \cdot H_2O$. The same applies to the interactions in the catalytic site of molecule 1', except for the difference in SER 195 O, position already discussed for The catalytic region generally undergoes some small rearrangements upon inhibitor binding at pH 3.6, probably a result of the displacement of the sulfate ion bridging monomers of the dimer (94).

As with TOS and PMS and all boronic acid derivatives used in this study, the sulfate ion, present in the active

site region of native α -CHT adjacent to SER 195 0_{γ} , must be displaced by the sulfonyl or boronate group. In examining the inhibitor orientation by the difference Fourier method, the analysis in the catalytic region of the active site is complicated because the inhibitor density occupies the region of the displaced sulfate electron density

 $^{\rho}$ protein $^{-}$ $^{\rho}$ protein $^{-}$ $^{\rho}$ sulfate $^{+}$ inhibitor $^{-}$ $^{\rho}$ sulfate

Since the sulfate in native α -CHT links HIS 57, SER 195, GLY 193 and TYR 146' by hydrogen bonding and charge interactions, the presence of an inhibitor, whether covalently bound or weakly coordinated to SER 195 0_{γ} , will cause a reorientation of this cluster of residues.

The SER 195 changes associated with PEBA pH 3.6 are both smaller and opposite in direction from those observed in TOS and PMS. At pH 3.6, PEBA produces larger changes in the vicinity of MET 192-GLY 193 than near SER 195 which results from the orientation of the boronate group. HIS 57 appears to rotate about C_{α} - C_{β} as in TOS and PMS but the associated peak is somewhat smaller in PEBA pH 3.6, while TYR 146' retracts from its position in the native structure by an apparent rotation about C_{α} - C_{β} of about +45°.

The PEBA derivative at pH 5.4 is most notable because of a shift in position of the boronate group of approximately 1 \mathring{A} which results from a rotation of 120° around the inhibitor CA-CB bond from that of the pH 3.6 derivative. The effect of this reorientation is to double the number of interactions within a range of 3.5 \mathring{A} between α -CHT and PEBA (Table 12). The increased interaction at pH 5.4 has already been noted in the specificity region so that the number of van der Waals contacts and the potential hydrogen bonds have increased markedly with the pH 5.4 conformer.

Although PEBA at pH 3.6 assuredly contains a trigonal $-B(OH)_2$ group, the configuration in the pH 5.4 α -CHT complex will be dependent upon the pH of its local microenvironment. The pH of the conformers of α -CHT referred to here represents the hydrogen ion concentration of the mother liquor in which the crystals have been soaking. The pH of the catalytic site is taken to be the same as the soaking solution. The value of pH 5.4 is close to the transition of the boronate group from its trigonal to tetrahedral form. Due to the lack of atomic resolution, determination of the exact boronate configuration is not possible from the electron density. However, the difference electron density map suggests that the interaction between SER 195 0_{γ} and the boronate forms a generally

more intimate complex than that at pH 3.6. The observed boron-SER 195 0_{γ} distance in the pH 5.4 complex is about 2.5 Å.

A change of the native α -CHT conformation upon PEBA inhibition at pH 5.4 is suggested by difference electron density gradients around the region CYS 191-SER 195. The rotation of SER 195 $\mathrm{O}_{_{Y}}$ in PEBA pH 5.4 is both larger and opposite in direction to that at pH 3.6 (a rotation of $\sim +90^{\circ}$ about the $C_{\alpha}-C_{\beta}$ bond). The other shifts in this region cannot be analyzed definitely but would appear to indicate an increased interaction between the inhibitor and GLY 193, probably through its amide group. remainder of the catalytic triad (HIS 57 and ASP 102) remains intact, probably because the boronate occupies approximately the same position vacated by the sulfate ion and interacts in a similar manner (except for the shift in SER 195 O_{γ} . It has already been observed by Vandlen and Tulinsky that the two active sites become more similar at pH 5.4 and this is in good agreement with the occupancies of PEBA pH 5.4 (Table 16). reorientation of SER 195 $\mathbf{0}_{\gamma}$ could thus be a pH effect which is either more pronounced because of the interaction with the inhibitor, or easier to observe in the latter.

At pH 7.3, PEBA is oriented with its boronate group in yet another position. The activity profile of $\alpha\text{-CHT}$

would suggest even a greater interaction might occur between the enzyme and a substrate. Moreover, at pH 7.3, it can be assumed that the boronate is tetrahedral (pK = 9.2). Thus, in the pH 7.3 conformer the boron is positioned about 1.8 Å from SER 195 0_{γ} . However, the electron density distribution in this region at pH 7.3 neither proves nor disproves tetrahedral boronate.

It should be noted that the orientation of SER 195 is unique to each pH conformer and is greatly affected by the presence of PEBA. There is no apparent reorientation of SER 195 in PEBA pH 7.3. The conformational changes between CYS 191-SER 195 involve MET 192-GLY 193 and result in a rotation of the $\mathrm{C}_{\alpha}\mathrm{-C}_{\mathrm{g}}$ bond of ASP 194, which affects the crucial ASP 194-ILE 16 ion pair. The rotation of ASP 194 appears to be a precursor to the reorganization observed with the pH 8.6 conformer (43), and from solution studies (10) is thought to be largely responsible for the high pH fall-off of the α -CHT-pH activity profile. The pH 8.6 conformer shows an apparent difference in the pK of the ASP 194-ILE 16 ion pair in the two molecules of the asymmetric dimer. reorganization of the active site of molecule 1 could be responsible for the decrease in occupancy of PEBA observed in molecule 1 on raising the pH from 5.4 to 7.3 (Table 16).

The asymmetry of the orientation of PEBA in α -CHT dimer can be seen from Tables 16, 17 and in Figure 33. It would appear from the non-identical conformational changes which occur as a function of pH that the orientational asymmetry results from an attempt to maximize the interaction between PEBA and α -CHT. It is apparent that both the x-y and x-z inclination angles are relatively conserved with the largest deviation occurring in the aromatic rotation angle. While the inclination angles are responsible for the primary orientation of the aromatic group of PEBA in the specificity site, it is the aromatic rotation angle which produces the differences in the interactions observed between TOS and PMS, and between PEBA at pH 3.6, 5.4 and 7.3.

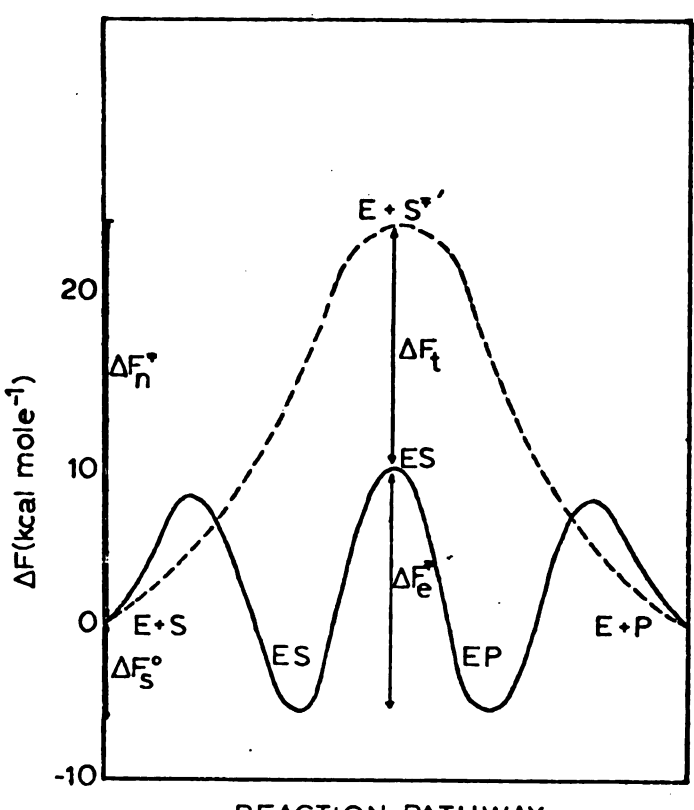
3. Evaluation of PEBA as a transition-state analog

The tetrahedral form of the boronate ion is expected to approximate the tetrahedral intermediate suggested in the mechanism of ester hydrolysis catalyzed by $\alpha\text{-CHT}$. This tetrahedral intermediate has been implicated in nonenzymatic ester hydrolysis by isotope exchange experiments so that it would be of great interest to understand the mechanism of the rate-enhanced hydrolysis by enzyme catalysis. The emphasis in current research is on those features of enzymatic catalysis which increase the catalytic efficiency: their cause and their effect. The

use of molecules which approximate the proposed transitionstate (structure of highest energy) and not the substrate itself should enable the investigation of the transitionstate of the enzyme-catalyzed mechanism.

A comparison between enzymatic and non-enzymatic catalysis is made in Figure 37 (96), if it is assumed that these proceed by the mechanisms indicated. The comparisons also assume that the transition-state structure of the substrate is identical in both the enzymatic and non-enzymatic process but that the enzyme allows lower free energy of activation to the transition-state (57). It has been suggested that this results from chelating effects within the active site (i.e., a high concentration of weak interactions such as hydrogen bonding, dipolar interactions, etc.) and within the specificity region of the enzyme which distort the substrate molecule to best accommodate these interactions.

The above ideas concerning enzymatic catalysis have been expanded to consider the design of analogs to the transition-state for use in probing the interactions responsible for high catalytic efficiency. It was anticipated that a molecule which resembled the transition-state of the substrate would be bound more closely to the enzyme than the substrate itself (56), thus permitting the examination of a complex approximating a species whose half-life is approximately 10^{-10} sec. Since these



REACTION PATHWAY

E = Enzyme

S = Substrate

P = Product

ES = Enzyme Substrate Complex

ES[†] = Complex Transition-State

S[†] = Substrate Transition-State

EP = Enzyme Product Complex

 ΔF_S° = Formation of ES from E and S

 ΔF_T = Formation of ES* from E and S[†]

 ΔF_N = Formation of S^{\dagger} from S

 ΔF_{E}^{\dagger} = Formation of ES from ES

FIGURE 37. Energy Diagram of Proposed Enzymatic Mechanism Involving a Transition-State for Catalysis (96)

complexes are stable, they can be studied by physical techniques such as X-ray diffraction (96). It should be noted that a perfect transition-state analog cannot be synthesized because the bonds differ in length, charge distribution, etc., and lead to minor differences in free energies of solvation, all of which ultimately disturb the transition-state equilibrium. Also, the more closely the analog resembles the substrate transition-state, the greater is its susceptibility to catalytic attack. The observed binding constants (inhibition constants), 10^{-3} to 10^{-4} mM, can differ appreciably from the theoretical values (97), 10^{-8} to 10^{-14} mM and both non-ideality and electronic interactions have been held responsible. The major consideration in choosing an analog is structural similarity in both the catalytic and specificity regions of the inhibitor molecule.

The methyl ester of phenylalanine is a primary substrate of α -CHT, its phenyl ethyl side-chain occupying the specificity pocket. This substrate has as an analog, phenyl ethane boronic acid, which is closely isosteric to the former. The use of the boronic acid group to approximate carbonyl compounds was pioneered by Antonov et al. (65) by studying the interactions of both alkyl and phenyl alkyl boronic acids with α -CHT. Philipp and Bender (98) examined substituted aryl boronic acids as inhibitors of both α -CHT and subtilisin. Koehler and



Lienhard (66) investigated the PEBA system in comparison to other competitive inhibitors, emphasizing the structural correspondence of PEBA to the proposed tetrahedral transition-state of the phenylalanine substrate. companion study of the subtilisin-PEBA system was performed by Lindquist and Terry (63). Kinetic studies of the reaction of benzene boronic acid with both subtilisin and α -CHT have been performed by Nakatani et al. (99) in an effort to understand the mechanism of catalysis. All these solution studies arrived at the same general conclusions concerning the applicability of transition-state analog theory to the serine proteases and alkyl or phenyl alkyl boronic acids.

Boronic acids, as a class, have been shown to inhibit α -CHT and subtilisin by the formation of a tightly bound complex; for PEBA α -CHT, $K_{\text{D}} = 4.7 \times 10^{-2} \text{ mM}$, for subtilisin, $K_D = 2.8 \times 10^{-2}$ mM. These values are larger than those predicted by transition-state theory, where

$$K_D = K_w \times k_n/(K_a \times k_e)$$
 (62)

where,

 K_{D} = transition-state dissociation constant

 K_{w} = dissociation constant of water

 K_a = dissociation constant of boronic acid

k_n = non-enzymatic rate constant (base

n (catalysis)
kp = enzymatic rate constant

The predicted K_D for α -CHT is 9 x 10^{-5} mM and 7 x 10^{-4} mM for subtilisin. These differences have been attributed to non-exactness of the transition-state analogs and overlap of pH transition ranges. In examining both the α -CHT and subtilisin interactions with PEBA, it has been observed that the inhibition constant is a function of both pH and side-chain length. The pH- K_i (K_i = $1/K_D$) profile for the two systems is identical below pH 8 and reflects the conformational transition of α -CHT which occurs at higher pH values with PEBA, hydrocinnamide and 2-phenyl ethane sulfonate (66). Although more extensive specificity studies have been performed on α -CHT, it is apparent that the substrate specificity is identical to that observed with the boronic acids.

A significant difference occurs in the interpretation of the specifics of the boronate-enzyme interaction.

While Antonov et al. (65) and Philipp and Bender (98) report the occurrence of the boronic acid:enzyme complex to be an interaction primarily with HIS 57, Koehler and Lienhard (66) implicate SER 195 as the primary site of interaction.

Hess <u>et al</u>. (100) have reported the existence of a tetrahedral intermediate in the complex of α -CHT and PEBA after examining the complex using laser Raman spectroscopic techniques. The appearance of a peak in the spectrum of the complex at pH 7.0, but not at pH 5.5, is



highly suggestive of the presence of a tetrahedral PEBA, but still requires a normal coordinate analysis of the boronate structure. The observation that the PEBA saturates the active site of α -CHT at pH 5.0 as well as at pH 7.0 (100) agrees with the results of the present study which indicate approximate full occupancy of PEBA at pH 3.6, 5.4 and 7.3 in crystalline α -CHT. This result does not conflict with the observations concerning the variation of binding strength versus pH since it was possible to wash out the PEBA from the pH 3.6 and pH 5.4 crystals with original PEBA-free mother liquor. The diffraction patterns returned to those of the native conformers at pH 3.6 and 5.4 after washing. At pH 7.3 the result was not definitive; changes were observed upon attempts to wash out the PEBA but without attainment of the pattern of the native pH 7.3 conformer. One possibility could be the removal of the inhibitor from one of the molecules of the dimer.

Matthews <u>et al</u>. (67) have investigated the structure of boronic acid adducts with subtilisin BPN (Novo) in the crystalline state. Their 2.5 \mathring{A} resolution study considered both benzene boronic acid (BBA) and PEBA, at pH 7.5. The initial phasing for the subtilisin structure was derived from the PMS-inhibited structure at pH 5.9. The phases used to examine both pH differences and inhibitor complexes were determined by a structure factor

calculation based on a Kendrew model constructed at pH 5.9 and were extended to 2.0 $\mathring{\text{A}}$ resolution. The interactions in the catalytic region of subtilisin correspond to those in α -CHT:PEBA (HIS 64, GLY 219, SER 221, subtilisin; HIS 57, GLY 193, SER 195, α -CHT) and would imply the same mode of binding of PEBA in subtilisin at pH 7.5 as with α -CHT at pH 7.3. The previous examination of the TOS (MSU) and TOS (MRC) structures lacked the exacting comparison necessary to evaluate the full influence of the choice of parent compounds for protein MIR phasing. Differences were observed between the native structures in the two studies. At less than atomic resolution the uncertainty caused by the weighting of the parent phasing structure upon detailed structural analysis, particularly when utilizing $\Delta \rho$ maps, should be examined at high resolution before attempting to make reliable, absolute comparisons of such results.

In summary, PEBA binds more directly to SER 195 than HIS 57 in α -CHT by interacting through the boron and SER 195 0_{γ} . At pH 7.3, it appears that the boron could be in a tetrahedral arrangement utilizing the 0_{γ} of SER 195 and the interaction of PEBA is consistent with observations both in solution and with subtilisin. However, lack of atomic resolution prevents the direct observation of this geometry. The interaction in the

catalytic region of the active site appears only slightly different at pH 5.4, but very different at pH 3.6. interpretation of both the substitution interaction and the concomitant conformational changes which occur upon binding are affected by the conformational variability previously observed in α -CHT with change in pH. would appear that the high occupancy observed at all three pH values results from a complementarity between PEBA and the α -CHT specificity and catalytic sites, while the degree of the interaction principally results from SER 195 and secondarily from GLY 193 (hydrogen bonding). This pH variability reflects a probable overlap of the pH "activation" of the active site (probably resulting from HIS 57 deprotonation) and the tetrahedral transformation of the boronic acid group. While the observed binding and interaction of PEBA with α -CHT do not in any way disprove the existence of a tetrahedral intermediate, they also do not permit a definitive proof that it occurs in this system.

4. <u>Comparison with enzyme:inhibitor (natural)</u> complex structures

Another crystallographic approach to the enzyme: substrate complex problem has utilized the inhibition of trypsin (T) by the natural protein inhibitors, pancreatic trypsin inhibitor (PTI) and soybean trypsin inhibitor



(STI). The applicability of such a complex to the α -CHT system would seem to be straightforward in view of the similarity in the catalytic mechanism of α -CHT and T. Such studies have been completed, on bovine PTI-T by Ruhlmann et al. (101), and on porcine T-STI by Sweet et al. (102). These crystallographic results are of particular interest since Blow and Huber had previously collaborated in predicting the manner of association of PTI with α -CHT and T based on model-building studies utilizing the structures of PTI, α -CHT and T (103). Huber's group had previously determined the structure of PTI at 1.5 Å resolution (104).

Crystals of the PTI-T complex yielded diffraction data to 2.8 Å resolution (101). Previous work had determined that the interaction between PTI and T involved the LYS 15I-ALA 16I link of PTI. The establishment of a tetrahedral configuration about this amide carbon came primarily from the position of SER 195 0_{γ} . Comparison of the PTI-T active site with that of the MRC α -CHT structure revealed the orientation of SER 195 0_{γ} to be in the "acylated" position observed in indoleacroyl-(48) and tosyl- α -CHT (49). The absence of electron density in the native orientation further suggested the involvement of SER 195 0_{γ} in an interaction other than a Michaelis complex, particularly as the bond between LYS 15I-ALA 16I appeared intact. Including the tetrahedral

configuration into a real space refinement produced a final orientation in agreement with the starting model. The stability of this complex ($\rm K_i > 10^{14}$) was thus thought to depend on the strain present in the tetrahedral carbon bond angles observed in the PTI structure, 121° and 98° compared with 109° (ideal). It was also concluded that the structural changes between the native structures and those in the complex represented the minimum changes necessary to accommodate PTI and T, and that this additionally lowered the energy of the transition-state. Further study suggested that the intermediate might be somewhat between the acyl-enzyme and the tetrahedral adduct due to a slightly extended $\rm C(151)-O_{\gamma}(195)$ distance.

Blow and his collaborators investigated the STI-T complex, in which STI can be reversibly hydrolyzed, because of its greater stability and homogeneity. Crystals of the complex yielded diffraction data to 2.6 Å resolution. Solution studies had shown that the scissle bond of STI, ARG 63I-ILE 64I, was reversibly cleaved but bound to the enzyme in an inhibitory way (102). The refinement procedure used a modified set of bovine coordinates, structure factor calculation and a combination with the MIR phases. They attempted to examine the nature of the scissle bond by deleting the constraint of the peptide linkage and allowing the independent refinement of

SER 195, ARG 63I and ILE 64I. A comparison was made of these results (C $_{\beta}(195)$ -C $_{\alpha}(63I)$ distance 3.7 Å and $\mathrm{C}_{\alpha}(63\mathrm{I})\mathrm{-C}_{\alpha}(64\mathrm{I})$ distance 3.9 Å) with those established for a Michaelis complex (5.2 $\overset{\circ}{A}$ and 3.8 $\overset{\circ}{A}$), tetrahedral intermediate (3.7 $\mathring{\text{A}}$ and 3.8 $\mathring{\text{A}}$), and acyl-enzyme (3.7 $\mathring{\text{A}}$ and 5.0 $\mathring{\mathsf{A}}$). The coordinates reflect a tetrahedral configuration, even though Huber et al. (101) have suggested that C(63I)-0 $_{_{\Upsilon}}$ (195) is longer than normal C-0 single bonds. Unlike PTI, STI was not observed to have strained angles about the scissle bond, and the complex stability $(K_i > 10^{11})$ is attributed to the availability of free energy from entropy driven effects. It is further hypothesized that the tetrahedral form is stabilized as a minimum of free energy of the total system and that the function of trypsin-like enzyme is to lower the activation energy of the overall reaction. This is accomplished by the delocalization of the negative charge on the tetrahedral group which also strengthens potential hydrogen bonds between carbonyl oxygen and NH (193) and NH (195) and improves alignment.

In accordance with the above, the tetrahedral intermediate has been assumed as fact; although conceivably it could be an artifact of the refinement procedures. It would appear imperative therefore in applications of this nature that the dependence of

refinement procedures upon the initial model be established in order to evaluate the reliability of the details resulting from these analytical approaches.

5. <u>Phenyl alkyl boronic acid orientation as a</u> function of alkyl chain length

The structures of α -CHT:PPBA and α -CHT:PBBA were studied to further probe the specificity requirement of α -CHT. The study was carried out at pH 4.6 and the cell parameters for these two derivative crystals proved to be identical; however, they differ markedly along the a-and b-axes from those observed in native α -CHT pH 4.6 crystals (Table 18). Both derivative crystals exhibit

TABLE 18
Cell Parameters for PPBA and PBBA

	a(Å)	b(Å)	c(Å)	β(°)	Volume (Å ³)
PPBA pH 4.6	49.54(4)	67.39(6)	66.00(7)	101.92(5)	215,600(600)
PBBA pH 4.6	49.54(2)	67.43(2)	66.03(3)	101.97(4)	215,800(300)
NAT pH 4.6	49.3 (1)	67.8 (1)	65.9 (1)	102.0 (1)	215,000(600)

cell volumes greater than that of the native pH 4.6 conformer. Although the variation in the cell parameters of all the boronic acid derivatives is probably indicative of changes occurring in the crystal, there are too few observations to make more conclusive statements. The variation in unit cell volume, although only slightly beyond the

estimated error for all the boronic acid derivatives and for TOS and PMS, appears significant and is of the same magnitude as the variation observed among the native pH conformers.

An examination of the difference electron density maps of PPBA and PBBA showed lower occupancies in the active site region for both derivatives (Table 19). The

TABLE 19

Comparison of Peak Heights of Difference Electron

Density in the Active Sites of the

PPBA and PBBA Derivatives

Derivative	Site	Molecule 1	Molecule l'
PPBA pH 4.6	catalytic	0.16 eÅ ⁻³	0.12 eÅ ⁻³
	specificity	0.31	0.20
PBBA pH 4.6	catalytic	0.17	0.14
	specificity	0.21	0.20

large difference in the occupancy between these two derivatives and that of PEBA initially generated some concern about the integrity of the inhibitors themselves, since PPBA and PBBA were from the same source and PEBA from a different source. However, a new sample of PPBA gave essentially identical results with respect to occupancy of the substitution and conformational changes throughout the molecule. The differences in occupancy

observed upon the lengthening of the alkyl chain appear to be due to a limitation imposed by the specificity pocket.

The x-y and x-z composite bounded difference electron density projections of PPBA and PBBA are shown in Figure 38. A comparison of these projections to those of the other inhibitors indicates the generally lower occupancy since all are drawn at approximately the same contour levels; however, the comparison shows excellent agreement with respect to orientation of the inhibitor both between the two independent molecules and even between PPBA and PBBA. This observation is further corroborated by the comparison of the centroid positions of the substitution densities as previously described (Table 20). The displacement observed in the y-direction with the other inhibitors upon rotation of molecule 1' about the two-fold axis is also apparent with the PPBA and PBBA derivatives. As with the other inhibitors, Kendrew models of PPBA and PBBA were fitted to the composite bounded electron density projections and the atomic coordinates were determined and are listed in Table A-1.

6. Orientation and interaction of phenyl alkyl boronic acids in the active site

It is apparent from examination of the composite bounded electron densities (Figure 38) that the orientation

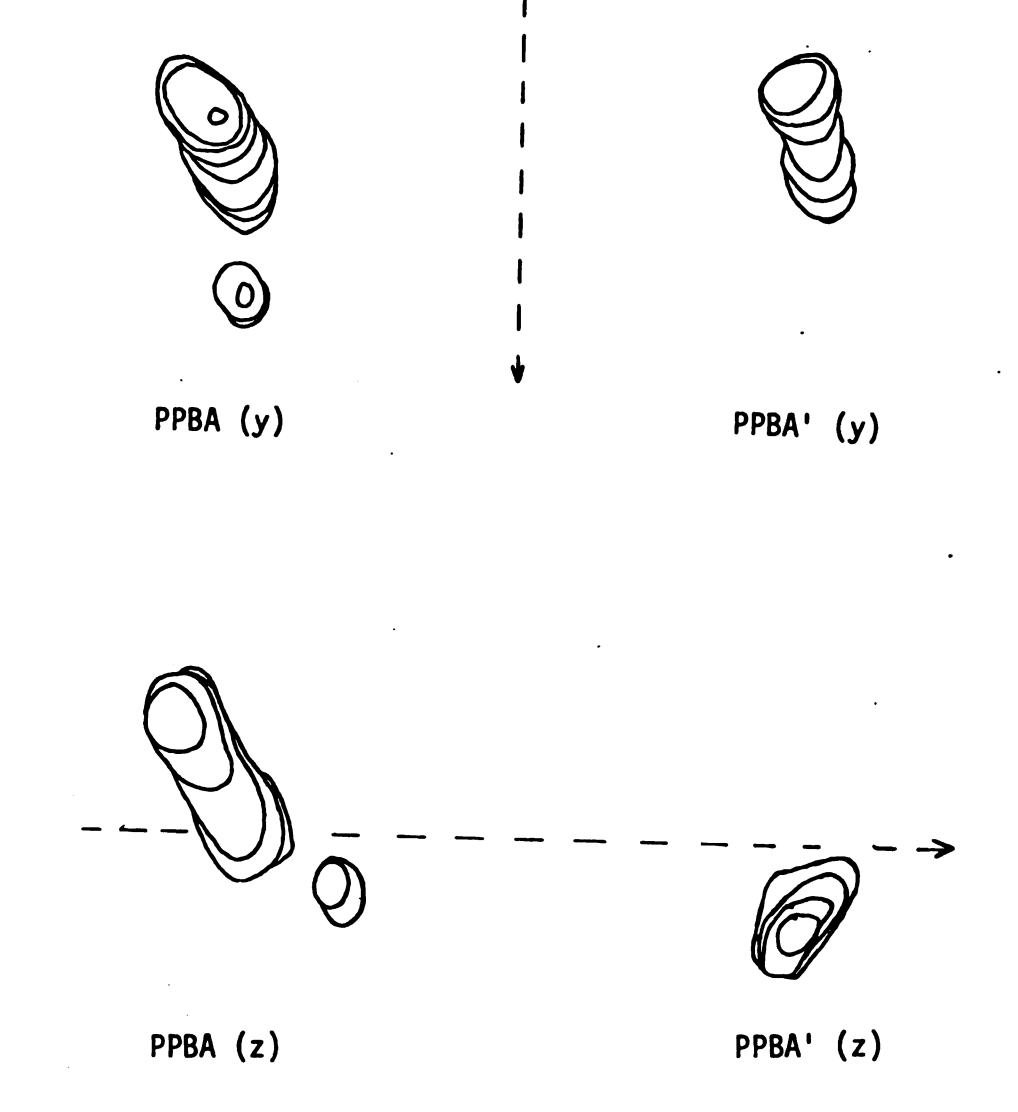
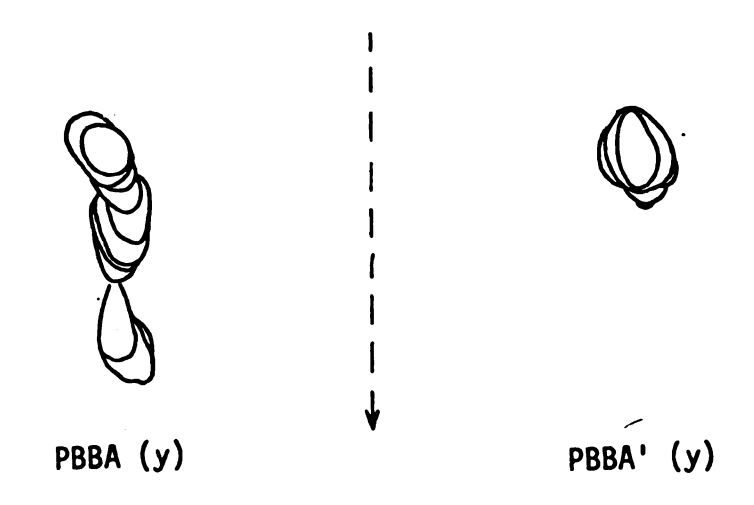


FIGURE 38a. PPBA in Region of Active Site, Viewed Down y,z-Axis, Contoured at 0.15 eA-3, with Approximate Two-Fold Representation



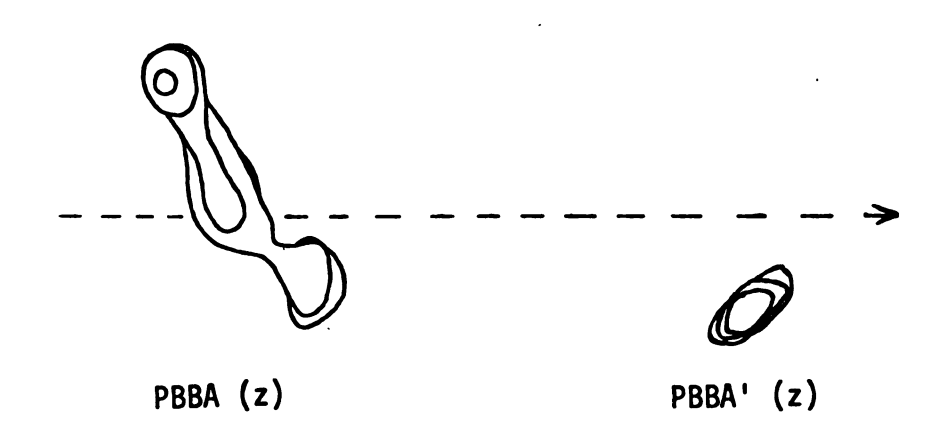


FIGURE 38b. PBBA in Region of Active Site, Viewed Down y,z-Axis, Contoured at 0.15 eA-3, with Approximate Two-Fold Representation

TABLE 20

Comparison of Centroid Positions of Substitution Density in the Active Sites of Molecules 1 and 1' (PPBA and PBBA)

Comparison of Rotation About Two-Fold Axis Performed on the Substitution in Molecule 1', Followed by Averaging the Deviation from Molecule 1 . م

PBBA	PBBA
$\Delta \bar{z} = 0.13 \text{ Å}$	$\triangle \bar{z} = 0.00 \text{ Å}$ PPBA'
Δ <u>y</u> = -0.83 Å	$\Delta \bar{y} = 0.25 \text{ Å}$ PPBA'
PPBA	PPBA

PBBA'	PBBA'	
$\Delta \bar{z} = -0.06 \text{ Å}$	∆y = 0.44 Å	988A
Δz = -0.02 Å	Δ <u>y</u> = -1.36 Å	9BBA

Comparison of Competitive Inhibitor Substitution in Each of the Independent Molecules of the Crystalline α -CHT Dimer ۵.

۰۷	۰۷	
90	05	
-0.06	0.05	PBBA
ıı l	11	PB
ΔZ	Σ∇	
	,	
۰۷	۰۷	
24	57	
0.24 Å	. 0.57 Å	PBBA
11		PB
Δÿ	Δÿ	
		,
34	34	
PPBA	PPBA	

$\Delta \bar{z} = 0.00 \text{ Å}$	ΔZ = -0.04 Å	PBBA'
$\Delta \bar{y} = 0.16 \text{ Å}$	Å 69.0- = ½ A	PBBA '
PPBA'	PPBA'	•

<pre>specificity pocket (x < 49/76)</pre>	catalytic pocket (x <u>></u> 50/76)
0 Å	04 Å

The deviation between the centroid positions of PBBA (Molecule 1) and PBBA (Molecule 1') are 0.44 Å ($\Delta \bar{y}$) and -0.06 Å ($\Delta \bar{z}$) in the catalytic pocket. Example:

of PPBA and PBBA are essentially the same in the specificity region of molecule 1. The occupancy in molecule 1 is lower than that observed with PEBA, but is higher than that observed in molecule 1' where only the PPBA density appears above the three sigma level. In the catalytic region of the active site, significant density is only present for the substitution in molecule 1. The net result is that the binding orientations and interactions between the independent molecules cannot be accurately compared.

It is interesting to note the similarity of both the orientation and interaction of PPBA and PBBA in the specificity site (Figure 39). Although initial examination of the Kendrew model of native $\alpha extsf{-}\mathsf{CHT}$ indicated that side-chains longer than phenyl ethyl could possibly be accommodated by the specificity site, comparison of the coordinates of the bound inhibitor molecules indicates that there is an apparent length limitation in this region. The same number of van der Waals contacts, within 3.5 Å, between α -CHT and the aromatic group of the inhibitor occur with PPBA and PBBA as occur with PEBA, but the number of closer contacts increases markedly (within 3.0 A-PPBA (17), PBBA (16), PEBA pH 7.3 (12), PEBA pH 5.4 (9) and PEBA pH 3.6 (7)). The interactions in the catalytic site involve van der Waals contacts between the inhibitor alkyl chain and α -CHT and the



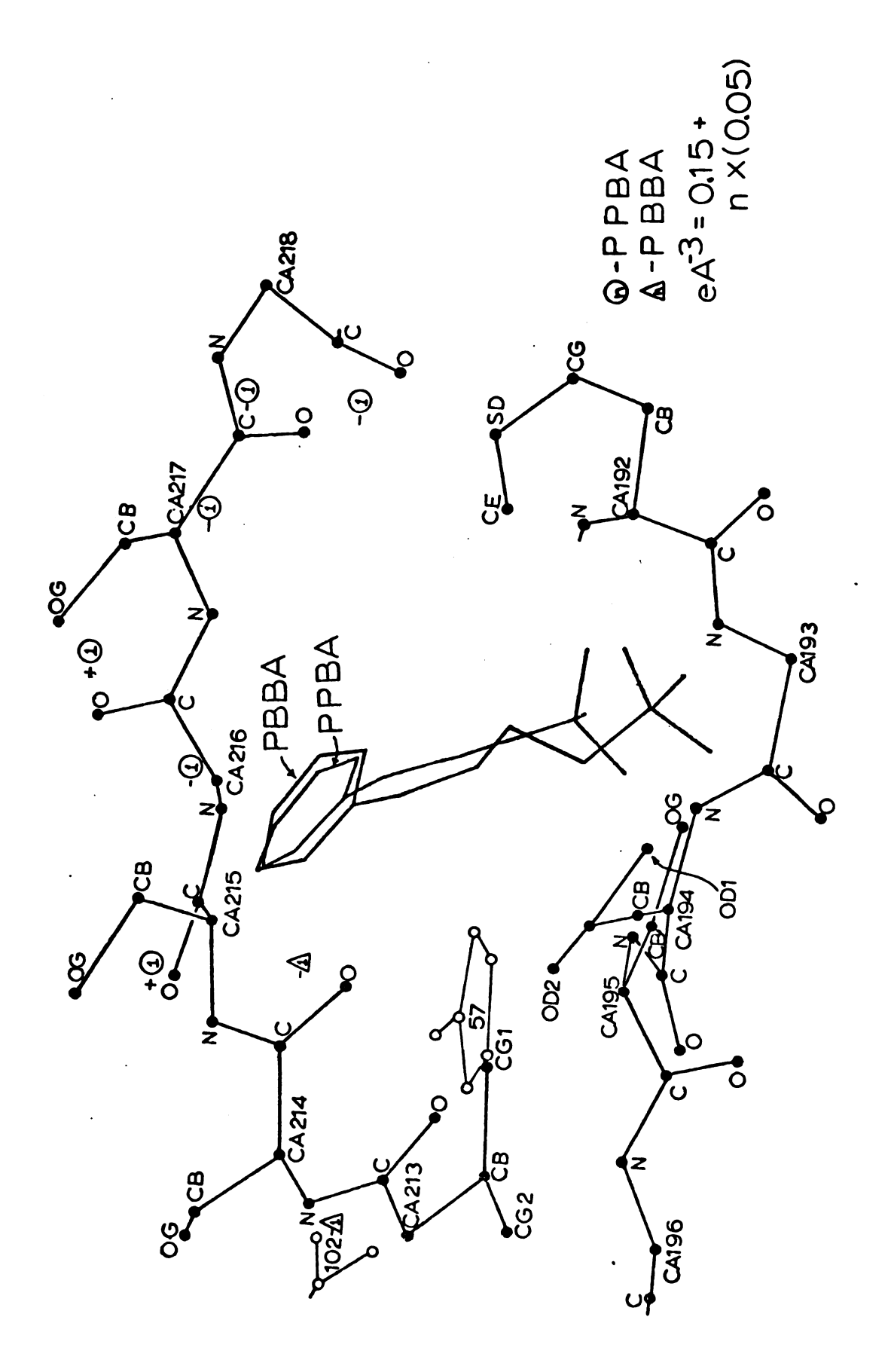


FIGURE 39. PPBA and PBBA Orientation in x-z Projection of Active Site



boronic acid group is oriented in a "weak" binding orientation near SER 195 (~ 3.5 Å). The alkyl chain, instead of extending into the vacant area of the active site and thereby minimizing conformational strain, attempts to maintain an interaction between the boron and SER 195 0_{γ} . The gradient peaks along the 214-219 chain lining the rear of the specificity pocket resemble the changes observed in PEBA pH 3.6.

It would appear that the lower occupancy of PPBA and PBBA results from a strain imposed upon the "bidentate"-like binding in the active site. An apparent cooperativity exists between the specificity region and the catalytic region of the active site. The specificity of α -CHT is determined by its ability to interact correctly in both regions. It would also appear that the importance of this cooperativity is reflected in the weak binding of PPBA and the weaker affinity towards PBBA. An increase of the alkyl chain appears sufficient to strain the interactions between the specificity and catalytic regions and prevents higher occupancy in the active site.

7. Substrate specificity of α -CHT

In attempting to discuss the high efficiency of enzyme catalysis, it is necessary to examine the sources and types of interactions which determine enzymic

specificity. The initial binding (complexing) of a substrate or inhibitor which is specific for a given enzyme must rely on the enzyme's ability to interact selectively with a limited segment of a multi-component pool in vivo. The serine protease enzyme class contains members of different species origin with similar but varying structures and specificities. Although each member of this class exhibits a unique response to pH, temperature and other external perturbations, the reaction and interaction between the enzymes and their substrates provides evidence of those forces most critical to natural processes. Probably similar forces enable a polypeptide chain to conform to a pre-determined tertiary structure as it is produced on the ribosome and form the basis of all biochemical processes. inhibitors used in this study provide a means to examine the specificity requirements of α -CHT and to compare results obtained from solution studies.

As indicated in Table 10, α -CHT exhibits specificity with respect to both size and stereoisomerism, but enzymatic activity exists over a wide range of structures with varying efficiency. The reactivity can be evaluated in terms of two parameters, the relative binding constant, K_m , and the catalytic rate constant, k_{cat} . Various attempts have been made to quantitize the interaction

specificity, most notably using reactivity parameters, steric fit, hydrophobicity, and molecular size considerations (105,106). Based on the phenyl alkyl boronic acid results obtained in this study, it would appear from the cooperativity implied between the catalytic and specificity regions of the active site that molecular size is of prime concern within a homologous series. This idea does not ignore the effects of reactivity, steric effect and hydrophobicity. However, the limited number of orientations and interactions in the binding region suggests a selectivity based on volume, surface area, potential van der Waals contacts and packing within the binding region, in combination or separately.

Solution studies of α -CHT specificity have also been performed using homologous substrate and inhibitor series. Some of these, N-acetyl-L-amino acids esters (107), phenyl alkyl-para-nitro phenyl esters (108), alkyl boronic acids (65) and phenyl alkyl boronic acids (64), are discussed below in terms of side-chain volume and surface area.

The van der Waals volumes and surface areas of various side-chains have been determined using the approximate method of Bondi (109) (Table 21). That portion of the side-chain which extends into the specificity region of the active site (beyond C_{α}) is compared in Figure 40. Because of the diversity of experimental

TABLE 21

Comparison of Homologous Series of Inhibitors, Substrates and Potential Transition-State Analogs of $\alpha\text{-CHT}$

1. N-acetyl-L-amino acids (methyl esters), Jones et al., J. Amer. Chem. Soc. 87, 8 (1965).

	CH3-EH3	сн ₃ -с-ин-сн-с-сн ₃ ^L (сн ₂) _п н				
~	>	SA	K* (mM)	Krel	$k_0 (sec^{-1})$	krel
I	2.5	0.8	33		0.013	0.0
сн ₃	13.7	2.12	739	0.0	1.27	0.09
C ₂ H ₅	23.9	3.47	53.5	0.03	1.05	0.08
nC ₃ H ₇	34.1	4.82	10.2	0.16	2.70	0.20
nC4H9	44.4	6.17	6.7	0.24	8.39	0.63
ոշերյ	54.6	7.52	1.6	1.0	13.4	1.0
nc ₆ H ₁₃	64.8	8.87	2.9	0.55	6.23	0.46

Table 21. (cont'd.)

Table 21. (cont'd.)

0.10 0.11 0.67 2. para-nitro-phenyl esters, Dupaix et al., Biochem. Biophys. Res. Commun. 41, 2 (1970). $k_3^* \times 10^2 \text{ (sec}^{-1})$ 1.88 1.85 17.8 12.0 SA (R) 6.78 8.03 9.38 45.8 76.5 13.7 56.1 66.3 $(c_6H_5)(cH_2)_2$ $(c_6H_5)(cH_2)_3$ $(c_6H_5)(cH_2)_4$

Table 21. (cont'd.)

0.86

2.09

2.48

19.2

12.2

с1-сн₂

22.5

32.1

 $c1 - (cH_2)_3$

 $C1-(CH_2)_4$

1.82

3.17

4.52

5.87

5.18

4.45

 $C1-(CH_2)_2$

Table 21. (cont'd.)

R'	V (R)	SA (R)	$k_3^* \times 10^2 (sec^{-1})$	^k 3rel
Ŧ	2.5	0.8	150	
CH ₃	13.7	2.1	0.99	1.0
сн(сн ₃) ₂	23.9	3.46	0.34	0.34
с(сн ³) ³	34.1	5.01	0.018	0.02
3. phenyl alkyl boronic		Antonov et al.,	acids, Antonov et al., FEBS Letters 20, 37 (1972).	
1 ⁹ 0	с ₆ н ₅ -(сн ₂) _n -в(он) ₂		$R' = c_6 H_5 - (cH_2)_n$ less cH_2	
R'	۸	SA	κ <mark>*</mark> (mole ⁻¹)	K, rel
НО			10.	
(⁶ H ⁹)	37.8	3.98	780.	0.07
(² H ²)(CH ²)	56.1	6.68	10950.	1.0
$(c_6H_5)(cH_2)_3$	66.3	8.03	5200.	0.47
$(c_{6}H_{5})(cH_{2})_{4}$	76.5	9.38	3300.	0.30
Table 21 (cont'd)				

Table 21. (cont'd.)

Table 21. (cont'd.)

4. alkyl boronic acids, Antonov et al., FEBS Letters 7, 23 (1970).

	K _i rel	0.03	90.0	0.13	0.32	1.0	1.0	1.0
$R' = H(CH_2)_n$ less CH_2	K_{j}^{\star} (mole ⁻¹)	.01	16.	40.	100.	310.	310.	310.
	SA	0.8	2.12	3.47	4.82	6.17	7.52	8.87
$H(CH_2)_n - B(OH)_2$	>	2.5	13.7	23.9	34.1	44.4	54.6	64.8
	-	НО	н(сн ₂) ₂	н(сн ₂) ₃	$H(CH_2)_4$	$H(CH_2)_5$	$H(CH_2)_6$	н(сн ₂) ₇

*k3, k₀ are k_{cat};

/K_i = [enzyme][inhibitor] [enzyme complex]

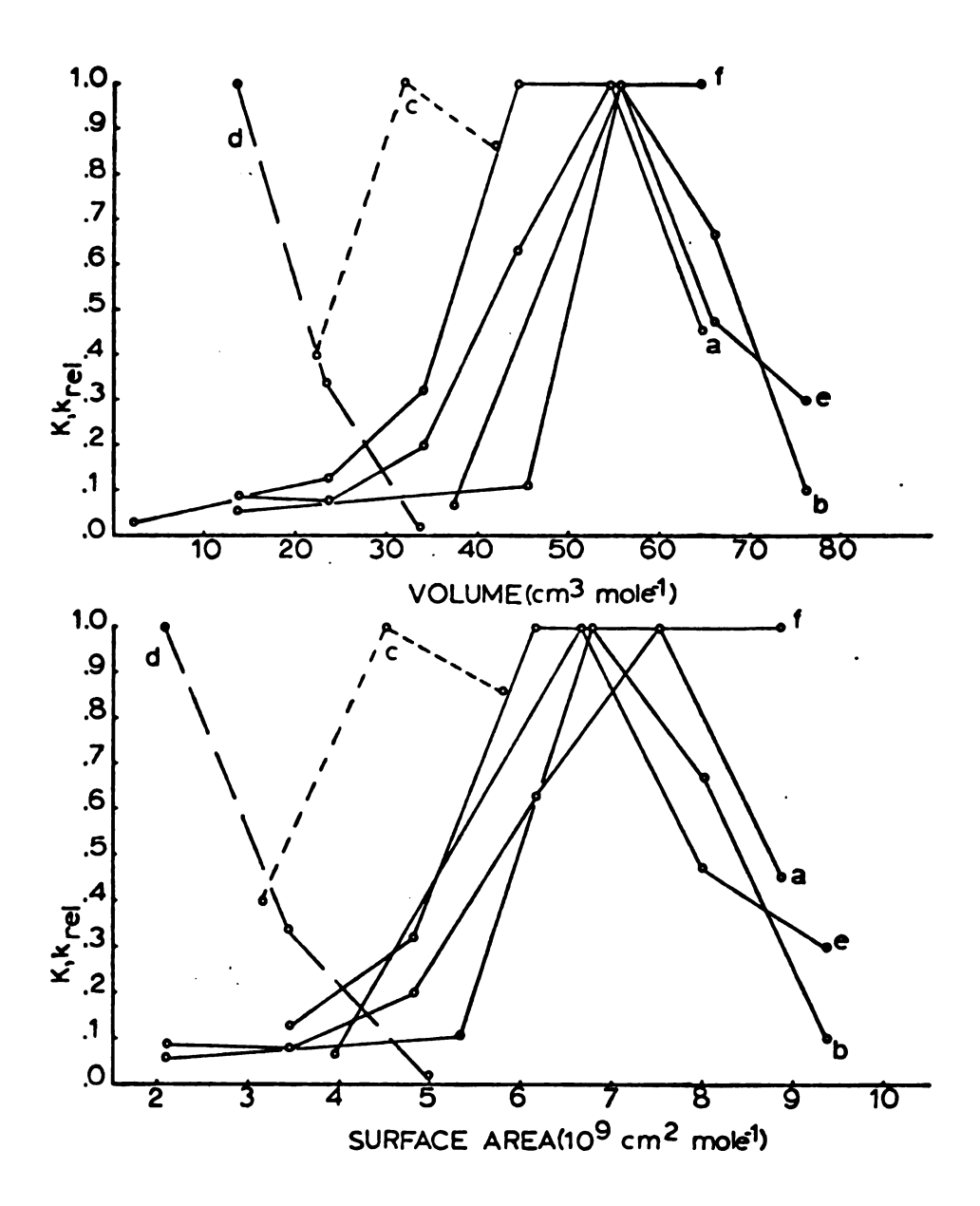


FIGURE 40. Substrate/Inhibitor Side-Chain Specificity in $\alpha\text{-CHT}$

parameters and procedures, it is of particular interest to note the bell-shape of these steric relationships. The optimal surface area (\sim 120 \mathring{A}^2 /molecule) and volume (\sim 92 \mathring{A}^3 /molecule) occur with the same structures, and if a spherical approximation is used for the inhibitor sidechain, the approximate van der Waals radii are 3.1 Å and 2.8 Å. respectively. It appears that as the side chain is increased in size, it passes through an optimal size for interaction in the specificity region. This has been observed with the contacts in TOS, PMS, PEBA (3.6, 5.4, 7.3) and PPBA and PBBA. Further expansion of the side-chain would require either reorientation of the group within the specificity region or would strain the interactions within the catalytic site. If the interactions in the catalytic site are weak by nature (i.e., van der Waals contacts and hydrogen bonding only), it is conceivable that the multiple contacts in the specificity region would govern the orientation and conformation of the inhibitor. This apparently occurs with PPBA and PBBA, and is suggestive of the similar observations made recently with alkyl isocyanates (110). Although there is a slight displacement of the phenyl ring by about 0.3 Å along the x-direction away from SER 195, it is apparent from the available free volume of this region (193-312 \mathring{A}^3), that the aromatic group does not reposition itself, but maintains apparently

optimal interactions as observed with PEBA within the specificity region. However, the alkyl chain of PPBA is forced to reorient in an attempt to maximize its interaction in the catalytic region. Thus the boronate group is forced to extend past SER 195 0_{γ} , which weakens their interaction and accounts for the low occupancy. This interpretation also explains the smaller occupancy observed with PBBA in the catalytic region. These results are indicative of the cooperativity which exists between the specificity and catalytic regions of the active site and indicate that the specificity pocket establishes the initial orientation of the substrate for subsequent interaction and catalysis at SER 195.

The results further confirm the hydrophobic nature of the specificity of $\alpha\text{-CHT}$ as did the comparisons made between alkyl and phenyl alkyl side-chains. The electronic factors involved in substrate specificity were not specifically detailed in this study although further analysis of the data of Dupaix et al. (108) indicates complexities with halo-alkyl side-chains. A further point of interest concerns the behavior of branched alkyl side-chains. $\alpha\text{-CHT}$ appears to exhibit restrictive catalytic behavior if extensive branching occurs at C_α with the restriction decreasing for C_β branching. This is most probably due to strained interactions in the catalytic region of the active site, particularly the



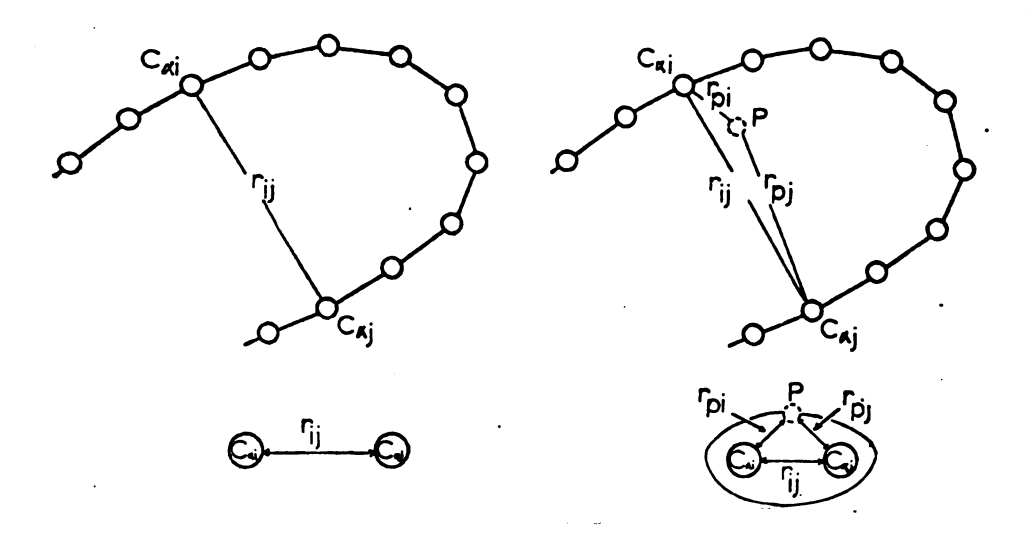
inability of the apparently important hydrogen bond with GLY 193 NH to form.

V. DIAGONAL PLOT ANALYSIS

A. Analysis of the Distance Diagonal Plot of α -CHT (Native, pH 3.6)

Because inhibitor binding affects the conformation of the active site of native α -CHT and produces conformational changes in regions of the molecule removed from the catalytic site, the structure of α -CHT (Native, pH 3.6) will be discussed in terms of a distance plot representation. The distance diagonal plot comprises one diagonal half (i > j or i < j) of a square matrix of order N, where N is the number of amino acids in a polypeptide chain with the point (ij) indicating the separation (in \mathring{A}) of alpha carbon atoms i and j (Figure 41). The plot of the native α -CHT structure is shown in Figure 42, with all regions < 15 $\ddot{\text{A}}$ darkened. Using the alpha carbon positions for each of the independent molecules of the α -CHT dimer, both molecules can be represented in the same diagonal plot, one above and the other below the diagonal. This permits convenient comparisons to be made across the diagonal between the independent monomers.

The inherent organization of a distance plot provides a natural progression between sequential relationships and secondary and tertiary structure. Closed segment features include nearest-neighbor interactions ($|i-j| \ge 0$),



DISTANCE DIAGONAL PLOT COORDINATES

DIFFERENCE DISTANCE DIAGONAL PLOT COORDINATES

FIGURE 41. Distance Diagonal Plot Definitions

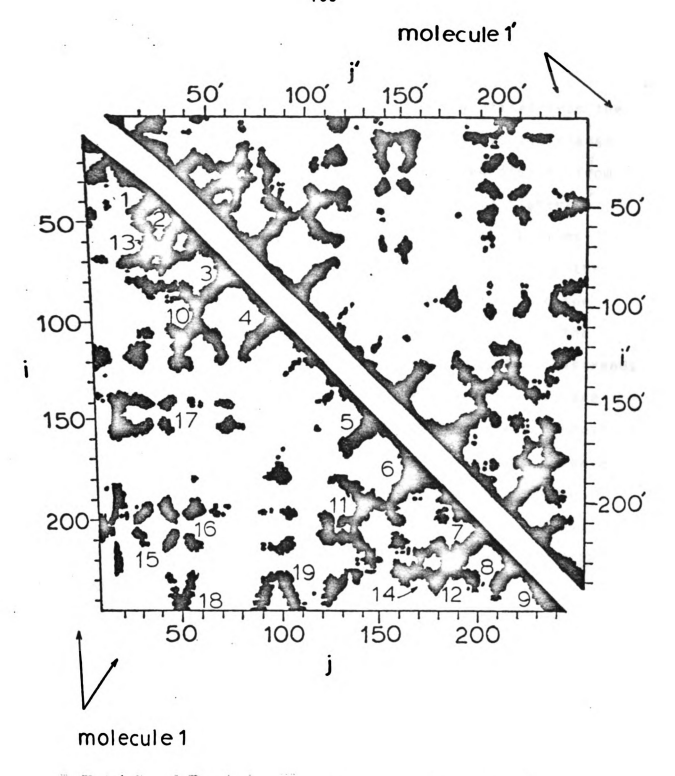


FIGURE 42. Distance Diagonal Plot of α -CHT Dimer Depicting Representative Structural Features, Contoured at 15 Å (Solid Regions)

which occur at or along the diagonal, mid-range distance interactions ($|i - j| \sim N/4$) are slightly offset from the diagonal, while open segment features involve long-range interactions (|i - j| > N/4) and are located distant from the diagonal. Although α -helices (broadened segments along the diagonal) are nearest-neighbor interactions, anti-parallel β-strands (extending perpendicular to the diagonal) are mid-range or long-range depending on the length of the polypeptide chain segment connecting the strands of the β -loop (Table 22) (111). Parallel β -strands (features parallel to but offset from the diagonal) are typically long-range. Table 22 summarizes these several features as well as others of tertiary structure observed in α -CHT. These examples are idealized as distortion from these occurs in actual diagonal maps of proteins. The mid-range features are primarily those discussed by Kuntz (112).

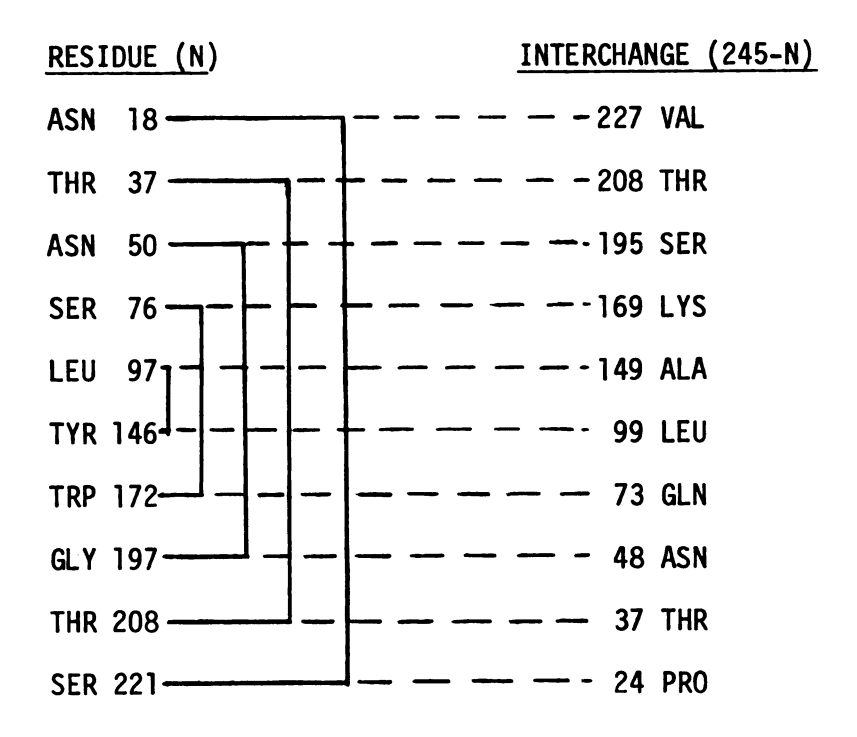
Further examination of the distance diagonal plot of α -CHT shows the presence of long-range features related by mirror planes of symmetry, oriented about 45° to the diagonal and located distantly from it. These off diagonal long-range interactions of α -CHT displaying mirror symmetry have not heretofore been discussed. The regions are designated in numbered blocks in Figure 42 and will be called: crosses (1), anti-crosses (2), "v's" (3) and inverted "v's" (4) and they arise from the

TABLE 22 $\begin{tabular}{ll} \textbf{Structural Features of α-CHT} \\ \textbf{Diagonal Plot} \end{tabular}$

Structure	Backbone Conformation	Theoretical Feature	Feature (Figure 42)
l. α-helix	7000-		9
2. β-loop			
3. Multi-strand	ANTI-PARA:LEL PARALLEL	<u>\</u>	1,2,3,4,5,6,7,8 10,11
Loops		<u>y</u>	12 12
4. Loop-loop			12,13
4. Loop-100p		×	15 16,17
5. Loop-helix	(200 <u>0</u>)	<u>\</u>	18 19

structural features shown schematically in Table 22. The β -strand- β -strand interaction gives rise to mm symmetry in the diagonal plot and the particular strands involved in the interaction can be identified from the intersection of the symmetry elements with the diagonal. The positions of the intersections define the sequential position of the bend of the β -strand. For instance, the crosses of Figure 42 arise from β-strands with bends near (37-148) and (49-204), respectively (Table 23). The intersection of the mirror plane of the "v's" and inverted "v's" can be interpreted in the same manner. Thus, the "v" of Figure 42 arises from the interaction of the carboxyl terminal helix of α -CHT with a β -strand possessing a bend near residue 49 while the inverted "v" arises from a similar interaction but with a bend near 97 and with the helix running in an opposite sequential sense. It should be noted that these interactions are all of an interdomain type.

The long-range interactions which appear as symmetrical features in the region i \geq 123, j < 122 reveal the interdomain contacts to involve beta structures. It should be apparent that by examining these diagonal plots on a finer contour scale and extending them to three-dimensional surfaces, observation of distance gradients (sharpness, etc.) would allow the calculation of distortions from the idealized interactions of



Palindromy observed in α -CHT

------ Predicted by interchange (245-N)

Table 22. It would thus be possible to approximate separation angles between sheets and helices, sheet strand separation, etc.

Nishikawa and Ooi (45) have noted that the distance plot of α -CHT (Figure 42) possesses an approximate mirror plane of symmetry perpendicular to the diagonal, which separates the molecule into two similar structural domains (domain A, residues 1-122 and domain B, 123-245). This qualitative feature based on a comparison of the plot contoured at a 15 Å level is indicative of the presence of two segments of chain of approximately equal length (122 residues) and conformation. Matthews (38) originally noted that the main chain hydrogen bonding scheme of α -CHT implied the presence of two approximately cylindrical surfaces of anti-parallel pleated sheet structure. Birktoft and Blow (49) later reported the details of these cylindrical surfaces in terms of six adjacent antiparallel chains and four disulfide bridges. Their examination of this intramolecular symmetry led them to conclude that α -CHT contained two structurally similar halves in one segmented polypeptide chain, and suggested this was the result of gene duplication (49). This type of folding is not unique since Shotton et al. (91) have made similar observations with sequentially homologous elastase. However, the domain structure in the distance diagonal plot contradicts the possibility of gene

duplication, since the cylinders show greatest similarity in structure when the sequence in one of the domains is reversed. The algorithm for generating the corresponding residue in domain B from domain A simply involves subtracting the sequence number of the residue from the length (245) of the peptide chain termed "interchange." This observation suggests that the implication of gene duplication is incorrect since the latter does not give rise to a palindromic or interchanged polypeptide sequence. Although sequence homologies do not exist between the two domains, various structural features are observed to be present in both.

Five interchain loops occur in α -CHT, three of which are closed by disulfide bridges and two of which are approximately palindromic to two others (Table 24).

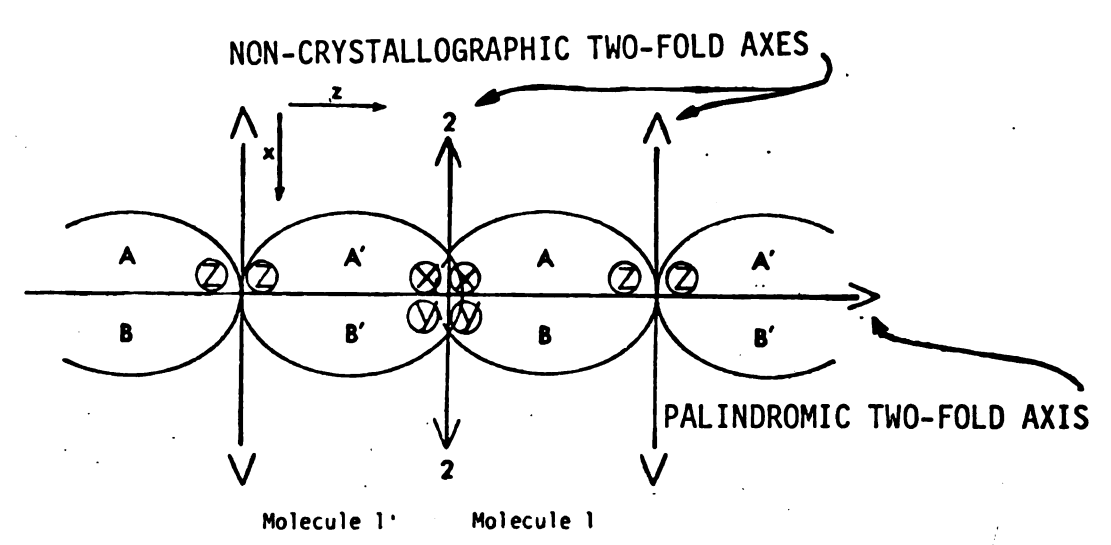
TABLE 24
Intrachain Loop Palindromy

Loop Name	Residues (N)	Interchange (245-N)
Histidine	42-58*	203-187
Methionine	168-182*	78-63
Serine	190-220*	55-25
Aspartic Acid	84-110	161-135
Autolysis	133-164	81-112

where (*) denotes loop closure by disulfide bridge

It can be further noted that part of the specificity pocket of the active site TRP 215-SER 217 is sequentially palindromic with part of a secondary binding site of α -CHT formed by a cluster of three tryptophan residues (TRP 27, TRP 29 and TRP 209) (42).

The segments with mirror symmetry reveal several interesting points concerning the inter-domain interactions and the dimeric structure. Locating the residues involved at the beta-bends (intersection points on the diagonal) shows that they are on the surface of the molecule, within approximately 5 Å from one of two noncrystallographic two-fold axes which are approximately parallel to the a*-axis (Figure 43). The construction of line segments connecting the alpha carbons of each pair of these palindromically related residues in the threedimensional structure gives a series of lines with colinear mid-points. A new intra-molecular dyad axis can now be constructed passing approximately through the midpoints of these line segments. This dyad passes through the active site region and is perpendicular to the noncrystallographic two-fold axes discussed above (Figure There is only one pair of residues which does not show this relationship (TYR 146-LEU 97). If a correction is made to the TYR 146 position based on the position of this residue in the zymogen (51), the pair then satisfies the new dyad. Thus the α -CHT dimer can be approximated



x = CATALYTIC BINDING POCKET

y = SPECIFICITY POCKET

z = SECONDARY BINDING SITE

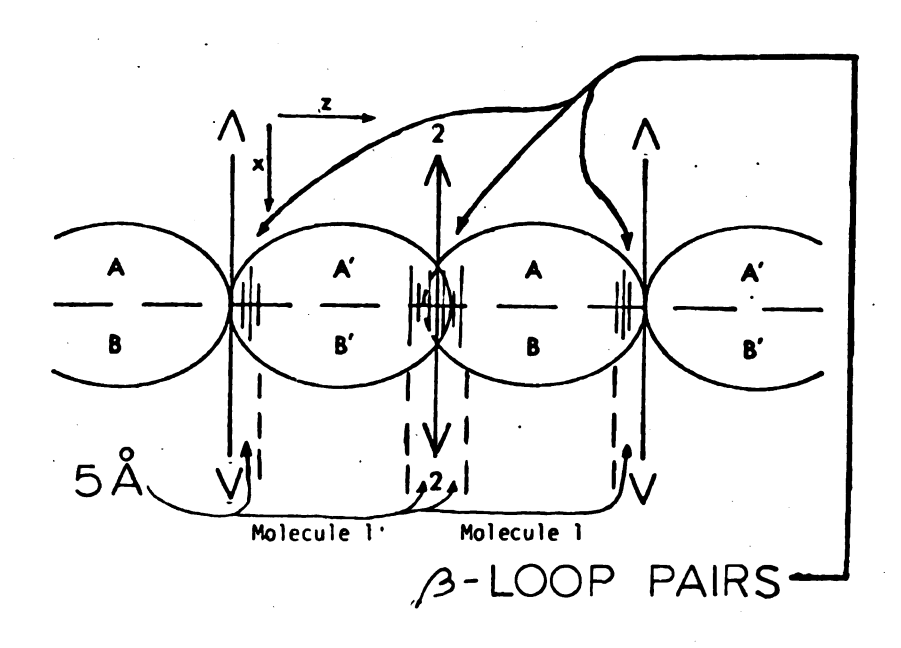


FIGURE 43. Domain Configuration of $\alpha\text{-CHT}$ Dimer

by a tetramer comprised of domains A, B, A', and B'. Such a tetrameric organization of quaternary structure might be a basic format observed in nature in other macromolecular systems. The new dyad might exist to define the region of intra-domain contact; it is interesting that both the active site and the secondary site (tryptophan cluster) (42) are situated around this dyad (Figure 43). In the crystal, the domains of α -CHT occur as alternative rows of A and B type, extending parallel to the crystallographic c-axis.

An additional point of interest related to the domain structure but which is not yet fully understood, centers around the location of the ordered sulfate molecules of α -CHT (identified by sulfate-selenate exchange experiments) (94). Each of the sulfates can be assigned to a specific amino acid residue according to proximity. Except for CYS 1, all residues so indicated (Table 25) are in domain B. CYS 1-122 constitutes both termini of domain A and is located on the intramolecular dyad.

The foregoing construction arises from the fact that the bio-architecture of α -CHT relies on the presence and interaction of structurally similar domains. It is therefore of particular interest to study the correlation of both the domain sub-structure with other members of a particular enzyme class, and the domain conformational changes which occur upon inhibitor binding or chemical

TABLE 25
Residues in Proximity of Localized Sulfate Ions (94)

Sulfate (Residue #)	Domain Location
195/195'	B, B'
1/1'	Terminus of A domain: covalently linked to 122, A'
149/149'	B, B'
154/154'	B, B'
177	В
192/192'	B, B'
217/217'	B, B'
236/236'	B, B'

modification with respect to variability in protomer structure. Potentially, this can form a basis for molecular recognition. Since domain structures occur in other proteins and enzymes, the basic concepts operative in the α -CHT system might, in fact, be of more general application.

B. Comparison of the Structures of α -CHT with Pancreatic Trypsin Inhibitor by Use of Distance Diagonal Plots

Due to the similarity in the active site regions of enzymes belonging to the serine protease class, it is of interest to examine their three-dimensional structures in an attempt to recognize common structural features which might provide a basis for better understanding the structure-function relationship of this enzyme class. It would appear that the distance plot affords an efficient means by which to catalog these structures for detailed comparisons.

The domain of α -CHT centers around an observed betabarrel. The representation of this region in the distance plot has been discussed above as a "multi-loop superhelix" in α -CHT, but Kuntz (112) also assigned this feature to extended segments of anti-parallel β -sheet structure. It would be of particular interest to further evaluate these conformations, as described above, in terms of the packing of ideal sheet and helical structures to establish

whether these configurations are possibly formed as functional segments of the polypeptide chain, or as simple minima on conformational energy surfaces. This aspect appears even more significant upon the examination of the crystallographic structure of PTI.

PTI (101) is a natural inhibitor of trypsin found in bovine pancreas as well as other organs. It consists of 58 amino acid residues, with a molecular weight of 6500 amu. It is anomalously stable towards standard denaturants, chemical agents and heat, and resists proteolytic digestion, while being capable of inhibiting either α -CHT or T in a stoichiometric (1:1) complex. The three-dimensional structure of PTI has been determined by Huber's group (101).

The folding of PTI is based on a twisted double-stranded anti-parallel β -sheet from ALA 16 to GLY 36. The N-terminal segment is in an extended conformation and is anti-parallel to the first strand of the β -sheet. The remaining C-terminal segment consists of a short extended region (39-43) and three turns of α -helix, both of which are anti-parallel to the second strand of sheet and the N-terminal segment. Thus, the folding consists of four anti-parallel and two parallel structural features with about 12 and 10 residues between turns.

The overall folding of PTI is similar to half of that of cylinder 1 of $\alpha\text{-CHT}.$ The latter is based on six

 β -sheet features arranged in a fairly distorted cylindrical fashion with about 12, 10, 15 and 22 residues between turns. The resemblance can be seen from Figure 44 which compares the diagonal distance map of α -CHT and with that of PTI translated by 21 residues from the N-terminal to obtain the best congruence in folding with α -CHT. This suggests that the folding of an α -CHT cylinder might be based upon and related to that of PTI. The closest structural similarity occurs between the double-stranded anti-parallel sheet of PTI (CYS 14-39) and the doublestranded sheet of the HIS loop of α -CHT (CYS 42-58). The principal difference between the two occurs in the vicinity of and beyond residue 60 in a α -CHT (37 in PTI): from Figure 44, it can be seen that the C-terminal α -helix of PTI leads to a broader interaction perpendicular to the diagonal at residue 60. In the folding of PTI, the α -helix corresponds closely to the position of the fourth strand of the α -CHT cylinder so that the PTI folding resembles part of the cylindrical well. Removal of the helix and duplication of the remainder of the chain could conceivably lead to a cylinder.

The distance plot of PTI is shown in Figure 44, along with that of a 58 amino acid segment of α -CHT which bears a structural resemblance to PTI. It is apparent that this segment of α -CHT which occurs in domain A (residue 24-81) is quite similar to PTI when comparing alpha-carbon

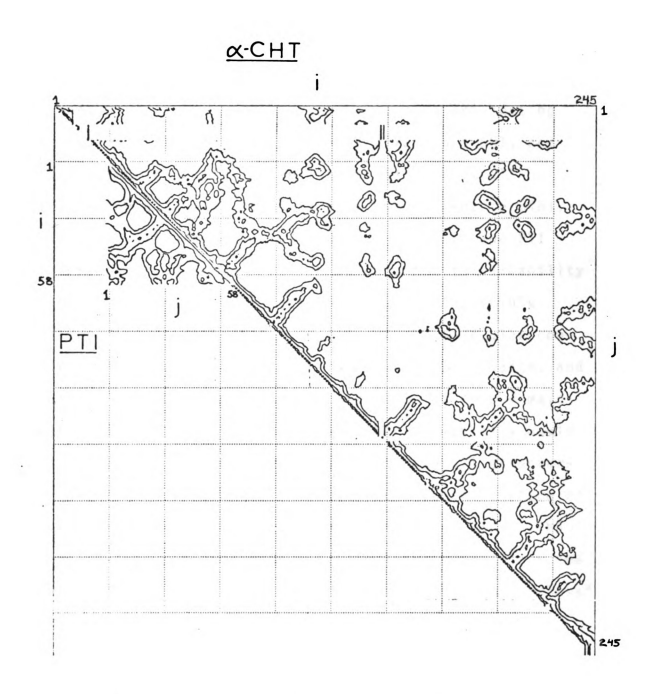


FIGURE 44. Comparison of Distance Diagonal Plots of $\alpha\text{-CHT}$ and PTI [contouring program courtesy of S. Ernst (18)].

separation distances although the comparison of their respective amino acid sequences does not yield the same conclusion (Table 26). The distance plots show similar placement of anti-parallel sheet structure originating at residues 37(221), 49(204) and 75(172) in α -CHT, and 10, 23 and 48 in PTI, as well as similar "helical" thickening along the diagonal near the segment termini. The major differences between domain A(24-81) and PTI interestingly involve a region which exhibits variability between domains A and B in native α -CHT. A possible interpretation is that this region of the molecular conformation is more susceptible to evolutionary change, and this is further buoyed by the comparison of this domain with elastase as described (45). This variability would not produce significant changes in the overall structure of α -CHT as the residues involved occur on the surface of the molecule, frequently with exposed side-chains. The three segments approximate a single loop (class C) of the multi-loop super helix. α -CHT also exhibits other "class" examples as previously indicated, most notably the approximately three strand loop beta structure (class B) which encompasses the region 75(172) to 97(146).

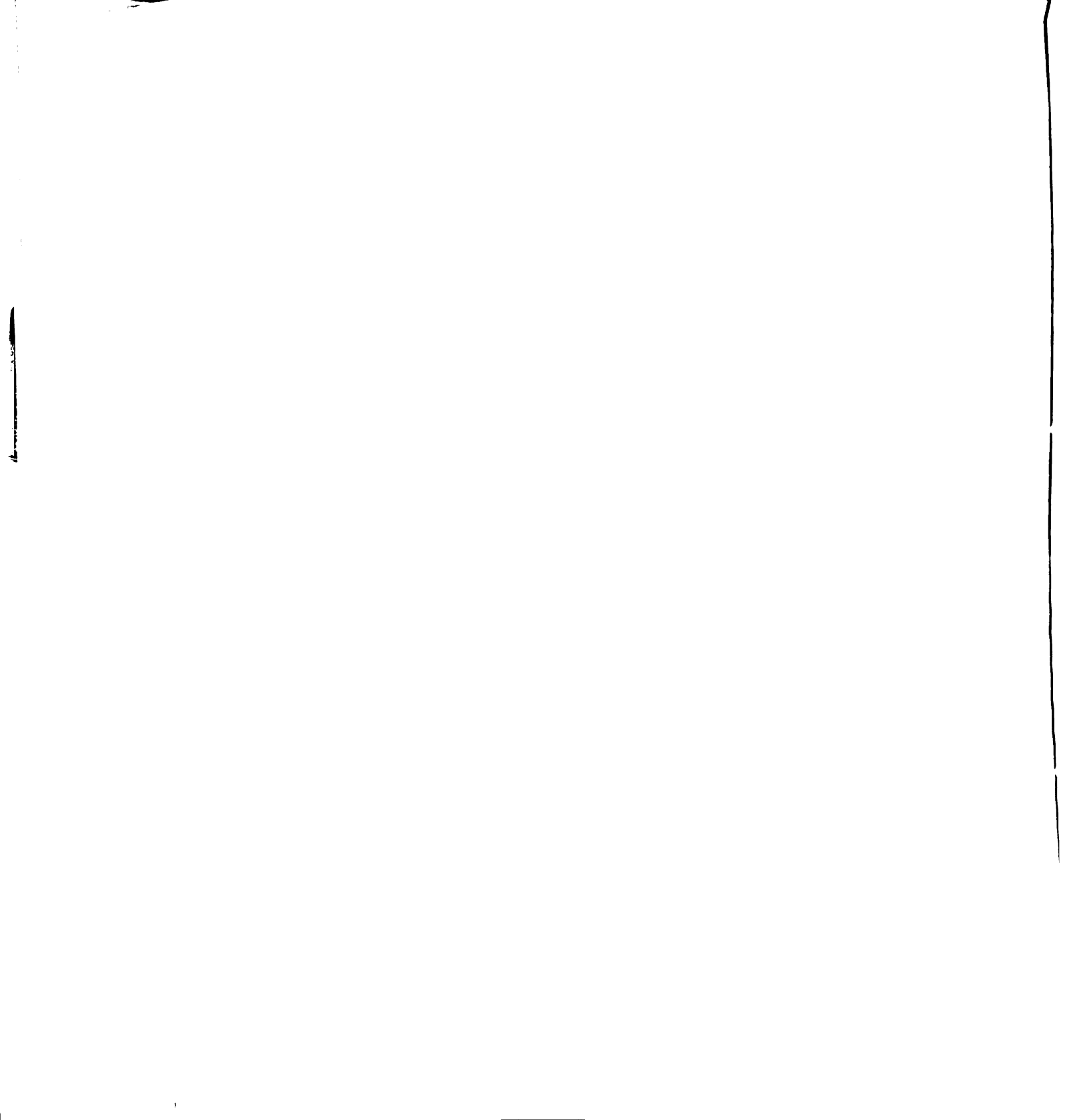
Concerning the possible structure-function relationship present in PTI, it should be noted that there are three disulfide bridges within the 58 residue chain. It is observed in α -CHT that only one disulfide appears in

TABLE 26

Sequence Comparison of PTI and $\alpha extsf{-CHT}$ Domain A Based on Alignment of Distance Diagonal Plots

α_CHT	 -	PTI		113 p	α-CHT	<u>+</u>	PTI		113 p
Residue #	Residue	Residue #	Residue		Residue #	Residue	Residue #	Residue	
24	P.RO		ARG	4	53	VAL	30	CYS	Ξ
25	GLY GLY	2	PRO	12	54	TH	3]	GLN	=
56	SER	က	ASP	12	55	ALA	32	THR	15
27	TRP	4	PHE	41	26	ALA	33	PHE	4
28	PR0	2	CYS	4	22	HIS	34	VAL	9
53	TRP	9	LEU	က	28	CYS	35	TYR	_
30	GLN	7	GLU GLU	14	29	GLY	36	GLY GLY	53
31	VAL	æ	PRO	∞	09	VAL	37	GLY	7
32	SER	6	PRO	Ξ	19	TH	38	CYS	6
33	LEU	10	TYR	9	62	TH	39	ARG	9
34	GLN	=	THR	Ξ	63	SER	40	ALA	33
35	ASP	12	GLY GLY	Ξ	64	ASP	41	LYS	2
36	LYS	13	PRO	∞	65	VAL	42	ARG	വ
37	TH	14	CYS	6	99	VAL	43	ASN	∞
38	GLY	15	LYS	7	29	VAL	44	ASN	∞
39	PHE	16	ALA	4	89	ALA	45	뮖	4
40	HIS	17	ARG	20	69	GL Y	46	LYS	7
41	PHE	18	ILE	Ξ	70	GLU	47	SER	=
42	CYS	19	ILE	ი	71	뿚	48	ALA	4
43	GLY	20	ARG	4	72	ASP	49	GLU	9
44	GLY	21	TYR	_	73	GLN	20	ASP	14
45	SER	22	뭂	4	74	GLY	51	CYS	9
46	LEU	23	TYR	9	75	SER	52	MET	∞
47	ILE	24	ASN	7	9/	SER	53	ARG	7
48	ASN	25	ALA	12	77	SER	54	THR	<u> </u>
49	GLU GLU	5 6	LYS	9	78	GL U	52	CYS	ည
20	ASN	27	ALA	12	79	LYS	26	GLY	7
51	TRP	58	GL.Y	_	80	ILE	22	GLY	9
52	VAL	53	LEU	15	81	GLN	28	ALA	11
Σp = 539	= <d></d>	9.3 ≡ random	selection (113	(113)					

 $\langle p \rangle = 9.3 \equiv random selection (113)$



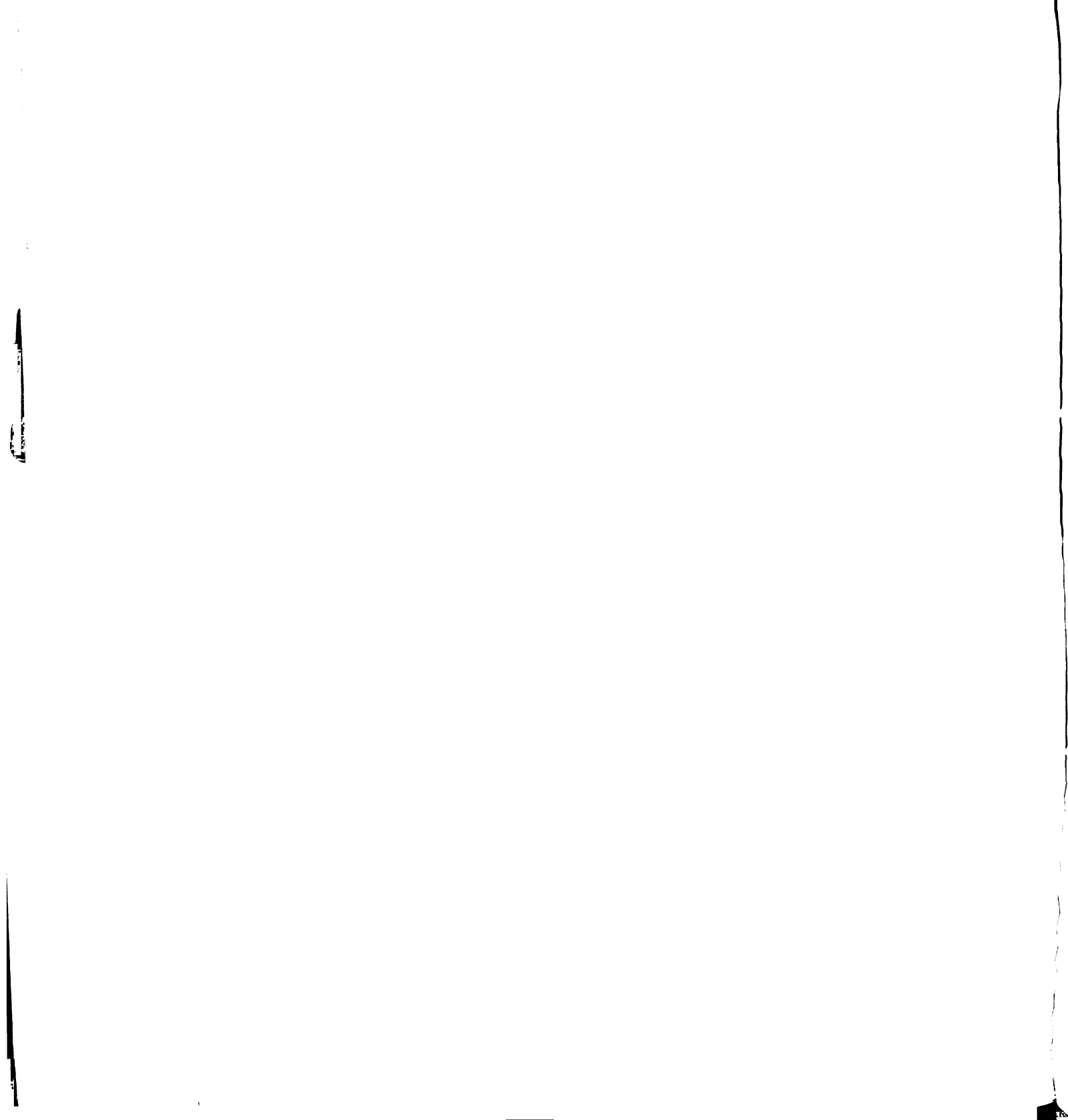
domain A (CYS 42-CYS 58), while three appear in domain B (136-301; 168-182; and 191-220), and two of the latter are linked externally to the 58 residue segment. It is possible that the disulfide links, themselves, are responsible for the relative chemical stability of the inhibitor molecule as compared to the serine proteases, in general. This conjecture is supported by the observation that upon the reduction of the disulfide bond CYS 14-38, the LYS 15-ALA 16 peptide bond is cleaved by T (114).

Based on the above observations, it is interesting to hypothesize on the evolution of the class of serine proteases and their natural inhibitors. It is possible that the domains of α -CHT represent conservative structures present in all serine proteases (cylinders have been identified in elastase) (91) resulting from a common evolutionary gene, and that the different specificities and three-dimensional structures are representative of presently stable gene mutations. The observation of domains in other protein classes suggests that proteins consist of several building blocks (domains), which might have specific conformational properties or functions associated with them. It is interesting to note that several of the bacterial serine proteases (e.g., Staphylococcus aureus) are of a molecular weight about 12,000-13,000 daltons (approximately 100-110 residues in



length), consistent with the size of the α -CHT domain. PTI is one-half this size (58 residues) which might imply the presence of still smaller domains or domain cores. The comparison with other members of this enzyme class and its inhibitors should prove most useful in establishing domain conservation. The functional importance with respect to α -CHT:inhibitor interactions is discussed below, examining both the reversible and irreversible inhibitors used in this study.

One last hypothesis incorporates the concept of a master macromolecule comprised of both the zymogen (inactive enzyme) and its natural inhibitor. This, in effect, would provide a bio-feedback mechanism by which a single molecule, consisting of sub-segments (domains), could be employed to generate the independent zymogen, the active enzyme and/or its natural inhibitor by appropriate cleavage. This concept is particularly of interest when one considers that the activation of the serine proteases from their zymogens appears to function with cleavage by other serine proteases--principally tryptic or chymotryptic attack. The idea of a single macromolecule structured as an internally complete system would further explain the observation of the large, apparently non-allosteric enzyme structures necessary to maintain a small, concerted active site configuration.



C. <u>Perturbations to the Tertiary Structure Accompanying</u> Active Site Binding

The intermolecular cooperativity exhibited by the tetrameric hemoglobin molecule gave early indications of the manner in which protein transmits conformational changes through its three-dimensional structure. In describing his theory of proton fluctuation, J. G. Kirkwood (88) stated:

Relatively distant groups may influence local interactions of complementary sites on two protein molecules by serving as sources or sinks of mobile charges supplied or withdrawn from the interacting sites.

And more recently, R. W. Lumry (89) has proposed the notion of mobile defects:

Proteins in solution are in a constant state of restless conformational fluctuation due to the presence of 'mobile defects' resulting from the evolution of imperfect bonding solutions. In addition to high mobility in most regions of protein, the mobile defects provide a store of potential energy necessary for specific function.

Both of these ideas emphasize the importance of mid- and long-range tertiary interactions and the dynamic nature of the three-dimensional structure of an enzyme, suggesting the ability to recognize and accommodate a substrate or inhibitor molecule and transmit this information through conformational changes. The group of structurally/functionally related inhibitors used in this study provides an excellent basis for the comparison of such structural adaptability. This will be accomplished

using a new technique developed in the course of this study, a distance plot of the difference electron density of a derivative which will be referred to as a difference diagonal plot. The construction of these difference diagonal plots has been described in the Methods section.

The difference diagonal plot considers the distance of a peak in a difference electron density map from the alpha-carbon atoms of residues i and j. The quantity plotted in the difference diagonal plot is the sum of the magnitudes of these distances (Figure 41b). The derivative difference distance plot shows structural changes on two levels. The primary level identifies the difference electron density peaks associated with individual alpha-carbon atoms (or residues) as contours along the diagonal. These represent the close approach of a peak in the difference electron density to a residue although, presently, positive and negative difference peaks are not distinguished. The peaks which appear offdiagonal are representative of changes occurring in the tertiary structure at both mid-range $(C_{\alpha i} - C_{\alpha i}, i = j)$ and long-range (i > j). Since the diagonal plot is symmetrical about the diagonal, the difference diagonal plot of the two monomers of α -CHT can be plotted on either side of the diagonal. Thus, any asymmetry about the diagonal represents an asymmetry in response of the

dimer to a perturbation. Some maps displaying the application of this new approach are shown in Figure 45(a-e), from which it is immediately apparent that, in general, mirror symmetry about the diagonal is not present, thus showing the asymmetrical response of the dimeric molecule. The difference peaks used in generating the plots of Figure 46(a-e) are listed in Appendix C. The asymmetry simply reflects the variability in structure observed in the dimer and between domains A and B.

The optimum correlation between the difference electron density distance plot and the structure of the native enzyme comes only after the distance diagonal plot of the enzyme itself has been elucidated. The detailed interpretation of the features of the three-dimensional structure which have been found in the distance diagonal plot of α -CHT (Figure 42) suggests the capability of this technique. It would be of further interest to determine the variability in interaction that could be caused by rotation, twisting or bending of adjacent regions of helices, β -sheets, random coils or combinations thereof. As this mode of examination of tertiary interactions of macromolecular structure is still under development, the interpretations and comparisons reported here may be subject to some revision.

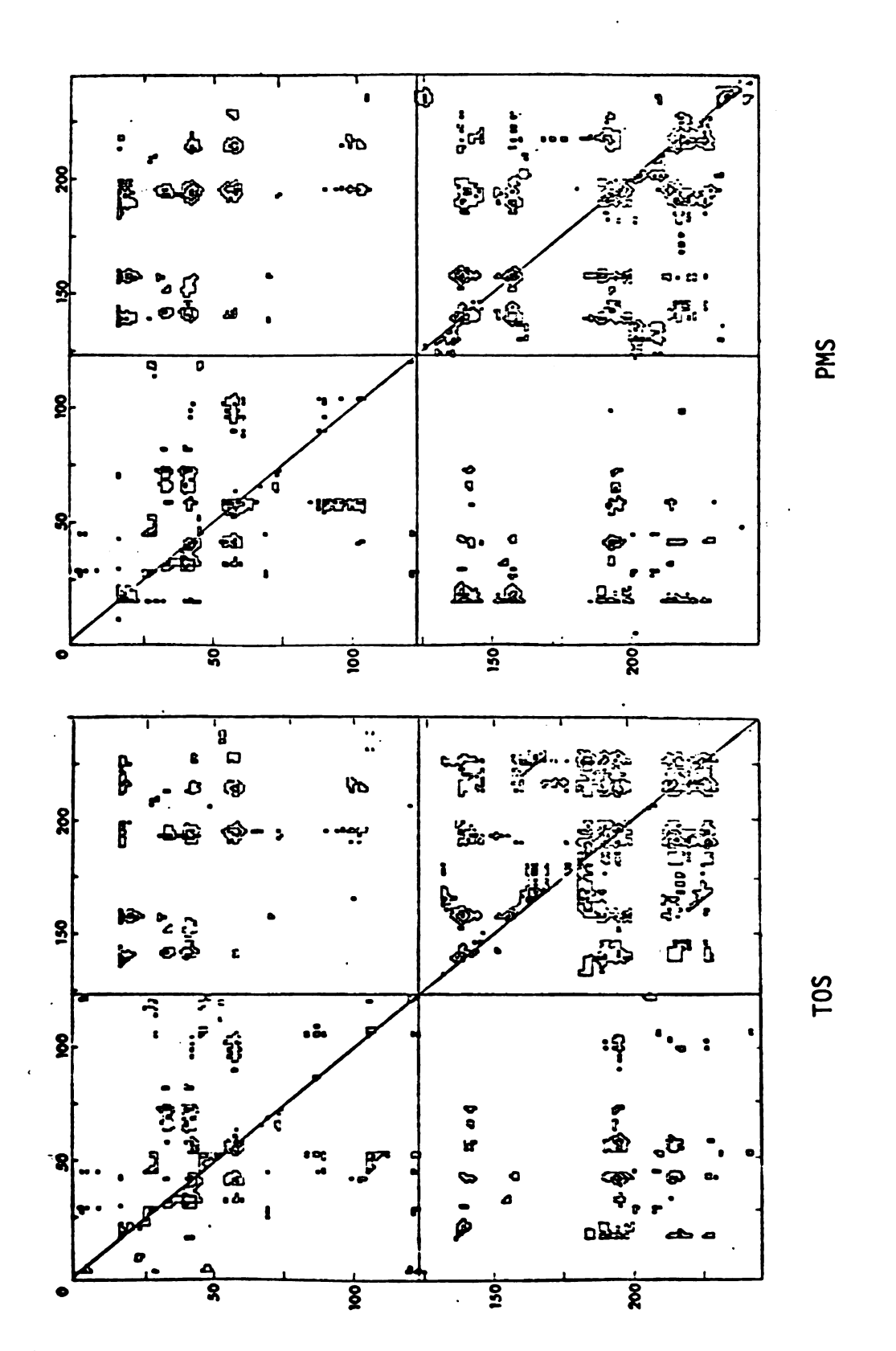
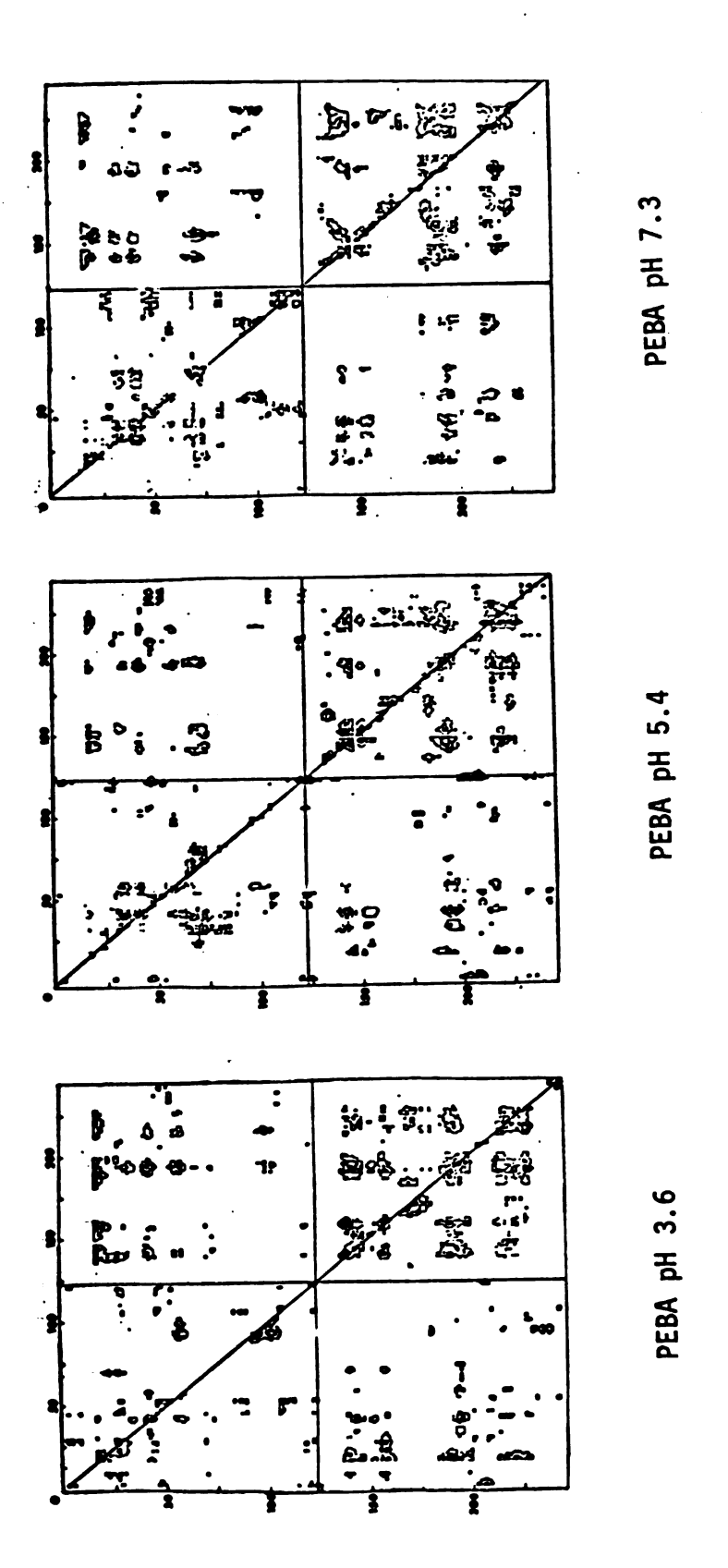
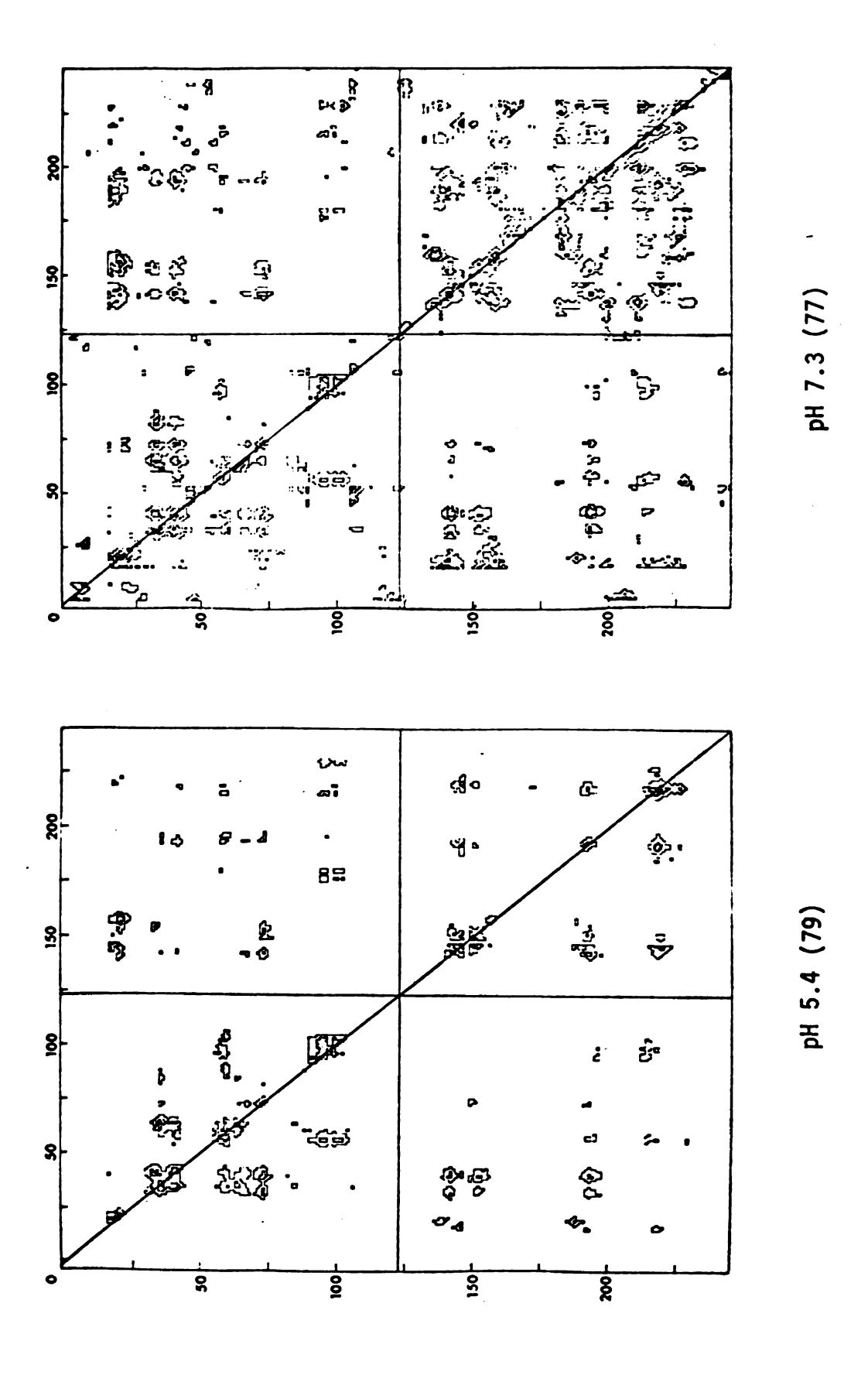
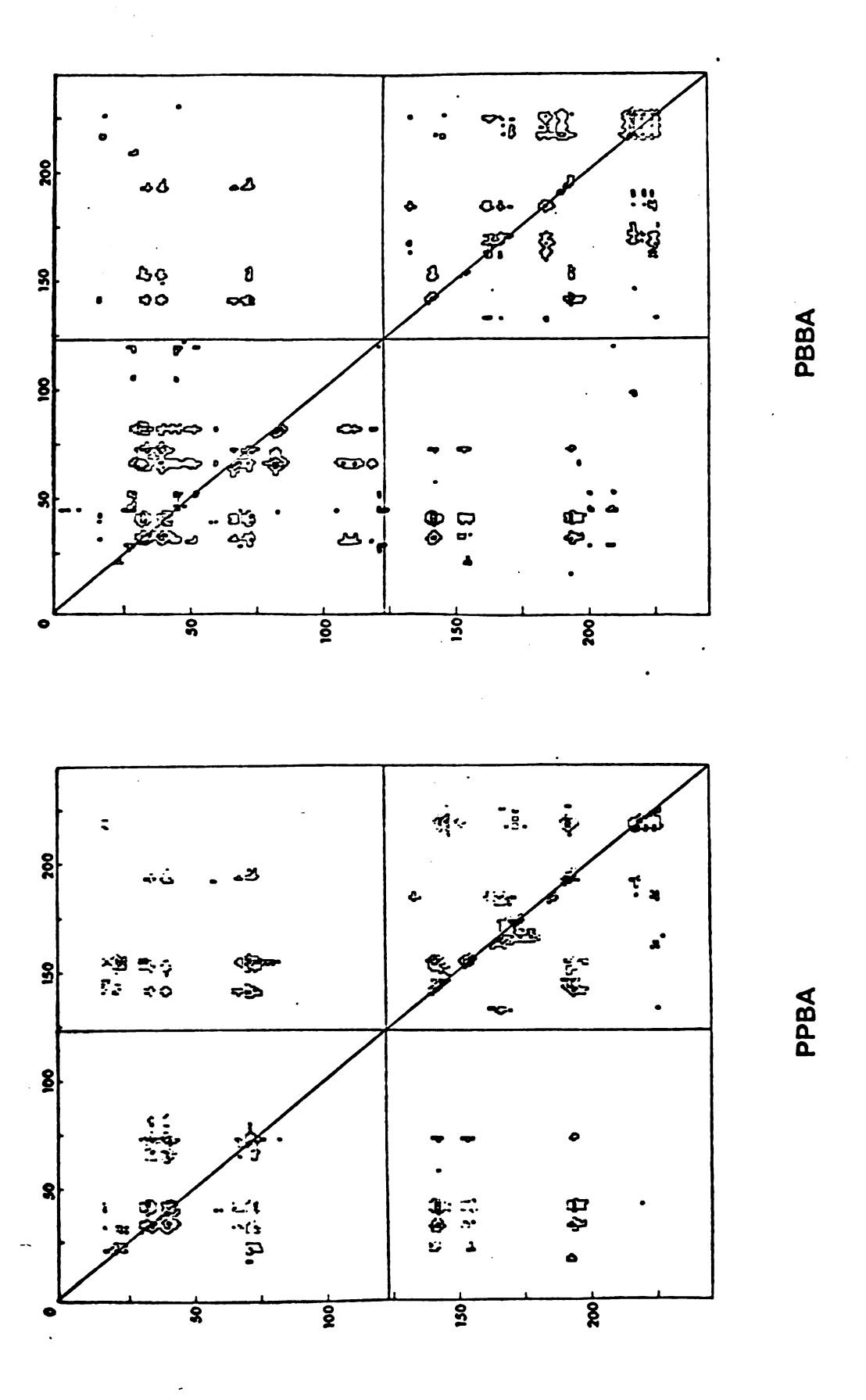
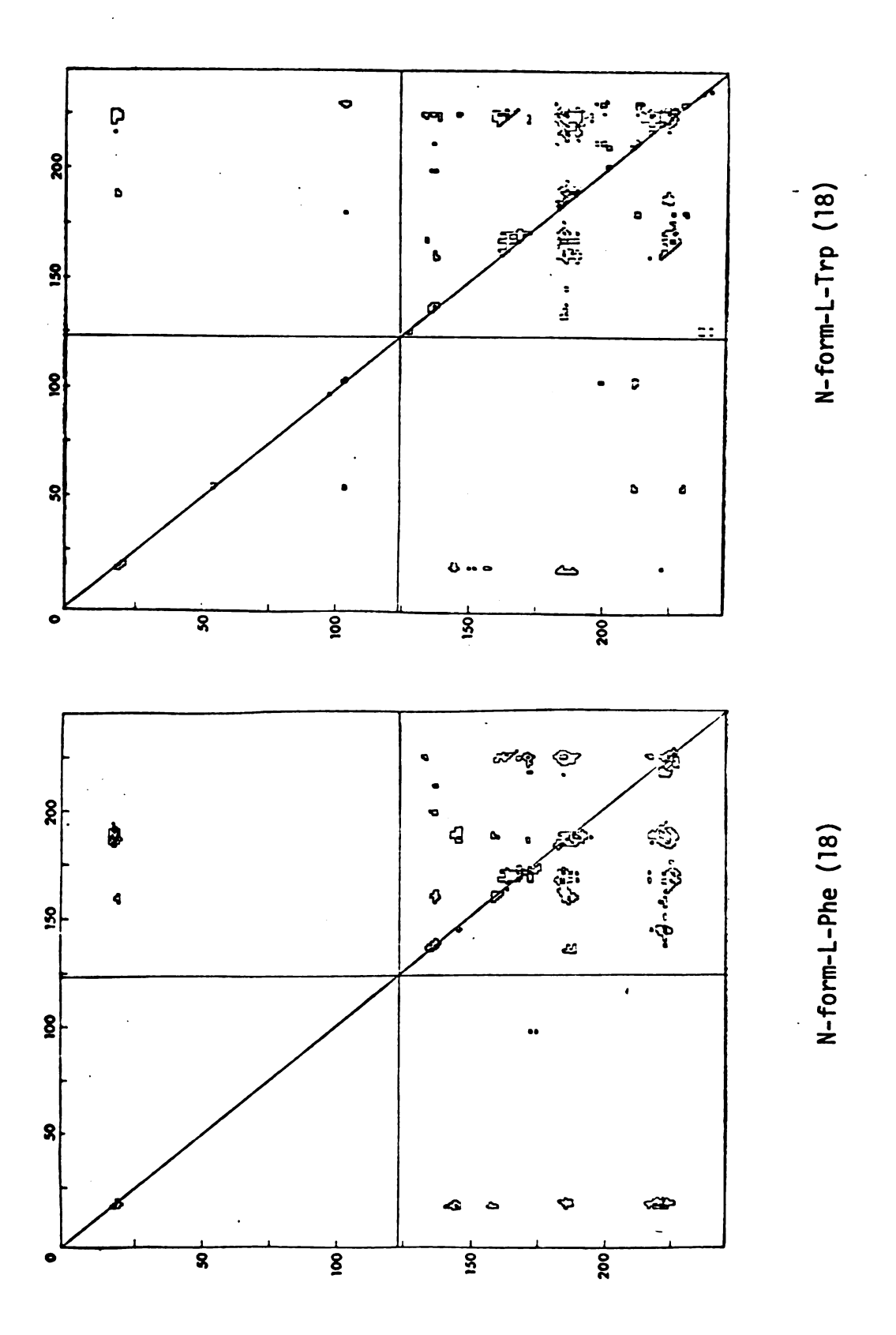


FIGURE 45. Difference Diagonal Plots



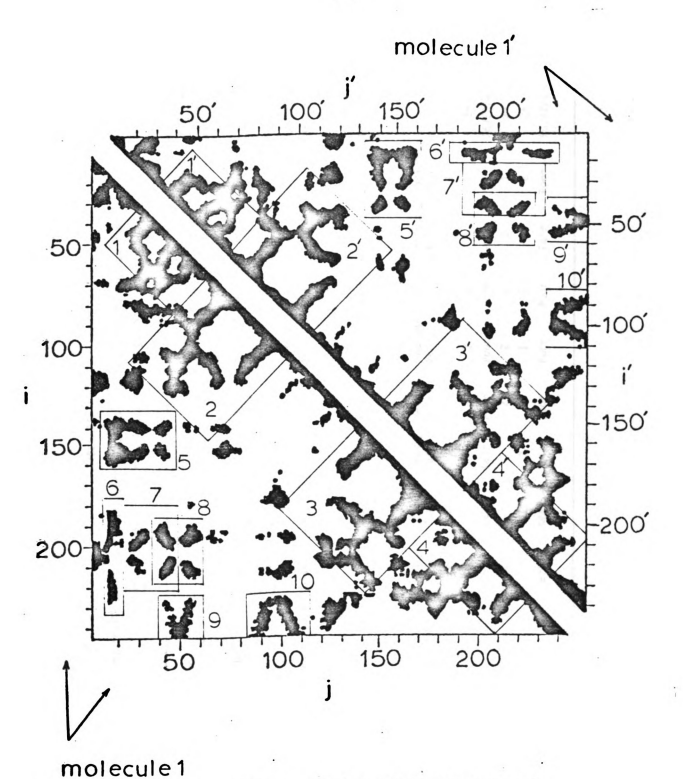






The features of the difference diagonal plots to be discussed below are denoted as 1-10 and 1'-10' in the distance diagonal plot of native α -CHT shown in Figure 46 and detailed in Table 27. These correspond to the β -barrel (cylinder), β -sheet loops and β -sheet stacking which were discussed in the previous section. Several observations can be made from this comparison which relate to the relative adaptability of the structural facets represented by these features.

- Features (1,1') and the domain-symmetry related 1. features (4,4'), are regions of the structure which show the greatest tendency to change, with (4,4') being generally more susceptible. (1,1') appears to be more sensitive to pH change than (4,4') due to the presence of ILE 16, 16' and HIS 40, 40'. The local twofold agreement appears to improve with pH in (1,1') and with duality of interaction within the catalytic region and specificity region of the active site for (4,4'). Comparison of (4,4') with PMS points out the variability in specificity site dimensions discussed above for the two independent molecules and might be indicative of differences in specificity.
- 2. Features (2,2') and the domain-symmetry related features (3,3') exhibit a greater fluctuation



OIECUIE | FIGURE 46. Identification of Diagonal Plot Features of Native α-CHT to be Compared in Difference Diagonal Plots

TABLE 27

Individual Analysis of Difference Electron Density Distance Diagonal Plots (Interactions: Heavy = 3; Medium = 2; Light/None = 1)

Domain/Feature	105	PMS	PEBA pH 3.6	PEBA pH 5.4	pH 5.4	PEBA pH 7.3	рн 7.3	PPBA	PBBA	N-form- &-PHE	N-form- e-trp	Average Overall
Domain A Substitution/	Medium/	Medium/	Light/	Medium/	Medium/	Heavy/	Medium/	Medium/	Medium/	None	None	
	2	2 2	<u> </u>	7007 2	7007 2	rair 2	. 2	rair 2	7a17			8
-	2	_	- 2	ო	7	က	က	2	8			.
Two-Fold	Poor	Poor	Poor	Fair	Good	Fair	Fair	Fair	Fair			P4/F4/G1
2	_	_	7	_	_	_	_	_	8			_
2,	_	_	_	_	8	ო	8	-	-			±
Two-Fold	ı	•	Poor	•	Poor	Poor	Poor	ř	Poor			P5/F0/G0
Domain B												
Substitution/ Two-Fold	Heavy/ Fair	Medium/ Good	Heavy/ Fair	Heavy/ Fair	Light/ Good	Heavy/ Fair	Medium/ Poor	Medium/ Poor	Light/ Poor	Medium/ Fair	/ Medium/ Poor	
ო	_	8	ო	7	2	ო	2	-		_	, -	2
m	2	2	. 2	ო	2	ო	m	2	8	-	_	
Two-Fold	Poor	Poor	Fair	Fair	6 000	Fair	Poor	Poor	Poor		•	
4	ო	ო	ო	2	2	8	2	2	_	2	,- -	*
4	ო	_	ო	2	2	က	ო	_	2	-	2	5+
Two-Fold	B ood	Poor	Good	600d	9009	Fair	Poor	Poor	Poor	Fair .	Poor	P5/F2/G4

Table 27. (cont'd.)

Table 27. (cont'd.)

Domain/Feature	T0S	PMS	PEBA pH 3.6	PEBA pH 5.4	pH 5.4	PEBA pH 7.3	рн 7.3	PPBA	PBBA	N-form- &-PHE	N-form- &-TRP	Average Overall
Domain AB												
Substitution/ Two-Fold	Medium/ Fair	Light/ Fair	Light/ Fair	Light/ Poor	Light/ Poor							
ĸ	_	2	ო	2	2	ო	2	2	2	_	_	
5.	2	2	ო	2	_	m	က	2	2	-	_	
Two-Fold	Poor	Good	Good	Fair	Fair	Good	Fair	Fair	Fair	Fair	Poor	P2/F6/G3
Q	2	. 8	m	, 2	_	2	2	_	_	-	_	
•9	2	2	ო	2	_	2	2	_	_	-	_	
Two-Fold	Good	Fair	Poog	Fair	Poor	Fair	Fair	•		Fair	Fair	P1/F6/G2
7	2	2	2	2	_	2	2	_	_	_	_	±
7 .	2	2	2	2	_	2	2	_	_	_	-	±
Two-Fold	Fair	Fair	Good	Fair	Fair	Fair	Good	Fair	Fair	ı	•	P0/F7/G2
∞	ო	2	_	ო	_	2	က	~	_	_	~	
8	က	က	2	2	_	_	8	_	_	_	,-	
Two-Fold	Po og	Fair	Fair	Fair	Fair	Fair	Fair	•	•	•	•	P0/F6/G1
6	_	_	_	-	_	_	_	_	_	_	_	_
6	_	-	-	7	-	_	_	_	_	_	_	
Two-Fold			•	Fair		•	•	•	•		•	-/F1/-
10	_	_	_	_	_	_	_	-	_	_		_
10.	_	_	_	_	7	~	7	_	-	_	_	_
· Two-Fold		•	•	•	Fair	•	Fair	•	•			-/F2/-

in their variability with only light occupancy in (2,2') and slightly heavier occupancy in (3,3'), indicative of respective conformational adaptability. In (2,2'), of domain A, there again appears a greater pH susceptibility, now due to the presence of ASP 102, while in (3,3') the pH fluctuation appears to function cooperatively with the side-chain specificity difference. Neither feature exhibits extremely good or consistent two-fold correspondence.

- 3. The features (5,5'), (6,6'), (7,7') and (8,8') are the tertiary interactions of the β -strands (loops) between the two domains and along with (9,9') and (10,10') reveal the conformational adaptability in the inter-domain interface. The interactions of α -helix and β -loop, (9,9') and (10,10') (Table 22), show only slight if any change upon inhibitor binding. The principal change observed occurs only with (10,10') upon pH variation and only in molecule l'. This adaptability is tempered (eliminated) upon incorporation of PEBA.
- 4. Feature (5,5') represents conformation fluctuation which includes the segmented loop containing TYR 146, 146'. Although this feature is somewhat complex, involving two interactive

features, one with ILE 16 and one with HIS 40 (Figure 19), perturbations to this feature are combined in this discussion. These features exhibit the best two-fold symmetry of the more heavily changing features. There is no apparent correlation other than a greater degree of fluctuation occurring at pH 7.3 (with/without PEBA), or at pH 3.6 where the orientation of the boronate implies a more direct interaction than simple conformational adaptability.

5. Features (6,6'), (7,7') and (8,8') reflect the interactions between the loop involving LYS 203 and ILE 16, HIS 40 and ASN 48, respectively.

In general, these features exhibit fairly good two-fold agreement, indicative of their generally non-dimer interface involvement. (6,6') reveals a greater density of adaptation as would be expected when considering that the 203 loop includes MET 192, SER 195 and both CYS 191 and CYS 201. Feature (7,7') exhibits a similar degree of adaptability and the best two-fold agreement of any of the features examined. Feature (8,8') reveals fairly good two-fold symmetry between molecule 1 and 1', but

differences in the intensity of the adaptability, with pH influencing molecule 1 more than mole-cule 1'.

The availability of the difference electron density maps of two competitive reversible inhibitors, N-formyl- ℓ tryptophan and N-formyl- ℓ -phenylalanine (unpublished results of this laboratory), permitted an interesting but tentative generalization to be made from an examination of their difference electron density distance plots (Figure 45). The implication of the map is that changes which result from the occupation of the specificity region of the active site, as with these two inhibitors, are confined to the B domain of the structure. It is of interest to note that the two distance plots are very similar, generally differing in magnitude. The two-fold symmetry of the distance plots is best in the (4,4')The (3,3') features shows less change than with region. inhibitors which interacted more directly with both the catalytic and specificity regions of the active site. Thus it becomes apparent that TYR 146, 146' is essentially not involved in the interaction and its importance lies in the catalytic triad interaction in the dimer interface. Among the off-diagonal features, (5,5') exhibits the same changes in both derivatives, but only a fair degree of two-fold symmetry and is very light in substitution. The (6,6') feature exhibits greater substitution,

two-fold symmetry and similarity between the two derivatives.

Another comparison of changes in structure accompanying the introduction of inhibitors or pH change has been carried out using difference electron density peaks within the active site region. Only those peaks which occur within \pm 8 Å of the center of the active site in the x and y directions, but extending across the local two-fold axis separating the active sites of the dimer in the z direction, were considered. The correlation among those peaks is presented in Table 28, where further delineation is made between the catalytic and the specificity regions of the active site. Two peaks were assumed to be equivalent if both appear above the three sigma (difference electron density) level, both had the same sign and were located within 1 Å of one another.

It is apparent from examination of Table 28 that, in general, the difference electron density peaks other than the substitution are fairly conserved and reproducible in terms of observation of combined effects of inhibitor and pH change. This conservation is in agreement with concepts of molecular recognition and conformational adaptability. One intention of this work was to introduce and explore these concepts by X-ray crystallographic methods and studies in order to establish the feasibility of such approaches. Although this work cannot expound

Correlation (%) of Difference Electron Density Peaks (Other Than Substitution) Within the Active Site Region of $\alpha\text{-CHT}^{\star}$ TABLE 28

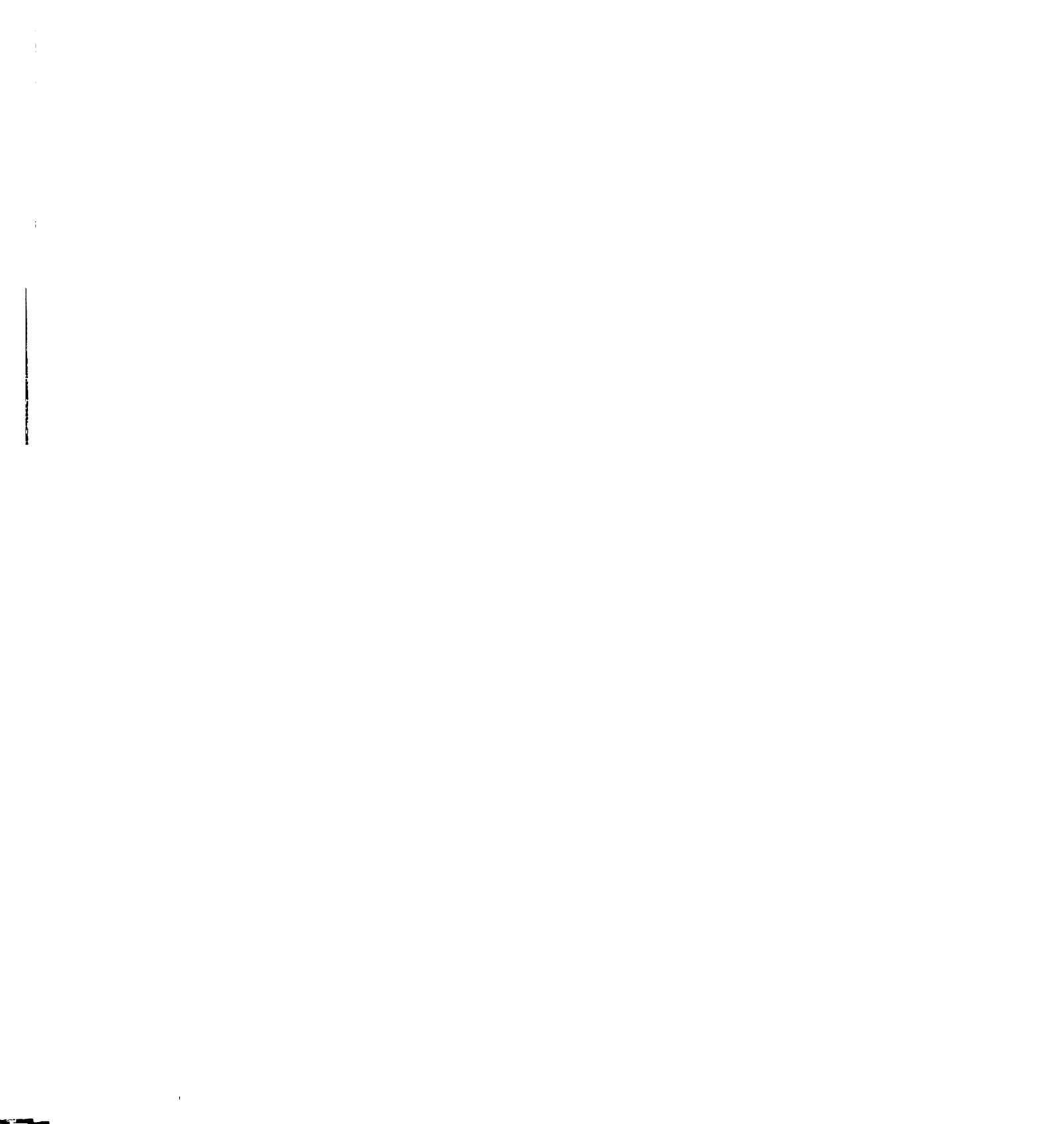
The second secon	The second name of the last of				The same and the s	-				
Specificity	Specificity Region (x < 49/7 # Peaks TOS	49/76) T0S	PMS	PEBA pH 3.6	PEBA pH 5.4	pH 5.4	PEBA pH 7.3	pH 7.3	PPBA	PBBA
TOS PMS PEBA PH 3.6 PEBA PH 5.4 PEBA PH 5.4 PEBA PH 7.3 PPBA		100 20 50 0 44 0 0	75 - 20 39 20 28 18 25 33	75 80 - 17 0 33 9	50 80 80 60 61 33 33		75 80 50 67 40 - 18 75	20 10 100 100 28 28 25 0	39 39 39 100 100	38 0 40 33 20 50 50 0 75
Catalytic Region	legion (x > 50/76 # Peaks TO	0/76) T0S	PMS	PEBA pH 3.6	PEBA pH 5.4	рН 5.4	PEBA pH 7.3	рн 7.3	PPBA	PBBA
TOS PMS PEBA PH 3.6 PEBA PH 5.4 PEBA PH 5.4 PPBA PH 7.3 PPBA	6 7 7 8 9 8 8 8	-888 50 12 12 12 00	100 - 60 29 14 31 0 17	50 - 24 0 33 33 20	33 33 33 43 45 65 65 65	24 0 24 - 100 17	88 8 9 13 3 1 4 8 8 8 8 8 8 8 8 8 8 8 8 8 8 8 8 8 8	29 0 0 100 17 20 20	0 30 18 44 22 100	17 13 20 24 43 54 83
			:		0					

*Peaks are considered to match if they occur within 1 Å of one another and are of the same sign although from different derivatives. % = # peaks (same)/# peaks (total).

with finality of ultimate results, it has established new methods and techniques with which to examine concepts of bio-molecular architecture utilizing specific enzyme inhibitors and potential transition-state analogs.

REFERENCES

- Hartley, B. S., <u>Nature</u> <u>201</u>, 1284 (1964).
 Hartley, B. S. and Kauffman, D. L., <u>Biochem. J.</u> <u>101</u>, 229 (1966).
- Meloun, B., Kluh, I., Kostka, V., Morávek, L., Prusik, Z., Vavécék, J., Keil, B. and Sorm, F., <u>Biochim. Biophys. Acta</u> 130, 543 (1966).
- 3. Blow, D. M., Birktoft, J. J. and Hartley, B. S., Nature 221, 337 (1969).
- 4. Blow, D. M., <u>The Enzymes</u>, P. D. Boyer, editor, Vol. III, 3rd. Edition, Academic Press, Chapter 6.
- 5. Kunitz, M. and Northrop, J. H., <u>J. Gen. Physiol</u>. <u>18</u>, 433 (1935).
- Bernal, J. D., Fankuchen, I. and Perutz, M. F., <u>Nature</u> 141, 523 (1938).
- 7. Bergmann, M. and Fruton, J. S., <u>Science</u> <u>83</u>, 306 (1936).
- 8. Bender, M. and Brubacher, L., <u>Catalysis and Enzyme</u> <u>Action</u>, McGraw-Hill, New York, 1973.
- 9. Zerner, B. and Bender, M. L., <u>J. Am. Chem. Soc</u>. <u>85</u>, 357 (1963).
- 10. Bender, M. L., Clement, G. E., Kezdy, F. J. and Heck, H. d'A, J. Am. Chem. Soc. 86, 3680 (1964).
- 11. Sprinson, D. B. and Rittenberg, D., Nature 167, 484 (1951).
- Jansen, E. F., Nutting, M. D. F., Jang, R. and Balls,
 A. K., J. Biol. Chem. 179, 189 (1949).
- 13. Shaffer, N. K., May, S. C. and Summerson, W. H., J. Biol. Chem. 202, 67 (1953).
- 14. Oosterbaan, R. A. and van Adrichem, M. E., <u>Biochim.</u> <u>Biophys. Acta</u> <u>27</u>, 423 (1958).
- 15. Baker, B. R., <u>Design of Active-Site-Directed</u>
 <u>Irreversible Enzyme Inhibitors</u>, Wiley, New York,
 1967.



- Ray, W. J., Ruscica, J. J. and Koshland, D. E., J. Am. Chem. Soc. 82, 4739 (1960).
- 17. Schoellmann, G. and Shaw, E., <u>Biochemistry 2</u>, 252 (1963).
- 18. Unpublished results of this laboratory.
- 19. Henderson, R., <u>Biochem. J.</u> 124, 13 (1971).
- Wright, C. S., Hess, G. P. and Blow, D. M.,
 J. Mol. Biol. 63, 295 (1972).
- 21. Dayhoff, M. O., Atlas of Protein Sequence and Structure, National Biomedical Research Foundation, Washington, D. C., Vol. 5, 1972, p. D-107.
- 22. Goodwin, T. W., Harris, J. I. and Hartley, B. S., Structure and Activity of Enzymes, FEBS Symposium #1, March 24, 1964, Academic Press.
- 23. Wright, C. S., Alden, R. A. and Kraut, J., <u>Nature</u> 221, 235 (1969).
- 24. Koshland, D. E., Strumeyer, D. H. and Ray, W. J. Brookhaven Symp. Biol. 15, 101 (1962).
- Schramm, H. J. and Lawson, W. B., <u>Hoppe-Seyl. Z</u>. 332, 97 (1963).
 Lawson, W. B. and Schramm, H. J., <u>Biochemistry 4</u>, 377 (1965).
- 26. Taylor, R. P., Vatz, J. B. and Lumry, R., <u>Biochemistry</u> 12, 2933 (1973).
- 27. Hartley, B. S., <u>Phil. Trans. Roy. Soc. London</u> <u>B257</u>, 77 (1970).
- 28. Horbett, T. A. and Teller, D. C., <u>Biochemistry 12</u>, 1349 (1973).

 Gladner, J. A. and Neurath, H., <u>J. Biol. Chem</u>. <u>206</u>, 911 (1954).
- 29. Rydon, H. N., Nature 182, 928 (1958).
- Cohen, J. A., Oosterbaan, R. A., Jansz, H. S. and Berends, F., <u>J. Cell. Comp. Physiol</u>. <u>54</u>, Suppl. 1, 231 (1959).

- Schneider, F., <u>Hoppe-Seyl. Z. 332</u>, 38 (1963).
- Smith, E. L., Light, A. and Kimmel, J. R., Biochemical Society Symposia No. 21, The Structure and Biosynthesis of Macromolecules, A61, Cambridge University Press, p. 88.
- 31. Bernhard, S. A., Berger, A., Carter, J. H., Katchalski, E., Sela, M. and Shalitin, Y. J. Am. Chem. Soc. 84, 2421 (1962).
- 32. Gutfreund, H. and Sturtevant, J., <u>Biochem. J.</u> 63, 656 (1956).
- 33. Fersht, A. R. and Sperling, J., <u>J. Mol. Biol</u>. <u>74</u>, 137 (1973).
- 34. Tulinsky, A., Mani, N. V., Morimoto, C. N. and Vandlen, R. L., <u>Acta Cryst</u>. <u>B29</u>, 1309 (1973).
- 35. Medical Research Council, Laboratory of Molecular Biology, Cambridge, England.
- 36. Blow, D. M., Rossmann, M. G. and Jeffrey, B. A., J. Mol. Biol. 8, 65 (1964).
- 37. Matthews, B. W., Sigler, P. B., Henderson, R. and Blow, D. M., <u>Nature</u> <u>214</u>, 652 (1967).
- 38. Birktoft, J. J., Matthews, B. M. and Blow, D. M. Biochem. Biophys. Res. Commun. 36, 131 (1969).
- 39. Sigler, P. B., Jeffrey, B. A., Matthews, B. W. and Blow, D. M., J. Mol. Biol. 15, 175 (1966).
- 40. Department of Chemistry, Michigan State University, East Lansing, Michigan.
- 41. Vandlen, R. L. and Tulinsky, A., Biochemistry 12, 4193 (1973).
- 42. Tulinsky, A., Vandlen, R. L., Morimoto, C. N., Mani, N. V. and Wright, L. H., <u>Biochemistry</u> 12, 4185 (1973).
- 43. Mavridis, A., Tulinsky, A. and Liebman, M. N. Biochemistry 13, 3661 (1974).
- 44. Nishikawa, K., Ooi, T., Isogai, Y. and Saito, N., J. Phys. Soc. Japan 32, 1331 (1972).

- 45. Nishikawa, K. and Ooi, T., <u>J. Theor. Biol</u>. <u>43</u>, 351 (1974).
- 46. Sigler, P. B., Blow, D. M., Matthews, B. M. and Henderson, R., <u>J. Mol. Biol</u>. <u>35</u>, 143 (1968).
- 47. Steitz, T. A., Henderson, R. and Blow, D. M. J. Mol. Biol. 46, 337 (1969).
- 48. Henderson, R., J. Mol. Biol. <u>54</u>, 341 (1970).
- 49. Birktoft, J. J. and Blow, D. M., <u>J. Mol. Biol</u>. <u>68</u>, 187 (1972).
- 50. Freer, S. T., Kraut, J., Robertus, J. D., Wright, H. T. and Xuong, NgH, Biochemistry 9, 1997 (1970).
- Wright, H. T., <u>J. Mol. Biol</u>. <u>79</u>, 1 (1973).
 Wright, H. T., <u>J. Mol. Biol</u>. <u>79</u>, 13 (1973).
- 52. Segal, D. M., Powers, J. C., Cohen, G. H., Davies, D. R. and Wilcox, P. E., <u>Biochemistry</u> 10, 3728 (1971).
- 53. Wright, C. S., Alden, R. A. and Kraut, J., <u>Nature</u> 221, 235 (1969).
 - Alden, R. A., Birktoft, J. J., Kraut, J., Robertus, J. D. and Wright, C. S., <u>Biochem. Biophys. Res.</u> Commun. 45, 337 (1971).
 - Robertus, J. D., Kraut, J., Alden, R. A. and Birktoft, J. J., Biochemistry 11, 4293 (1972).
 - Drenth, J., Hol, W. G., Jansonius, J. N. and Koekoek, R., Cold Spring Harbor Symposium on Quantitative Biology, Vol. XXXVI, Cold Spring Harbor Laboratory, 1971, p. 107.
- 54. Shotton, D. M., Watson, H. C., <u>Phil. Trans. Roy.</u> <u>Soc. London</u> <u>B257</u>, 111 (1969).
 - Watson, H. C., Shotton, D. M., Cox, J. M. and Muirhead, H., <u>Nature</u> <u>225</u>, 806 (1970).
- 55. Stroud, R. M., Kay, L. M. and Dickerson, R. E.

 Cold Spring Harbor Symposium on Quantitative

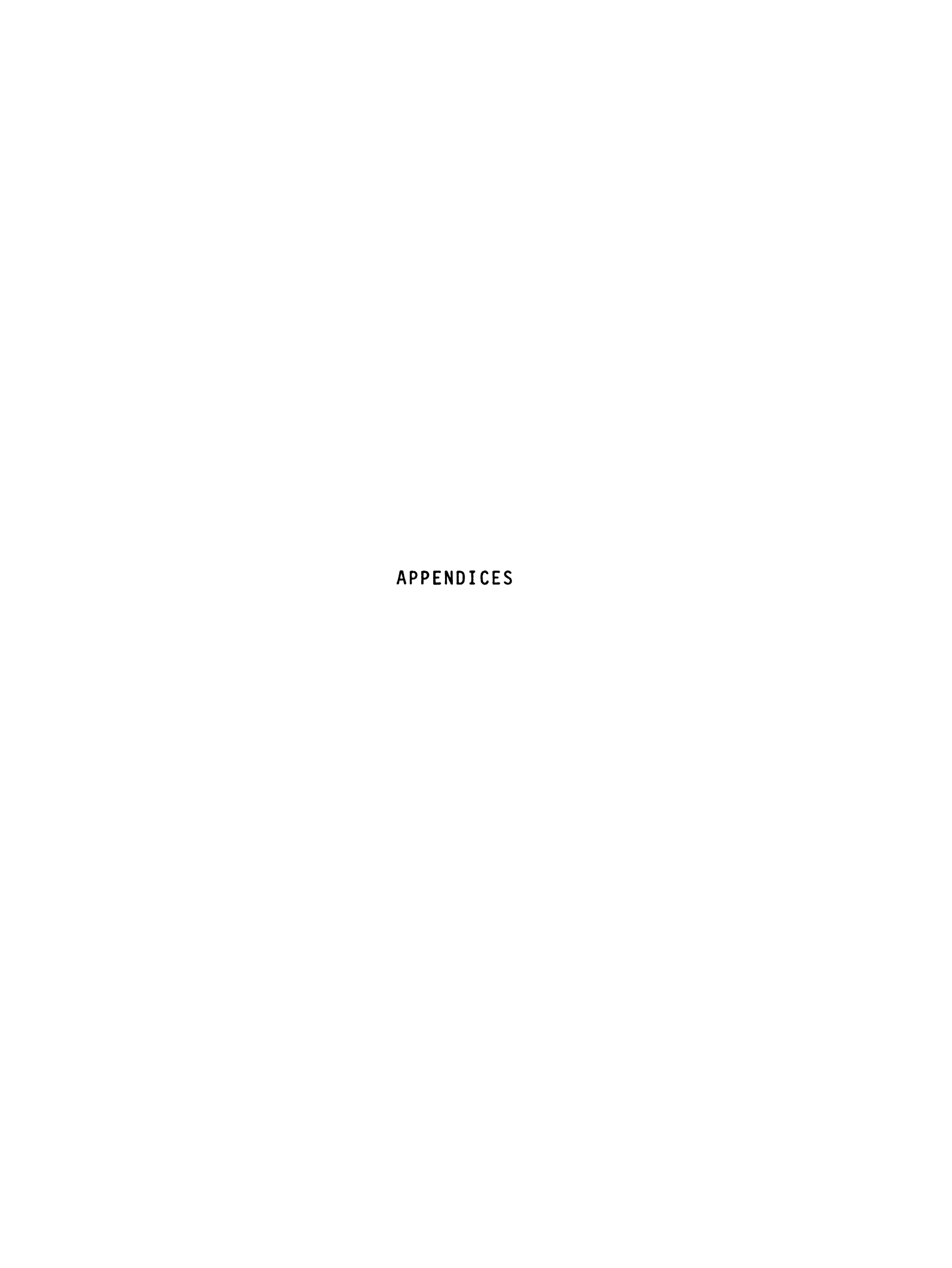
 Biology, Vol. XXXVI, Cold Spring Harbor Laboratory,
 1971, p. 125.

- Stroud, R. M., Kay, L. M. and Dickerson, R. E. J. Mol. Biol. 83, 185 (1974).
- 56. Pauling, L., Chem. Eng. News 24, 1375 (1946).
- 57. Wolfenden, R., Acc. Chem. Res. 5, 10 (1972).
- 58. Bender, M. L., J. Am. Chem. Soc. 73, 1626 (1951).
- 59. Thompson, R. C. and Blout, E. R., <u>Biochemistry</u> 12, 44 (1973).
- 60. <u>International Tables for X-Ray Crystallography</u>, Vol. III, p. 202, Kynoch Press, Birmingham, 1962.
- 61. Bell, R. P., Edwards, J. O. and Jones, R. B., The Chemistry of Boron and Its Compounds, Muetterties, E. L., Editor, Wiley, New York, Chapter 4.
- 62. Rawn, J. D. and Lienhard, G. E., <u>Biochemistry</u> <u>13</u>, 3124 (1974).
- 63. Lindquist, R. N. and Terry, C., Arch. Biochem. Biophys. 160, 135 (1974).
- 64. Antonov, V. K., Ivanina, T. V., Berezin, I. V. and Martinek, K., FEBS Letters 7, 23 (1970).
- 65. Antonov, V. K., Ivanina, T. V., Ivanova, A. G., Berezin, I. V., Levashov, A. V. and Martinek, K. FEBS Letters 20, 37 (1972).
- 66. Koehler, K. A. and Lienhard, G. E., <u>Biochemistry</u> 10, 13 (1971).
- 67. Matthews, D. A., Alden, R. A., Birktoft, J. J., Freer, S. T. and Kraut, J., <u>J. Biol. Chem.</u> 250, 7120 (1975).
- 68. Worthington Biochemical Corporation, Freehold, New Jersey.
- 69. Schwert, G. W. and Kaufman, S., <u>J. Biol. Chem.</u> 190, 807 (1951).
- 70. para-toluene sulfonyl fluoride purchased from Aldrich Chemical Company, Milwaukee, Wisconsin, #11,745-5.

- 71. Department of Chemistry, Ohio State University, Columbus, Ohio.
- 72. Department of Chemistry, University of New Hampshire, Durham, New Hampshire.
- 73. Institute for Chemistry of Natural Products, USSR, Academy of Science, Moscow, USSR.
- 74. Operating Manual, Leeds-Northrup general purpose pH meter, Model 4711.
- 75. King, M. V., <u>Acta Cryst</u>. <u>7</u>, 601 (1954).
- 76. Personal communication, Bud Suddath, Department of Chemistry, Massachusetts Institute of Technology, Cambridge, Massachusetts.
- 77. Hunt, P., <u>Senior Honors Report</u>, Department of Chemistry, Michigan State University, East Lansing, Michigan.
- 78. Vandlen, R. L. and Tulinsky, A., <u>Acta Cryst</u>. <u>B27</u>, 437 (1971).
- 79. Vandlen, R. L., Ph.D. Thesis, Department of Chemistry, Michigan State University, East Lansing, Michigan, 1973.
- 80. Henderson, R. and Moffat, J. K., <u>Acta Cryst</u>. <u>B27</u>, 1414 (1971).
- 81. Luzzati, V., <u>Acta Cryst</u>. <u>6</u>, 142 (1953).
- 82. Ford, L. O., Johnson, L. N., Macin, P. A., Phillips, D. C. and Tjian, R., <u>J. Mol. Biol</u>. <u>88</u>, 349 (1974).
- 83. Phillips, D. C., <u>British Biochemistry</u>, <u>Past and Present</u>, T. W. Goodwin, Editor, Academic Press, London, 1970, pp. 11-28.
- 84. Richards, F. M., <u>J. Mol. Biol</u>. <u>37</u>, 225 (1968).
- 85. The Chemical Society, <u>Tables of Interatomic Distances</u> and <u>Conformations in Molecules and Ions</u>, Special Publication #10, Burlington House, W.1, 1958.
- 86. Hass, B. S., Willoughby, T. V., Morimoto, C. N., Cullen, D. L. and Meyer, E. F., Acta Cryst. B31, 1225 (1975).

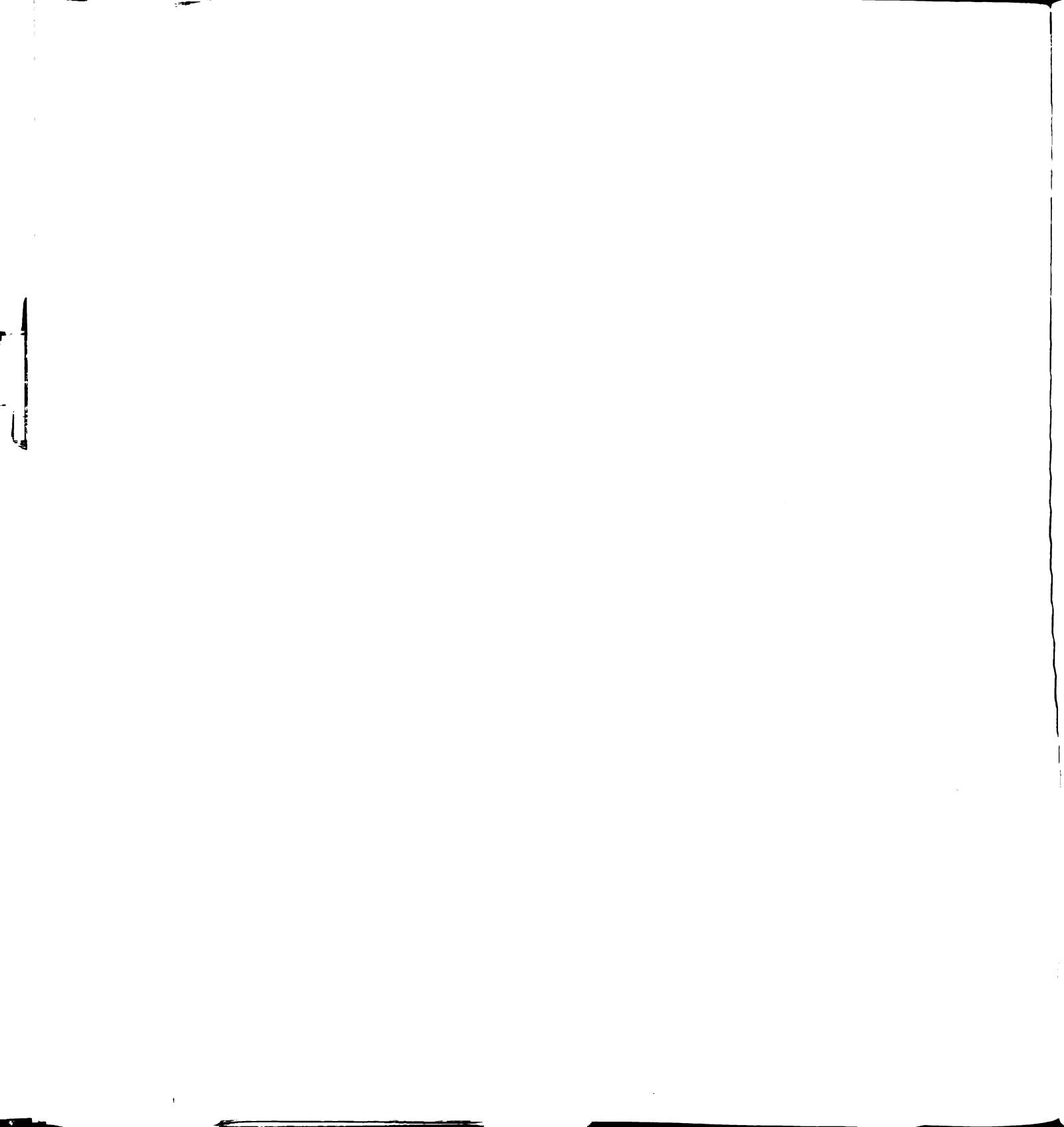
- 87. Diamond, R., Acta Cryst. 21, 253 (1966).
- 88. Kirkwood, J. G., "The Nature of the Forces Between Protein Molecules in Solution," The Mechanism of Enzyme Action, Johns Hopkins Press, Baltimore, (1954).
- 89. Lumry, R., "Fundamental Problems in the Physical Chemistry of Protein Behavior," <u>Electron and Coupled Energy Transfer in Biological Systems</u>, Vol. I, Part A, King and Klingenberg, Editors, Marcel Dekker, New York, 1971.
- 90. Adams, M. J., Buehner, M., Chandrasekhar, K., Ford, G. C., Hackert, M. L., Liljas, A., Rossmann, M. G., Smiley, I. E., Allison, W. S., Everse, J., Kaplan, N. O. and Taylor, S., Proc. Nat. Acad. Sci. USA 70, 1968 (1972).
- 91. Shotton, D. M., White, N. J. and Watson, H. C., Cold Spring Harbor Symposium on Quantitative Biology, Vol. 36, 187 (1971).
- 92. Liljas, A. and Rossmann, M. G., <u>Annual Review of Biochemistry</u> 43, 475 (1974).
- 93. M. G. Rossmann, Purdue University, West Lafayette, Indiana, personal communication.
- 94. Tulinsky, A. and Wright, L. H., <u>J. Mol. Biol</u>. <u>81</u>, 47 (1973).
- 95. Cotton, F. A. and Wilkinson, G., Advances in Inorganic Chemistry, 2nd Edition, Interscience Publishers, New York.
- 96. Lienhard, G., Science 180, 13 (1973).
- 97. Schray, K. and Klunman, J. P., <u>Biochem. Biophys.</u> Res. Commun. <u>57</u>, 641 (1974).
- 98. Philipp, M. and Bender, M. L., <u>Proc. Nat. Acad. Sci. USA</u> 68, 478 (1971).
- 99. Nakatani, H., Hanai, K., Uehara, I. and Hiromi, K., <u>J. Biochem</u>. <u>77</u>, 905 (1975).
- 100. Hess, G. P., Sybert, D., Lewis, A., Spoonhower, J. and Cookingham, R., Science 189, 384 (1975).

- Ruhlmann, A., Kukla, D., Schwager, P., Bartels,
 K. and Huber, R., <u>J. Mol. Biol</u>. <u>77</u>, 417 (1973).
- 102. Sweet, R. M., Wright, H. T., Janin, J., Chiotia, C. H. and Blow, D. M., <u>Biochemistry</u> <u>13</u>, 4212 (1974).
- 103. Blow, D. M., Wright, C. S., Kukla, D., Ruhlmann, A., Steigemann, W. and Huber, R., <u>J. Mol. Biol</u>. <u>69</u>, 137 (1972).
- 104. Huber, R., Kukla, D., Ruhlmann, A., Epp, O., and Formanek, H., Naturwissenschaften 57, 389 (1970).
- 105. Yoshimoto, M. and Hansch, C., <u>J. Med. Chem</u>. <u>19</u>, 71 (1976).
- 106. Simon, Z., Angew. Chem. Int. Ed. 13, 719 (1974).
- 107. Jones, J. B., Kunitake, T., Niemann, C. and Hein,
 G. C., J. Am. Chem. Soc. 87, 8 (1965).
- Dupaix, A., Bechet, J. and Roucous, C., <u>Biochem.</u> Biophys. Res. Commun. 41, 464 (1970).
- 109. Bondi, A., Physical Properties of Molecular Crystals, Liquids and Glasses, Wiley, New York, 1968.
- 110. Brown, W., Biochemistry 14, 5079 (1975).
- 111. Rossmann, M. G. and Liljas, A., <u>J. Mol. Biol</u>. <u>85</u>, 177 (1974).
- 112. Kuntz, I. D., <u>J. Am. Chem. Soc</u>. <u>97</u>, 15 (1975).
- 113. Dayhoff, M. O., Atlas of Protein Sequence and Structure, 1972, Vol. 5, National Biomedical Research Foundation, Silver Springs, Maryland, 1972.
- 114. Kress, L. F. and Laskowski, M., <u>J. Biol. Chem.</u> 242, 4925 (1967).



APPENDIX A

Coordinates of Inhibitors Determined in This Study (a = 49.2 Å, b = 67.2 Å, c = 65.95 Å, β = 101.8°)



APPENDIX A-1

Coordinates of Inhibitors Determined in This Study

 $(a = 49.2 \text{ Å, b} = 67.2 \text{ Å, c} = 65.95 \text{ Å, B} = 101.8^{\circ})$

T0S

		Molecule 1			Molecule 1'	
Atom Name	×	>	2	×	۶,	Z
C 2	0.5675	0.2548	0.3770	0.5681	0.3354	0.5321
C J	0.6440	0.2875	0.3850	0.6426	0.3040	0.5599
C 5	0.6330	0.2824	0.4023	0.6336	0.3202	0.5702
ဗ	0.6080	0.2719	0.3996	0.6098	0.3308	0.5609
C 4	0.5943	0.2660	0.3798	0.5936	0.3241	0.5421
CP3	0.6058	0.2706	0.3626	0.6014	0.3070	0.5326
CP2	0.6304	0.2816	0.3651	0.6266	0.2976	0.5410
S	0.6768	0.3012	0.3884	0.6736	0.2901	0.5721
0 1	0.6821	0.3114	0.4088	0.6899	0.2850	0.5562
0 2	0.6749	0.3162	0.3717	0.6653	0.2717	0.5814
0 3	0.6997	0.2872	0.3875	0.6908	0.3026	0.5883

Appendix A-1 (cont'd.)

Appendix A-1 (cont'd.)

		Molecule 1			Molecule 1'	
Atom Name	×	۶.	2	×	አ	2
C J	0.6379	0.2897	0.3825	0.6339	0.3033	0.5526
C 2	0.6278	0.2831	0.3997	0.6334	0.3184	0.5672
ဧ	0.6055	0.2697	0.3969	0.6159	0.3348	0.5619
C 4	0.5938	0.2626	0.3771	0.5971	0.3353	0.5429
CP3	0.6045	0.2687	0.3600	0.5960	0.3195	0.5290
CP2	0.6263	0.2825	0.3627	0.6154	0.3039	0.5334
CA	0.6618	0.3040	0.3854	0.6526	0.2857	0.5581
S	0.6945	0.2902	0.3926	0.6879	0.2942	0.5690
0 1	0.7010	0.2806	0.3740	0.7051	0.2926	0.5531
0 2	0.7172	0.3041	0.4015	0.7001	0.2818	0.5871
0 3	0.6918	0.2749	0.4081	0.6870	0.3153	0.5756

Appendix A-l (cont'd.)

Appendix A-l (cont'd.)

			PEBA pH 3.6	9		
		Molecule 1			Molecule 1'	
Atom Name	×	>	2	×	۲	2
L 0	0.6238	0.2876	0.3803	0.6334	0.3262	0.5474
C 2	0.6062	0.2831	0.3614	0.6346	0.3459	0.5544
ဧ ၁	0.5888	0.2665	0.3597	0.6105	0.3576	0.5510
C 4	0.5872	0.2554	0.3774	0.5848	0.3490	0.5421
CP3	0.6031	0.2609	0.3967	0.5833	0.3289	0.5366
CP2	0.6225	0.2764	0.3980	0.6078	0.3177	0.5383
CA	0.6424	0.3055	0.3821	0.6591	0.3137	0.5511
CB	0.6729	0.2987	0.3885	0.6512	0.2916	0.5528
æ	0.6921	0.3175	0.3940	0.6768	0.2781	0.5516
0 1	0.6893	0.3345	0.3795	0.6994	0.2859	0.5420
0 2	0.7130	0.3181	0.4136	0.6785	0.2577	0.5600

Appendix A-l (cont'd.)

Appendix A-1 (cont'd.)

PEBA pH 5.4

		Molecule 1			Molecule 1'	
Atom Name	×	>	Z	×	۶,	Z
C J	0.6320	0.2691	0.3815	0.6331	0.3177	0.5524
C 2	0.6168	0.2677	0.3611	0.6268	0.3318	0.5664
င ၁	0.5945	0.2544	0.3564	0.6031	0.3438	0.5609
C 4	0.5860	0.2438	0.3723	0.5845	0.3404	0.5421
CP3	0.5998	0.2465	0.3929	0.5897	0.3253	0.5288
CP2	0.6237	0.2584	0.3973	0.6146	0.3146	0.5335
CA	0.6559	0.2834	0.3866	0.6584	0.3049	0.5583
89	0.6834	0.2720	0.3879	0.6513	0.2864	0.5700
æ	0.7082	0.2871	0.3921	0.6763	0.2714	0.5732
0 1	0.7041	0.3024	0.3756	0.6808	0.2646	0.5528
0 2	0.7096	0.2968	0.4124	0.7016	0.2814	0.5846
0 3	0.7345	0.2763	0.3922	0.6700	0.2540	0.5852

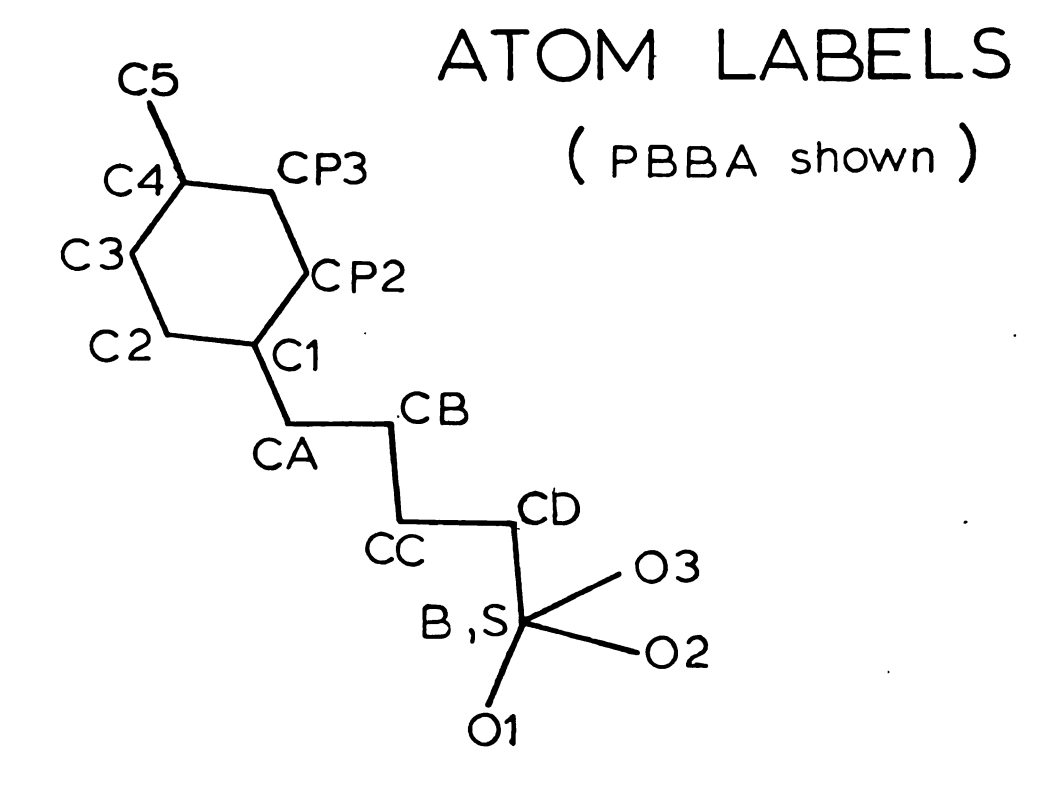
Appendix A-1 (cont'd.)

Appendix A-l (cont'd.)

			•			
		Molecule 1			Molecule 1'	
Atom Name	×	y	2	×	>	2
ر 1	0.6186	0.2793	0.3795	0.6271	0.3149	0.5546
C 2	0.5980	0.2775	0.3615	0.6078	0.3129	0.5674
ဗ	0.5817	0.2599	0.3584	0.5835	0.3244	0.5636
C 4	0.5844	0.2456	0.3741	0.5775	0.3366	0.5461
CP3	0.6035	0.2484	0.3928	0.5958	0.3374	0.5324
CP2	0.6215	0.2648	0.3950	0.6212	0.3273	0.5372
CA	0.6361	0.2977	0.3831	0.6530	0.3025	0.5585
CB	0.6646	0.2926	0.3966	0.6456	0.2807	0.5621
മ	0.6837	0.3115	0.3991	0.6717	0.2672	0.5623
0 1	0.6742	0.3251	0.3814	0.6682	0.2562	0.5424
0 2	0.7127	0.3054	0.3995	0.6746	0.2528	0.5796
0 3	0.6821	0.3218	0.4186	0.6968	0.2798	0.5649

Appendix A-l (cont'd.)

	PPBA		
		Molecule 1	
Atom Name	x	y	Z
C 1	0.6003	0.2711	0.3727
C 2	0.5725	0.2707	0.3621
C 3	0.5578	0.2527	0.3600
C 4	0.5700	0.2356	0.3699
CP3	0.5971	0.2364	0.3819
CP2	0.6126	0.2539	0.3824
CA	0.6161	0.2903	0.3750
СВ	0.6467	0.2862	0.3745
CC	0.6623	0.3061	0.3745
В	0.6938	0.3019	0.3748
0 1	0.7010	0.3099	0.3557
0 2	0.7111	0.3117	0.3931
0 3	0.6988	0.2802	0.3759
	PBBA		
		Molecule 1	
Atom Name	x	У	Z
· C 1	0.6017	0.2697	0.3691
C 2	0.5748	0.2672	0.3574
C 3	0.5610	0.2491	0.3580
C 4	0.5730	0.2341	0.3717
CP3	0.5990	0.2373	0.3847
CP2	0.6139	0.2546	0.3826
CA	0.6166	0.2891	0.3685
СВ	0.6479	0.2852	0.3705
CC	0.6644	0.3039	0.3789
CD	0.6835	0.3100	0.3641
В	0.7142	0.3040	0.3739
0 1	0.7265	0.2935	0.3582
0 2	0.7145	0.2907	0.3918
0 3	0.7306	0.3221	0.3808



APPENDIX A-2

Bond Distances and Bond Angles of Inhibitors Determined in This Study

As described in the text, the deviations in bond distances and bond angles for the inhibitors determined in this study are very similar to ideal values, as summarized below:

1) Carbon-Carbon Distances

$$_{aromatic}$$
 = 1.40 \pm 0.05 \mathring{A}
 $_{phenyl-alkyl}$ = 1.50 \pm 0.05 \mathring{A}
 $_{alkyl}$ = 1.54 \pm 0.05 \mathring{A}

2) Carbon-Sulfur Distances

$$< r>_{C-S} = 1.83 \pm 0.05 \text{ Å}$$

3) <u>Carbon-Boron Distances</u>

$$< r>_{C-B}$$
 = 1.57 \pm 0.05 Å

4) Oxygen Distances

$$< r>_{S-0}$$
 = 1.47 \pm 0.05 Å
 $< r>_{B-0}$ = 1.48 \pm 0.05 Å

5) Aromatic Ring Bond Angles

6) Alkyl Chain Bond Angles

$$<\theta>_{phenyl-alkyl}$$
 = $120 \pm 1^{\circ}$
 $<\theta>_{alkyl}$ = $109.45 \pm 1^{\circ}$

7) Boronate/Sulfonate Bond Angles

$$^{<\theta>}_{-B(OH)_2} = 120 \pm 1^{\circ}$$

 $^{<\theta>}_{-SO_3} = ^{<\theta>}_{-B(OH)_3} = 109.45 \pm 1^{\circ}$

8) <u>Deviations from Planarity of Phenyl Rings</u>

$$<\Delta r>$$
 = ± 0.02 Å from least-squares plane



APPENDIX B

Calculated van der Waals Contacts of TOS, PMS, TOS (MRC), PEBA pH 3.6, PEBA pH 5.4, PEBA pH 7.3, PPBA and PBBA

APPENDIX B-1

Calculated van der Waals Contacts Between Native $\alpha\text{-CHT}$ and Irreversible Inhibitors (TOS and PMS) Inhibitor Coordinates from Appendix A

Inhibitor Atom	Residue #	TOS Contact Atom (Distance Å)	Residue #	PMS Contact Atom (Distance Å)
C5	215	C (3.2), 0 (3.3)	3 8 1	
	216	C ₂ (1.5), N (2.5), C (2.7)		
	217	N (3.0)		
C4	215	C (3.3)	215	C (3.2), 0 (3.3)
	216	C ₂ (2.3), N (2.6), C (3.5)	216	C ₂ (2.3), N (2.7)
CP3	216	CŽ (3.0), N (3.2)	216	CŽ (2.9), N (3.1)
CP2	191	0 (3.5)	}	3
E3	214	0 (3.4)	214	0 (3.5)
	215	C (3.3)	215	C (3.4), 0 (3.5)
	216	N (3.2)	216	N (3.3), C ₂ (3.4)
C2	195	N (3.5)	195	N (3.5)
	213	(3.0)	213	c ₂ (3.0)
	214	0 (3.3)	214	0 (3.1)
C1	!		!	
CA	;		195	0,(3.2)

(cont'd.)



(cont'd.)

		T0S		PMS
nibitor Atom	m Residue #	Contact Atom (Distance Å)	Residue #	Contact Atom (Distance A)
ν	195	0_{χ} (2.4), N (2.9), c_{β} (3.0), c_{ζ}^{χ} (3.3)	195	0_{γ} (2.4), N (3.0), c_{β} (3.3), c_{ζ} (3.2)
10	57	N ₅ (3.4)	191	0 (2.5), c (3.0)
	195	$0.(2.5), c_{R}(2.9)$	192	N (3.0), C_{α} (2.3), C (2.8)
		1	193	N (2.5)
			194	N (3.5)
02	194	N (3.0), C_{κ} (3.2), C (2.5)	193	N (3.4), C (3.0)
	195	N (1.3), 0_{\vee}° (1.9), C_{R} (2.5),	194	N (2.2), C_{R} (3.1), C_{R} (2.5),
		c, (1.9), c (3.3)		c (2.2), 0 (3.4)
	213	ر _{کا} (3.4)	195	N (1.3), 0_{γ} (2.4), c_{β} (2.9),
		<u>-</u>		c (2.5)
			213	ເຼັ (3.4)
03	191	0 (3.3)	193	N (3.2)
	192	c _~ (3.0), c (3.0)	195	0_{\sim} (1.9), $c_{\rm g}$ (3.1)
	193	$N(2.1), C_{\mathcal{R}}(3.1), C(3.4)$		1
	194	N (3.0)		
	195	N (3.4), 0_{γ} (2.9)		

	PEBA	PEBA pH 3.6	PEBA	PEBA pH 5.4	PEBA	PEBA pH 7.3
Inhibitor Atom	Residue #	Contact Atom (Distance Å)	Residue #	Contact Atom (Distance Å)	Residue #	Contact Atom (Distance Å)
2	216	N (3.4), C _N (2.8)	190	c (3.2), 0 (3.0), C _R (2.9)	190	c (3.4), 0 (3.1), c _g (3.0)
	217	N (3.3)	216	c _~ (2.5)	216	N (3.4), C ₂ (2.4)
CP3	216	C _A (2.8), N (3.4)	190	0 (3.1)	190	0 (2.9), c (3.2)
	217	Ç (3.3)	191	c (3.2), c _a (3.0)	161	c (3.3), 0 (3.5), c _a (3.3)
	•	:	192	S_{δ} (3.1), N (3.4)	516	c _a (3.1)
	•			C ₂ (3.4)	•	1
	•	. ,		N (3.2), 0 (3.4)	1	
	٠.		220	S _v (3.4)	•	
CP2	•		191	$c(2.8), 0(3.1), c_{\alpha}(3.4)$	191	c (3.2), 0 (3.0)
	ı		192	N (2.8), C, (3.3), S ₈ (2.7)	•	
ន		c (2.8), 0 (2.9)	190	C _B (2.9), 0, (3.5)	190	c _g (3.5)
	216	$N(2.7), C_{\alpha}(2.7)$	215	0 (3.4)	215	c (2.9), 0 (2.8)
	•	ì	516	N (3.5), C _A (3.1)	516	N (2.8), C _R (2.5)
23	213	ري (3.4)	213	رم، (3.0)	214	0 (2.9)
	214	0 (2.7)	•	<u>:</u>	215	c (2.7), 0 (3.0), c _x (3.4)
	215	C (3.4)	•		216	N (2.7), C, (3.1)
	216	N (3.4)			•	5
១	214	0 (3.3)	191	0 (3.5)	216	N (3.5)
క	214	0 (3.3)	•		214	0 (3.4)
8	195	N (3.3), C _A (3.4), 0 ₂ (2.7)	191	0 (3.4)	193	N (3.3)
	•		193	N (3.2)	194	N (3.5)
,						

	PEBA	PEBA pH 3.6	PEBA	PEBA pH 5.4	PEB/	PEBA pH 7.3
Inhibitor Atom	Residue #	Contact Atom Residue # (Distance A) Re	sidue #	Contact Atom Residue # (Distance Å)	esidue #	Contact Atom Residue # (Distance A)
			194	N (3.2)	195	N (3.2), 0, (3.0)
	•		195	N (2.8), 0 ₂ (2.9)	•	-
&	195	0, (2.0), c _g (2.8)	193	N (3.4)	195	N (3.0), C ₂ (3.2), C _A (2.5),
		.	195	O_{χ} (1.7), C_{β} (2.7), C_{α} (3.3), N (3.0)	•	0, (1.7) y
6	•		195	0, (2.9)	195	0, (2.8)
05	22	C_{62} (3.5), N_{e2} (2.7)	22	N _E (3.1)	22	N ₅ (3.0)
	195	ca (3.2), c _B (2.0), 0 _y (1.9) 195		$N(3.0), C_{\alpha}(2.7), C_{\beta}(1.7),$	195	$N(2.8), C_{\alpha}(2.5), C_{\beta}(2.1),$
03	193	N (3.1)	193	N (2.5), C (2.6), 0 (3.4),	193	c (3.4)
	195	Cg (3.0), 0, (1.7)		C <u>,</u> (2.6)	194	N (3.3), C (3.1)
		-	194	N (2.6), C (3.4)	195	N (2.0), C (3.4), C _A (2.3),
			195	N (2.6), c_{α} (3.3), c_{β} (3.0), o_{γ} (1.7)		c _β (1.7), 0 _γ (0.7)

(cont'd.)

Calculated van der Waals Contacts between Native $\alpha\text{-CHT}$ and PPBA and PBBA Inhibitor Coordinates from Appendix A

		PPBA		PBBA
Inhibitor Atom	Residue #	Contact Atom (Distance A)	Residue #	Contact Atom (Distance Å)
C4	190	c (3.2), 0 (2.8), c _{\(\infty\)} (3.5),	190	c (2.9), 0 (2.5), c_{α} (3.2),
		c _k (3.0)		c _g (2.8)
	216	c <u> </u>	216	ເ _ດ (2.8)
CP3	190	$C'(2.5)$, 0 (2.3), $C_{S'}(3.2)$,	190	$C'(2.6), 0 (2.4), C_{\alpha}(3.3),$
		c _g (2.8)		c _g (2.9)
	191	N (3.0), C ₂ (3.4)	191	N (3.1)
	216	ິ (3.2)	216	(0.8) %
CP2	190	c (3.4), c _g (3.4)	190	ເຊື (3.5)
	191	C (3.3), O (3.1), N (3.4)	191	0 (3.4)
	ı		216	c, (3.3)
C3	215	c (2.8), 0 (2.4)	215	c (3.1), 0 (2.7)
	216	N (2.6), C ₂ (1.8)	216	c (3.1), N (2.9), c_{κ} (2.0)
C2	215	c (2.0), 0° (2.2), c_{\sim} (3.2)	215	C (2.4), 0 (2.4)
	216	c (3.5), N (1.9), C (2.0)	216	N (2.4), C ₂ (2.3)
[]	215	C (3.2)	215	c (3.3)
	216	N (2.8), C ₂ (2.9)	216	N (3.0), C ₂ (3.1)
CA	214	0 (3.2)	214	0 (2.9)
	216	N (3.3)	216	N (3.5)

(cont'd.)

 c_{g} (3.4), o_{γ} (2.9) c_{g} (3.3) c_{g} (3.3) c_{g} (2.5), c_{g} (1.7), c_{g} (1.5) c_{g} (3.0), c_{g} (1.9), c_{g} (0.7) c_{α} (2.1), c_{β} (1.7), 0_{γ} (1.1) N (1.9), C (2.9), O (2.9), Contact Atom (Distance Å) N (3.3), C (2.8), O (3.5) N (3.5), 0_{γ} (2.3) S_{γ} (3.3) C_{β} (2.7), 0_{γ} (1.8) C_{α} (3.3), C_{β} (3.2) C (3.2), 0 (3.5) N (2.4), C_{α} (3.2) N (3.5) Residue # 195 195 57 195 195 192 193 195 42 195 194 193 194 42 N (2.3), C (2.9), C_{α} (3.0) N (2.5), C (3.5), C_{α} (3.4) N (2.6), C_{β} (3.4), O_{γ} (2.4) N (2.4), C_{α} (2.8), C_{β} (2.4), O_{γ} (1.5) c_{α} (1.5), c_{β} (0.7), o_{γ} (1.3) o_{γ} (2.0), c_{β} (3.0) N (3.3), c_{β} (3.4), o_{γ} (3.0) N (2.2), C (2.8), 0 (3.5), Contact Atom (Distance Å) N (3.3), C (3.5) N_{E2} (3.3) C (3.5) **PPBA** N (3.5) Residue # 195 195 194 195 195 195 194 195 192 193 191 194 Inhibitor Atom ဗ 8 05 03 5 മ

(cont'd.)

APPENDIX B-2 Calculated van der Waals Contacts Between $\alpha\text{-CHT}$ (MRC) and Tosyl Inhibitor (MRC Results) (49)

nhibitor Atom	Residue #	Contact Atom (Distance Å)
C5	216	C _o (3.6), N (3.9), C (4.0)
	217	0 (4.0), N (4.0)
C4	215	C (3.8)
	216	N (3.5), C _g (3.8)
CP3	216	N (4.0)
CP2	191	C (3.8), O (3.9)
	192	N (4.0)
	195	0 _Y (3.9)
C3	215	c'(3.8)
C2	191	0 (3.7)
	195	0 _γ (3.0)
	213	$c_{\gamma 1}^{'}$ (3.7)
Cl	191	0'(3.4), C (3.9)
	195	c _β (3.9), 0 _γ (2.6)
S	191	0້(3.8)
	195	N (3.5), C_{α} (3.5), C_{β} (2.5)
		0, (1.5)
0E1	191	C'(3.2), O (2.7), N (3.3)
	192	C _α (3.2)
	195	0 _γ (2.8)
0E2	191	0 (2.9)
	192	C _o (3.3), N (3.1)
	193	ที่(3.5)
	194	N (2.9)
	195	C_{α} (3.5), C_{β} (2.9), O_{γ} (2.5)
0 _Y	194	ที่(2.6)
Ť	195	C_{α} (2.4), C_{β} (1.8), O_{γ} (0.8)

APPENDIX C

Coordinates of Difference Fourier Peaks Used in Calculation of Difference Diagonal Plots (a = 49.2 Å, b = 67.2 Å, c = 65.95 Å, β = 101.8°)

APPENDIX C Coordinates of Difference Fourier Peaks Used in Calculation of Difference Diagonal Plots (a = 49.2 Å, b = 67.2 Å, c = 65.95 Å, β = 101.8°)

TOS

Peak Height*	Derivative	X	У	Z
-9	TOS	0.197	0.716	0.000
- 9	TOS	0.328	0.333	0.650
-9	TOS	0.552	0.333	0.500
- 9	TOS	0.684	0.366	0.350
-9	TOS	0.697	0.266	0.600
9	TOS	0.802	0.216	0.000
12	TOS	0.815	0.366	-0.016
-8	TOS	0.302	-0.050	0.333
8	TOS	0.460	0.416	0.600
8	TOS	0.500	0.266	0.400
-8	TOS	0.526	0.316	0.433
-8	TOS	0.552	0.250	0.400
-8	TOS	0.578	0.250	0.333
-8	TOS	0.605	0.350	0.583
-8	TOS	0.697	0.450	0.666
-8	TOS	0.828	0.283	0.433
8	TOS	0.881	0.283	0.400
8	TOS	0.907	-0.033	0.266
-8	TOS	0.947	-0.033	0.433
8	TOS	1.000	0.500	-0.050

PMS

Peak Height*	Derivative	X	У	Z
10	PMS	0.118	0.783	0.600
-10	PMS	0.157	0.783	0.566
10	PMS	0.250	0.800	0.616
10	PMS	0.276	0.616	0.366
10	PMS	0.289	0.816	0.650
-10	PMS	0.289	0.783	0.466
11	PMS	0.302	0.633	0.666
-10	PMS	0.315	-0.050	0.333
-14	PMS	0.447	0.750	0.600
10	PMS	0.473	0.666	0.916
10	PMS	0.526	0.166	0.083
-12	PMS	0.526	0.316	0.450
-14	PMS	0.552	0.250	0.400
10	PMS	0.684	0.366	0.350
11	PMS	0.697	0.133	0.333
-10	PMS	0.697	0.450	0.666
-10	PMS	0.710	0.316	0.350
-10	PMS	0.710	0.283	0.533
10	PMS	0.723	0.116	0.633
10	PMS	0.750	0.300	0.383
12	PMS	0.815	0.366	-0.016
-10	PMS	0.842	0.283	0.433
10	PMS	0.881	0.283	0.400

Appendix C (cont'd.)

PEBA pH 3.6

Peak Height*	Derivative	X	У	Z
9	PEBA	0.592	0.366	0.383
-11	PEBA	0.605	0.300	0.416
-9	PEBA	0.644	0.266	0.516
-9	PEBA	0.697	0.283	0.516
-9	PEBA	0.750	0.283	0.466
9	PEBA	0.763	0.283	0.550
9	PEBA	0.789	0.333	0.500
10	PEBA	0.802	0.216	0.000
10	PEBA	0.815	0.383	-0.016
8	PEBA	0.236	0.266	0.266
8	PEBA	0.355	-0.050	0.433
8	PEBA	0.381	0.650	0.633
-8	PEBA	0.434	0.233	0.433
-8	PEBA	0.434	0.350	0.433
-8	PEBA	0.434	0.016	0.766
-8	PEBA	0.565	0.250	0.333
-8	PEBA	0.565	0.516	0.233
8	PEBA	0.618	0.150	0.366
-8	PEBA	0.631	0.300	0.416
8	PEBA	0.657	0.450	0.566
-8	PEBA	0.684	0.450	0.666
-8	PEBA	0.710	0.266	0.366
8	PEBA	0.723	0.316	0.416
-8	PEBA	0.736	0.300	0.500
-8	PEBA	0.802	0.116	0.266

PEBA pH 5.4

Peak Height*	Derivative	X	y	Z
-13	PEBA	0.171	0.166	0.383
12	PEBA	0.171	-0.050	0.500
14	PEBA	0.315	0.433	0.566
12	PEBA	0.355	0.650	0.466
-13	PEBA	0.434	0.233	0.433
-12	PEBA	0.539	0.250	0.383
12	PEBA	0.644	0.150	0.533
-13	PEBA	0.684	0.166	0.500
-14	PEBA	0.684	0.183	0.533
-14	PEBA	0.684	0.416	0.416
-13	PEBA	0.802	0.233	0.616
12	PEBA	0.828	0.450	0.500
14	PEBA	0.855	0.333	0.616
-13	PEBA	0.881	0.350	0.783
-13	PEBA	0.894	0.400	-0.050
-13	PEBA	0.947	-0.016	0.433
21	PEBA	0.947	0.000	0.400
-12	PEBA	0.986	0.233	-0.116

pH 5.4

Peak Height*	Derivative	X	у	Z
-11	pH 5.4	0.052	0.066	0.416
-11	pH 5.4	0.052	0.633	0.416
-9	pH 5.4	0.078	-0.033	0.550
- 10	pH 5.4	0.289	0.066	0.366
9	pH 5.4	0.381	-0.066	0.600
9	pH 5.4	0.434	0.616	0.366
9	pH 5.4	0.565	0.116	0.633
11	pH 5.4	0.565	0.266	0.466
9	pH 5.4	0.631	0.433	0.400
-13	pH 5.4	0.684	0.166	0.533
-9	pH 5.4	0.684	0.416	0.416
-10	pH 5.4	0.723	0.566	0.633
-9	pH 5.4	0.763	0.333	0.483
-9	pH 5.4	0.789	0.466	0.383
9	pH 5.4	0.868	0.000	0.000
12	pH 5.4	0.881	0.316	0.600
-9	pH 5.4	0.921	0.333	0.583
-9	pH 5.4	0.934	0.400	0.450
-11	pH 5.4	0.947	0.133	0.583
-11	pH 5.4	0.947	0.566	0.583

PEBA pH 7.3

Peak Height*	Derivative	X	y	z
11	PEBA	0.118	-0.066	0.333
11	PEBA	0.315	0.416	0.566
-13	PEBA	0.434	0.250	0.433
-11	PEBA	0.500	0.300	0.466
-12	PEBA	0.526	0.250	0.483
12	PEBA	0.578	0.250	0.483
-12	PEBA	0.592	0.300	0.516
11	PEBA	0.605	0.400	0.600
11	PEBA	0.684	-0.083	0.433
-14	PEBA	0.684	0.183	0.533
-11	PEBA	0.763	0.300	0.483
11	PEBA	0.881	0.433	0.666
12	PEBA	0.947	0.000	0.400

pH 7.3

Peak Height*	Derivative	X	у	z
13	pH 7.3	0.052	0.500	0.600
-11	pH 7.3	0.092	0.516	0.633
-13	pH 7.3	0.276	0.066	0.366
- 15	pH 7.3	0.315	-0.083	0.583
11	pH 7.3	0.368	-0.066	0.600
-11	pH 7.3	0.605	0.233	0.533
11	pH 7.3	0.631	0.433	0.400
-18	pH 7.3	0.671	0.183	0.533
-14	pH 7.3	0.671	0.416	0.416
-13	pH 7.3	0.723	0.566	0.633
14	pH 7.3	0.789	0.200	0.016
-12	pH 7.3	0.828	0.300	0.583
11	pH 7.3	0.881	0.316	0.600
-11	pH 7.3	0.907	0.016	0.366
-11	pH 7.3	0.921	0.333	0.583
13	pH 7.3	0.947	0.000	0.400

PPBA

Peak Height*	Derivative	X	y	Z
-9	PPBA	0.171	0.283	0.466
-9	PPBA	0.233	0.266	0.166
10	PPBA	0.315	0.583	0.566
10	PPBA	0.328	0.100	0.250
-9	PPBA	0.368	-0.033	0.083
-10	PPBA	0.434	0.250	0.433
-9	PPBA	0.644	0.466	0.933
-9	PPBA	0.671	0.350	0.466
10	PPBA	0.671	0.600	0.750
10	PPBA	0.684	-0.066	0.433
12	PPBA	0.855	0.333	0.616
10	PPBA	0.868	0.550	0.616
9	PPBA	0.894	0.433	0.666
10	PPBA	0.947	0.000	0.400
-10	PPBA	0.947	0.283	0.433

PBBA

Peak Height*	Derivative	X	У	Z
9	PBBA	0.052	0.350	0.200
11	PBBA	0.052	0.500	0.600
10	PBBA	0.315	0.433	0.566
9	PBBA	0.328	0.100	0.250
-9	PBBA	0.368	-0.033	0.083
-19	PBBA	0.434	0.233	0.433
9	PBBA	0.486	0.333	0.500
9	PBBA	0.671	0.600	0.750
9	PBBA	0.789	0.333	-0.016
12	PBBA	0.855	0.333	0.616
11	PBBA	0.868	0.333	0.616
-9	PBBA	0.947	0.283	0.433
11	PBBA	0.947	0.000	0.400
-9	PBBA	1.000	0.316	0.300

^{*}Electrons/ \mathring{A}^{-3} = (Peak Height)/50.